Martin-Luther-Universität Halle-Wittenberg

Institut für Physik

der Naturwissenschaftlichen Fakultät II

Structure, Formation and Thermodynamic Properties of Polymer Networks as Studied by NMR

Dissertation zur Erlangung des akademischen Grades

doctor rerum naturalium (Dr. rer. nat.)

vorgelegt von

Diplom-Physiker

Walter Chassé

geboren am 31.07.1981 in Halle (Saale)

Halle (Saale), September 27, 2012

Gutachter:

1. Prof. Dr. Kay Saalwächter, Martin-Luther-Universität Halle-Wittenberg

2. Prof. Dr. Wolfgang Paul, Martin-Luther-Universität Halle-Wittenberg

3. Prof. Dr. Matthias Ballauff, Helmholtz Zentrum Berlin

Öffentliche Verteidigung: 20. Februar 2013

Contents

1. Introduction

Polymers are macromolecules whose properties and functionality are determined by the type, number, sequence and spatial arrangement of their basic monomeric units. The extraordinary variability of the composition substantiates the incredible diversity of the natural occurrence and the technical applications of polymers. The undisputedly most important representatives are biological polymers such as proteins and peptides which consist of well-defined sequences of amino acids and form the fundamental building blocks of all known forms of life. Also in our everyday life we constantly meet polymeric materials as versatile engineering materials. They are used in different kinds of plastic, sealants, tires, paints and varnishes, adhesives and important biomedical applications, to name just a few examples.

An important and unique property of flexible polymer chains is their elasticity. This is based on the macromolecular construction of the polymers and the ability to alter their conformation by thermal motion and external mechanical stress. In an unloaded condition the polymer chains in a network adopt their entropically favored random-coil conformation, which is typically described by Gaussian statistics. By deformation of the network, the polymer chains behave as entropic springs. The induced tension can almost solely be attributed to the increase of entropy, due to the stretching respective change in conformation of the individual network strands between their cross-links. In contrast to polymer networks, very small deformations on an atomic scale cause a huge increase of internal energy in solids like crystals, metals and ceramics. The increase of internal energy is several orders of magnitude higher than for comparable deformations of polymer networks.

The elastic response of a polymer network is independent of the nature of the cross-links, i.e. physical or chemical cross-links, whereas major differences in the time scale of the elastic response are observed. In a melt of long entangled polymer chains, the tension can be released by reptation of the polymer chains along the one-dimensional confining tube. Such systems show an elastic response to external mechanical deformation only on comparable short time scales. The time scale of this response is determined by the

disentanglement time, which defines the time a chain needs to pass the confining tube once. The introduction of permanent cross-links through chemical connections of the chains leads to an ultimate prevention of reptative motions. The mechanical stress induced to the network can be conserved over long time scales. This rubber-like elasticity of permanent chemical cross-linked networks enables reversible elongation of many time the original length.

Permanent elastic polymer networks emerge by *formation* of irreversible covalent bonds between the polymer chains during the cross-link reaction forming a giant three dimensional macromolecule. The *structure* of the resulting polymer networks is strongly dependent on the *formation* mechanism. One of the best-known cross-linking reactions is the vulcanization of natural rubber with sulfur, which was already discovered in the 19th century by Charles Goodyear. Other often used methods are the irradiation by electrons [1, 2], gamma- and X-rays [3, 4], the curing by peroxide or other additives [5, 6]. These methods establish an irregular connectivity between the individual chains and with that between all monomers. The random character of the cross-link processes leads to polymer networks having complex *structures* [7, 8] with broad molecular weight distributions of the network strands between the cross-links. Among these the mechanical properties of polymer networks are determined by the functionality of the cross-links, clustering, polydispersity, and defects, as for example dangling chains and self loops. For special applications the properties of polymer networks can be enhanced, e.g., by additional fillers like carbon black [9, 10, 11].

Polymer networks have been subject to intense scientific research for several decades. Complementary theoretical and experimental methods, which of course are the most important, and computer simulations are used for the investigation. An impressive number of different experimental methods such as scattering experiments, rheology, raman spectroscopy, etc. were applied. An often-used approach is the investigation of the deformation behavior of polymer networks in dependence on different external influences. Therefore especially mechanical tests, which investigate the elastic response of networks to deformations of different duration and amplitude, as well as equilibrium swelling experiments are conducted. These experiments are easily feasible and produce reliable conclusions about the macroscopic properties of polymer materials as shown in innumerable scientific publications. Due to the macroscopic character of these methods of investigation only little or even no information about the distribution of network strand lengths and potential heterogeneities of the network is obtained. Furthermore, a quantitative estimation of the elastically ineffective network defects and the precise

quantification of the influence of entanglements on the mechanical properties of polymer networks are hardly possible.

On the other hand several competing and partly contradicting theoretical models were developed to describe rubber-like elasticity. Thereby the main problem is the correct description and identification of the microscopic origin of the change of entropy due to the deformation of networks. Another big challenge is the incorporation of distributions of the length of network strands between two cross-links [12]. Since the latter are hardly accessible by experiments, many theories for the description of rubber-like elasticity are based on the assumption of ideal, defect-free, monodisperse polymer networks. Two of the most common network models used are the affine model by Hermans, Flory and Wall [13, 14], and the phantom model by James and Guth [15, 16]. The affine model assumes that the individual chains of the network are deformed according to the deformation of the complete network. The network is regarded as not-fluctuating elastic background onto which the individual network strands are fixed permanently. In contrast the phantom model assumes that the cross-links are free to fluctuate around an average position without topological restriction by neighboring chains. These fluctuations can be described by Gaussian statistics. The constrained-junction model uses this approach and adds an additional potential constraining the fluctuation of the cross-links [17]. The latter is described by virtual chains which are connected to the non-fluctuating elastic background. An important point of this model is that the fluctuations of the virtual chains are changing affinely with the deformation and thus the constraining potential, too. A progress is represented by the Edwards tube model [18], which expands the influence of the confining environment on the whole chains between two cross-links. With that, the assumed chain fluctuations are restricted to a tube defined by a non-fluctuating elastic background. The non-affine tube [19] and slip tube model [20] also apply the concept of virtual chains for the modeling of fluctuation confining potentials. Major differences arise from the number, distribution and possibilities of displacements of the virtual chains along the contour of the polymer chain. The above mentioned models as well as others [21] are used in many studies in order to describe results especially of mechanical and swelling experiments [22, 23]. Thereby they reveal problems in the quantitative estimation of measurement results. Other physically more precise models of rubber-like elasticity fail due to an excessive number of free fitting parameters and/or the mathematical complexity, therefore a high effort and often numerical solutions are required to solve these.

The third approach of rising importance is the investigation of polymer networks using

computer simulations. One of the key advantages here is the generation of networks with well-defined *structures* by immediate control of the *formation* mechanism. This enables the direct investigation of the local microscopic *structure*, e.g., the functionality of cross-links, defects and the molecular weight distribution of elastically active network strands [24, 25], which are hardly or not at all experimentally accessible. Furthermore, information about the dynamic behavior and relaxation processes in polymer networks and melts can be obtained [26, 27]. Thereby especially the parallel determination of several microscopic and macroscopic properties allows rich insights into polymer networks. For such studies mainly molecular dynamics simulations [28] and bond-fluctuation Monte Carlo simulations [29] are used. A major problem is caused by the partly very long relaxation times in polymer networks which, for example, have to be taken into consideration for the calculation of shear moduli. This is one of the reasons why especially the macroscopic elasticity is hard to simulate. Nevertheless, due to their ability to vary the *formation* mechanism, numerical methods provide an extraordinary possibility to investigate and to verify theoretical models for the local origin of rubber-like elasticity. Furthermore, the comparison with results of experimental studies helps to verify these, or to contribute to their understanding and interpretation [25, 27, 28].

Nowadays nuclear magnetic resonance (NMR) offers a variety of possibilities to assess the *structure* and dynamics of polymer networks and melts on different length and time scales [30]. For the investigation of polymer networks the fact is used that the NMR response is partially solid-like [31]. In melts and solutions of unentangled polymers well above the glass transition temperature inter- and intra-monomer dipolar couplings are averaged out completely by fast isotropic segmental fluctuations of the chains. The latter are restricted in polymer networks by the presence of topological restriction, i.e., entanglements and permanent chemical cross-links. This leads to non-isotropic chain segment fluctuations leaving weak residual dipolar couplings, D_{res}, which give rise to solid-like NMR properties [32, 33, 34]. The partially averaged interactions are directly proportional to a dynamic order parameter of the polymer backbone, S_{b} [35], and reflect the physical and chemical cross-link density of polymer networks [33, 36, 37].

The residual dipolar interactions left by rapid segmental motions, which are fast on the time scale of NMR experiments, are reflected by various NMR parameters in different ways. The weak residual interactions among abundant spins lead to a coherent dipolar dephasing and thus are related to the relaxation of transverse magnetization [31]. The latter can be determined quantitatively by relaxometry which is an often used method for the investigation of polymer networks [38]. However, the presence of slower

cooperative motion on the time scale of the experiments, i.e., excursions attributed to whole chain reorientations, and other thermal motion random in nature lead to incoherent relaxation and thus to a complex interplay of relaxation effects and dephasing. The shapes of relaxation curves are commonly evaluated by multi-parameter functions in order to separate the coherent dipolar effect. This gave rise to certain criticism since inadequacies of the applied fitting models and parameter interdependencies play a crucial role for the meaningfulness of the results usually obtained from global fits of complete relaxation functions or line shapes [39, 40]. Among alternative methods [34, 41] especially ^{1}H double-quantum (DQ) NMR [42] has demonstrated to be a versatile and reliable technique for the determination of residual dipolar couplings in the recent years [36, 43, 44, 45]. The main advantage of ^{1}H DQ experiments is the determination of two signal functions, i.e., a build-up curve dominated by DQ spin-pair coherences and a fully dipolar-refocused decay function, which show an almost comparable time-dependence in the long-time limit of the experiment. This allows for a normalization of the DQ build-up curve for effects of slow motions and other relaxations. The so-obtained relaxation compensated normalized build-up curve solely depends on the *structure* of the investigated networks and therefore permits even the estimation of distributions of residual dipolar couplings [36].

Equilibrium swelling is an easy feasible and often used experiment for the determination of the molecular weight between two cross-links, M_c, and thus the cross-link density, γ_c. The equilibrium degree of swelling is characterized by the exact compensation of the gain in free energy upon mixing, as described by the Flory-Huggins solution theory [46, 47], by the free energy loss due to network deformation. Swelling experiments are usually evaluated in terms of the Flory-Rehner theory [48] which postulates the additivity of the free energy of mixing and the elastic free energy whereas the latter is described by molecular theories of rubber-like elasticity as mentioned above. Hence the results obtained by swelling are strongly model dependent.

In this work polymer networks are studied by ^{1}H DQ low-field NMR in dry and swollen state in order to precisely characterize their *structure* in dependence on their *formation* condition and to investigate their *thermodynamic properties* as reflected directly by segmental orientation correlations. The results are used to examine the impact of the network *structure* on the evaluation of equilibrium swelling experiments and to explore the applicability of the Flory-Rehner theory for the description of the thermodynamic state of swollen polymer networks.

For this purpose poly(dimethylsiloxane) (PDMS) networks are prepared by cross-

linking end- and randomly functionalized pre-polymers at various reaction conditions. For the evaluation of the DQ NMR experiments an improved protocol for fast Tikhonov regularization, *ftikreg*, is developed and presented which uses a new generic build-up function to extend the fitting limit of conventional fitting functions enabling the precise determination even of broad or multimodal coupling constant distributions [49]. The cross-link density of randomly cross-linked PDMS networks with systematically varied defect fractions is investigated by ^{1}H DQ NMR and equilibrium swelling experiments. The results are compared with absolute-value results obtained by calculations based on a statistical theory of cross-linking and used to investigate different approaches to consider network defects, as determined with high accuracy in swollen networks samples by NMR data decomposition, in the evaluation of equilibrium swelling experiments by Flory-Rehner theory employing the phantom model [37].

In order to investigate the applicability and limitations of the classical Flory-Rehner theory the equilibrium degree of swelling of different PDMS networks in various solvents of different quality is determined temperature-dependent. The results are used for a novel construction of solvent independent swelling master curves and yield information about the temperature- and cross-link density-dependence on the Flory-Huggins interaction parameter. The results are supported by DQ measurements on networks swollen to equilibrium in various solvents at different temperatures [50]. This allows to investigate predictions of the Flory-Rehner model for the relation between the two directly measurable quantities and to study the influence of excluded volume effects on chain statistics in terms of scaling laws [51]. As a matter of fact, it demonstrates nicely the sensitivity of segmental orientation correlations on the thermodynamic state of polymer networks.

The influence of the preparation condition on the network *structure*, i.e., coupling constant distributions and network defects, is studied by cross-linking end-functionalized PDMS chains in presence of different amounts of solvent during the network *formation*. The results of equilibrium swelling and ^{1}H DQ NMR experiments for two network series prepared by different pre-cursor polymer length are evaluated with respect to the overlap of the chains in the solution during cross-linking. In order to obtain detailed information about the cross-link kinetics and the *formation* of the elastically effective network the end-cross-linking process in presence of solvent is investigated by liquid- and solid-state NMR in dependence on the reaction temperature [52]. Besides the *structure* of dry and the *thermodynamic properties* of equilibrium swollen end- and randomly cross-linked PDMS networks, the samples are investigated by ^{1}H DQ NMR at well-defined swelling

degrees below equilibrium in order to obtain information about the deformation behavior as reflected by changes in the residual dipolar coupling distributions. The results are evaluated in terms of an introduced back-extrapolation procedure leading to a coincidence of the apparent change of the average residual dipolar coupling constant upon swelling for all investigated networks. This behavior is further compared to the affine prediction for deformation of Gaussian chains.

This cumulative thesis is organized in two main parts. In the first part the theoretical and conceptual background of this work is explained. The basic theoretical description of statistical, dynamic and *thermodynamic properties* of polymers in bulk and solution is presented and the conceptual background of the used NMR method is explained. The second part deals with the results of this work. The published results are briefly summarized and the articles presented. At the end of this chapter unpublished results obtained during this work are shown. The Appendix contains some experimental details.

2. Conceptual and Theoretical Background

In this chapter the basic physical principles of the experiments used in this work are explained in detail. At first, typical length scales used for the characterization of single chain conformations and their dependence on the degree of polymerization, N, are discussed using Gaussian chain statistics for the description of the statistical spatial orientation of the individual chain segments. This is the basis for the description of the *thermodynamic properties*, i.e., entropy elasticity, of ideal polymer chains. Afterwards the Flory-Huggins solution theory is explained. The latter is an important model of the *thermodynamic properties* of polymers in solution and the basis for the evaluation of equilibrium swelling experiments. This paragraph focusses especially on the influence of the solvent quality on the Flory-Huggins interaction parameter, χ, which affects the excluded volume interactions that in turn determine the chain conformation. Afterwards, the dynamical properties of polymer chains are discussed in terms of the Rouse model and the Edwards tube model. The derived characteristic time- and length-scales are used to introduce the time-dependent orientation autocorrelation function, $C_\alpha(t)$, of the chain segments and with that to define the dynamic backbone order parameter, S_b, of polymer chains in networks. This order parameter quantifies the influence of topological constraints on the ability of polymer chains to alter their conformation and thus is a measure for the cross-link density, γ_c, of polymer networks. Finally, it is shown that these segmental orientation correlations are directly reflected by the residual dipolar coupling constant, D_{res}, of dipolar coupled spins connected to the backbone of network strands which can be quantitatively determined by nuclear magnetic resonance (NMR) experiments.

2.1. Statistical Chain Conformation

The characterization of the fundamental entropic properties of macromolecules is generally performed by statistical models for the spatial arrangement of the individual monomeric units of a polymer chain. The simplest model is the freely jointed chain model [53]. Thereby $N + 1$ equal monomer units are connected through N rigid bonds of constant length b, which are completely free to rotate, without consideration of intermolecular interactions. Therefore, the orientation of inter-monomeric connecting vectors $\vec{b}_i$ is of purely statistical nature. The conformation of the polymer chain can be described mathematically by a random walk. The overall length of the chain, the contour length l_0, is obtained by a simple summation over the length of all inter-monomeric connections (Eq. 2.1).

$$l_0 = \sum_{i=1}^{N} |\vec{b}_i| = bN \tag{2.0}$$

The root mean square (rms) end-to-end distance, $\sqrt{\langle \vec{r}^2 \rangle}$, of the terminal monomers of each polymer chain is another important quantity for the characterization of their properties. Whereby $\vec{r}$ denotes the connecting vector between the two end monomers, which is the sum of N independent, statistically oriented vectors and thus also a random quantity. The probability distribution of the end-to-end vectors $P_N(\vec{r})$ is described by a Gaussian distribution function (Eq. 2.1) for a sufficient number of chain segments.

$$P_N(\vec{r}) = \left(\frac{3}{2\pi b^2 N}\right)^{3/2} \exp\left(-\frac{3\vec{r}^2}{2b^2 N}\right) \tag{2.0}$$

The second moment of this distribution function in three dimension yields the dependence of the rms end-to-end distance of the chain ends on the number of monomer units of the polymer chain.

$$\sqrt{\langle \vec{r}^2 \rangle} = bN^{1/2} \tag{2.0}$$

The rms end-to-end distance is distinctly smaller than the contour length and stresses again the random coil conformation. An important feature of this treatment is the applicability of the statistical description for the whole chain as well as for parts of the chain, as long as the number of monomers is sufficiently large. This self-similarity of the polymer conformation allows that the chains between two cross-links in a polymer network can be described by the same statistics. The nature of the crosslinks, i.e., physical or chemical, and the crosslink mechanism for the *formation* of networks, i.e., end-linked or randomly linked, is unimportant for the statistical description of the chain

conformation between two crosslinks.

The distribution function of the rms end-to-end distance, as described by the Gaussian distribution in Eq. 2.1, can be used to determine the *thermodynamic properties* of an ideal polymer chain.

$$S(N, \vec{r}) = k_B \ln P_N(\vec{r}) = -\frac{3}{2} \frac{k_B \vec{r}^2}{b^2 N} + S(N, 0) \tag{2.0}$$

The so-obtained entropy S (Eq. 2.1) is composed of an end-to-end distance dependent and independent part. The latter is resulting from the normalization prefactor of the Gaussian distribution in Eq. 2.1. The Helmholtz free energy, $F = U - TS$, is in the case of the ideal chain model reduced to the entropic contribution, since the chain is assumed to be free of internal interactions ($U = 0$).

$$F(N, \vec{r}) = \frac{3}{2} \frac{k_B T \vec{r}^2}{b^2 N} - F(N, 0) \tag{2.0}$$

If the chain is deformed by an external force, the amount of accessible micro-states is reduced and with that the entropy of the system. On a microscopic scale the deformation leads to a change Δr of the end-to-end distance.

$$f_{\text{el}} = -\left. \frac{\partial F}{\partial r} \right|_{r = \Delta r} = -\frac{3 k_B T}{b^2 N} \Delta r \tag{2.0}$$

The force f_{el} induced by the deformation is opposite to it and of pure entropic origin. That illustrates the natural desire of the system to return to the state of maximum entropy. This behavior is denoted as 'entropy elasticity' and is the molecular respectively statistical reason of rubber-like elasticity.

In contrast to the ideal chain discussed above, the orientation of the inter-monomeric connecting vector $\vec{b}_i$ in a real polymer chain between two consecutive monomers is not completely random. The latter is determined by the chemical structure of the monomer units and hence the steric restrictions as well as the bond properties. Therefore the orientations of the connecting vectors of successive monomers in a polymer chain are correlated. The number of monomers n_{k} over which this orientation correlation vanishes is specific for the polymer material and characterizes the flexibility of the chain. For the statistical description of a real polymer the whole chain is dived in N_{k} completely freely rotating segments as indicated in Figure 2.1. These so-called 'Kuhn-segments' are assumed as stiff rod of the length $l_{\text{k}} = b n_{\text{k}}$. Through this parametrization by l_{k} as material-specific scaling factor, all polymer chains can be described by the same statistics independently of their chemical structure. Chains with a contour length smaller than a

$$\sqrt{\langle \vec{r}^2 \rangle} = bN^\nu \qquad \sqrt{\langle \vec{r}^2 \rangle} = l_k N_k^\nu \qquad \sqrt{\langle \vec{r}^2 \rangle} = l_R N_R^\nu$$
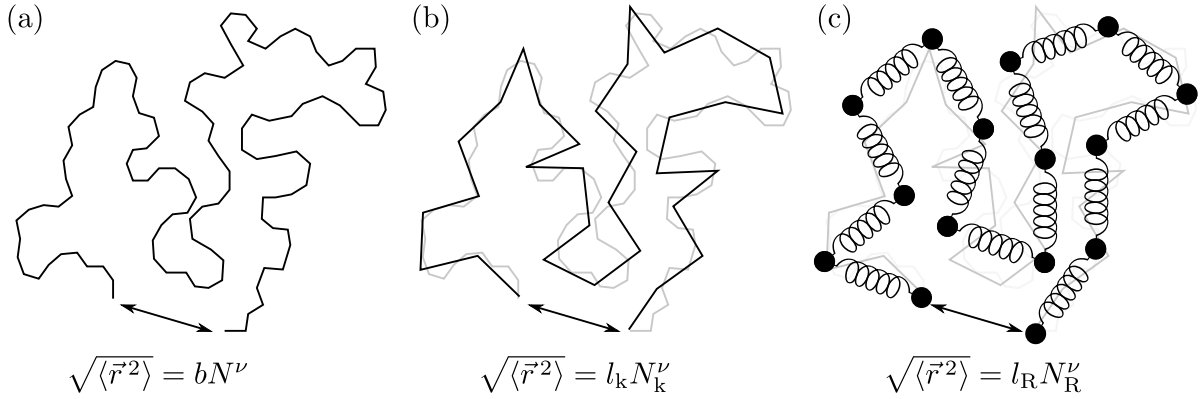
Fig. 2.1.: Representation of chain conformation by a (a) ideal chain, (b) chain of Kuhn segments, and (c) Rouse chain.

Kuhn segment are not flexible, whereas polymers with $l_0 \gg l_k$ are represented by the above discussed Gaussian statistics, and the mean-square end-to-end distance (Eq. 2.1) is obtained analogously to Eq. 2.1.

$$\langle \vec{r}^2 \rangle = N_k (b n_k)^2 = N_k l_k^2 \qquad (2.0)$$

A measure for the stiffness of a polymer chain can be specified by Flory's characteristic ratio C_∞.

$$C_\infty = \frac{\langle \vec{r}^2 \rangle}{N b^2} = \frac{l_k}{b} \qquad (2.0)$$

Polymer chains with strong steric interactions and large bond angles exhibit high values for the characteristic ratio, which is additionally highly dependent on the size of specific side groups attached to the monomers along the backbone. For an ideal chain the characteristic ratio is 1.

More generally, the dependence of the rms end-to-end distance on the degree of polymerization respectively the number of monomers of the chain, N, can be expressed as scaling law.

$$\sqrt{\langle \vec{r}^2 \rangle} \sim N^\nu \qquad (2.0)$$

The scaling exponent of the chain-models considered so far is $\nu = 0.5$. Since the segments of the chain have a spatial expansion and two segments can not occupy the same volume, a part of the space has to be assumed as 'excluded volume'. The latter is defined by the own volume of the chain and makes real chains non-ideal. Possible crossings of the polymer chain with itself become more probable in between more remote monomers. The mathematical description of the chain conformation is performed according to a self

avoiding random walk (SAW). This leads to an increase of the volume of the random coil and with that to a larger rms end-to-end distance. The scaling exponent in Eq. 2.1 with consideration of excluded volume effects is $\nu = 0.6$, as obtained by the Flory-Fischer argument [53, 54], or more precisely, as obtained by renormalization group-theory [55, 56], $\nu = 0.588$. Independently of excluded volume effects the scaling exponent for polymers with $l_0 \leq l_k$ is always $\nu = 1$. In this case the end-to-end distance is equivalent to the contour length.

The statistical conformation of a polymer chain as random coil can approximately be described by a sphere. The size of this sphere is determined by the radius of gyration r_G, which is the root-mean-square distance of all monomers of a polymer chain from its center-of-mass, averaged over all possible chain conformations. The radius of gyration is an important characteristic size for polymers and directly related to the end-to-end distance of the chain.

$$\langle r_G^2 \rangle = \frac{1}{6} \langle \vec{r}^2 \rangle \sim N^{2\nu} \tag{2.0}$$

The volume of the sphere defined by r_G is only filled for a rather small part by the defining polymer chain. In a polymer melt this free volume can be occupied partly by other polymer chains leading to an overlap of different polymer coils. The concentration of the monomers in the melt can be assumed as constant in space and is in particular independent of r_G. Since it is unimportant for a monomer if a neighboring one belongs to its chain or not, no additional expansive forces arise by the overlap of the individual random coils. Thus, the polymer chains adopt their unperturbed, statistical conformation as stated by the 'Flory ideality hypothesis' [57, 53] which conveys that intra- and interchain excluded volume effects compensate each other for strongly overlapping chains as is the case in melts [58].

By dilution of a polymer melt by suitable solvent the overlap, i.e., the interpenetration of the individual chains, can be reduced or removed. This is especially important for the processing of polymers and the investigation of single chain conformation by scattering techniques. Partially overlapping polymer chains are referred to as semi-dilute solution and for very low solvent concentrations as concentrated solution. At the critical overlap concentration, c^*, the complete volume of the solution is occupied by polymer coils without overlap.

$$c^* \sim N^{1-3\nu} \tag{2.0}$$

Below c^* the solution is referred to as dilute and for extremely low polymer concentrations as infinitely dilute. The different concentration regimes are depicted in Figure 2.2.
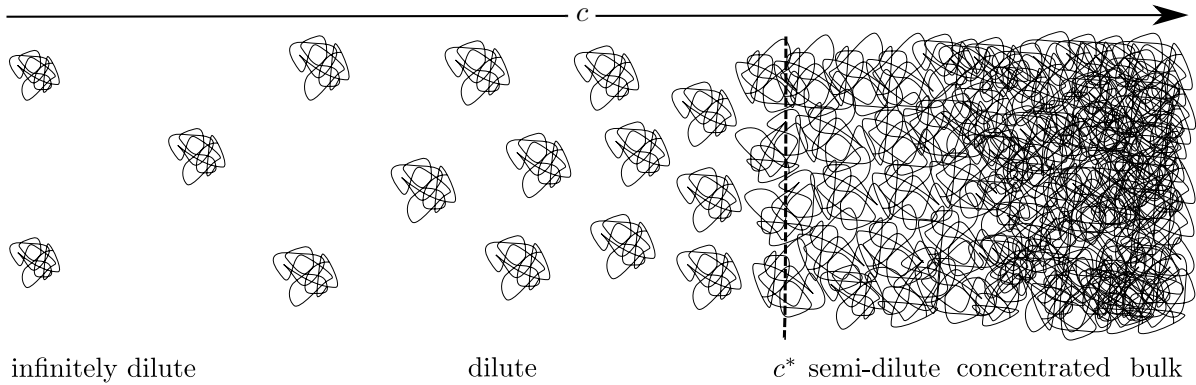
Fig. 2.2.: Concentration regimes of polymers in solution.

The dilution of the polymer melt leads to concentration fluctuations of the monomers and thus polymers, since their monomers are fixed permanently in the chain. These fluctuations increase with decreasing polymer concentration in the solution. Instead of the concentration usually the volume fraction of the polymers $\varphi_p = V_p/V$, which is obtained by the ratio of the polymer volume V_p and the overall volume V of the mixture, is used to quantify their amount in a solution.

2.2. *Thermodynamic Properties* of Polymers in Solution

The *thermodynamic properties* of a polymer solution are commonly described by the Flory-Huggins (FH) lattice theory [46, 47], which yields an expression for the change of the Gibbs free energy ΔG_{mix} upon mixing.

$$\Delta G_{mix} = \Delta H_{mix} - T\Delta S_{mix} \tag{2.0}$$

For the calculation of the mixing enthalpy and entropy, ΔH_{mix} and ΔS_{mix}, respectively, of a binary mixture the components are placed on a lattice. The distribution of the components on the lattice is random and therefore different possibilities for the arrangement exist. By counting all possible arrangements the thermodynamic probability can be estimated. The latter is directly related to the configurational entropy of a system through the Boltzmann's equation, one of the fundamental equations of statistical thermodynamics. The change of the entropy upon mixing is obtained by comparison of the pure system S_0 with the mixed system S_{mix}. Whereas the entropy of the pure systems

is equal to zero, since there is only one way for the arrangement on the lattice. The amount of the components is expressed by their volume fraction φ_i in the mixture, which is likewise the probability that a lattice cell is occupied by a molecule of the type i.

$$\Delta S_{\mathrm{mix}} = S_{\mathrm{mix}} - S_0 = -R \sum_{i=1}^{2} \frac{\varphi_i}{N_i} \ln \varphi_i = -R \left(\frac{\varphi_1}{N_1} \ln \varphi_1 + \frac{\varphi_2}{N_2} \ln \varphi_2 \right) \qquad (2.0)$$

In a mixture of polymers, additionally, it has to be taken into account that the monomers cannot be arranged independently of each other. Therefore, the entropy of mixing is reduced by the degree of polymerization N_i in Eq. 2.2. For very large polymers the entropy of mixing is distinctly smaller as compared to the mixing of simple solutions ($N_1 = N_2 = 1$). Therefore, the enthalpy of mixing governs the miscibility of a polymer solvent system.

Typical interactions between the components in the solution are short-ranged, e.g., hydrogen-bonding, dipole-dipole and van-der-Waals interactions. They are described by a mean-field approximation in the FH-theory. For this purpose the pairwise interaction energies, ε_{12}, ε_{11} and ε_{22}, respectively, of a component on a lattice cell with the components on the Z nearest neighbor cells are considered. The pairwise chemical and physical interactions are summarized by the dimensionless Flory-Huggins interaction parameter χ, which is a measure for the deviation of the system from an ideal system ($\chi = 0$).

$$\chi = \frac{Z}{RT} \left(\varepsilon_{12} - \frac{1}{2} \left(\varepsilon_{11} + \varepsilon_{22} \right) \right) \qquad (2.0)$$

The change of the mixing enthalpy is obtained by replacing one component by the other in the mean-field of the surrounding molecules on the lattice. The statistical occupation of the latter is determined by the respective volume fraction φ_i of the components in the mixture, which is the core assumption of the the mean field approach.

$$\Delta H_{\mathrm{mix}} = H_{\mathrm{mix}} - H_0 = RT\chi\varphi_1\varphi_2 \qquad (2.0)$$

Defining one component as solvent ($N_1 = 1$) and using $\varphi_{\mathrm{s}} = 1 - \varphi_{\mathrm{p}}$, the Flory-Huggins equation (Eq. 2.2) for polymers in solution is obtained.

$$\frac{\Delta G_{\mathrm{mix}}}{RT} = (1 - \varphi_{\mathrm{p}}) \ln(1 - \varphi_{\mathrm{p}}) + \frac{\varphi_{\mathrm{p}}}{N} \ln(\varphi_{\mathrm{p}}) + \chi\varphi_{\mathrm{p}}(1 - \varphi_{\mathrm{p}}) \qquad (2.0)$$

The change of the Gibbs free enthalpy by mixing polymers with a low molecular solvent is dependent on temperature, chemical interactions, volume fraction of components and the degree of polymerization of the chains. This already indicates the complexity of the

thermodynamic properties of polymer solutions and their experimental investigation. For polymer networks the second term on the right-hand side vanishes, since N is assumed to tend to infinity.

Besides the influence on the miscibility, the Flory-Huggins interaction parameter χ has a significant impact on the conformation of the polymer chains in a solution. In dependence on the intermolecular interactions between the monomers of the polymer chain and the solvent molecules, the solvent quality is specified. If solvent-monomer interactions are energetically favored ($\varepsilon_{12} > \varepsilon_{22}$), usually over a wide range of temperature, the solvent is denoted as 'good solvent'. In this case the polymer chain in the solution can be described by a self-avoiding random walk. In order to avoid monomer-monomer contacts, the chains expand and with that maximize the number of solvent-monomer contacts. By the expansion of the polymer chain the number of possible rotational isomeric states is reduced. The concomitant decrease of entropy inhibits the complete expansion of the chain. Thus, polymers in a solution with good solvents experience excluded volume effects for the chain conformations since the solvation of the chains impedes the screening of these in opposite to the melt state. This leads to a scaling exponent of $\nu = 0.6$ for the end-to-end distance in Eq. 2.1. The mentioned excluded volume effects are progressively screened for increasing polymer concentrations in a good solvent [59]. In contrast, for 'bad' or 'poor solvents' the monomer-monomer interactions are energetically favored ($\varepsilon_{22} > \varepsilon_{12}$). The polymer coils shrink or collapse to reduce solvent contacts leading to a scaling exponent for the end-to-end distance of $\nu = 0.333$, as expected for packed spheres. This globular state is an especially important conformation for bio-polymers like proteins. If the interaction energies of the monomer-monomer and solvent-monomer contacts are indistinguishable ($\varepsilon_{22} = \varepsilon_{12}$), the solvent is referred to as 'athermal-solvent'. This is usually the case when polymer chains are diluted by their own monomer or by a comparably very short-chain polymer of the same species. Solvents which do not mix with a polymer are 'non-solvents'.

In the θ-state the repulsive excluded volume forces and the solvent-induced attractive monomer-monomer interactions cancel each other. The scaling exponent of the end-to-end distance is $\nu = 0.5$, since polymer chains have the same conformation as in an unperturbed melt. The equation of state of the solution is usually formulated in terms of the osmotic pressure π. For small polymer concentrations in interacting mixtures the virial expansion is used to quantify the influence of the interactions, whereas the virial

coefficients A_i denote the interactions between i molecules in the solution.

$$\frac{\pi}{RT} = \sum_{i=1}^{p} A_i \varphi^i = \frac{\varphi}{M} + A_2 \varphi^2 ... \tag{2.0}$$

The second virial coefficient A_2 describes the pairwise interactions (ε_{12}, ε_{11}, ε_{22}) and can be expressed by the Flory-Huggins interaction parameter χ. The higher order coefficients are usually neglected for polymers in solution.

$$A_2 = \frac{1}{2}\left(1 - 2\chi\right) \sim \frac{T - \theta}{T} \tag{2.0}$$

In the θ-state the χ-parameter has the characteristic value of 0.5 and thus the second virial coefficient, A_2, vanishes. For lower χ-values the solvent-monomer interactions dominate and for higher the monomer-monomer interactions. In general the interactions are temperature-dependent and therefore the θ-state is also defined by a certain temperature θ as indicated in Eq. 2.2. Polymer chains in a solution at the θ-temperature have the same properties as in the unperturbed melt state.

Polymer chains in a melt or a solution are no rigid objects with time-constant conformations. Due to thermal fluctuations the polymer chains show internal segmental relaxations and center-of-mass diffusion. The former permanently interchange between all possible conformations, and in the long time limit all accessible conformations are adopted. The dynamics of these conformational changes are dependent on temperature, length and spatial structure of the chains and their chemical composition. Thereby the mobility of the polymer chains is governed by the local chemical environment and restricted by topological constraints.

2.3. Polymer Dynamics

A frequently used and intuitively accessible method for the description of the chain dynamics in unentangled polymer melts is the Rouse model [60, 61]. The ideal Gaussian chain is replaced by a model chain where beads represent several monomers connected by hypothetical Hookian springs. Therefore the chain is subsumed in N_{R} equal segments, as shown in Figure 2.1, long enough to be described by Gaussian statistics. The distance between two beads is determined by the end-to-end distance l_{R} of the segments. The Hookian springs thus quantify the entropy elastic behavior of a part of the polymer chain. For small changes Δr of the end-to-end distance the counteracting entropic force

f_{el} is proportional to its origin and is expressed by the spring constant k. The latter is temperature-dependent due to its entropical origin.

$$f_{\mathrm{el}} = k\Delta r = -\frac{3k_B T}{l_{\mathrm{R}}^2}\Delta r \tag{2.0}$$

The mobility of the Rouse chain in a melt or a solution is dominated by viscous friction forces ζ of the beads with their environment. The combined motion of the beads connected by Hookian springs can be described mathematically by a differential equation of coupled linear oscillators in the over-damped limit. The position of the beads is denoted by $\vec{r}_n$.

$$\zeta\frac{\partial \vec{r}_n}{\partial t} = k(\vec{r}_{n+1} - 2\vec{r}_n + \vec{r}_{n-1}) + \vec{f}_s \tag{2.0}$$

The Langevin equation (Eq. 2.3) is valid for the inner segments of the chain. Thermic collisions with the environment are considered through the uncorrelated stochastic force $\vec{f}_s$ which quantifies the influence of Brownian motions of surrounding polymer chains or solvent molecules on the segment. The relaxation times τ_p of the individual modes p of the equation of motion (Eq. 2.3) are obtained by decomposition via a Fourier transformation.

$$\tau_p = \frac{\zeta N_{\mathrm{R}}^2 l_{\mathrm{R}}^2}{3\pi^2 k_B T}\frac{1}{p^2} \approx \tau_0\left(\frac{N_{\mathrm{R}}}{p}\right)^2 \tag{2.0}$$

The relaxation times of the individual modes enable the characterization of the time-dependent response of polymer chains to deformation on different time scales. Thereby τ_0 is the relaxation time of a single Rouse segment which is the shortest time occurring and it appears if the number of all unrelaxed modes is equal to the number of segments of the chain, $p = N_{\mathrm{R}}$. For times $t < \tau_0$ the polymer chain exclusively responses elastically to deformations, because the introduced tension is not yet compensated by relaxation. Lower-index modes comprise more Rouse segments and thus relax slower. The mode $p = 1$ corresponds to the relaxation of the end-to-end distance. It is the longest relaxation time of the Rouse chain and called 'Rouse time' τ_{R}. Above the Rouse time the stress due to deformation is completely released by relaxation. In this case the chain shows no longer an elastic response and performs just diffusive motions in the viscous melt. At times between the segmental relaxation time and the Rouse time, $\tau_0 < t < \tau_{\mathrm{R}}$, the chain has a complex visco-elastic behavior to deformations since some of the modes are not yet relaxed. The Rouse time τ_{R} is material-specific and corresponds to the relaxation time of the end-to-end vector of an extended linear chain to its most probable random coil conformation.

$$\tau_{\mathrm{R}} \sim N_{\mathrm{R}}^2 \sim N^2 \tag{2.0}$$

In general, Eq. 2.3 can be expressed by the above introduced scaling exponent ν, whereas the consideration of excluded volume effects leads to longer relaxation times [26].

$$\tau_{\mathrm{R}} \sim N^{1+2\nu} \tag{2.0}$$

In this treatment the relaxation is not restricted by topological constraints and is therefore referred to as free Rouse relaxation.

At a certain length the polymer chains start to entangle, which leads to topological restriction of the polymer dynamics. The influence of these entanglements is very clearly illustrated by the viscosity of a melt. In an unentangled melt the viscosity η scales linearly with the chain length, $\eta \sim N$, whereas in an entangled melt a $\eta \sim N^{3.4}$ dependence of the viscosity on the degree of polymerization is observed experimentally. The number of monomers between two entanglements, N_{e}, defines the entanglement length and is characteristic for each polymer material. The number of entanglements and with that of topological restrictions per chain is increasing by rising the molecular weight of the polymer. The probability of lateral movements is drastically reduced due to the entanglement points. The influence of the entanglements on the polymer dynamics and the center of mass diffusion is commonly described by the Edwards tube model [18], which reduces the polymer motions on a tube. The latter is defined by a field of topological constraints on the chain mobility created by the surrounding polymers in the melt. Along the contour of the tube, which is in itself described by a random walk, the polymer chain moves unrestrictedly, whereas motions perpendicular to the contour are restricted to the diameter d_{t} of the tube. The latter is defined by the rms end-to-end distance of a chain with N_{e} segments.

$$d_{\mathrm{t}} = \sqrt{\langle \vec{r}^{\,2}(N_{\mathrm{e}}) \rangle} \sim N_{\mathrm{e}}^{\nu} \tag{2.0}$$

The polymer chain in the tube is described by the so-called 'primitive path', which is defined by the shortest way to connect the two ends of a chain subject to topological constraints. Therefore the primitive path is defined by the end-to-end vectors of the individual segments with N_{e} monomers and a length equivalent to the tube diameter d_{t}. These N/N_{e} segments of the length d_{t} of the primitive path in the tube determine the contour length l_{t} of the chain as well as of the tube.

$$l_{\mathrm{t}} = l_{\mathrm{pr}} \approx d_{\mathrm{t}} \frac{N}{N_{\mathrm{e}}} \tag{2.0}$$

The dimension of the confining tube, i.e., length and diameter, are thus material specific values which are determined by chemical configuration of the polymer chain.

Due to the finite expansion of the tube, the chain mobility is still unrestricted at short time scales and behaves analogously to the free Rouse dynamics. At a certain time, the entanglement time τ_e, the chains feel the influence of their restricting environment. The entanglement time thus corresponds to the time a chain segment requires to diffuse $d_t/2$ and is proportional to N_e^2.

$$\tau_e \sim N_e^2 \tag{2.0}$$

A part of a polymer with N_e monomers shows the same characteristics as a polymer with N_e monomers due to the self-similarity of the chain conformation. Therefore, the entanglement time τ_e defines the number of monomers N_e, which are still relaxed by a free Rouse process. For times longer than the entanglement time the Rouse dynamics is restricted to one dimension. This can be interpreted as local reptation of the chain along the primitive path inside the confining tube [62]. The time required by the chain to move exactly once the contour length l_t is denoted as reptation-time or disentanglement-time τ_d.

$$\tau_d \sim N^3 \tag{2.0}$$

The disentanglement time τ_d exhibits the longest relaxation time in an entangled melt, since it characterizes motions of the whole polymer chain. During this motion the primitive chain diffuses out of the tube. Meanwhile the chain ends establish continuously a new tube in the melt, which has a random orientation with respect to the original tube. The time τ_d can thus be understood as time that is required by the chain to form a tube which is completely uncorrelated with the original one. At times larger than the disentanglement time, $t > \tau_d$, the entanglement induced topological restrictions are immaterial. The polymer chain conducts a free three-dimensional diffusive motion in the melt. The mean-square-displacement of the polymer chain's segments, $\langle (\vec{r}(0) - \vec{r}(t))^2 \rangle$, whereby $\vec{r}$ denotes the position of the segment, is thus analogous to free particles and is linearly proportional to time.

At shorter times than the disentanglement time the mean square displacement of the segments is slower as compared to free particles. This is related to the dominant influence of different relaxation mechanisms and topological restrictions on the chain dynamics on different time scales. Thereby two essential limitations on the mobility have to be considered. For the displacement of a particular segment also the adjacent segments need to move on due to the permanent chemical connection of the segments to a chain. Therefore r^2/b^2 segments of the chain are involved in a displacement of a segment of r^2. For diffusion times less than the Rouse time τ_R the mean-square-displacement of a
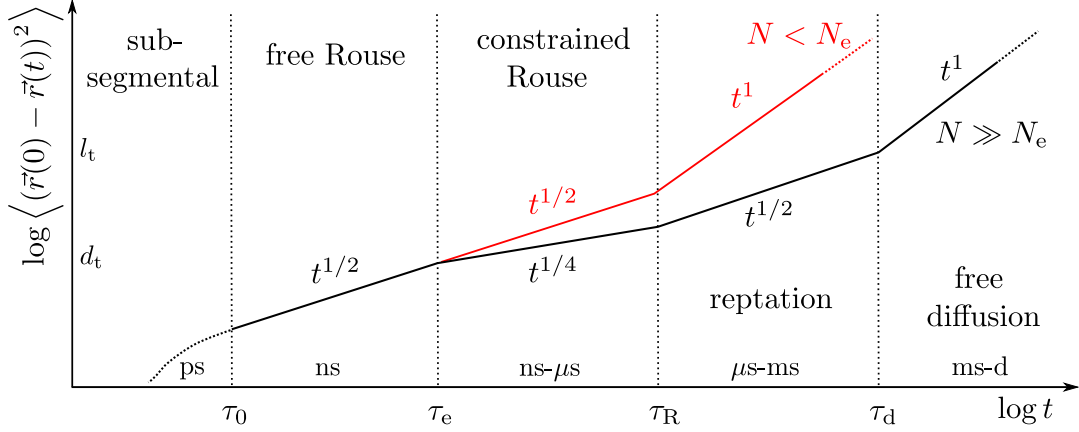
Fig. 2.3.: Dynamic regimes and crossover times predicted by the Rouse and tube model for the mean-square-displacement of chain segments in an unentangled (red line) and an entangled melt (black line).

segment is proportional to $t^{1/2}$. In entangled melts of long polymer chains ($N \gg N_e$) the impact of the present topological restrictions have to be considered additionally. For diffusion times larger than the entanglement time τ_e the motions of the segments are restricted to the random-walk profile of the confining tube. This leads to a $t^{1/2}$ dependence of the mean-square-displacement of the segments up to the disentanglement time τ_d. For diffusion times between the entanglement time and the Rouse time, $\tau_e \leq t \leq \tau_R$, the simultaneous existence of the two restrictions of the polymer mobility combine to a $t^{1/4}$ dependence of the mean-square-displacement. For times between $\tau_0 \leq t \leq \tau_e$ and $\tau_R \leq t \leq \tau_d$ the same time dependence of the mean-square-displacement is obtained but due to different reasons.

The previously discussed time and length scales and their effects on the diffusion respectively the mean-square-displacement of the individual segments of a polymer chain are summarized in Figure 2.3. Despite this simplified description of the polymer dynamics by models with rather strong assumptions, the Rouse model as well as the tube model show a surprisingly good agreement with a variety of experimental studies and simulations [63, 64]. The key strength of the two theories is in the universality of the description of polymer properties, which is achieved by the reduction to material-specific length and time scales.

2.4. Residual Order in Polymer Networks

The introduced time and length scales, used for the quantification of the mean-square-displacement of individual chain segments, can also be used for the investigation of the orientation of chain segments and its time-dependent evolution. The orientation of a vector along a chain segment, i.e., a Kuhn-segment, is regarded with respect to a reference direction, which is usually chosen parallel to the z-direction in a Cartesian coordinate system. The orientation of the segment is defined by the angle α between segment vector and reference direction. The latter is time dependent, $\alpha = \alpha(t)$, due to the thermal fluctuations of the chain segments. In a polymer melt all orientations of the segments have the same probability, as these are determined by a random walk. The probability to find a segment under the same orientation after a certain time t as it was observed at $t = 0$ is reflected by the time-dependent autocorrelation function $C_\alpha(t)$ [36].

$$C_\alpha(t) = \langle P_2(\alpha(0)) P_2(\alpha(t)) \rangle_{t, N_k, n} \tag{2.0}$$

The square brackets $\langle ... \rangle$ in Eq. 2.4 represent an average over the elapsed time t and the Kuhn segments N_k of all individual chains n. Thus the correlation function yields information about the average orientation of all segments whereas $P_2(\alpha)$ is the second-order Legendre polynomial.

$$P_2(\alpha(t)) = \frac{1}{2} \left(3 \cos^2 \alpha(t) - 1 \right) \tag{2.0}$$

The mobility of the polymer chains induced by thermal fluctuations leads to a continuous loss of orientation correlation of the segments in a melt. The decrease can roughly be subdivided into a strong decay of the autocorrelation function due to fast local and semi-local reorientation processes and a rather slight decay due to slow cooperative reorientation motions. On time scales on the order of $10^{-12} - 10^{-9}\,\mathrm{s}$, very fast, localized intra-monomeric processes, e.g., conformational isomerizations and vibrations, lead to a loss of orientation correlation of the individual monomers. These very fast processes describe reorientations of monomers within the statistical Kuhn segment. The time-dependent orientation of the latter, which is investigated by the autocorrelation function (Eq. 2.4), is therefore already partially pre-averaged.

The orientational change of a single Kuhn segment involves a certain number of adjacent segments due to the permanent chemical interconnections of the monomers. Large changes of the orientation are slower since more segments are incorporated in this process. The number of those is determined by the amount of segments which are already
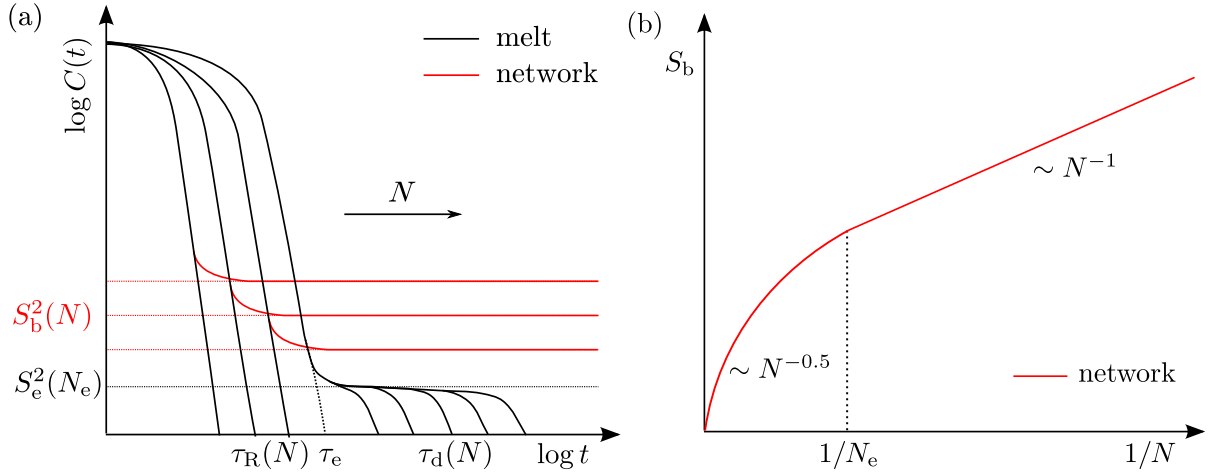
Fig. 2.4.: (a) Time-dependent orientation correlation function, $C_\alpha(t)$, in dependence of different chain lengths, N, and (b) scaling of the dynamic backbone order parameter, S_b, with respect to the number of monomers, N, between two crosslinks.

relaxed by the Rouse process. By progression of time the number of the latter increases enabling the involvement of larger chain parts in the reorientation motions of a segment. With that the decrease of the autocorrelation function $C_\alpha(t)$ is directly proportional to the number of relaxed Rouse modes at a time t, and thus dependent on the degree of polymerization N of the chain. These can diffuse freely in a melt of short polymers, $N < N_e$, above the Rouse time enabling complete whole-chain reorientations. This leads to a complete loss of orientation correlation and thus the polymer chains in the melt behave analogously to low-molecular liquids.

In melts of long polymer chains, $N \gg N_e$, the confinement of the polymer motion and reorientations to the tube defined by the surrounding polymer chains distinctly slows down the loss of correlation. This slow cooperative process conserves partially the orientation correlation for a certain time interval. These long-time correlation (ms-s) can be expressed by an order parameter S_e which quantifies the entanglement-induced average residual orientation of the polymer chain segments along the polymer backbone. The order parameter S_e is defined by the value of $C_\alpha(t)$ at the entanglement time τ_e [63, 64].

$$S_e^2 = C_\alpha(\tau_e) \sim \frac{1}{N_e^2} \tag{2.0}$$

The magnitude of the order parameter S_e in an entangled melt is thus characteristic for each polymer material. Nevertheless the reptation of the polymer chains along the confining tube leads to a further decrease of the orientation correlation. As soon as

the chain moved once along its contour length, whole chain reorientations are possible. Thus, the correlation is lost completely above the disentanglement time τ_d. The time interval of more or less slow decay of the autocorrelation function is dependent on the length of the polymer chain in the melt [64].

In polymer networks the individual chains are inter-connected permanently by physical and chemical cross-links, i.e., covalent bonds. Reptation and whole-chain reorientation processes are definitely not possible. Therefore, a certain amount of the orientation correlation is permanently conserved in the long time limit. The resulting plateau value of the time-dependent orientation auto-correlation function (Eq. 2.4) is used to define the dynamic backbone order parameter S_b of the polymer chains in the network.

$$S_\mathrm{b}^2 = \lim_{t \to \infty} C_\alpha(t) \tag{2.0}$$

The amount of this remaining average residual orientation is dependent on the number of statistical chain segments between two crosslinks and the spatial separation of the crosslinks.

The possibilities of reorientation are decreasing with less monomers between two crosslinks, since less neighboring monomer units can be involved into reorientation processes. Therefore the residual orientation of the chain segments increases with decreasing length of network strands. The order parameter of polymer networks with strand length $N < N_\mathrm{e}$ is thus proportional to the inverse number of monomers between two crosslinks. For longer strand lengths, $N > N_\mathrm{e}$, the order parameter reflects a combination of the chain length and the entanglement length, $S_\mathrm{b} \sim (NN_\mathrm{e})^{-1/2}$, due to a decorrelation of segmental order by the sliding motion of chain segments along the confining tube [65]. The dependence of the order parameter, S_b, on the number of monomers between two cross-links, N, is summarized in Figure 2.4

In a polymer network the distance between two crosslinks or topological constrains can be described by the above introduced Gaussian statistics for the mean squared end-to-end distance due to the self-similarity of the statistical chain conformations. The spatial separation of two crosslinks of a network strand with N monomers is equivalent to the end-to-end distance $\langle \vec{r}^2 \rangle_0$ of a polymer chain with the same number of monomers in a melt. The deformation of a network by external forces leads to a spatial separation of those, due to the permanent chemical connection of the chains by crosslinks. The latter is characterized by the end-to-end distance $\langle \vec{r}^2 \rangle_d$ of the deformed network strands. Thus, in networks with invariant, time-constant stress, such as equilibrium swollen networks, the number of accessible chain conformations is reduced permanently. This leads to an

higher residual orientational order of the chain segments. The order parameter S_b is thereby proportional to the ratio $r^2 = \langle \vec{r}^2 \rangle_d / \langle \vec{r}^2 \rangle_0$ of the end-to-end distances of the deformed to the unperturbed network strand. In combination with the above discussed $1/N$ dependence S_b can be expressed according to Eq. 2.4 for ideal chains, where the pre-factor was introduced due to the Gaussian statistics [66].

$$S_b = \frac{3}{5} \frac{r^2}{N} \tag{2.0}$$

The r^2-dependence clearly illustrates the sensitivity of the backbone order parameter, S_b, and with that of segmental orientation correlations on solvent effects, i.e., excluded volume effects of polymer chains in good solvents. Thus, the *thermodynamic properties* of polymers in solution are directly reflected by S_b .

Usually the motions of the segment vectors are not axial symmetric. Additionally, it is irrelevant for the description of the orientation at which direction the vector points along the segment. Therefore and to consider segmental motions with respect to all spatial axes, the orientation tensor S of the segments can be used as alternative description.

$$S_{\alpha\beta}^k = b_\alpha^k b_\beta^k - \frac{1}{3} \delta_{\alpha\beta} \tag{2.0}$$

b_α, b_β are the Cartesian coordinates ($\alpha, \beta = x, y, z$) of the vector $\vec{b}$ along an investigated segment k and $\delta_{\alpha\beta}$ is the Kronecker symbol. The order parameter S of a segment is obtained according to Eq. 2.4 by the time average of the respective orientation tensor.

$$S_b^2 = \left\langle \frac{3}{2} \mathrm{Tr} \left(S^k \right)^2 \right\rangle_t \tag{2.0}$$

The so-obtained 'tensor order parameter' S_b is a scalar measure for the strength of residual tensorial orientations. Thus, it is directly reflected by tensor orientation dependent interactions within the polymer chain as for example dipolar couplings between nuclear spins.

Atomic nuclei with a non-zero nuclear spin $\vec{I}$ have a magnetic moment $\vec{\mu}$. The latter is directly related to the spin via $\vec{\mu} = \gamma \vec{I}$ and originates a small magnetic field. The dipolar interaction results from the interaction of a nuclear spin with the magnetic field generated by other neighboring nuclear spins. Due to this direct mutual interaction in their associated magnetic fields the spins are coupled. The resulting dipolar coupling of the nuclei with each other can be described by a Hamilton operator (Eq. 2.4).

$$H_{\mathrm{DD}} = \sum_{i<j} \frac{\hbar \mu_0}{4\pi} \frac{\gamma_i \gamma_j}{r_{ij}^3} \left(\vec{I}_i \cdot \vec{I}_j - 3 \frac{(\vec{I}_i \cdot \vec{r}_{ij})(\vec{I}_i \cdot \vec{r}_{ij})}{r_{ij}^2} \right) = \sum_{i \neq j} \vec{I}_i \vec{\vec{D}}^{ij} \vec{I}_j \tag{2.0}$$

The direct through-space coupling of the spins, which can be inter- and intramolecular, is dependent on their respective gyromagnetic ratio, γ_i, as well as on the internuclear distance, r_{ij}, of the center of the nuclei. The coupling tensor, D^{ij}, reflects the dependence of the interaction energy on the orientation of the spins with respect to each other. The second rank tensor is traceless and symmetric, meaning that no dipolar coupling exists in the limit of fast isotropic motion, and the interaction between two spins is symmetric, respectively.

The molecular parameters of a spin-pair, $\vec{I}_i$ and $\vec{I}_j$, are summarized by the dipole-dipole coupling constant, ν_{D},

$$\nu_{\mathrm{D}} = \frac{\hbar\mu_0}{4\pi}\frac{\gamma_i\gamma_j}{r_{ij}}, \tag{2.0}$$

which is a measure for the strength of the dipolar coupling and thus for the distance between spins. The latter is constant and known when the nuclei are fixed inside one molecule. Thus, the experimental estimation of the coupling constant and its orientation dependence in solids enables the experimental determination of the local and global spatial structure of molecules. The typical magnitude of the coupling constant is in the order of several kHz for protons.

In strong static magnetic fields, B_0, as used in NMR experiments, the nuclear spins are aligned parallel or anti-parallel with respect to the direction of the magnetic field. Speaking quantum mechanically, the degeneration of the spin eigen-states regarding the magnetic quantum number m, $m = -I, ..., I$, is abolished yielding a well-defined quantized projection of the spin on the axis specified by the direction of the magnetic field. The latter is usually parallel to the z-direction leading to $2I+1$ states of different energy E_m, $E_m = -\gamma m B_0$, of the z-component, I_z, of the spin. The population of the spin states is defined by a Boltzmann distribution in thermal equilibrium and can be manipulated by resonant irradiation of a magnetic radio frequency (rf) field perpendicular to B_0, inducing transitions between the particular states. In NMR experiments the response of the spin system on the perturbation by these rf-pulses is detected in a time-resolved fashion. Therefore a variety of specifically composed sequences of rf-pulses of different duration can be applied for the selective determination of molecular properties.

The Zeeman interaction is in general several orders of magnitude stronger as compared to the dipolar interaction, so the secular approximation applies for the corresponding

dipolar Hamiltonian, H_{DD}.

$$
\begin{aligned}
H_{\mathrm{DD}} &= \nu_{\mathrm{D}} \frac{1}{2} \left(3 \cos \theta - 1\right) \left(3 I_{1z} I_{2z} - \vec{I_1} \cdot \vec{I_2}\right) \\
&= \nu_{\mathrm{D}} \frac{1}{2} \left(3 \cos \theta - 1\right) \left(2 I_{1z} I_{2z} - \frac{1}{2} \left(I_1^+ I_2^- + I_1^- I_2^+\right)\right)
\end{aligned}
\tag{2.0}
$$

This secular form considers the parts of the dipolar Hamiltonian of a homo-nuclear spin-pair, I_1 and I_2, which commute with the Hamiltonian of the Zeeman interaction [67]. I^+ and I^- represent the raising and lowering spin operators, respectively, and the angle θ describes the orientation of the internuclear vector, r_{12}, relative to the static magnetic field, B_0.

The local magnetic field, B_{loc}, of a dipolar coupled spin is determined by the static magnetic field, B_0, and the magnetic field generated by the spins the spin is coupled to. According to the secular approximation the contributions of the latter to the local magnetic field are additive and thus a spin can have different energy states depending on which state the nearby spins have. This is expressed by a shift of the resonance frequency in comparison to an uncoupled spin and leads to a splitting of the NMR signal. The latter is dependent on the magnitude of the dipolar coupling and thus on the distance of the spins, r_{12}, and the orientation of the internuclear vector with respect to the applied static magnetic field. Additionally, in powdered solids all orientations are represented and have the same probability. Thus, the combination of multi-spin couplings and the orientation-dependence of the dipolar coupling lead to complex NMR spectra with usually very broad lines requiring specific experiments for the investigation of certain molecular aspects.

For an isolated pair of equal spin half nuclei only one dipolar coupling is present. The spin system has three states of different energy corresponding to the combination of the spin eigen-states among the two nuclei and their mutual dipolar interaction. This leads to two resonance frequencies which are shifted equal in magnitude positively and negatively with respect to the resonance frequency in absence of the dipolar interaction, ν_0.

$$
\nu = \nu_0 \pm \frac{3}{4} \frac{\hbar \mu_0}{4\pi} \frac{\gamma^2}{r_{ij}^3} (3 \cos \theta - 1)
\tag{2.0}
$$

In a powdered sample the orientation dependence of the dipolar interaction (Eq. 2.4) leads to the characteristic Pake doublet shown in Figure 2.5a . The maxima correspond to an inter-nuclear vector perpendicular to the static magnetic field which has more possible realizations in comparison to the parallel orientation. The separation between the maxima of the Pake doublet is $3/2 \nu_D$.
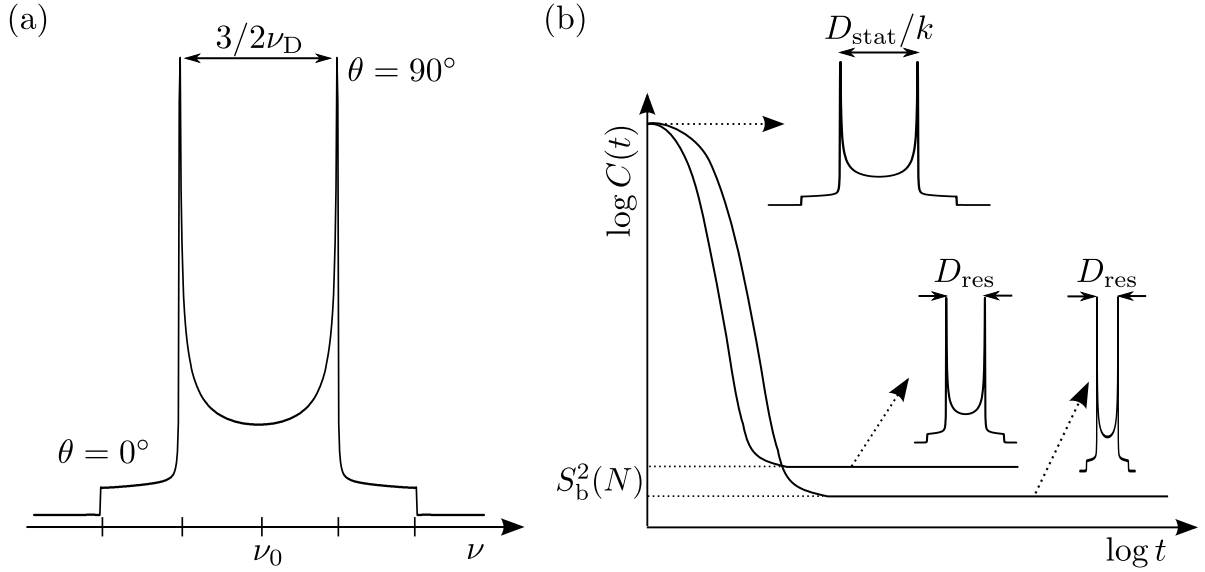
Fig. 2.5.: (a) Pake-doublet of a powdered sample of an isolated pair of equal spin half nuclei, and (b) time-dependent orientation autocorrelation function with corresponding partially motion-averaged Pake-doublets.

In isotropic liquids the fast Brownian motions rapidly change molecule orientations. These motions are fast on the timescale of NMR experiments and therefore the dipolar couplings are averaged out completely. In solids, i.e., crystals, the positions of the nuclei are fixed in space leading to a static time-constant coupling constant, D_{stat}. Polymer networks behave partially solid-like. Topological restrictions, i.e., entanglements and permanent chemical crosslinks, lead to anisotropic motions of the individual chain segments of the network strands as discussed above. Therefore, the internuclear vector of dipolar coupled nuclei attached on the backbone of the polymer chain cannot adopt all orientations with respect to the static magnetic field. Thus, their dipolar couplings are not averaged out completely and some persist. The magnitude of these residual dipolar couplings, D_{res}, directly reflects the motion averaging of the dipolar coupling constant by conformational changes of network strands as shown in Figure 2.5b. Thus, the ratio of the residual dipolar coupling and its static counterpart is an estimate of the dynamic backbone tensor order parameter, S_{b}, of the segments of a polymer chain.

$$S_{\mathrm{b}} = k\frac{D_{\mathrm{res}}}{D_{\mathrm{stat}}} = \frac{3}{5}\frac{r^2}{N} \tag{2.0}$$

Eq. 2.4 represents the connection between the experimental accessible quantity by NMR, the residual dipolar coupling constant, D_{res}, and the *structure* of polymer networks, i.e.,

the network strand length, N, and the *thermodynamic properties* as reflected by r^2. The static dipolar coupling, D_{stat}, characterizes the strength of the dipolar coupling in a network without thermal motions and is usually obtained by spin-evolution simulations of the spin system. The pre-factor k in Eq. 2.4 takes into account that the coupling constant can also be pre-averaged by properties of the local intra-segmental spin system which are not related to conformational changes of the polymer chains, e.g., fast rotations of methyl groups attached to the polymer backbone [43, 44].

2.5. ^{1}H Double-Quantum NMR

A reliable quantitative method for the determination of homonuclear residual dipolar couplings, D_{res}, in polymer networks is static ^{1}H multiple-quantum (MQ) NMR [43]. The experiment is based on the excitation of coherences between two or more dipolar coupled spins. Coherences between spin states that differ by more than one unit in the magnetic quantum number are called MQ coherences. These produce no magnetization and thus have to be detected indirectly. The typical stages of a static MQ experiment are depicted in Figure 2.6a. In the first part MQ coherences are excited. The second part reconverts the excited MQ coherences into detectable magnetization. In the acquisition period the intensity related to the different MQ coherences is detected selectively by appropriate phase-cycling [43].

The improved Baum-Pines MQ pulse sequence shown in Figure 2.6b is characterized by a pure average dipolar double-quantum hamiltonian which excites all even-order MQ coherences [68]. Thus the spin system is assumed to evolve according to this hamiltonian and the spins become correlated. The correlation is dependent on the time the spin system evolves with respect to the hamiltonian and on the strength of the dipolar coupling, D_{res}. The intensity related to different MQ coherences is detected as function of the evolution time, τ_{DQ}, by increasing the delays between the pulses. The applied 4-step phase-cycle leads to two signal functions, i.e., a double-quantum (DQ) build-up curve $I_{\mathrm{DQ}}(\tau_{\mathrm{DQ}})$ and a reference intensity decay curve $I_{\mathrm{ref}}(\tau_{\mathrm{DQ}})$ as shown in Figure 2.5a. The double-quantum intensity, I_{DQ}, comprises contributions of all $4n+2$ quantum order. However, the initial slope of the build-up function is dominated by DQ coherences, as demonstrated by spin counting experiments and simulations [43, 68]. The higher quantum orders give rise to minor contributions at longer evolution times, τ_{DQ}. This justifies the nomenclature 'double-quantum' (DQ) used throughout this work. The reference intensity, I_{ref}, comprises contributions from all $4n$ quantum orders and of all signals
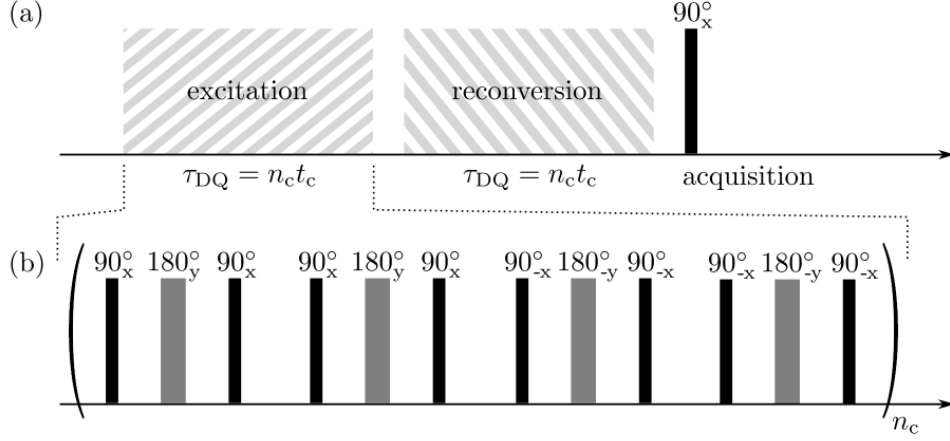
Fig. 2.6.: (a) Schematic representation of a multi-quantum experiment, and (b) particular pulse sequence used for multi-quantum excitation and reconversion [43].

that do not have evolved into MQ coherences, i.e., the signal of non-coupled spins as present in isotropically mobile molecules. In polymer networks the latter represent the contribution of elastically ineffective defects to the signal which is characterized by a rather slow exponential decay in comparison to coupled network components [69]. This enables a reliable quantitative identification of networks defects.

The sum intensity, $I_{\sum MQ} = I_{ref} + I_{DQ}$, which is a fully dipolar refocused intensity, decays due to incoherent processes, i.e., molecular motions on the time scale of the experiment, and imperfections related to the pulse sequence [43]. The DQ intensity as well as the reference intensity after substraction of the non-coupled contribution are subject to the same relaxation effects. The effect of such apparent relaxations can be removed by a normalization of the double-quantum build-up curve. This is performed through a point by point division of the DQ build-up function, I_{DQ}, by the sum relaxation function, $I_{\sum MQ}$. The normalized double-quantum intensity, I_{nDQ}, is dominated by pure dipolar spin-pair interactions that are only related to the network structure after substraction of the contribution of the isotropically mobile network components.

$$I_{nDQ} = \frac{I_{DQ}}{I_{\sum MQ} - \text{defects}} = \frac{I_{DQ}}{I_{DQ} + I_{ref} - \text{defects}} \qquad (2.0)$$

The resulting normalized double-quantum build-up function is in very good approximation temperature-independent (see Figure 2.7b) and must reach a relative amplitude of 0.5 in the long-time limit after a proper substraction of the contribution of non-coupled network defects (Figure 2.7a) since the DQ intensity, I_{DQ}, contains only half of the excited quantum orders.
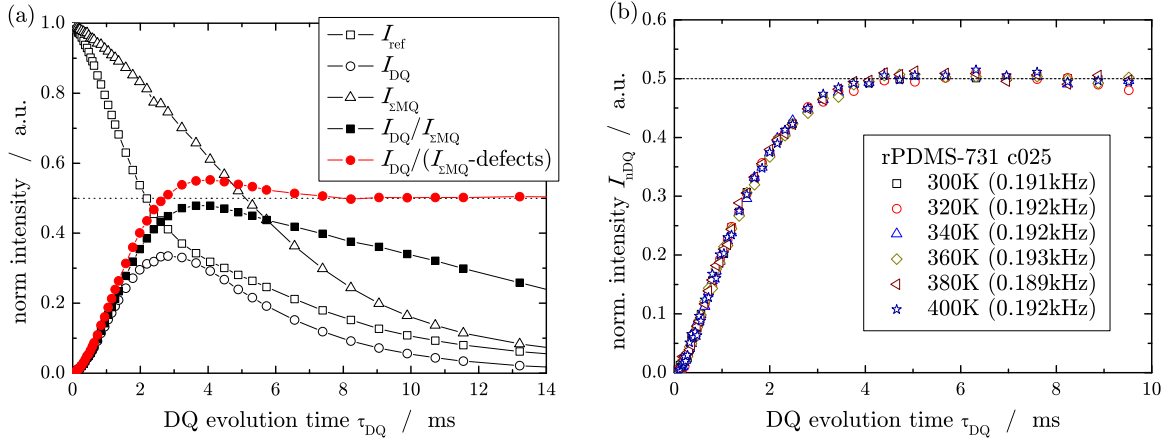
Fig. 2.7.: (a) Experimental DQ, reference and sum intensities as well as normalized DQ intensity before and after substraction of defect contribution, and (b) nDQ build-up curves, I_{nDQ}, at different temperatures.

Normalized double-quantum (nDQ) build-up curves are independent of NMR relevant relaxation effects and comprise the *structure* information about polymer networks. The latter are obtained in the form of residual dipolar couplings, D_{res}, by fitting the build-up curve to appropriate functions. The commonly used fitting function (Eq. 2.5) based on a static second-moment approximation yields an apparent average D_{res} and is limited to the initial part of the build-up curve [36].

$$I_{\mathrm{nDQ}}(D_{\mathrm{res}}, \tau_{\mathrm{DQ}}) = 0.5 \left(1 - \exp\left\{-\tfrac{2}{5}D_{\mathrm{res}}^2 \tau_{\mathrm{DQ}}^2\right\}\right) \tag{2.0}$$

However, the anisotropy of the segmental fluctuations of polymer chains fixed at their ends by permanent chemical crosslinks is determined by the spatial separation of the crosslinks and with that dependent on the length of the network strands. Usually the latter have a certain length distribution and thus a measured build-up curve is a superposition of all residual dipolar spin-pair couplings of the investigated network sample. For a proper extraction of D_{res} and especially its distribution, which is encoded in the build-up curve, numerical methods have to be applied since the conventional fitting functions are not appropriate. For that purpose fast Tikhonov regularization (*ftikreg*) is used [70, 71]. The program employs a stable numerical variation algorithm for the solution of inverse Fredholm integral equations in dependence of an error parameter quantifying the noise of experimental data. The impact of the error parameter on the calculated distributions was studied in detail in the present work and a consistent criterion for the estimation of the most reliable distribution could be identified leading to an improved

and timesaving protocol for the evaluation nDQ build-up curves by *ftikreg* [49].

The fitting function stated in Eq. 2.5 fails in the description of the overall shape of build-up curves especially in the case of very homogeneous or heterogenous networks. Furthermore, as Eq. 2.5 is used as kernel function for *ftikreg*, the above mentioned fitting limit has a crucial influence on the precision of the calculated coupling constant distributions, since contributions of the build-up curve beyond the fitting limit are disregarded. Therefore, a new generic build-up function (Eq. 2.5) was designed during this work using results of samples well-described by Eq. 2.5 for the calibration of the exponent and the numerical factors [49].

$$I_{\mathrm{nDQ}}(D_{\mathrm{res}}, \tau_{\mathrm{DQ}}) = 0.5 \left(1 - \exp \left\{ - (0.378 D_{\mathrm{res}} \tau_{\mathrm{DQ}})^{1.5} \right\} \right) \times \cos[0.583 D_{\mathrm{res}} \tau_{\mathrm{DQ}}] \qquad (2.0)$$

The (A-l) function (Eq. 2.5) describes the whole shape of build-up curves properly and thus the fitting limit could be extended up their end. Using Eq. 2.5 as kernel function in *ftikreg* the build-up curves of different monomodal natural rubber (NR) and PDMS network samples systematically mixed in different weight fractions were investigated. The determined coupling constant distributions are in very good agreement with weighted superpositions of the respective monomodal distributions and the weight fractions of the mixed components could be estimated within deviations of 1-2 % even for mixtures with weight fractions of 0.95 of one component despite the already strong domination of the build-up curve by that component [49]. The results demonstrate that the improved protocol for *ftikreg* in combination with the new fitting function represents an advance for the reliability and accuracy of coupling constant distributions [72, 45]. This is rather important for the further investigation of the latter in dry and swollen networks where the introduced approach is used as standard procedure for the evaluation of DQ NMR experiments.

3. Results and Discussion

In this chapter the main results of the present work will be summarized. Therefore, some of the important conclusions of the published and unpublished results are shown and discussed. The first parts include the published articles of this cumulative thesis. The last two sections present results of the investigation of end-linked polymer networks which were cross-linked in bulk, and in concentrated and semi-dilute solutions and are not yet published. This study focuses especially on the influence of the polymer volume fraction during the network *formation* on the *structure* of the resulting networks. In the last part, results of partial-swelling studies of end- and randomly linked PDMS networks are presented. This is the linkage between the investigated *structure* of dry polymer networks and the *thermodynamic properties* of polymer networks in the equilibrium swollen state.

The aim of this work was the investigation of the *structure* and *thermodynamic properties* of polymer networks in order to test and validate theoretical models for the evaluation of readily available routine experiments used for the characterization of polymer networks and to improve their understanding. Therefore PDMS networks with systematically changed properties were investigated by ^{1}H double-quantum (DQ) low-field NMR and by equilibrium swelling experiments. The sample characterization and preparation as well as experimental details of the swelling experiments are explained in the Appendix.

In section 3.1 an improved approach for the evaluation double-quantum build-up curves, which is already discussed in section 2.5, is presented. In section 3.2 the cross-link density of PDMS networks is investigated by DQ NMR and swelling experiments. The evaluation of swelling experiments in terms of the Flory-Rehner model is strongly dependent on the model used to consider elastic contribution. In this study the phantom model is used. The precisely determined *structure* of the networks, i.e., the defect fraction and the weight average functionality of the cross-links, is considered in different ways and compared to absolute-value results of Miller-Macosko calculations which are model independent. The comparison of the results demonstrates the importance of a

proper consideration of the actual network *structure* and constitutes a validity test of the phantom model.

In section 3.3 the applicability and validity of the classical Flory-Rehner model for network swelling is investigated. Therefore, equilibrium swelling experiments and DQ NMR measurements on swollen samples are performed at various conditions yielding two directly measurable quantities, which are compared to predictions of the Flory-Rehner model. The comparison shows that the Flory-Rehner model is well applicable in the range of poor solvents to slightly above the θ-condition. In the good solvent regime the Flory-Rehner model fails as revealed by the deviation of experimental results and theoretical predictions. This demonstrates that excluded volume effects on the chain statistics have to be included in Flory-Rehner model for the correct prediction of order parameters as obtained by DQ NMR.

Section 3.4 investigates the cross-link kinetics of end-functionalized polymers in presence of solvent by a Pt-catalyzed hydrosilylation reaction in order to obtained detailed information about the cross-link mechanism. Despite this is an often used approach to cross-link polymers which has been studied intensively just little detailed knowledge about the mechanistic details of the network formation is available and different reaction orders are reported for the hydrosilylation. The presented results reveal multi-stage reaction kinetics, which could be related to a different reactivity of the cross-linker molecules in dependence of the number of already reacted functional sites. The different cross-linker species show first-order reaction kinetics whereas the different population of those reasons the observed complex overall kinetics.

At this point some of the results presented in the following publications are discussed in more detail and supporting information are given. Polymer networks are complex constructs. The length of network strands, their distribution and defects strongly influence the *structure* of polymer networks and thus their mechanical and *thermodynamic properties* [73]. Network defects, i.e., dangling chains, loops, etc., usually arise during the *formation* of polymer networks and do not contribute to the elastic response on deformations. This leads directly to a reduction of the number of elastically effective polymer chains per unit volume. Dangling chains are only fixed at one end permanently to the infinite gel and therefore are isotropically mobile as far as they are shorter than the entanglement length N_e. In NMR experiments, i.e., Hahn echo and DQ NMR, this is reflected by a rather different relaxation behavior in comparison to the elastically active network fraction. The signal of the latter decays much faster while defects show a slow exponential decay [69] enabling a quantitative estimation of the defect fraction.
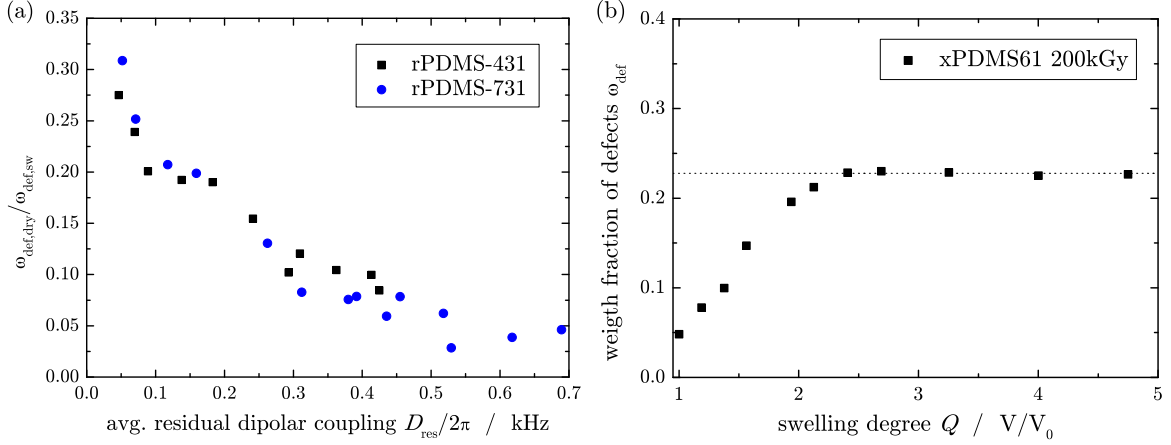
Fig. 3.1.: (a) Dependence of the fraction of identified defects in dry samples with respect to their amount determined in the corresponding equilibrium swollen samples on the average residual dipolar coupling constant, D_{res}, and (b) estimation of defect fraction, ω_{def}, at different degrees of swelling.

In randomly cross-linked polymer networks the statistic distribution of cross-links along the backbone of the polymer chains leads to a certain fraction dangling chain defects in dependence on the length of the pre-polymers and the number of cross-links per chain. The investigation of randomly cross-linked PDMS networks (rPDMS-431 and rPDMS-731) in dry state and swollen to equilibrium by DQ NMR shows that the defect fractions, $\omega_{\text{def,dry}}$ and $\omega_{\text{def,sw}}$, respectively, increase continuously with less used amount of cross-linker during the preparation of the samples. However, the defect fractions determined in dry state are rather low whereas the defect fractions determined in the corresponding swollen networks are considerably higher. This behavior was observed for all networks investigated in this work including natural rubber samples not reported here [45] and can be related to topological restrictions or packing effects in dry networks which inhibit fast isotropic motions of defects and thus a fraction of the latter is observed as elastically effective on the time scale of the NMR experiment. This assumption is strongly supported by the increasing relative fraction of the identified defects in dry state with respect to the corresponding swollen networks for samples having a lower D_{res}, which is a measure for the density of topological constraints, as shown in Figure 3.1a. By swelling the restrictions are released and distinctly higher defect fractions are observed. The latter are in very good agreement with results obtained by Miller-Macosko calculations [74] demonstrating that in dry state the defect fraction in distinctly under-

estimated. This and the saturation of the determined defect fraction at swelling degrees below equilibrium (Figure 3.1b) demonstrates that DQ NMR experiments on equilibrium swollen samples allow for a reliable and precise estimation of the defect fraction in polymer networks.

Network defects also essentially influence the functionality, f, of cross-links. The latter is reduced directly by the number of elastically ineffective network chains attached on a cross-link. Thus, according to the phantom model [15, 16], fluctuations of cross-links around their average position in the network are less constrained. The results of Miller-Macosko calculations show that the weight average functionality, f_{wa}, of the investigated randomly cross-linked PDMS networks varies in between 3.6 and 2.5. These values are significantly smaller than the expected functionality of 4 and are strongly dependent on the used amount of cross-linker.

The molecular weight of polymer chains between two cross-links, M_{c}, is often determined by swelling of networks with suitable solvents using the Flory-Rehner (FR) equation [48, 75]. At the equilibrium degree of swelling, Q_{eq}, the gain in free energy upon mixing of the components as described by the Flory-Huggins equation is compensated completely by the increase of the conformational entropy due to the network dilation. Thus, the length of network strands and the network *structure* are directly reflected by the solvent uptake of networks. The latter is characterized by the volume fraction of rubber, φ_{p}, in equilibrium swollen samples which can be estimated by simple gravimetric measurements. For the evaluation of swelling experiments performed on the rPDMS samples according the phantom model the weight average functionality, f_{wa}, and network defects were considered. Thereby, the precisely determined defect fraction, ω_{def}, was used to estimate volume fraction of elastically active chains in the swollen state, $\varphi_{\mathrm{p,el}}$, in order to correct the elastic contribution to the FR equation.

$$\varphi_{\mathrm{p,el}} = (1 - \omega_{\mathrm{def}})\varphi_{\mathrm{p}} \tag{3.0}$$

The comparison of the so-obtained molecular weights by swelling to results of absolute-value Miller-Macosko calculations yields nearby the expected linear correlation between the two methods. In contrast, the neglection of f_{wa} and/or $\varphi_{\mathrm{p,el}}$ during the analyzation of swelling experiments leads to distinctly non-linear correlations. This demonstrates that the network *structure* has to be accounted properly for a reliable evaluation of swelling experiments. Unfortunately, especially the functionality of cross-links is hardly accessible experimentally. The comparison of these two methods to results obtained by DQ-NMR evaluated according to Eq. 3 shows again a close-to linear correlation of the

determined molecular weights.

$$M_c = \frac{1266\,\text{Hz}}{D_{\text{res}}/2\pi} \frac{f-2}{f}\,\text{kg/mol} \tag{3.0}$$

This again shows that the results are strongly dependent on the weight average functionality of the cross-links in the network and constitutes a validity test of the phantom model since the results of the Miller-Macosko calculations are independent on model considerations for the fluctuations of network chains. Thereby, quantitative deviations of the results obtained by the different approaches can be attributed mainly to shortcomings of the underlying model for the calculation of the constant of proportionality in Eq. 3 and of the Flory-Rehner model for the evaluation of swelling experiments, in particular ambiguities related to the Flory-Huggins interaction parameter and its volume fraction-dependence.

The ^{1}H DQ NMR experiment is not only sensitive to the *structure* of polymer networks but also to their *thermodynamic properties*. These are directly reflected by a change of the segmental orientation correlations as characterized by the backbone order parameter, S_b, upon network deformation and polymer-solvent interactions, i.e., excluded volume effects, in swelling experiments since the length of the network strands remains invariant. The classical Flory-Rehner treatment predicts a linear relation of the order parameter to the inverse equilibrium swelling degree in the good-solvent limit, $S_b \sim Q_{\text{eq}}^{-1}$. By consideration of the impact of excluded volume effects on the chain statistics a dependence according 3 is obtained by FR theory [51].

$$S_b(Q_{\text{eq}}) \sim D_{\text{res}}(Q_{\text{eq}}) \sim Q_{\text{eq}}^{-3/2} \tag{3.0}$$

The residual dipolar coupling constants, D_{res}, determined in a series of randomly- and end-link PDMS networks swollen to equilibrium in a good solvent are in excellent agreement with the predicted scaling behavior of D_{res} on Q_{eq} [51]. Additionally, the good-solvent limit scaling exponent is confirmed by an extensive study of the residual dipolar coupling constant of networks swollen to equilibrium in dependence of the solvent quality ranging from the bad solvent up to the good solvent regime. The so-obtained apparent scaling exponents converge towards the predicted exponent of $-3/2$ with increasing solvent quality. This demonstrates the influence of the solvent condition on the orientation statistics of chain segments in a swollen network and shows that the Flory-Rehner model only provides reliable predictions for the order parameter in the good solvent case when excluded volume effects are taken into account.

The Flory-Huggins solution theory which describes the *thermodynamic properties* of

polymers in a solution, and thus is the basis for the evaluation of swelling experiments in terms of the Flory-Rehner model, features several theoretical limitations [76]. Besides the above discussed negligence of energetically (un)favored arrangements of solvent molecules and polymer segments in a solution, the theory is only applicable to sufficiently concentrated solutions. This is directly related to the emergence of concentration fluctuations of polymers in a solution which increase at lower polymer volume fractions, φ_p, and thus corrupt the mean-field approach of the FH theory. In that way the latter is restricted to the investigation of networks with low swelling degrees having comparable volume fractions as concentrated solutions. In order to test this limitation, temperature-dependent equilibrium swelling experiments of randomly- and end-linked PDMS networks for various solvents ranging from the bad solvent regime over theta solvents up to good solvent regime were performed. The results, which are evaluated in terms of a novel construction of solvent-independent swelling master curves, were fitted by the FR equation showing a rather good agreement when the fit is limited to low swelling degrees obtained in the range of poor solvents to slightly above the θ-condition. For higher swelling-degrees obtained in the good-solvent regime the fit fails completely. This confirms the limitation of the FH theory to concentrated polymer solutions and displays again the importance of the consideration of polymer-solvent interactions in terms of excluded volume effects for a correct description of the *thermodynamic properties* of polymers in good solvents.

3.1. Precise dipolar coupling constant distribution analysis in proton multiple-quantum NMR of elastomers

The article presents an improved approach for the evaluation of normalized ^{1}H double-quantum (nDQ) build-up data. Conventional fitting methods for nDQ build-up data based on a static second-moment approximation are limited to the initial part of nDQ build-up data. This further only works for the rare case of very homogeneous networks. Therefore, a new generic build-up function (A-l function) is introduced, which allows to extend the fitting limit up to the end of the plateau of nDQ build-up data enabling a more accurate description of the build-up data of very homogeneous polymer networks and superpositions. The new A-l function is implemented as kernel function in fast Tikhonov regularization (*ftikreg*) which employs an improved protocol for a precise determination of residual dipolar coupling distributions.

The applicability of the new approach for the characterization of scientifically and practically important inhomogeneous network *structures* is tested and validated on examples of different bimodal networks. Therefore, a set of bimodal nDQ build-up meta-data, comprising simple superpositions of monomodal build-up curves of natural-rubber networks with different cross-link density, and silicone networks as well as co-cross-linked PDMS model networks are investigated. The shown results prove a precise characterization of the mass fractions of the components and thus the potential modality of networks. Especially for networks where the nDQ build-up is dominated by a highly coupled component, and thus the more lowly coupled component is first obvious beyond the fitting limit of the conventional fitting functions, the extended fitting limit of the (A-l) function represents a rather significant improvement for the evaluation of the coupling constant distribution.

The introduced new analysis method of nDQ build-up curves was used throughout the present thesis for the evaluation of all performed ^{1}H DQ measurements.

Authors Contributions. W.C. designed and implemented the new *ftikreg* fitting protocol. J.L.V. and G.D.G. prepared the NR and PDMS model networks, respectively. W.C. performed the measurements and analyzed the data. W.C. wrote the manuscript, assisted K.S..

Precise dipolar coupling constant distribution analysis in proton multiple-quantum NMR of elastomers

Walter Chassé,[1,a)] Juan López Valentín,[2] Geoffrey D. Genesky,[3] Claude Cohen,[3] and Kay Saalwächter[1,b)]

[1]*Institut für Physik – NMR, Martin-Luther-Universität Halle-Wittenberg, Betty-Heimann-Str. 7, D-06120 Halle, Germany*
[2]*Institute of Polymer Science and Technology (CSIC), C/ Juan de la Cierva 3, 28006 Madrid, Spain*
[3]*School of Chemical and Biomolecular Engineering, Olin Hall, Cornell University, Ithaca, New York 14853, USA*

In this work we present an improved approach for the analysis of ^{1}H double-quantum nuclear magnetic resonance build-up data, mainly for the determination of residual dipolar coupling constants and distributions thereof in polymer gels and elastomers, yielding information on crosslink density and potential spatial inhomogeneities. We introduce a new generic build-up function, for use as component fitting function in linear superpositions, or as kernel function in fast Tikhonov regularization (*ftikreg*). As opposed to the previously used inverted Gaussian build-up function based on a second-moment approximation, this method yields faithful coupling constant distributions, as limitations on the fitting limit are now lifted. A robust method for the proper estimation of the error parameter used for the regularization is established, and the approach is demonstrated for different inhomogeneous elastomers with coupling constant distributions. © *2011 American Institute of Physics*. [doi:10.1063/1.3534856]

I. INTRODUCTION

The precise analysis of elastomer or gel components and microstructure is an important challenge for polymer physics, as this information is key to understanding their intriguing properties in applications as performance materials, separation membranes, and many more. In the recent years, simple time-domain ^{1}H solid-state NMR, possibly performed on simple low-field instruments, was demonstrated to be a powerful and versatile tool to investigate quantitatively the crosslink density of polymer networks.[1–8] The NMR effect is due to the restrictions to fast segmental fluctuations posed by the crosslinks and other topological constraints such as entanglements, leading to nonisotropic orientation fluctuations. Therefore, intrasegmental dipole–dipole couplings are not averaged out completely and residual dipolar couplings (RDC) persist, which are directly related to the crosslink density and thus the network structure.[9–11] Residual dipolar couplings are most simply reflected in the T_2 relaxation behavior,[9] and despite the ambiguities related to the unknown shape of Hahn-echo decay curves,[12] attempts have been made to extract even RDC distributions and, thus, information on crosslink density inhomogeneities.[13]

Reliable numerical approaches to the determination of dipolar coupling constant distributions have for instance been reported for the case of heteronuclear couplings as obtained from the REDOR (rotational-echo double-resonance) NMR experiment,[14,15] or for the case of electron–electron dipolar couplings from pulsed-electron paramagnetic resonance data.[16,17] These situations are favorable in that experimental data are composed of a sum of relaxation-free single-pair responses, which follow the theoretical prediction more or less exactly. The situation is less favorable for homonuclear dipolar couplings in systems with abundant spins, since the response of such a multispin system is homogeneous in nature and cannot be treated by analytical theory. Our previous work, as reviewed in Ref. 5, has demonstrated that static ^{1}H multiple-quantum (MQ) NMR spectroscopy is the tool of choice to quantitatively measure homonuclear RDCs and their distribution in soft materials.[3] Up to now, we have used a generic yet rather approximate single-RDC Gaussian signal function based upon a second-moment approximation. Here, we present a substantially improved approach based on a new generic signal function and a reliable protocol for data analysis, yielding reliable RDC distributions.

The clear advantage of the MQ NMR experiment arises from the acquisition of two different sets of data, i.e., a double-quantum (DQ) build-up curve $I_{DQ}(\tau_{DQ})$ and a reference intensity decay curve $I_{ref}(\tau_{DQ})$, see Fig. 1. The experiment is based upon a pure DQ Hamiltonian which generally excites all even quantum orders (thus the nomenclature MQ NMR). However, the initial rise of the build-up function is dominated by DQ coherences (thus its nomenclature DQ), yet at longer pulse sequence times τ_{DQ}, it also comprises higher $2n + 2$ quantum orders. Similarly, the initial decay of the reference curve is dominated by dipolar-modulated longitudinal magnetization (quantum order 0), yet contains contributions from higher $2n$ quantum orders at long times.

With the two signal functions, it is possible to obtain structure information about the polymer network independently of relaxation effects by normalizing the DQ

a)Electronic mail: walter.chasse@physik.uni-halle.de.
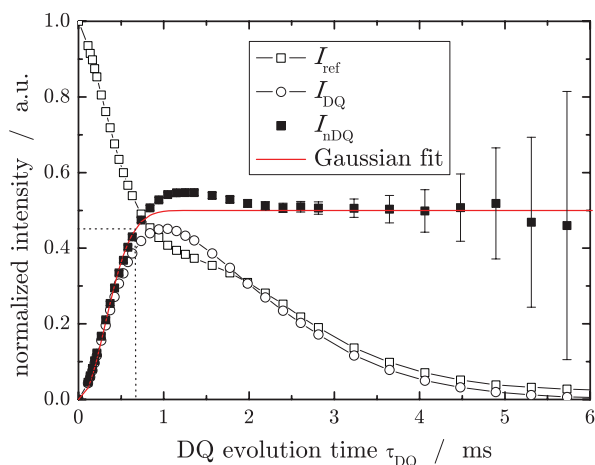b)Electronic mail: kay.saalwaechter@physik.uni-halle.de.

134, 044907-1

FIG. 1. Experimental double-quantum (I_{DQ}), reference (I_{ref}), and normalized DQ (I_{nDQ}) intensities for the natural rubber sample NR-C8, as well as the result of a fit of the latter with Eq. (3) yielding $\overline{D}_G/2\pi = 595$ Hz and $\sigma_G/2\pi = 166$ Hz. The dashed lines indicate the fitting limit. Note that the uncertainty for I_{nDQ} increases at long times due to the division of increasingly small quantities.

buildup through point by point division by the sum relaxation function $I_{\Sigma MQ} = I_{DQ} + I_{ref}$, possibly after subtraction of (usually exponential) long-time signal tails related to network defects or solvent: $I_{nDQ} = I_{DQ}/(I_{\Sigma MQ} - tails)$. The resulting normalized DQ build-up function must reach a relative amplitude of 0.5 in the long-time limit for theoretical reasons (equal partition among all excited even quantum orders) and is to a good approximation independent of temperature. The structural information in the form of RDCs is obtained by fitting such data to appropriate functions.

As mentioned, up to now we have used an approximated build-up function based on a static second-moment approximation:[3, 11, 18]

$$I_{nDQ}(\tau_{DQ}, D_{res}) = 0.5 \left(1 - \exp\left\{\tfrac{2}{5} D_{res}^2 \tau_{DQ}^2\right\}\right), \quad (1)$$

where D_{res} is an apparent RDC characteristic of the whole monomer unit representing of course the averaged action of many pair couplings. This build-up function was shown to fit very well both simulated data of multispin systems as well as data measured on homogeneous single-component elastomers. In the latter, the segmental fluctuations are all subject to the same crosslink induced anisotropy, and a discussion of this *a priori* unexpected finding and the polymer-physical implications is found in Ref. 19.

In case of RDC distributions, i.e., in inhomogeneous polymer networks with broad or even multimodal distribution of RDCs, such as in swollen polymer networks or networks with spatially separated bimodal or multimodal chain length distributions, the above function does not give a proper fit, because it only considers a single RDC constant D_{res}. The response is then generally given by a Fredholm integral equation (a distribution integral):

$$g(\tau_{DQ}) = \int_0^\infty K[D_{res}, \tau_{DQ}] f(D_{res}) dD_{res}, \quad (2)$$

where the function $g(\tau_{DQ})$ represents the measured data and $f(D_{res})$ is the RDC distribution. Taking Eq. (1) as (approximate) kernel function $K[D_{res}, \tau_{DQ}]$ and assuming that the distribution is Gaussian with the average RDC denoted as $\overline{D}_G$ and the standard deviation σ_G, one can obtain an analytical fitting function:[3]

$$I_{nDQ}(\tau_{DQ}, \overline{D}_G, \sigma_G) = \frac{1}{2}\left(1 - \frac{\exp\left\{-\frac{\frac{2}{5}\overline{D}_G^2 \tau_{DQ}^2}{1 + \frac{4}{5}\sigma_G^2 \tau_{DQ}^2}\right\}}{\sqrt{1 + \frac{4}{5}\sigma_G^2 \tau_{DQ}^2}}\right), \quad (3)$$

which applies for moderate distributions with $\sigma_G < \overline{D}_G$. Note that from now on, Eq. (1) is referred to as "Gaussian fitting function," while Eq. (3) is the "Gaussian-distributed fitting function."

More generally, one may try to fit linear superpositions of Eqs. (1) or (3) in order to model a multimodal distribution or resort to a numerical inversion procedure. The latter means that Eq. (2) has to be inverted to obtain $f(D_{res})$, which is an ill-posed problem, related to the well-known case of the inverse Laplace transformation. The program *ftikreg*,[20, 21] based on the fast Tikhonov regularization algorithm, combined with the Gaussian build-up function [Eq. (1)] as kernel function, was until now our method of choice to obtain an estimate of the distribution function.

However, one needs to keep in mind that Eq. (1) approximates simulated as well as true data only for nDQ intensities up to ~0.45, corresponding to a time limit of $\tau_{DQ}^{max} = 2.4/D_{res}$, see Fig. 1, resulting in systematic errors in the component fractions or the distribution shape obtained by *ftikreg*, in particular for networks with a dominating high-D_{res} component. In addition, the regularization result is sensitively dependent on a user-defined error parameter ε, which should ideally reflect the uncertainty for each data point. This uncertainty, however, is not constant for normalized I_{nDQ} data, as the noise-related error in the two experimental functions is constant, but its relative importance increases at long times due to division of small quantities. Due to these limitations to numerical regularization, in most of our previous papers we used results from multicomponent fitting as the more quantitative strategy for quantitative evaluations.

In this work, we introduce a new build-up function which allows for a more accurate description of the build up of very homogeneous polymer networks and thus to extend the fitting limit and further improve the accuracy of multicomponent fits. We further present an improved protocol for using *ftikreg*,[22] which includes the new kernel function and a reliable estimation procedure of the most probable error parameter ε, enabling a precise determination of the RDC distribution. We demonstrate the applicability of the new approach on examples of different bimodal networks, comprising simple mixed samples as well as cocrosslinked poly(dimethyl siloxane), (PDMS), model networks, proving the precise characterization of the potential modality of a network, including the correct RDCs and the mass fractions of the components.

II. EXPERIMENTAL SECTION

A. Samples

The studied natural rubber (NR) compounds were based on standardized poly(cis-1,4-isoprene) natural rubber kindly supplied by Malaysian Rubber (SMR-CV60). A conventional sulfur-accelerator recipe was used. Samples contain zinc oxide (five parts per hundred of rubber, phr) and stearic acid (2 phr) as activators, and different amounts of the accelerator N-cyclohexyl-2-benzothiazolesulphenamide and sulfur. The accelerator/sulfur ratio was always 0.2, and the sulfur contents were 1.3 phr (C2) and 11.1 phr (C8). Samples were prepared in an open two-roll mill using standard mixing procedures and vulcanized in a laboratory press at 150 °C at their respective optimum times (t_{97}), deduced from the rheometer curve (Monsanto Moving Die Rheometer, model MDR 2000E).

The sample ePDMS-t400 is a so-called PDMS "model network," prepared in high dilution by using vinyl end-functionalized PDMS with $M_w \approx 5.2$ kDa and a four-functional crosslinker. The uncrosslinked polymer was dissolved in 400 wt. % toluene with respect to the used amount of polymer. After adding the crosslinker and a platinum catalyst, the sample tube was sealed. For details of the reaction mechanism see Ref. 23. After the completed crosslink reaction, the toluene was carefully evaporated and the uncrosslinked network components were extracted by equilibrium swelling. The sample rPDMS-c040 was prepared by using a PDMS pre-polymer with randomly distributed vinyl groups on the backbone. The polymer, the two-functional crosslinker, and the platinum catalyst were diluted by only 20 wt. % toluene just in order to facilitate homogeneous mixing of the components. The amount of crosslinker was chosen so as to react just 40% of the vinyl groups. The uncrosslinked components were also extracted by equilibrium swelling.

A third, very similar series of end-linked monomodal and bimodal PDMS model networks comprises precursor chains of high ($M_n = 91$ kDa) and low ($M_n = 4.5$ kDa) molecular weight at different mass fractions. The same samples were previously investigated by Genesky, Cohen and co-workers, who also published details on their preparation.[24,25]

B. NMR spectroscopy

The ^{1}H MQ solid-state NMR experiments were carried out on a Bruker minispec *mq*20 spectrometer operating at a resonance frequency of 20 MHz ($B_0 \approx 0.5$ T) with 90° pulse length of 2.2 μs and a dead time of 13 μs. The experiments and the analysis of the measured raw data were performed following the previously published procedures,[5] including the subtraction of small contributions of signal tails related to network defects prior to calculating I_{nDQ}. This fraction was in all cases on the order of a few percent.

III. DATA ANALYSIS

A. Improved fitting function

As mentioned, in many polymer networks as well as in simulations, the nDQ curve shows not only the typical build-up behavior to a plateau of 0.5, but also a local maximum (see Fig. 1). This maximum is particularly well pronounced in very homogeneous networks which are characterized by a narrow RDC distribution ($\sigma_G/\overline{D}_G \leq 0.3$). In our first publication on the topic[3] using PDMS model networks, we used spin-counting experiments to show that this maximum in fact results from multiple-quantum dynamics: it arises from the growing importance of four-quantum coherences, which are created from the DQ coherences that dominate the primary buildup. The DQ selection phase cycle, more precisely, the complementary phase cycle used for the reference experiment, ensures that $4n$-quantum coherences are part of I_{ref}, which means that their appearance reduces I_{DQ}. Initially, I_{ref} is of course composed of longitudinal magnetization with apparent quantum order 0. One could expect a minimum after the maximum due to the growing importance of six-quantum coherences, again detected as part of I_{DQ}, but this is almost undiscernible due to low overall intensity of higher quantum orders. Thus the data quickly approaches the plateau of 0.5, arising from equal partition of all the different quantum orders in the long-time limit.

While our previous work showed that vulcanized NR samples can be extremely homogeneous, with $\sigma_G/\overline{D}_G \leq 0.1$,[8] most PDMS networks showed a significantly broader RDC distribution, always around $\sigma_G/\overline{D}_G \approx 0.3$.[3] We attribute this to inhomogeneities inherent in the preparation of the previously investigated samples, and to prove this point, the measured DQ build-up curves of an end-linked PDMS network which was crosslinked in high dilution (ePDMS-t400) and a randomly linked PDMS network (rPDMS-c040) are plotted in Fig. 2(a).

The end-linked network shows a clear maximum in the buildup, whereas the randomly linked network shows a monotonic increase of the double-quantum intensity to the plateau value of 0.5, indicating a more homogeneous structure of the former, see Fig. 2(a). The average RDC constants obtained by fitting with Eq. (3) are quite similar (ePDMS-t400: $\overline{D}_G/2\pi \approx 150$ Hz; rPDMS-c040: $\overline{D}_G/2\pi \approx 140$ Hz), while the relative distribution widths $r_G = \sigma_G/\overline{D}_G$ are rather different: $r_G \approx 0.1$ for the solution end linked and $r_G \approx 0.6$ for the bulk randomly linked network.

It becomes again obvious that the homogeneity of a polymer network is indicated by the maximum in the build-up curve, and it is now clear that end linking of highly dilute chains provides more homogeneous networks (after deswelling), probably as a result of better mixing, thus better controlled network structure. This statement is further supported by the corresponding RDC distributions plotted in Fig. 2(b). These distributions were obtained by using the *ftikreg* software with the old Eq. (1) as kernel function.

As mentioned, the previously used inverted Gaussian fitting functions (1) and (3) cannot fit the local maximum, requiring a fitting limit $I_{nDQ} < 0.45$. This leads to the systematic errors mentioned in the Introduction. It should be stressed that the main problem does not arise for the estimation of the average residual dipolar coupling constant, for which Eq. (3) is always a suitable choice, but for the proper characterization of the actual distribution. Especially for the regularization procedure with *ftikreg*, the kernel function representing
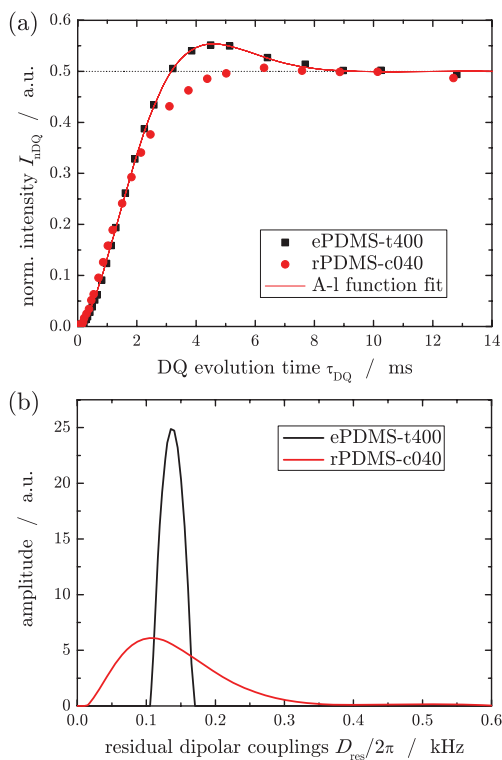
FIG. 2. (a) Normalized DQ build-up curves of end-linked ePDMS-t400 and randomly linked rPDMS-c040, and (b) corresponding coupling constant distributions obtained by Tikhonov regularization.

the response of a single monomer unit (or a segment thereof) has to be as accurate as possible.

For this reason, we introduce a new fitting function, which we have derived by resorting to the data of the most homogeneous networks at our disposal, i.e., NR-C2 and ePDMS-t400. We were inspired by the so-called "Abragamian" function, which is a product of a Gaussian and a sinc function and was used by Abragam to fit free-induction decays (FIDs) of single crystals of fluorides,[26] and gained some popularity in fitting FIDs of rigid ^{1}H systems like crystalline components of polymers dominated by CH_2 spin pairs,[27] or other systems with similar local order.[28] However, an inverted Abragamian, $0.5[1 - A(x)]$, did not fit our MQ build-up data well, yet a modified version using a Weibullian and a cosine function fitted the data almost perfectly, see Fig. 2(a):

$$I_{nDQ}(\tau_{DQ}, D_{res}) = 0.5(1 - \exp\{-(0.378 \, D_{res}\tau_{DQ})^{1.5}\}$$
$$\times \cos[0.583 \, D_{res}\tau_{DQ}]). \quad (4)$$

The numerical factors and the exponent 1.5 of the Weibullian in this "Abragam-like" (A-l) function were calibrated so as to result in the same RDC as obtained from fits using Eq. (1). For all used reference networks, the deviation between the fitted average D_{res} was below 1% for the given prefactors in Eq. (4). It should be mentioned that the samples on which the function optimization was performed still had relative distribution widths $\sigma_G/\overline{D}_G \approx 0.1$ when fitted with the Gaussian-distributed function, Eq. (3). This means that Eq. (4)

contains some *a priori* bias (it is, in a sense, the convolution of the "correct" unimodal result and a narrow point-spread function), and its use will always lead to a slight underestimation of the actual distribution width, which, however, is only relevant in extremely homogeneous samples with similarly narrow distributions.

The new A-l build-up function enables a precise fitting of the maximum in the build-up curves of homogeneous polymer networks. This means that the fitting range for DQ build-up curves can be extended beyond the potential maximum of the build-up curve, even until the last reliable points in the plateau region. For samples with wide distributions, the maximum in the experimental data of course vanishes [see Figs. 2(a) or 3(c)], which means that all data points up to $I_{nDQ} \leq 0.5$ can be fitted. As opposed to the previous use of the Gaussian or Gaussian-distributed functions, the component fractions will be precise because the signal functions of the individual subcomponents are faithfully represented. This gain in precision is central for a much improved analysis of RDC distributions. Equation (4) can be used in simple linear superpositions, modeling multimodal distributions with sharply peaked maxima, or one can also combine it with a Gaussian distribution of RDCs (in this case, the result is not analytical, requiring a least-squares fit to a numerically computed function, which is easily possible in modern data analysis software).

To appreciate the improvements on implementing the A-l function as kernel function in *ftikreg*, Figs. 3(a) and 3(b) display build-up data of two NR samples and a bimodal mixture, respectively. Note that the experimental data of the latter is virtually identical to a superposition of single-component build-up curves. The two horizontal lines indicate the fitting limits used for the Gaussian kernel. The solid lines correspond to the build-up curves calculated with the A-l kernel, which is in good agreement with the whole range of meaningful data. In Fig. 3(c), the associated coupling constant distributions are plotted. Note that the NR-C8 sample contains a minority component with high crosslink density. Such impurities have been observed before,[11] and we attribute them to imperfect mixing before or during vulcanization.

Apart from the weak high-D_{res} contribution, the distribution obtained for the mixture with the old kernel fails to comply with the expected bi- (or rather tri-) modality. This is because the initial buildup is mainly dominated by the highly crosslinked (highly dipolar-coupled) component in the mixture that is excited at shorter τ_{DQ}, and the bimodal character of the build-up curve is only obvious beyond the fitting limit of the Gaussian kernel, Eq. (1). In contrast, the distribution obtained from the regularization with the A-l kernel shows a clearly bimodal behavior which is also in very good agreement with the weighted sum of the monomodal distributions. Thus, the new fitting function, with its extended fitting range, ensures access to the whole information about the RDC distribution encoded in the build-up curve, which is an essential improvement for the analysis of multimodal polymer networks. For very homogeneous samples with narrow distributions, the Gaussian-distributed fitting function will of course still give faithful results as long as its fitting/validity limit is taken into account.
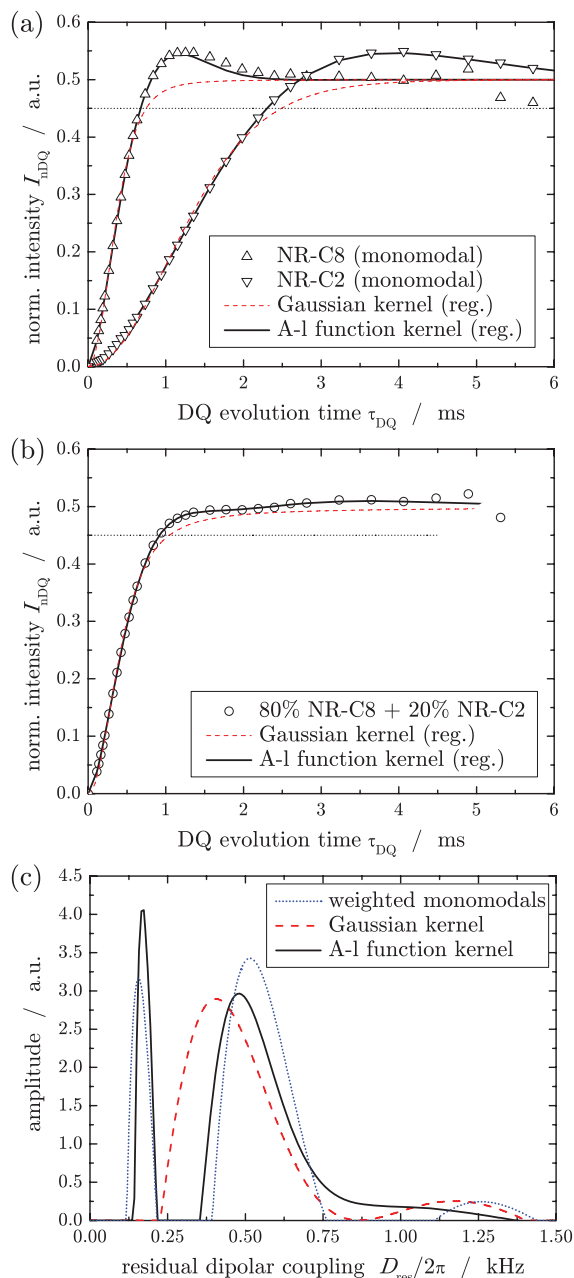
FIG. 3. Build-up curves of NR-C2 and NR-C8 (a), and of a bimodal mixture (b), along with build-up curves obtained by regularization with the Gaussian (dashed line) and A-l (solid line) kernels; the horizontal lines indicate the fitting limit for the former. (c) Corresponding RDC distributions.

It is important to note that the A-l function fits the data for NR and PDMS (as well as butadiene rubber,[11] data not shown) equally well. This stresses that the nDQ build-up curves of such elastomers, all with dense ^1H spin systems directly attached to the main chain, are quite universal, and that the new function can thus be considered generic. Problems arise with copolymers such as SBR (styrene-butadiene rubber) or EPDM (ethylene propylene diene monomer rubber), which have broad D_{res} distributions simply because the spin systems of the different monomer units are different.[29] This pertains to different average spin distances as well as geometries of the fast local bond fluctuations. Therefore, simple isomerism

such as *cis* versus *trans* configurations in poly(butadiene) also leads to differences in apparent residual couplings,[30] and the same can be expected for monomers with side chains that are dynamically decoupled from the main chain by more than one bond, such as in poly(alkyl acrylates). Investigations along these lines, taking advantage of the good site resolution provided by ^1H DQ experiments under high-resolution magic-angle spinning (MAS) conditions,[1,30] based on improved re-coupling pulse sequences, are ongoing.

B. Improved protocol for Tikhonov regularization

Experimentally not directly accessible distributions f are often connected to a measurable quantity g by an operator equation

$$g = \mathbf{A} f, \tag{5}$$

and therefore the inverse of Eq. (5) is of interest:

$$\mathbf{A}^{\dagger} g = f. \tag{6}$$

Commonly, instead of exact data, just noisy data g_ε with a noise level ε is available:

$$\|g_\varepsilon - g\| \le \varepsilon. \tag{7}$$

If the inverse operator $\mathbf{A}^{\dagger}$ of $\mathbf{A}$ exists but is discontinuous, Eq. (5) is called ill-posed and the solution has to be calculated numerically. In order to solve this problem, Tikhonov proposed a variation algorithm where the regularization parameter α, which quantifies a smoothing of the fitted distribution and stabilizes the result, is found such that Eq. (8) is fulfilled:

$$\|\mathbf{A} f_\alpha - g_\varepsilon\| = \varepsilon. \tag{8}$$

The main advantage of Tikhonov regularization is that it calculates the regularization parameter α and thus the resulting distribution for a given error parameter ε, which in turn is directly related to the known noise of the measured input data g_ε. In contrast, other algorithms such as continuous inversion (Ref. 31) calculate the result in dependence of a given regularization parameter α, the value of which leading to the most realistic fitting result is subject to uncertainties.

In the original *ftikreg* program by Weese,[20,21] the regularization is performed in dependence of an error parameter ε which should, thus, reflect the average uncertainty of the measured input data. As the regularization results highly depend on the used error parameter (see Fig. 4), which is not constant over the whole build-up curve (see Fig. 1), a strong criterion needs to be identified in order to obtain a reliable distribution of coupling constants. A possible resolution is of course to use as input to the program the absolute error for each point, as for instance determined via conventional error propagation and the known noise. The use of individual realistic error estimates has in fact been shown to give substantial improvements in the determination of relaxation time spectra in dynamic light scattering.[32] For the present case, where we have to expect other small systematic errors arising from the still approximative nature of the improved Kernel function, we suggest an alternative protocol, implemented in a
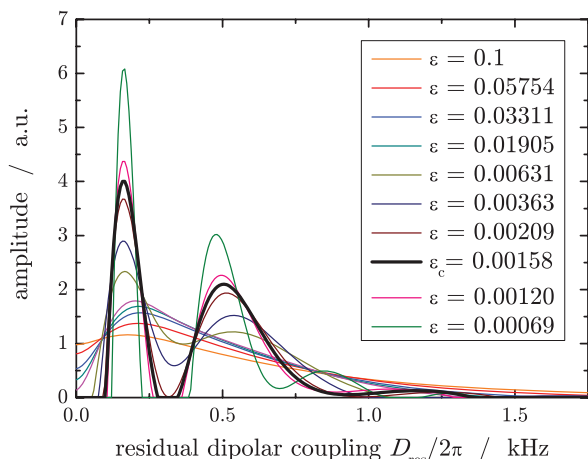
FIG. 4. Coupling constant distributions calculated with *ftikreg* for the sample mixture with 40 wt. % of NR-C2 for different error parameters ε.

user friendly way via several new subroutines[22] in the original source code of *ftikreg*.

In the first step, an automated variation of the error parameter ε was implemented. This enables the program to perform the regularization in consecutive calculations within a given error interval range with a predefined number of logarithmic equidistant steps. For every obtained distribution $f(D_{\text{res}})$, a build-up curve $g(\tau_{\text{DQ}})$ is calculated in a simple iteration by evaluating directly the integral Eq. (2) in a discrete form using the same Kernel function as for the regularization of the inverse problem. To gauge the precision of the distribution, a χ^2 test that simply calculates the mean square deviation between fit and data is used to compare the experimental build-up curve and the build-up curve obtained from the distribution resulting from the regularization procedure. Figure 5 shows the dependence of χ^2 on the used error parameter ε for the regularization.

In a double logarithmic representation, χ^2 is decreasing linearly with decreasing error parameter ε over several decades. At a certain error ε_c the χ^2 dependence of ε is chang-
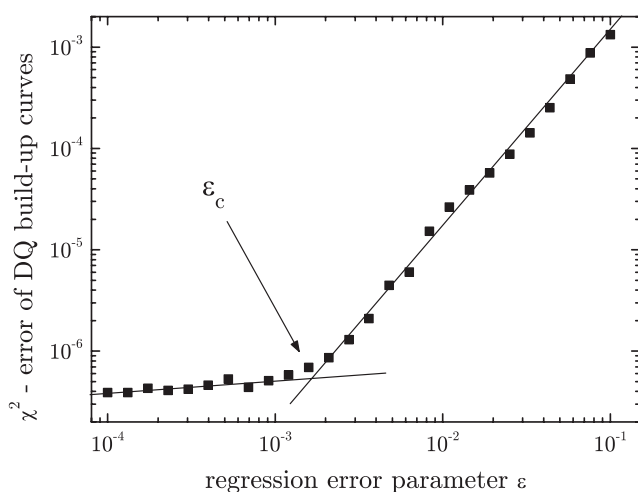
FIG. 5. Calculated χ^2 for a series of error parameters ε. The arrow indicates the physically meaningful ε_c.

ing, and a further reduction of the error parameter is not reflected in a comparably significant improvement of the accuracy of the calculated distribution. We assume that starting with the value ε_c, the accuracy of the measured data is becoming overestimated and, therefore, a further reduction of the error parameter is not physically meaningful. As a strong indication, the regularization result in the lower ε range becomes multiply peaked, which is obviously not realistic. Similar dependencies of χ^2 on the regression error parameter ε were observed for all investigated natural rubber and PDMS networks and also for more complex filled rubber compounds, which are not discussed in this work.

At this point we conclude that the error parameter ε_c corresponds to the most reliable measure of the uncertainty of the measured input data, and a further reduction leads to an overinterpretation of experimental noise. For further evaluations and investigations, the program also now automatically calculates the average $\overline{D}_{\text{reg}}$ and the variance σ_{reg} of the distribution of residual dipolar coupling constants obtained by the regularization.

Finally, we should discuss the consequences of the special property of nDQ build-up curves to reach a plateau of 0.5. It was until now necessary to add a number of additional long-time data points with $I_{\text{nDQ}} = 0.5$ to externally enforce the resulting best-fit build-up curve to reach the expected plateau. For a more practical strategy, we realize that *ftikreg* was initially conceived for inverse Laplace transformations (i.e., with a falling exponential as kernel function), so it has the built-in option to enforce $I = 0$ in the long-time limit. In order to use this option and to obviate the use of an arbitrary number of additional points, the program now internally fits *decay* data of the form $0.5 - I_{\text{nDQ}}$ to a correspondingly inverted fitting function.

IV. RESULTS AND DISCUSSION

A. Coupling constant distribution analysis of mixed monomodal NR compounds

In order to obtain information about the applicability and the accuracy of the new generic A-l build-up function, Eq. (4), and the new strategy for coupling constant distribution analysis, we prepared "metadata" corresponding to a series of bimodal rubber mixtures with known weight fractions ω of the individual monomodal components. Metadata simply means artificial datasets that were obtained by averaging experimental data for monomodal samples, which exhibit a realistic noise level. We calculated averages of the build-up curves of a rubber with lower (NR-C2: $\overline{D}_G/2\pi \approx 165$ Hz) and higher (NR-C8: $\overline{D}_G/2\pi \approx 600$ Hz) average RDC, weighted by their respective mass fraction ω. Since the RDC distributions of NR-C2 and NR-C8 have virtually no overlap, the distributions correspond to clearly bimodal samples. The weight fractions used for the bimodal mixtures are given in Table I. We note that we have also performed measurements on a few mixtures, and the results were virtually identical to the metadata (see Fig. 3).

The build-up curves were evaluated with the Gaussian-distributed fitting function (3) and by regularization. For the

TABLE I. Average RDC constants and standard deviations obtained from the fit with the Gaussian-distributed function ($\overline{D}_G$, σ_G) and from improved regularization analysis ($\overline{D}_{reg}$, σ_{reg}, fraction ω_{C2} of NR-C2, all obtained by numerical integration of the distributions). The fractions in the last column are from two-component fits according to Eq. (9).

| | Fit with Eq. (3) | | Regularization with Eq. (4) | | | Eq. (9) |
Ratio C2/C8	$\overline{D}_G/2\pi$ Hz	$\sigma_G/2\pi$ Hz	$\overline{D}_{reg}/2\pi$ Hz	$\sigma_{reg}/2\pi$ Hz	ω_{C2}	ω_{C2}
100/0	165	33	163	23	1.000	0.968
95/05	178	57	180	93	0.961	0.925
90/10	193	78	196	110	0.911	0.878
80/20	227	125	246	188	0.803	0.781
70/30	265	194	288	216	0.7	0.685
60/40	312	222	331	233	0.601	0.592
50/50	364	238	373	242	0.506	0.522
40/60	416	229	416	244	0.404	0.493
30/70	465	211	459	239	0.301	0.625
20/80	512	203	505	234	0.188	0.806
10/90	551	160	544	200	0.102	0.885
0/100	596	166	583	147	0.000	0.926

FIG. 6. Average RDC constants from the Gaussian fit, $\overline{D}_G$, and by regularization, $\overline{D}_{reg}$, in dependence of the fraction ω of the lower crosslinked rubber NR-C2. The right ordinate shows the fractions of NR-C2 obtained via integration over the regularized RDC distributions and the fitted results of the two-component with Eq. (9).

Gaussian fit, all data points of the normalized double quantum build-up curves I_{nDQ} up to the fitting limit of $I_{nDQ} = 0.45$ were taken into account. The average RDC constants $\overline{D}_G$ and the standard deviations of the assumed Gaussian distribution σ_G are stated in Table I. A continuous increase of the coupling constant $\overline{D}_G$ with increasing weight fraction of the more densely crosslinked rubber NR-C8 can be observed, and expectedly, the standard deviation σ_G is increasing up to a weight fraction $\omega = 0.5$ of NR-C8, and is decreasing for higher weight fractions of NR-C8. These results, thus, correctly reflect the averaged properties of the bimodal rubber mixtures, but of course do not carry any information on the actual microstructure.

For the determination of the RDC distribution of the different mixtures, the improved version of *ftikreg* including the new build-up kernel was used, evaluating all data points up to the maximum of the different build-up curves. From the actual full RDC distributions, the average RDC $\overline{D}_{reg}$, the standard deviation σ_{reg} (square-root of the variance), and the weight fractions of the two rubbers were extracted by numerical integration of the two separate peaks of the distributions. See Fig. 3(c) for an example of the clearly bimodal distributions that were observed in all cases. All results are listed in Table I.

The average RDC constants $\overline{D}_{reg}$ calculated with the regularization method show almost the same dependence on the fraction ω of the higher crosslinked rubber NR-C8 as the coupling constants $\overline{D}_G$ obtained with the Gaussian fitting function, the two coupling constants differing only by a couple of Hz. Notably, even the coupling constants of the monomodal samples and the bimodal samples with a high amount of one component are in very good agreement. The relative deviations of the two coupling constants for fractions of the less crosslinked rubber NR-C2 reaching from $\omega_{C2} = 0 - 0.4$ and $\omega_{C2} = 0.9 - 1$ are not bigger than 1% or 2%, and for in-between cases, the deviations are only as large as 8%.
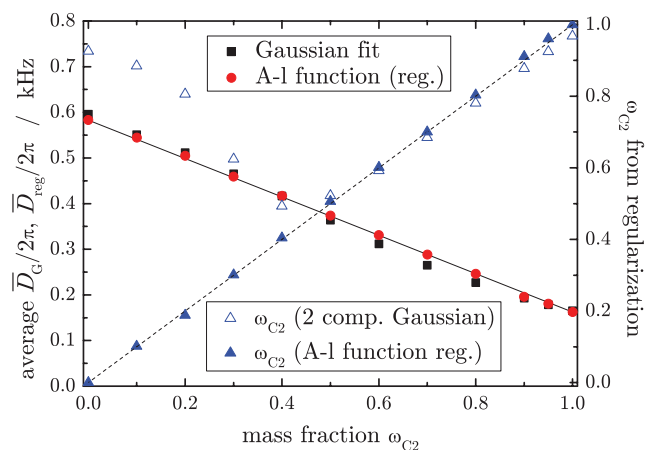
In Fig. 6 we plot the coupling constants from the regularization and the Gaussian fit versus the mass fraction of NR-C2. The straight solid line would correspond to the assumption that the RDCs of the bimodal mixture comply with a simple linear mixing law of the two components. The average coupling constants from the regularization $\overline{D}_{reg}$ are in very good agreement with this assumption, while the coupling constants obtained from the Gaussian-distributed fitting function (3) show more apparent deviations. This is of course due to the approximative nature of the underlying approximate build-up function, but we note that the deviations are not too large, which means that this simple fitting function is still of practical use to estimate the degree of inhomogeneity of a given unknown sample, with in fact rather good-quality results for the average RDC constant of inhomogeneous or bimodal or higher-modal networks or mixtures.

The comparison of the given fractions with the fractions obtained from regularization demonstrates an extremely good agreement over the whole range of the investigated bimodal mixtures. Especially for mixtures in which neither of the two rubbers is dominating ($\omega_{NR-C2} = 0.3 - 0.8$), the deviation between given and estimated fractions is less than 1%. This error is slightly increasing up to 2% when one of the two components becomes dominant. For the lightly crosslinked (lowly coupled) rubber NR-C2, precise quantitative results for the fraction could be obtained up to a given fraction of $\omega_{NR-C2} = 0.95$. For the highly crosslinked rubber NR-C8 it works just as well up to a fraction of $\omega_{NR-C8} = 0.9$. Beyond this, the build-up curve of the bimodal mixture is so strongly dominated by this component that the influence of the lightly crosslinked component is readily apparent only beyond the maximum of the build-up curve.

For an alternative determination of the component fractions, we also tested a two-component fit based on the inverted Gaussian build-up function, Eq. (1):

$$I_{nDQ}(D_1, D_2, \omega_1) = \omega_1 I_{nDQ}(D_1) + (1 - \omega_1)I_{nDQ}(D_2). \quad (9)$$

This strategy worked rather well in our previous work,[3] where we have investigated bimodal PDMS model networks with a rather large chain-length contrast, corresponding to RDCs differing by a factor of 6. In this study, it was possible to obtain good fit results for contents of highly crosslinked chains up to 70%. The results for the present mixtures, where the RDC contrast is only about half as large, are also listed in Table I and plotted in Fig. 6. A comparison of the given fractions with the fractions obtained from the two-component fit also demonstrates a satisfactory agreement for lower fractions of NR-C8. However, for higher fractions beyond 50%, the fit fails completely in a sense that D_2 assumes unreasonably high values and D_1 takes on an average value between the expected RDCs, thus giving meaningless results for the fraction. The situation can be somewhat improved by actually fixing the D_i values based on the pure components, but systematic errors at low ω_{C2} prevail.

In conclusion, the improved regularization analysis based on the new generic A-l build-up function (4) presents itself as the most robust and precise method to obtain information on the average RDC constants and the shape of the RDC distribution function for cases with no *a priori* knowledge, making it the tool of choice for the initial characterization of rubber compounds. This of course also holds for copolymer samples (such as SBR or EPDM), where apparent distributions partially arise from the different responses (different average D_{res}) of the different monomer units. In the present case, the A-l function was shown to yield extremely faithful mass fractions of the components in bimodal mixtures of homoelastomers over the whole range of compositions. For unknown samples, it can be used to check for a potential modality of the distribution, and then, bicomponent or multicomponent fits, also based on the new function, can be used to characterize the subcomponents even more reliably.

B. Distribution analysis of bimodal PDMS networks

In order to obtain further insights into practical applications and the precision of the regularization method for the analysis of elastomer structure, a new series of bimodal PDMS model networks were investigated. See Refs. 24 and 25 for in-depth investigations of these samples consisting of precursor polymers of $M_n = 91$ and 4.5 kDa. For the in-depth characterization of the bimodal networks, the double-quantum build-up curves of the bimodal as well as the monomodal network samples were measured. In addition, mixtures of the high- and low-molecular weight monomodal networks were also measured, with mass fractions identical to the ones used for the preparation of the different bimodal networks. For a further comparison, I_{nDQ} build-up curves of the monomodal networks were summed up according to the respective mass fraction in the bimodal networks.

In Fig. 7 the nDQ build-up curves of the monomodal networks and a bimodal network with a mass fraction of 48 wt. % short and 52 wt. % long chains are displayed, along with the measured mixed monomodal networks and a weighted superposition of the pure-component build-up curves of the same weight ratio. The superposed build-up curves and the build-
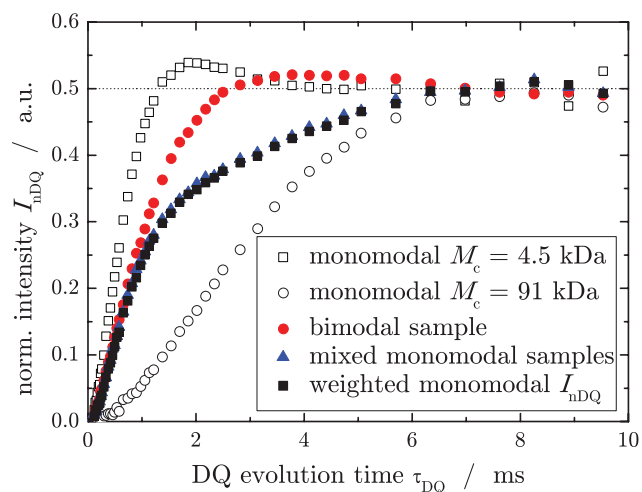

FIG. 7. Experimental nDQ build-up curves of monomodal networks (M_c = 91 and 4.5 kDa), a bimodal network (48 wt. % short and 52 wt. % long chains), and an experiment of a corresponding mixture of monomodal networks as well as a simple stoichiometric superposition of pure-component I_{nDQ} build-up curves.

up curve of the mixed monomodal networks are expectedly nearly identical and show a clearly bimodal behavior. In contrast, the response of the bimodal network, while being quite similar for small evolution times, is significantly different at longer evolution times (1–5 ms) and shows no apparent two-step behavior as is the case for clearly bimodal samples. Thus, while being chemically bimodal, the dynamics of the different chains in this network is not as dissimilar as expected from their length.

In Fig. 8 the corresponding residual dipolar coupling constant distributions are plotted, which were obtained by using the improved *ftikreg*. The results from the experiment on the mixed monomodal networks and the regularization result for the superposed metadata both show a clear bimodal distribution of coupling constants, proving that the components in the actual bimodal network could be resolved if they be-
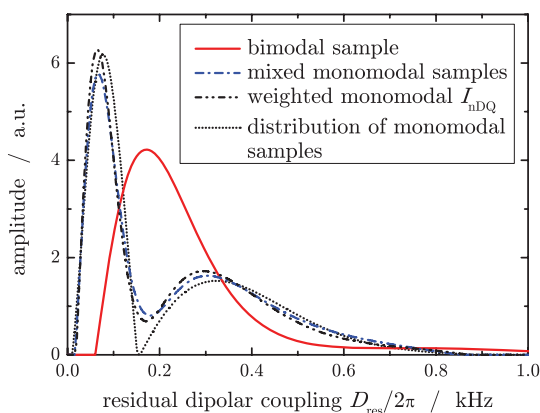

FIG. 8. Coupling constant distributions of the bimodal sample (48 wt. % short and 52 wt. % long chains, solid line), of the corresponding monomodal networks (M_c = 91 and 4.5 kDa), scaled to the same mass fractions (dotted lines), and for the results on the corresponding mixture of monomodal networks (dashed-dotted line) as well as the superposed pure-component I_{nDQ} metadata (dashed-dotted-dotted line).

haved the same as in the pure networks. While the regularization results for the mixed cases overestimate the width of the individual component distributions only somewhat, it is remarkable that the overall shape of the distribution, characterized by an asymmetric shape for the more highly crosslinked component, is in fact reproduced very well.

In contrast, however, the true bimodal network shows a broad monomodal distribution of coupling constants with no apparent bimodality. Such coupling constant distributions were observed for all other investigated bimodal PDMS networks, ranging in mass fraction of short chains from 7 to 71 wt. %, and this fact deserves some further discussion. First of all, this observation is in stark contrast to our previous investigations,[3] where PDMS chains of 47 and 0.78 kDa, i.e., with a chain-length contrast factor of 60, were co-crosslinked. In this latter case, the bimodal networks showed clearly bimodal RDC distributions (even using the less reliable Gaussian fitting function), indicative of more or less complete spatial separation of "short" and "long" subnetworks. Therefore, we conclude that a chain-length contrast of a factor of 20 is not enough to lead to subnetwork formation on a mesoscopic scale, i.e., to domains that span at least a few R_g.[19]

Such a spatial separation is in fact necessary for the observation of pronounced inhomogeneity or (as a limit that is observed in special samples) true bimodality or multimodality. This is easily proven by experiment, because when short and long chains are intimately interlinked, as is for instance trivially the case in a vulcanized (statistically crosslinked) rubber having a continuous and rather broad most-probable M_c distribution, rather narrow distributions are still observed, see for instance Fig. 3(c). It is important to remember that the NMR response is representative of the superposition of isolated monomer responses, as NMR measures all protons locally. In such a system, the orientation fluctuations of the individual monomers are, thus, homogenized and do not reflect either the length nor the end-to-end separation of the chain they are part of. Otherwise, the RDC distribution function of a vulcanized rubber could never be as narrow.

Some reasons for this interesting and unexpected yet generic behavior were already discussed in Ref. 19. Currently, by aid of computer simulations, we are trying to explore further the origin and consequences of this interesting phenomenon, which should have implications for the validity of the common models of rubber elasticity. One possibility is that given no significant spatial separation of interlinked short and long network chains, internal force balances may reduce the orientational order in the short chains at the expense of the long chains.[33] In other words, the crosslink positions fluctuate and adapt themselves so as to minimize the forces on them, thereby rendering the orientation dynamics of the attached chains similar. Further, entanglements effects further aid in homogenizing the system response.[34] The latter is presumably the main reason why the 4.5 kDa network (see Fig. 8) has a relatively broader distribution than the 91 kDa sample. Note that the entanglement spacing of NR (=polyisoprene) is about 5 times lower than that of PDMS, which explains that NR samples appear very homogeneous up to rather high-crosslink densities.

Now for the present case, we therefore believe that the 4.5/91 kDa system simply does not spatially separate upon co-endlinking as completely as the systems with larger chain-length contrast. Consequently, the dynamic behavior of the individual chains changes when these chains are co-endlinked. Once the distributions of one or both components become significantly modified/broadened, they cannot be clearly separated any more via ^{1}H NMR of the full system. Even though the M_c distribution is clearly bimodal, the orientational order in the individual chains as reflected in the RDC is subject to connectivity effects and is thus not clearly distinguishable any more.

This stresses the use of specific (and of course synthetically rather demanding) ^{2}H labelling schemes, which allow for a separate observation of the individual chain populations. A ^{2}H NMR study on the given type networks was recently published[25] and has in fact demonstrated that at short-chain contents significantly lower than 50 wt. %, it is mainly the short component that changes its behavior. The short chains presumably still form clusters, yet possibly smaller ones as in systems with larger chain-length contrast, and monomer fluctuations in these smaller clusters are more sensitive to the average mobility in the matrix that surrounds them, in particular when approaching the percolation threshold of the short-chain subnetwork. A great potential, yet to be explored, is the combination of ^{1}H MQ spectroscopy and the as yet more common ^{2}H lineshape analysis. This should enable us to better understand the influence of segmental dynamics, which leads to some additional broadening of ^{2}H spectra, but is is absent in ^{1}H MQ NMR via the intensity normalization procedure.[3]

V. CONCLUSIONS

^{1}H time-domain multiple-quantum NMR spectroscopy, in combination with a new generic fitting function for the normalized DQ build-up and an improved Tikhonov regularization procedure, represents a powerful tool to investigate the residual dipolar coupling constant distribution in polymer elastomers and gels. The essential improvements addressed in this work concern a new fitting function, which was developed by way of fitting data of exceptionally homogeneous networks. Further, we have outlined a strategy to determine the most probable error parameter for use in the fast Tikhonov regularization program *ftikreg* and have thus established a method to obtain truly reliable distribution functions. See Ref. 22 for information on the software. We have demonstrated the potential of the approach in applications to monomodal and bimodal natural rubber and poly(dimethyl siloxane) samples, mixtures, and corresponding metadata. Having demonstrated that different components in bimodal samples can faithfully be separated, our application on bimodal samples that do not exhibit bimodal coupling distribution provides new support for the fact that segmental orientation fluctuations in short and long chains have a similar anisotropy when they are crosslinked in an intimately mixed state.

On the methodological side, we note that the distribution analysis using the new generic fitting function is not limited to

static MQ experiments. Applying an improved and more robust version of the popular magic-angle spinning BaBa pulse sequence,[35] DQ build-up curves with exactly the same shape but of course a different scaling factor can be obtained and analyzed with the same approach, as will be published shortly. This again demonstrates that the shape of the generic build-up function is mainly determined by multiple-quantum coherence dynamics rather than by orientation dependence, which of course differs for static and MAS recoupling pulse sequences. Further research will show whether other DQ MAS experiments, such as the ones based on γ-encoded pulse sequences, yield the same generic response in ^{1}H NMR of soft-matter systems.

ACKNOWLEDGMENTS

[1] R. Graf, D. E. Demco, S. Hafner, and H. W. Spiess., Solid State Nucl. Magn. Reson. **12**, 139 (1998).

[2] M. Schneider, L. Gasper, D. E. Demco, and B. Blümich, J. Chem. Phys. **111**, 402 (1999).

[3] K. Saalwächter, P. Ziegler, O. Spyckerelle, B. Haidar, A. Vidal, and J.-U. Sommer, J. Chem. Phys. **119**, 3468 (2003).

[4] R. S. Maxwell, S. C. Chinn, D. Solyom, and R. Cohenour, Macromolecules **38**, 7026 (2005).

[5] K. Saalwächter, Progr. NMR Spectrosc. **51**, 1 (2007).

[6] J. L. Valentín, D. López, R. Hernández, C. Mijangos, and K. Saalwächter, Macromolecules **42**, 263 (2009).

[7] J. L. Valentín, I. Mora-Barrantes, J. Carretero-González, M.A. López-Manchado, P. Sotta, D. R. Long, and K. Saalwächter, Macromolecules **43**, 334 (2010).

[8] J. L. Valentín, P. Posadas, A. Fernández-Torres, M. A. Malmierca, L. González, W. Chassé, and K. Saalwächter, Macromolecules **43**, 4210 (2010).

[9] Yu. Ya. Gotlib, M. I. Lifshits, V. A. Shevelev, I. S. Lishanskij, and I. V. Balanina, Vysokomol. Soedin., Ser. A **18**, 2299 (1976).

[10] J. P. Cohen-Addad, B. P. Thanh, and H. Montes, Macromolecules **30**, 4374 (1997).

[11] K. Saalwächter, B. Herrero, and M. A. López-Manchado, Macromolecules **38**, 9650 (2005).

[12] K. Saalwächter, Macromolecules **38**, 1508 (2005).

[13] G. I. Sandakov, L. P. Smirnov, A. I. Sosikov, K. T. Summanen, and N. N. Volkova, J. Polym. Sci. B: Polym. Phys. **32**, 1585 (1994).

[14] T. Gullion and J. Schaefer, J. Magn. Reson. **81**, 196 (1989).

[15] K. T. Müller, T. P. Jarvie, D. J. Aurentz, and B. W. Roberts,. Chem. Phys. Lett. **242**, 535 (1995).

[16] G. Jeschke, A. Koch, U. Jonas, and A. Godt,. J. Magn. Reson. **155**, 72 (2002).

[17] Y.-W. Chiang, P. P. Borbat, and J. H. Freed, J. Magn. Reson. **172**, 279 (2005).

[18] K. Saalwächter and A. Heuer, Macromolecules **39**, 3291 (2006).

[19] K. Saalwächter and J.-U. Sommer, Macromol. Rapid Commun. **28**, 1455 (2007).

[20] J. Weese, Comp. Phys. Commun. **69**, 99 (1992).

[21] J. Weese, Comp. Phys. Commun. **77**, 429 (1993).

[22] See supplementary material at http//dx.doi.org/10.1063/1.3534856 for the Fortran source code, a Windows executable and documentation of the improved regularization software.

[23] A. J. Chalk and J. F. Harrod, J. Am. Chem. Soc. **87**, 16 (1965).

[24] G. D. Genesky, B. M. Aguilera-Mercado, D. M. Bhawe, F. A. Escobedo, and C. Cohen, Macromolecules **41**, 8231 (2008).

[25] B. M. Aguilera-Mercado, G. D. Genesky, T. M. Duncan, C. Cohen, and F. A. Escobedo, Macromolecules **43**, 7173 (2010).

[26] A. Abragam, *The Principles of Nuclear Magnetism* (Oxford University Press, Oxford, 1961).

[27] E. W. Hansen, P. E. Kristiansen, and B. Pedersen, J. Phys. Chem. B **102**, 5444 (1998).

[28] W. Derbyshire, M. van den Bosch, D. van Dusschoten, W. MacNaughtan, I. A. Farhat, M. A. Hemminga, and J. R. Mitchell, J. Magn. Reson. **168**, 278 (2004).

[29] K. Saalwächter, M. Klüppel, H. Luo, and H. Schneider, Appl. Magn. Reson. **27**, 401 (2004).

[30] R. Graf, A. Heuer, and H. W. Spiess, Phys. Rev. Lett. **80**, 5738 (1998).

[31] S. W. Provencher, Comm. Comp. Phys. **27**, 229 (1982).

[32] D. Maier, M. Marth, J. Honerkamp, and J. Weese, Appl. Opt. **38**, 4671 (1999).

[33] J.-U. Sommer, W. Chassé, J. L. Valentín, and K. Saalwächter, Phys. Rev. E **78**, 051803 (2008).

[34] M. Lang and J.-U. Sommer, Phys. Rev. Lett. **104**, 177801 (2010).

[35] M. Feike, D. E. Demco, R. Graf, J. Gottwald, S. Hafner, and H. W. Spiess, J. Magn. Reson., Ser. A **122**, 214 (1996).

3.2. Cross-Link Density Estimation of PDMS Networks with Precise Consideration of Networks Defects

In this work the cross-link density of randomly linked PDMS networks is studied by ^{1}H double-quantum (DQ) NMR, equilibrium swelling experiments and Miller-Macosko (MM) calculations focusing on the influence of network defects and the weight average functionality of the cross-links. Networks of different cross-link density were prepared by using a systematically varied amount of cross-linker during the reaction leading to a reasonable fraction of network defects. The latter was determined by DQ-NMR in dry as well as swollen networks, revealing that the defect fraction is significantly underestimated in dry networks. The defect fractions estimated in swollen gels are in very good agreement with the results obtained by the MM calculations. The precisely determined defect fraction is used to correct the elastic contribution to the Flory-Rehner (FR) equation, and therefore the elastically effective polymer volume fraction is introduced.

The correlation between the molecular weight obtained by DQ-NMR and equilibrium swelling experiments evaluated by the modified FR equation is investigated in terms of the phantom model. Thereby the weight average functionality of the cross-links calculated by MM is used to map the results of the DQ measurements on the phantom model. The so-obtained molecular weights are compared to the results of the as well performed MM calculations showing a nearby linear correlation for all three methods when the defects and the functionality are considered precisely.

Authors Contributions. W.C. planned the study, M.L. wrote the programm for MM calculations and presents details of the theory in the appendix. W.C. prepared the samples, performed the measurements and analyzed the data. W.C. wrote the manuscript with some input of K.S. and M.L..

Cross-Link Density Estimation of PDMS Networks with Precise Consideration of Networks Defects

Walter Chassé,*,[†] Michael Lang,[‡] Jens-Uwe Sommer,[‡] and Kay Saalwächter*,[†]

[†]Institut für Physik — NMR, Martin-Luther-Universität Halle-Wittenberg, Betty-Heimann-Strasse 7, D-06120 Halle, Germany
[‡]Leibniz-Institut für Polymerforschung Dresden, e.V., Hohe Strasse 6, D-01069 Dresden, Germany

ABSTRACT: Two series of randomly cross-linked poly(dimethyl-siloxane) (PDMS) networks with systematically varying and well-defined dangling chain and defect content were investigated by ^{1}H double-quantum low-field NMR (DQ NMR), equilibrium swelling, and high-resolution magic-angle spinning NMR (MAS NMR) experiments in order to obtain information about the absolute molecular weight of the polymer chains between two cross-links, M_c, and its distribution. A comparison of the experimental results from swelling and DQ NMR experiments with the results of Miller–Macosko calculations, based upon the reaction turnover determined by MAS NMR, clarifies the importance of a precise estimation of the defect fraction of the polymer network for a reliable determination of M_c. In order to properly account for network defects in the evaluation of equilibrium swelling as well as DQ NMR experiments, we use the elastically effective polymer volume fraction $\phi_{p,el}$ (that can be obtained from DQ NMR or simple Hahn echo experiments on samples swollen in deuterated solvent) and the variable weight-averaged functionality f_{wa} of the cross-links taken from Miller–Macosko calculations. On the basis of the dependence of the so-obtained M_c on f_{wa}, we are able to confirm the validity of the phantom model of rubber elasticity, and find good agreement between the results from the different methods. Small deviations only pertain to a proportionality factor different from unity, which for the case of equilibrium swelling is attributed to the shortcomings of the Flory–Rehner theory. We further address the quantitative interpretation of the residual dipolar coupling constant as the central result of DQ NMR on dry samples, which is confirmed to be proportional to the inverse M_c, but is also subject to systematic errors.
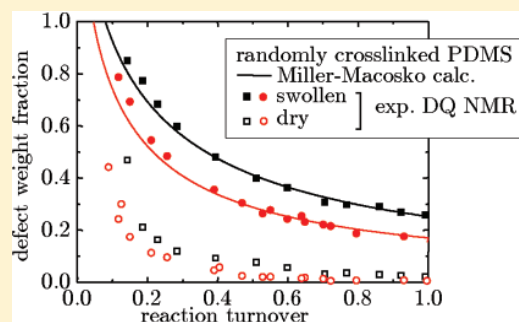
INTRODUCTION

Permanent elastomers are commonly formed via connecting linear polymer chains by chemical cross-links, resulting in a three-dimensional polymer network. Their elastic properties are governed by the length of network strands, functionality of cross-links, (trapped) entanglements and defects. The precise characterization of these topological parameters, especially the molecular weight of polymer chains between two cross-links, M_c, and its influence on the physical properties of the elastomers has been a major task in polymer physics and chemistry for decades, with many open questions to-date.

For the determination of reliable structure–property relationships for elastomers, knowledge of the network structure is essential. A variety of different methodological approaches, e.g., dynamical mechanical analysis,[1] osmometry,[2] inverse gas chromatography,[3] dielectric measurements, and neutron and X-ray scattering, has been applied for this purpose. The most often used experiments for the estimation of the cross-link density are equilibrium swelling, mechanical measurements, such as sulfur and NMR spectroscopy.

The network structure depends strongly on the formation process of the polymer network. Cross-linking techniques as sulfur vulcanization, peroxide curing, and electron or γ-irradiation[4,5] lead to highly complex structures with broad

distributions of network strand lengths and substantial defect fractions due to the random insertion of cross-links.[6−8] Therefore, well-defined model networks are commonly used to study theoretical models of rubber elasticity. An often used method is the controlled end-linking of polymers terminated with special reactive groups.[9,10] Measurements to characterize the polymer chains are performed prior to their cross-linking to determine the number-average molecular weight M_n and the molecular-weight distribution. After the cross-linking with multifunctional cross-linkers, the molecular weight between two cross-links M_c and its distribution is predetermined by the given functionalized polymer chains.[8] Additionally, the functionality of cross-links f is known and the amount of dangling-end defects is assumed to be negligible.[11] The quality of model networks is usually tested by investigating the unreacted amount of functional groups and the fraction of soluble polymer chains ω_{sol}. We note, however, that even a well-defined local structure of polymer networks does not imply a simple network topology, and topological disorder and various kinds of topological defects occur.[12]

Equilibrium swelling is a basic and easily feasible experiment for the determination of M_c. The thermodynamic description is commonly based on the Flory−Rehner treatment[13−15] of swollen polymer networks, which postulates the additivity of the free energy of mixing and the elastic free energy. A series of studies by Brotzman and Eichinger[16−18] indicates serious concerns related with this assumption. The elastic contribution is estimated by a variety of different molecular theories of rubber-like elasticity generally assuming Gaussian statics for the conformation of network strands between two cross-links. The classical and most often used theories are the affine model by Hermans, Flory, and Wall[19,20] and the phantom model by James and Guth.[21,22] These and other models of network elasticity[23] were put to a test in various extensive investigations of model polymer networks, especially of end-linked PDMS.[1,6] Comparisons with mechanical experiments generally show a good coincidence in the qualitative description of network parameters and dependencies, but difficulties are encountered when a quantitative interpretation is sought. Especially the neglect of the influence of defects and distributions in the classical models of network elasticity, and the strong dependence on the rather empirical Flory−Huggins interaction parameter hampers the exact determination of M_c by equilibrium swelling.

Therefore, a precise analysis of the influence of elastically inactive network defects, i.e., dangling chains, loop structures, etc., is essential for a complete account of the network structure and with that, a more quantitative understanding of the mechanical and thermodynamical (swelling) properties of elastomers. For this purpose, networks with well-defined defect content were the subject of previous investigations. Commonly, such networks were prepared by controlled stoichiometrically imbalanced cross-link reactions[24] or by the addition of monofunctional polymer chains.[25,26] Dangling chains, which are attached by only one end to the infinite gel, lead to a reduction of elastically effective polymer chains per unit volume.[27] In mechanical studies it was shown that the storage and loss moduli are quite sensitive to the fraction and molecular weight of pendant chains.[25,28−31] Thereby, the exact defect fraction of the networks is estimated based on the chemical cross-linking mechanism[10] or nonlinear polymerization (mean field) calculations,[26] since an independent quantitative determination on the basis of mechanical or equilibrium swelling experiments is not possible.

In the present work, we address the characterization of the network structure of randomly cross-linked poly(dimethylsiloxane) (PDMS) networks by ^{1}H double-quantum (DQ) low-field NMR and by equilibrium swelling experiments. The results of these readily available routine characterization methods, both of which rely on model assumptions, are compared with absolute-value results for the molecular weight between two cross-links M_c. The latter are taken from calculations based on the statistical theory of cross-linking published by Miller and Macosko,[32] using as input the known molecular weight and polydispersity of the precursor polymers and the extracted sol content, as well as the turnover of the cross-linking reaction as taken from integrated signals in high-resolution ^{1}H magic-angle spinninng (MAS) NMR spectra of the network samples. We demonstrate that the defect fraction of the investigated networks can be identified with high accuracy by decomposition of DQ NMR (alternatively Hahn-echo relaxation) data taken on samples swollen in deuterated solvent. The results are used to investigate different approaches to

considering network defects in the evaluation of equilibrium swelling experiments, and to assess the validity of M_c as calculated from residual dipolar coupling constants $D_{res} \propto M_c^{-1}$ measured on dry samples, where ambiguities arise from the specific model and the defect content of the network.

■ EXPERIMENTAL SECTION

Sample Preparation and Characterization. Two commercially available vinylmethylsiloxane-dimethylsiloxane trimethylsiloxy-terminated random precursor copolymers (rPDMS) with different vinylmethylsiloxane concentration, purchased from ABCR company and used as-received, were used to prepare the investigated silicone networks. Both prepolymers were characterized by gel permeation chromatography (GPC) to obtain information about the molecular weight and polydispersity. The ratio of dimethylsiloxane to vinylmethylsiloxane monomers was determined by ^{1}H solution NMR. For this purpose, the prepolymers were dissolved in deuterated toluene and ^{1}H spectra were recorded. The intensity of the measured signals is directly proportional to the amount of protons at the methyl and vinyl groups. Thus, a precise estimation of the average number of vinyl-functionalized monomers per dimethylsiloxane monomer, ρ_{vinyl}, was possible by comparing the integrals of the different signals. The results of the GPC and NMR measurements are given in Table 1. The two

Table 1. Results of Sample Characterization by GPC and ^{1}H Solution NMR

polymer	M_n/kDa (GPC)	M_w/kDa (GPC)	M_w/M_n (GPC)	ρ_{vinyl} (NMR)
rPDMS-431	11.2	29.4	2.6	0.0426
rPDMS-731	12.5	32.2	2.6	0.0776

prepolymers differ slightly in their molecular weight and by about a factor of 2 in the density of vinylmethylsiloxane comonomers.

The vinyl-functionalized polymers were cross-linked by using a 2-functional cross-linker (1,1,3,3-tetradimethyldisiloxan, ABCR) and *cis*-dichlorobis(diethyl sulfide)platinum(II) as catalyst. Because of monofunctional impurities, its average functionality is 1.81, as again determined by solution NMR. The un-cross-linked polymer and the cross-linker were dissolved in 20 wt % of toluene with respect to the used amount of polymer to facilitate homogeneous mixing of the components. After adding the catalyst, the sample tube was sealed and stored for 7 days at room temperature. The details of the cross-link reaction are described in ref 33. After the cross-link reaction was completed, the toluene was evaporated carefully.

For the preparation of networks with different cross-link densities, the amount of cross-linker was chosen so as to react with a defined percentage of the vinyl groups. The used amounts of cross-linker are based upon the known density of vinylmethylsiloxane monomers ρ_{vinyl} from the solution NMR measurements. For the estimation of the actual fraction of reacted vinyl groups during cross-linking, henceforth referred to as the reaction turnover p_r, high-resolution ^{1}H spectra of all networks were measured by magic-angle spinning (MAS) NMR. In Figure 1, the MAS spectra of polymer networks made of rPDMS-431 are shown, demonstrating the good resolution of the spectra, almost matching solution-state conditions. By comparing the integral ratio of vinyl and methyl groups of the prepared polymer networks to the ratio of these in the un-cross-linked prepolymers, the reaction turnover could be determined with high precision. The intended and measured reaction turnovers p_r of the vinyl-groups for the rPDMS-431 samples are listed in Table 2.

NMR Spectroscopy. The ^{1}H DQ solid-state NMR experiments were carried out on a Bruker minispec *mq*20 spectrometer operating at a resonance frequency of 20 MHz with a 90° pulse length of 2.8 μs and a dead time of 13 μs. The experiments and the analysis of the measured raw data were performed following the previously published procedures.[36−38] For the experiments on swollen networks, deuterated toluene was used as swelling solvent. The used sample amounts were
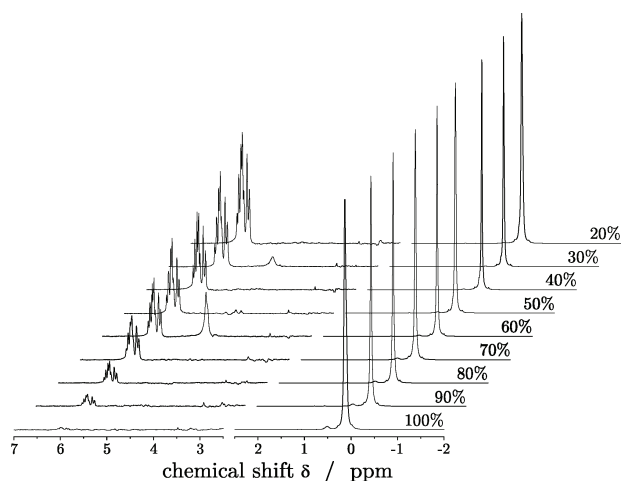
Figure 1. ^{1}H MAS spectra of rPDMS-431 networks cross-linked with different amounts of cross-linker, with the intended reaction turnover p_r indicated on the right. For clarity, the vinyl signal region (6.2–5.8 ppm) is amplified 100 times over the methyl signal (~0 ppm). The signal at 5 ppm is an unknown impurity, presumably water.

about 300 mg for measurements on dry networks and between 100 and 200 mg for measurements on swollen networks.

Equilibrium Swelling Experiments. The equilibrium swelling experiments were carried out at room temperature (21 °C) using toluene (molar volume V_s = 106.2 mL/mol, density ρ_s = 0.87 g/cm^3) as swelling solvent. The samples were weighed as-prepared (m_0) and swollen for 4 days to equilibrium. Swollen samples were blotted with tissue paper to remove the excess of toluene and weighed immediately (m_{sw}). Finally, the swelling solvent was evaporated carefully from the networks over a couple of days and the dry samples were weighed again (m_{dry}). For each sample, at least five pieces of different shape and weight of all prepared networks were investigated.

The sol content ω_{sol} is the fraction of polymer chains not coupled to the network after the cross-link reaction, and is was extracted from the samples during swelling. The sol fraction ω_{sol} was estimated by comparing the weight of the networks as-prepared m_0 and the weight of the dry networks m_{dry} corresponding to eq 1,

$$\omega_{sol} = \frac{m_{dry} - m_0}{m_0} \tag{1}$$

The equilibrium degree of swelling Q, and with that the volume fraction of polymer in the swollen network $\phi_p = 1/Q$ were calculated according to eq 2 using ρ_p = 0.97 g/cm^3 for PDMS.

$$Q = \frac{1}{\phi_p} = \frac{V_{sw}}{V_{dry}} = \frac{m_{dry}/\rho_p + (m_{sw} - m_{dry})/\rho_s}{m_{dry}/\rho_p} \tag{2}$$

All results of the swelling experiments with the rPDMS-431 networks are specified in Table 2. For their evaluation, we need the effective Flory−Huggins interaction parameter χ of the PDMS/toluene systems. It was investigated in several studies[4,39−43] by different experimental approaches, i.e., light scattering, osmometry and SANS. χ is generally not a constant and may attain different values in swollen networks vs solutions of linear polymers, highlighting the shortcomings of the Flory−Huggins mean-field theory as a basis for the calculation of the molecular weight between two cross-links, M_c.[44] See below for details. In this work, we use the volume-fraction dependent Flory−Huggins interaction parameter

$$\chi = 0.459 + 0.134\phi_p + 0.59\phi_p^2 \tag{3}$$

which was determined by osmotic deswelling experiments on different end-linked PDMS gels which were fitted to the Flory−Rehner model.[43]

METHODOLOGICAL BACKGROUND

Determination of M_c and the Network Defect Fraction by ^{1}H DQ NMR Experiments. ^{1}H multiple-quantum solid state NMR spectroscopy[38,45] is a robust quantitative and versatile technique for the investigation of structure and dynamics in polymer networks and melts. In contrast to more traditional approaches such as Hahn-echo relaxometry, the essential advantage of this method is the measurement of two qualitatively different sets of data, the decaying reference intensity I_{ref} and the DQ build-up intensity I_{DQ}, both measured as a function of the DQ evolution time τ_{DQ} in subsequent experiments that only differ in the phase cycling of the receiver. See Figure 2 for sample data. On the basis of the data processing procedure described below, it is possible to reliably distinguish between (and characterize) the elastically active network chains that contribute to I_{DQ} and network defects, sol, and solvent, which contribute to I_{ref} in particular at long times.

Data Processing and Determination of the Defect Fraction. I_{DQ} is dominated by spin-pair DQ coherences[36,45]

Table 2. Results of the Characterization of rPDMS-431 Network Samples, with the Intended Reaction Turnover in % as Part of the Sample Name (cXXX)[a]

| | MAS NMR | DQ NMR | | | | | swelling | | Miller−Macosko |
sample	p_r	$\omega_{def,dry}$	$\omega_{def,sw}$	$D_{res}/2\pi$ [kHz]	$\sigma/2\pi$ [kHz]	$r_G = \sigma/D_{res}$	ω_{sol} [% of m_0]	$Q = V/V_0$	f_{wa}
c100	0.991	0.022	0.257	0.425	0.273	0.557	4.45	2.70	3.60
c090	0.921	0.027	0.270	0.413	0.231	0.560	5.36	2.70	3.58
c080	0.860	0.030	0.290	0.362	0.215	0.593	5.66	3.02	3.55
c075	0.768	0.036	0.297	0.309	0.177	0.571	6.23	3.29	3.51
c070	0.705	0.031	0.308	0.293	0.168	0.574	7.03	3.36	3.48
c060	0.598	0.056	0.363	0.241	0.144	0.597	8.26	3.71	3.41
c050	0.510	0.076	0.400	0.183	0.100	0.548	9.84	4.34	3.33
c040	0.394	0.092	0.481	0.138	0.084	0.609	13.77	5.08	3.21
c030	0.284	0.120	0.598	0.089	0.050	0.565	20.37	6.85	3.01
c025	0.229	0.163	0.683	0.069	0.040	0.580	25.47	9.20	2.87
c020	0.187	0.213	0.773	0.047	0.025	0.542	30.28	12.07	2.72
c015	0.142	0.469	0.850	0.034	0.023	0.681	42.51	21.89	2.51

[a]D_{res} is the average of the coupling constant distribution obtained by regularization of the normalized DQ build-up curves by using fast Thikonov regularization,[34,35] and the distribution width is characterized by the variance σ. Note that D_{res} and σ are obtained from measurements on dry network samples.
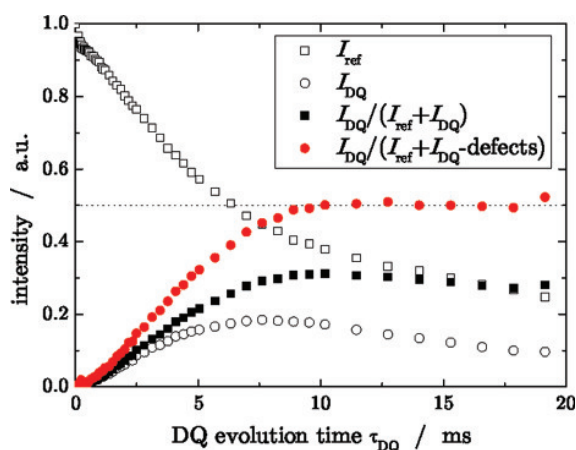
Figure 2. Experimental I_{DQ} and I_{ref} for the randomly cross-linked rPDMS-431 sample c020 and corresponding normalized I_{nDQ} data,

and comprises the structural information on the polymer chains, i.e., the residual dipolar coupling constant D_{res} and its distribution. Technically, I_{ref} contains signal from half of the quantum orders ($4n$) of the dipolar coupled network chains, as well as the signal from uncoupled components, i.e. isotropically mobile network defects like dangling chains and loops. The particular network fractions are characterized by a rather different relaxation behavior, as is apparent in Figure 3. The signals of
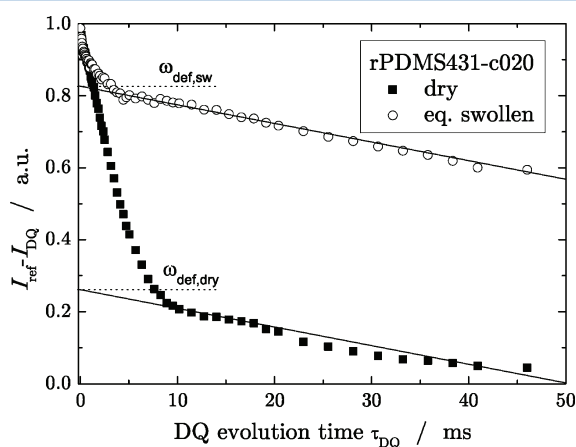
Figure 3. Experimental estimation of the defect weight fractions ω_{def} and $\omega_{def,sw}$ of the rPDMS-431 sample c020 from the difference of reference and DQ intensities ($I_{ref} - I_{DQ}$), measured in dry and equilibrium swollen state using deuterated solvent (closed and open symbols, respectively).

uncoupled, elastically ineffective defects show a slow exponential decay, while coupled network components relax much faster.[46] Plotting $I_{ref} - I_{DQ}$ amplifies this behavior and enables a quantitative identification and subtraction of the contribution of the network defects to the reference intensity I_{ref}; see ref 38 for details. The structural information on the polymer network (build-up due to D_{res}, see below) is separated from the relaxation effects due to chain dynamics by a point-by-point division of the DQ build-up by the sum of the corrected relaxation function (eq 4). The obtained normalized DQ build-up I_{nDQ} is then independent of relaxation effects and has to reach a

long-time plateau value of 0.5, since I_{DQ} contains only half of the excited quantum orders ($4n + 2$).

$$I_{nDQ} = \frac{I_{DQ}}{I_{DQ} + I_{ref} - \text{defects}} \qquad (4)$$

Note that both raw data intensities are, in the relevant data range of growing I_{DQ}, indeed dominated by spin dynamics among the quantum orders 0 (longitudinal magnetization) and 2, while higher-order coherences contribute only at later times and have a negligible effect.[36] We thus refer to the method as DQ NMR in the following.

The plateau of I_{nDQ} is only observed after a proper determination and subtraction of elastically ineffective defects (see Figure 2), providing a test for their precise quantification. Note that the apparent fraction of noncoupled network defects ω_{def} obtained by DQ NMR experiments can exhibit a significant dependence on cross-link density and in particular on temperature,[47] where the latter is related to the terminal relaxation of possibly large and branched structures being slow on the millisecond time scale of the DQ experiment (corresponding to slow mechanical relaxation processes in such imperfect networks). The defect fraction may thus be largely underestimated.

In dry networks, this problem can only be addressed by increasing the experimental temperature.[47] Another, more effective approach is the determination of defects in swollen networks by DQ NMR. Because of the network dilation by the solvent during the swelling process and the corresponding release of packing or topological constraints, the terminal relaxation of the defects is much accelerated. The solvent further acts as plasticizer, which also speeds up the chain dynamics. Motions of previously constrained defects thus become isotropic and the dipolar couplings ultimately average out. Figure 3 displays the change in the isotropically mobile fraction upon swelling. The detectable fraction of noncoupled and therefore elastically ineffective network defects in the equilibrium swollen sample $\omega_{def,sw}$ is considerably increased in comparison to the fraction in dry samples $\omega_{def,dry}$. Thus, the much decreased or even completely absent influence of restrictions on the relaxation time of defects in equilibrium-swollen samples allows for a reliable and precise quantitative estimation of the defect fraction in polymer networks. See below for an in-depth discussion of the observed drastic difference between $\omega_{def,sw}$ and $\omega_{def,dry}$ in the given samples.

The dependence of the detectable defect fraction and in particular of the residual coupling on the swelling degree below equilibrium will be discussed in more detail in an upcoming publication. Importantly, the observed defect fraction saturates already at solvent contents much below equilibrium swelling, which is equivalent to temperature variation, suggesting that the defect fraction is quantitatively determined under the given conditions. Note that the average residual coupling changes nontrivially upon addition of good solvent,[48] and its determination is further challenged by the appearance of swelling inhomogeneities, leading to broad D_{res} distributions.[49] Finally, it should be noted that simple Hahn−echo decay curves are in principle also suitable for a determination of the amount of slowly relaxing nonelastically active defects.[38]

Determination of M_c. After a proper subtraction of the defect contribution to I_{ref}, the normalized DQ build-up curve I_{nDQ} solely reflects the residual dipolar interactions that are related to the network structure. These are proportional to the

dynamic segmental order parameter that is associated with the degree of anisotropy of rotational motion of the monomers (cf. Appendix), arising from the fact that the chain in question is fixed at its ends, at least on the time scale of the experiment itself (i.e., many milliseconds). Usually, residual dipolar interactions are evaluated by fitting a distribution function, eq 5, to the initial rise of I_{nDQ} assuming a Gaussian distribution of dipolar couplings.[36,37]

$$I_{nDQ}(\tau_{DQ}, D_{res}, \sigma) = \frac{1}{2}$$
$$\left(1 - \frac{\exp\left\{ -\frac{\frac{2}{5}D_{res}^2\tau_{DQ}^2}{1 + \frac{4}{5}\sigma^2\tau_{DQ}^2} \right\}}{\sqrt{1 + \frac{4}{5}\sigma^2\tau_{DQ}^2}} \right) \tag{5}$$

The average apparent residual dipolar coupling constant D_{res} and its standard deviation σ, characterizing the width of the distribution, are obtained by this approach. In polymer networks with $M_c < M_e$, the experimental D_{res} is directly proportional to the cross-link density[50] and thus related to the molecular weight between two cross-links M_c. The proportionality factor depends on the investigated polymer, specifically, it involves a model accounting for chain stiffness (commonly characterized by Flory's characteristic ratio), and details on the spin dynamics among the protons in the monomer unit. On the basis of a fixed-junction model and explicit spin dynamics simulations, in ref 37 an approximate relation is derived for PDMS networks, eq 6, allowing for a direct determination of the average M_c from DQ NMR experiments:

$$M_c^{PDMS} = \frac{1266\ Hz}{D_{res}/2\pi} \frac{f - 2}{f}\ kg/mol \tag{6}$$

The factor $f - 2/f$ depending on the (average) functionality f of the cross-links discussed below is newly introduced in this work, and arises when the phantom model is taken as the theoretical basis. Details can be found in the Appendix. One of the purposes of this work is the evaluation of the validity of this relation, for which systematic errors on the order of 40% can be expected.

Polymer networks with spatially inhomogeneously distributed cross-links show a distribution of coupling constants. For relative distribution widths $r_G = \sigma/D_{res} \geq 0.3$ the initial buildup of I_{nDQ} is not well described by the Gaussian fitting function. Therefore, eq 5 gives just a rough estimate of the average coupling constant.[37] In order to obtain a more quantitative picture of the actual residual dipolar coupling distribution, numerical inversion procedures based on fast Tikhonov regularization (*ftikreg*) can be applied.[34,36] In a recent publication,[35] we have introduced a modified version of the fitting procedure using an improved Kernel function which provides precise and reliable results for the coupling constant distributions.

$$I_{nDQ}(\tau_{DQ}, D_{res}) = 0.5$$
$$(1 - \exp\{ -(0.378 D_{res}\tau_{DQ})^{1.5}\}$$
$$\times \cos(0.583 D_{res}\tau_{DQ})) \tag{7}$$

In Figure 4, the coupling constant distributions obtained by regularization with *ftikreg* are shown for some networks

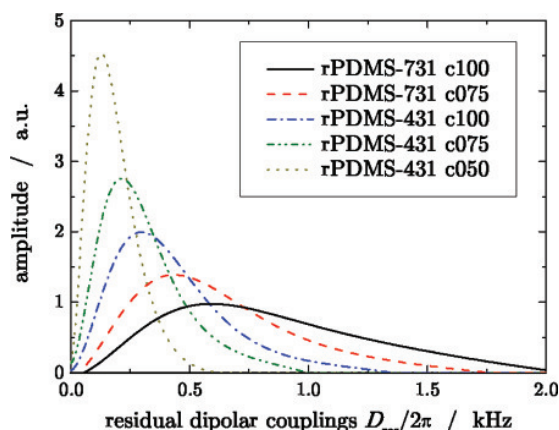**Figure 4.** Residual dipolar coupling distributions of rPDMS samples obtained by analysis of the normalized build-up curve I_{nDQ} with the improved *ftikreg* fitting routine.[35]

investigated in this study. The average residual dipolar coupling constant D_{res} and its variance σ are determined from the distributions. The results of this analysis are used for the characterization of the network structure and the calculation of the molecular weight between two cross-links according to eq 6.

Determination of M_c by Swelling Experiments: Flory–Rehner Theory. Bringing polymer networks in contact with appropriate solvents, the concentration difference causes an osmotic pressure, which is the driving force for the swelling process. The change of the total free energy ΔG^{tot} of the system depends thereby on the change due to the elastic deformation of the network ΔG^{el} and to the mixing of polymer and solvent ΔG^{mix}. The Flory–Rehner theory[13] for the thermodynamics of swollen polymer networks postulates that the two contributions to the free energy are separable and additive. This assumption has been discussed extensively and controversially in the literature.[16−18,51] According to Flory and Rehner, ΔG^{total} is expressed in terms of the change in the chemical potential of the swelling solvent, eq 8:

$$\frac{\Delta \mu_s^{total}}{RT} = \frac{\Delta \mu_s^{mix}}{RT} + \frac{\Delta \mu_s^{el}}{RT} \tag{8}$$

The mixing term, which considers the interaction between the polymer and the swelling solvent molecules, consist of an entropic and an enthalpic contribution. Commonly it is calculated according to eq 9, which is derived from the Flory–Huggins solution theory:[52,53]

$$\frac{\Delta \mu_s^{mix}}{RT} = \ln(1 - \phi_p) + \phi_p + \chi\phi_p^2 \tag{9}$$

As mentioned above, this simplified mean-field theory is subject to limitations, meaning that the Flory–Huggins polymer–solvent interaction parameter χ is experimentally found to depend explicitly on the polymer volume fraction at swelling equilibrium ϕ_p and temperature T.[54]

Furthermore, the estimate for the elastic contribution to the chemical potential depends the used network model. Classical approaches are the affine[19,20] and the phantom[21,22] models. In recent years, it was proposed that the phantom model should describe the behavior of swollen networks more appropriately.[44]

For this case, the following expression for $\Delta\mu_s^{el}$ holds:

$$\frac{\Delta\mu_s^{el}}{RT} = \frac{\rho_p V_s}{M_c}\left(1 - \frac{2}{f}\right)\phi_p^{1/3} \tag{10}$$

where f represents the functionality of the cross-links, and M_c is the number-average molecular weight between two cross-links.

At swelling equilibrium, the gain in free energy upon mixing is exactly balanced by the free energy loss due to network deformation. Hence, the total change in the chemical potential vanishes. Combining eq 9 and eq 10 at equilibrium yields the well-known Flory−Rehner equation, eq 11:

$$\ln(1 - \phi_p) + \phi_p + \chi\phi_p^2 = -\frac{\rho_p V_s}{M_c}\left(1 - \frac{2}{f}\right)$$
$$\phi_P^{1/3} \tag{11}$$

The difficulties in determining M_c by equilibrium swelling experiments are discussed in detail by Valentín et al.[44]

In order to consider the effect of network defects for the estimation of M_c, the mixing (eq 9) and elastic (eq 10) terms of the Flory−Rehner-equation must be treated differently. According to the Flory−Huggins theory, all monomer units belonging to the polymer network contribute equally to the mixing entropy and enthalpy in the calculation of the mixing term. Thus, a distinction between elastically effective and ineffective parts of the polymer network is not necessary, whereas the entropic elastic restoring forces only arise from elastically effective polymer chains. Therefore, just a certain fraction of polymer network ω_{el} is taken into consideration for the calculation of the elastic contribution, eq 10. The volume fraction of elastically effective polymer material in the equilibrium swollen sample $\phi_{p,el}$, eq 12, is estimated by using the results of the DQ NMR measurements of the defect fraction $\omega_{def,sw}$ in the polymer network.

$$\phi_{p,el} = \omega_{el}\phi_p = (1 - \omega_{def,sw})\phi_p \tag{12}$$

The molecular weight between two cross-links M_c is thus calculated using the modified Flory−Rehner equation, eq 13:

$$M_c = -\frac{\rho_p V_s(1 - 2/f)\phi_{p,el}^{1/3}}{\ln(1 - \phi_p) + \phi_p + \chi\phi_P^2} \tag{13}$$

Furthermore, the functionality of cross-links f plays an important role in the determination of M_c by swelling experiments. The functionality depends on the number of chemically linked polymer chains at a cross-link, and $f = 4$ should be expected for the given system. For networks in which a significant fraction of cross-links does not have f active connections to the network, one has to replace the functionality f by the weight-average number of attached active strands per cross-link, f_{wa}.

For the consideration of this effect, calculations based on the Miller−Macosko theory of cross-linking[32] are used to obtain information about the weight-averaged functionality f_{wa} of the investigated networks. Details of these calculations are given in the Appendix, and the results are given in Table 2. The actual computations are performed by a Fortran code that first reads in the precursor molecular weight distribution of the polymers. Then, equation eq A1 is computed numerically for all molecular weights of the sample. The following equations in the Appendix

are then evaluated step by step based on the numerical solutions of the distribution functions of previous steps. Note that the procedure was tested against exact solutions of the most probable and a uniform weight distribution. We note that the so-obtained f_{wa} is as low as 2.5 for the least cross-linked networks close the gel point, and reaches only values of about 3.6 at the highest conversions. The influence of $\phi_{p,el}$ and f_{wa} will be discussed in detail below.

■ RESULTS AND DISCUSSION

The main goal of this work is the determination of the molecular weight between two cross-links M_c in randomly cross-linked polymer networks with a precise consideration of defects. First, we will discuss the experimental results of the sample characterization by equilibrium swelling and DQ NMR experiments. The results are then compared with Miller−Macosko calculations based upon the experimentally determined sol fraction and the reaction turnovers from MAS NMR. Finally, M_c values obtained from the different approaches are correlated and the impact of network defects is demonstrated and discussed.

The desired reaction turnovers and the p_r determined by MAS NMR are in overall good agreement. In some cases, apparently more vinyl groups (2−6%) than expected were consumed during cross-linking (see Table 2), which appears counterintuitive. This can be attributed to the fact that the stoichiometric ratio of functionalized groups and cross-linking agent was adjusted to the average functionality 1.81 of the latter, due to an impurity fraction of monofunctional cross-linker. This latter fraction was probably slightly overestimated in the precharacterization. In any case, even samples with complete reaction turnover also contain some amount of consumed vinyl groups which do not lead to chemical cross-links.

Sol Fraction ω_{sol}. The fraction of polymer chains which were not connected to the infinite gel by permanent chemical cross-links during the network formation was obtained from the equilibrium swelling experiments. Figure 5 shows a continuous
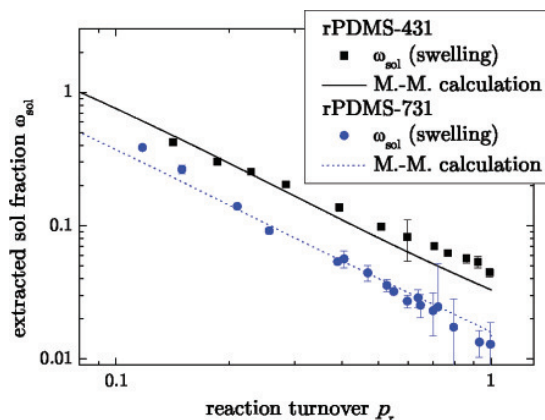
Figure 5. Variation of the extracted fraction of soluble network components ω_{sol} during equilibrium swelling as a function of the amount of reacted functional groups p_r during cross-linking along with results of Miller−Macosko calculations.

increase of extracted sol ω_{sol} from the networks with decreasing amount of used cross-link agent for sample preparation.

It is known for cross-linking reactions that a non-negligible fraction of cross-links is wasted in short dangling loops.[55]

Additionally, about 19% of the added cross-links are monofunctional. In order to determine the fraction of cross-linked sites wasted in dangling loops or connected to monofunctional cross-links, and to restrict the analysis to actual cross-links which connect different chains, we computed the sol fraction as a function of p_r based on the known fraction of cross-linked sites. Next, we assumed that a constant fraction p_b (cf. Appendix) of these reacted sites does not lead to dangling loops and determined $p_b \approx 0.72$ and 0.66 for rPDMS-431 and rPDMS-731 samples, respectively, simply as a scaling factor (shift in logarithmic units, see Figure 5) between the data points and the original theoretical prediction. The theoretical lines in Figure 5 show the predictions for a branching fraction of $p_b p_r$ cross-links. The good agreement between data points and theory indicate that the assumption of constant fraction of cross-links is reasonable and that ignoring the weight fraction of dangling loops is of minor importance, as also shown previously.[55] Note that all later computations are based on the reduced fraction $p_b p_r$ of cross-links. The already considerable fraction of sol extracted from networks with a high degree of cross-linking can be attributed to the broad molecular weight distribution of the precursor polymers. Chains with low molecular weight show a reasonable probability of having no functionalized monomer. This assumption is supported by molecular weight distributions of the extracted sol obtained by GPC measurements. The percentage of polymer chains with a molecular weight lower than the average weight between two functionalized monomers in the melt is extracted nearly completely. This fraction stays roughly constant for decreasing reaction turnovers while the amount of high-molecular-weight sol increases notably.

Defect Fraction ω_{def}. The fraction of network defects was determined by ^1H DQ NMR experiments on sol-extracted networks, providing an absolute and precise measure. Results of the measurements in dry and equilibrium swollen samples are shown in Figure 6. The amount of defects identified in dry
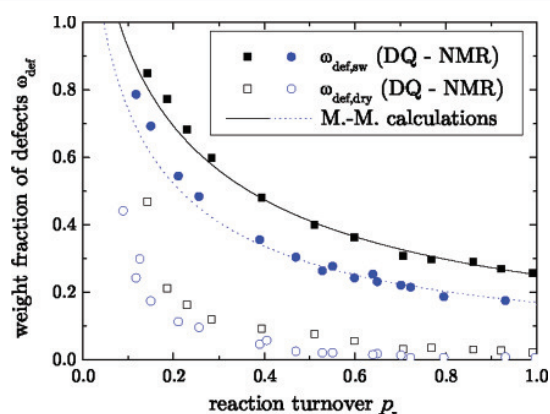
Figure 6. Fraction of network defects measured by DQ NMR in dry and equilibrium swollen rPDMS-431 (squares) and -731 (circles) samples, along with results of Miller–Macosko calculations in dependence of the reaction turnover p_r.

networks is of the order of a few percent and just slightly increases with decreasing reaction turnover. A significant increase of the measured defect fractions is observed only for reaction turnovers smaller than 50%. The accuracy of this low detected defect fraction is at least questionable, taking into account the way of cross-linking and the used prepolymers for

the studied samples. Because of the randomly distributed functionalized comonomers in the relatively short prepolymer backbones, even networks with 100% reaction turnover should have a nonzero amount of elastically inactive, dangling, and possibly branched material.

The fraction of defects depends primarily on the absolute number of possible cross-link sites along the polymer backbone and therefore, on the density of functionalized monomers ρ_{vinyl} and the length of the prepolymers. At low to moderate turnovers, at which the probability of simple chain extension reactions is higher, the molecular weight distribution of dangling chains is rather broad, and complex branched structures are present. An increase of the used amount of cross-linker primarily decreases the size of the dangling chain defects, and the defect fraction becomes dominated by linear dangling ends.[55] Because of the reasons discussed above, the used prepolymers with a broad molecular weight distribution generally causes an increase in the overall defect fraction.

The findings of a low fraction of nonelastic network defects measured in dry samples and the much increased fraction in swollen samples, see Figure 6, could be interpreted in different ways. Generally, if defects are present that are large or irregularly branched, their embedding in a dry cross-linked matrix renders them unobservable because the network constraints impede their terminal relaxation on the experimental time scale of the DQ NMR measurements. In this way, topological restrictions lead to similar nonisotropic motions of the associated chains on a time scale of ms as do chemical cross-links. A distinction between defects embedded in the network structure and elastically active polymer chains between two cross-links is thus not possible as they both contribute in a similar way (with similar apparent D_{res}) to the measured signal. Note that the slow relaxation of such defect structures contributes similarly to the mechanical properties, for instance, the stress relaxation modulus $G(t)$ or inversely, the time-dependent compliance $J(t)$, in defect-rich samples approach their rubber-elastic plateau values only very gradually.[56,57]

However in the given samples and in particular at high conversion, the defect fraction is expected to be dominated by dangling ends of moderate molecular weight around or below the entanglement threshold ($M \leq M_e$), since rather short precursor polymers were used.[55] While it cannot be fully excluded that the topological structure of the defects in the given samples differs from the theoretical expectation, this nevertheless raises the question why a large part of the expected linear structures may not be able relax on the experimental time scale. The clarification of this issue is the subject of ongoing work, and we here sketch the starting point.

Our previous studies on polymer melts have approximately confirmed that the outer M_e portion of a highly entangled linear chain moves isotropically and is thus elastically inactive.[58] One may speculate that the isotropic fraction decreases if the chain is embedded in a highly cross-linked matrix (corresponding to an effectively narrower "tube"), and/or that intermolecular packing correlations have an effect on the motional anisotropy of the chains. The latter effect was previously addressed theoretically as a possible additional contribution to network elasticity and segmental orientation phenomena as detected by NMR.[59] In any way, the relatively narrow observed D_{res} distributions, see Figure 4, suggest that the defect fraction that is not relaxed on the time scale of the experiment exhibits a similar motional anisotropy as the network component, as it does not appear as a separate peak in the distribution.

Whatever the nature of the restrictions, network dilation due to swelling of the network samples leads to two opposing effects. On one hand, elastically active polymer chains are stretched, possibly amplifying the nonisotropic character of their motions. On the other hand, the topological or packing restrictions for defects are released for the most part, speeding up their terminal dynamics and enabling isotropic motion on the experimental time scale. The dynamics is of course further enhanced as a consequence of the plasticizer effect of the solvent. The different dynamic behavior of elastically effective and ineffective network fractions is thus amplified in swollen polymers and allows a precise distinction of their contribution to I_{ref} and I_{DQ}. It can therefore be assumed that results obtained by measurements on samples in swollen state give an accurate estimation of the actual defect fraction in polymer networks.

This assumption is proven by the near quantitative agreement of the experimental defect fraction $\omega_{def,sw}$ measured in equilibrium swollen samples by DQ NMR and the Miller–Macosko calculations, see Figure 6, reminding that the theoretical prediction is based upon p_b (see Appendix) as an independently determined single constant which results from fitting the experimental sol fraction of all samples of one series. The agreement shows the consistency of our analysis and strongly supports that we can achieve an accurate quantitative analysis of network structure. We note again that the residual coupling D_{res} taken from I_{nDQ} in *swollen* networks is subject to a wide distribution arising from swelling heterogeneities,[49] and is further strongly influenced by excluded-volume interactions in good solvent,[48] posing challenges to its determination and interpretation

**Residual Dipolar Coupling Constants and Their Distribution.** Figure 7 shows the average residual dipolar
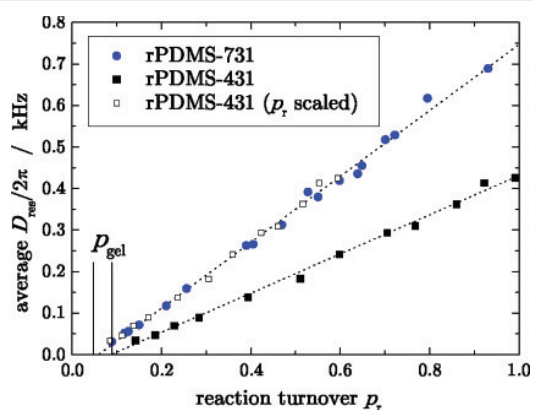
Figure 7. Relationship between the residual dipolar coupling constant D_{res} measured in dry rPDMS-431 (squares) and -731 (circles) samples, and reaction turnover p_r of vinyl-groups. D_{res} is the average of the coupling constant distribution obtained by regularization. The dashed lines represent linear fits of the data. The solid lines indicate the gel point obtained by the M.-M. calculations.

coupling constants D_{res} of the dry network samples in dependence of the reaction turnover p_r. The latter were obtained by using the numerical inversion procedure *ftikreg* for the evaluation of the normalized double-quantum build-up curves I_{nDQ}. For both series of polymer networks an apparent linear decrease of D_{res} with decreasing amount of cross-link agent is observed. In order to demonstrate the universality of the observation, the results of rPDMS-431 are scaled with respect to the ratio of the densities

of functionalized monomers ρ_{vinyl} in the two prepolymers. The near-perfect agreement of both prepared network series shows that the coupling constant mainly depends on the average number of monomer units between two chemical cross-links. We interpret the intercept of the linear fits of the data with the *x*-axis as an empirical measure of the minimum reaction turnover to obtain a network, in qualitative agreement with our previous observations.[60] These experimental estimations of the gel point, p_{gel}, are now again found to be in very good agreement to the results of Miller–Macosko calculations indicated by the vertical solid lines in Figure 7. It must be noted that this analysis is only possible because the used prepolymers are hardly entangled, meaning that the pure precursor melts do not exhibit measurable residual dipolar couplings arising from entanglements on the time scale of the DQ experiment at the given temperature. A detection of the gel point in terms of D_{res} would not be possible in systems of highly entangled, slowly reptating prepolymers.

In ideal monodisperse *f*-functional networks, the average residual dipolar coupling constant is related to the molecular weight between two cross-links, see eq 6. Since the measured coupling constant depends both on molecular weight between the cross-links and cross-link fluctuations,[50] a narrowing of the distribution of coupling constants as compared to the most probable weight distribution is expected and will be discussed in a forthcoming work. An important immediate consequence of this is that phantom-model considerations can be employed to provide a simple account of the cross-link fluctuations, as explained in the Appendix. This leads to the *f*-dependent correction factor for the DQ NMR results newly introduced in eq 6.

Since both, the average cross-link fluctuations and M_c, are roughly $\sim 1/p_r$, no significant changes in the width of the coupling constant distribution are expected as confirmed by Figure 8, which represents the ratio r_G between the variance σ
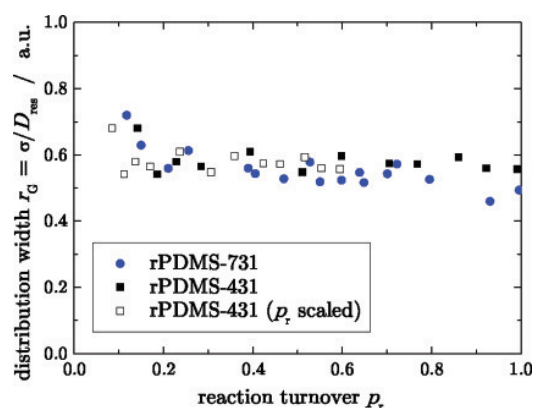
Figure 8. Variation of the relative width of the distribution of coupling constants as a function of reaction turnover p_r for samples rPDMS-431 and rPDMS-731. D_{res} represents the average and σ the variance of the coupling constant distribution obtained by regularization.

and the average D_{res} of the coupling constant distribution obtained by regularization of the normalized double-quantum build-up curve I_{nDQ} as a function of the reaction turnover p_r. The spatial distribution of cross-links has no significant dependence on the reaction turnover and ensures the comparability of the prepared networks. Additionally, this confirms a reasonably good mixing of the prepolymers and the cross-link agent prior to the cross-link reaction. We note again that even
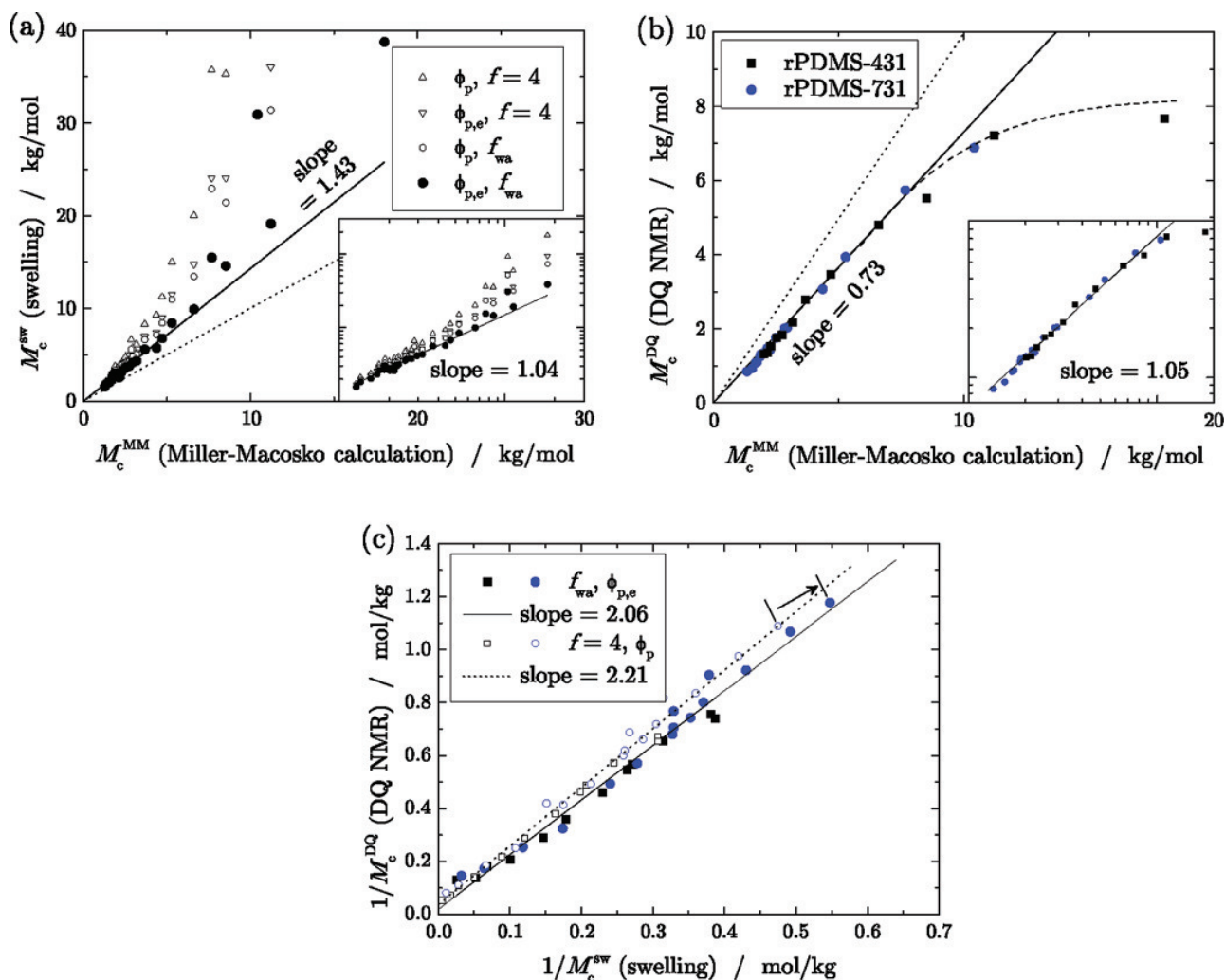
Figure 9. Comparison of the molecular weights between cross-links obtained by the different methods: (a) M_c for all samples from equilibrium swelling vs Miller−Macosko calculations, the former evaluated in different ways as discussed in the text, (b) M_c from DQ NMR using f_{wa} in eq 6 vs Miller−Macosko calculations, (c) cross-link density $1/M_c$ from DQ NMR vs swelling with or without consideration of defects in the analysis. The dotted lines in parts a and b have unity slope, and the insets show log−log representations of the data with fits allowing for a variable scaling exponent. The dashed line in (b) indicates the expected influence of entanglements. The arrow in part c connects two points from identical samples, demonstrating the magnitude of the f_{wa}- and $\phi_{p,e}$-dependent correction.

though a considerable amount (>20%) of defects with potentially low residual coupling contributes to the total D_{res} measured on dry networks (see Figure 6), it is not possible to discern these as separate component in the D_{res} distributions.

The results in Figure 8 compare well with previous findings,[36] but it should be noted that the width of the observed D_{res} distributions is still larger than those observed, for example, for vulcanized natural rubber.[37,47] In our recent paper concerned with the universality of I_{nDQ} curves for very homogeneous rubbers,[35] we have shown that even more homogeneous PDMS networks ($r_G \approx 0.1$) can in fact be prepared when the cross-linking is carried out at higher solvent content, facilitating mixing and diffusion of the reactants. This recent result demonstrates that the residual moderate inhomogeneity (distribution width) of the given samples is either due to spatial cross-linking inhomogeneities on a larger length scale (many mesh sizes), or to the mentioned defect fraction, or both.

Comparison of Molecular Weights between Cross-Links. Three completely different methods, DQ NMR, swelling experiments, and Miller−Macosko calculations based upon quantitative MAS NMR and the experimental sol content, were used to determine the molecular weight between two cross-links M_c. The D_{res} results of the DQ NMR measurements on dry network samples were evaluated according to eq 6, which takes into account the cross-link functionality-dependent correction arising from the phantom model (see Appendix). The Miller−Macosko approach, which we take as the standard for absolute (least model-dependent) M_c-determination, most directly yields the average number of monomers of an active network strand, cf. eq A2. The equilibrium swelling experiments were evaluated according to the Flory−Rehner treatment addressed above. For the calculation of the actual molecular weights, different values for the functionality of the cross-links, $f = 4$ vs variable f_{wa}, and the different volume fractions of the network component, ϕ_p vs $\phi_{p,el}$, were used.

We first focus on a comparison of the Miller−Macosko M_c^{MM} with the different swelling results, M_c^{sw}, plotted in Figure 9a. The functionality of cross-links in randomly cross-linked polymer networks is usually assumed to be four,[44] but the comparison shows that the relation to M_c^{MM} is then decisively nonlinear, see the triangles in the log−log inset. This can be attributed to an overestimation of the elastic contribution to the Flory−Rehner equation, related to an overestimation of the functionality of the networks. The results of the Miller−Macosko calculations for the weight-averaged cross-link functionality f_{wa}, see Table 2, confirm this assumption and reveal a distinct dependence of on the degree of cross-linking. For the polymers used in this study the number of possible cross-link sites is already defined before cross-linking by the number of functionalized monomers per polymer chain. The characterization of the prepolymers shows average numbers of 6 and 12 functionalized monomers per polymer chain for rPDMS-431 and rPDMS-731, respectively. The outer functional groups in the backbone of a single polymer chain have a functionality of at most $f = 3$ after cross-linking. If two outer functional groups are linked, the functionality reduces to $f = 2$, thus, with decreasing reaction turnovers less cross-links are established per chain, and the fraction of two- and three-functional cross-links increases drastically. This effect, in combination with the small number of functional groups per polymer chain leads to networks with average functionalities considerably smaller than four.

With the f_{wa} taken into account for the evaluation of the equilibrium swelling experiments, the correlation improves significantly, see the circles in the inset of Figure 9a. This clearly shows the importance of an approximately known functionality for a reliable determination of molecular weights by equilibrium swelling experiments.

In the previous section we introduced the elastically effective polymer volume fraction $\phi_{p,el}$ in equilibrium swollen samples. In this treatment it is assumed that the network defects do not contribute to the elastic term of the Flory−Rehner equation. Therefore, the volume fraction of polymer in an equilibrium swollen sample ϕ_p is reduced with respect to the defect fraction of the network. For this reason, the defect fraction obtained by DQ NMR experiments on the equilibrium swollen samples $\omega_{def,sw}$ was used to determine $\phi_{p,el}$ according to eq 12. Comparing the open and closed circles in the inset of Figure 9a, it is apparent that the neglect of this issue is again reflected in a significantly nonlinear relation between M_c^{sw} and M_c^{MM}.

With both quantities reflecting defects considered (f_{wa} and $\phi_{p,el}$), we obtain a log−log slope of 1.04, which is close to the expected linearity. Since the Flory−Rehner evaluation based on the affine model, see ref 44 for the corresponding formula, only depends very weakly on f, the evaluation using a constant $f = 4$ for all samples can be taken to represent the affine result up to a constant factor. We therefore interpret the near-linear correlation with variable f_{wa} considered (and the less linear correlation for constant $f = 4$) as a proof of the validity of the phantom model. Turning to the absolute values for M_c, we note that the swelling experiments yield results that are larger by a factor of 1.43. Considering the many potential shortcomings of the Flory−Rehner model, such as nonaffine swelling[12] and in particular the ambiguities related to the χ parameter and its potential dependence on concentration and cross-linking,[44] this deviation should be considered minor. One could of course use our absolute M_c^{MM} results for a recalibration of the used χ.

We now turn to gauging the M_c^{DQ} results from DQ NMR using the variable f_{wa} in eq 6 vs M_c^{MM}, see Figure 9b. The log−log inset demonstrates again a close-to linear relation, which also in this case can be taken as an additional and completely independent hint at the validity of the phantom network model, here without ambiguities related to the thermodynamic model. The direct comparison on the linear scale now indicates a deviation in the other direction, meaning that M_c^{DQ} appears to be underestimated by a factor of 0.73. A quick comparison with Figure 9a suggests that a factor of 2 can be expected in a direct comparison between M_c^{DQ} and M_c^{sw}, which will be addressed below. It is in any way clear that the omission of corrections due to f_{wa} and the elastically effective polymer volume fraction $\phi_{p,el}$ would only increase the deviation and increase the nonlinearity of the correlation at low M_c. Therefore, the absolute-value comparisons stress the importance of considering network defects.

A noticeable trend in Figure 9b is the apparent nonlinear behavior of M_c^{DQ} at higher molecular weights. This is the regime when M_c reaches the order of the entanglement molecular weight M_e, i.e. around 10−20 kg/mol for PDMS. Traditionally, the influence of entanglements was interpreted as being additive in the effective cross-link density ($1/M_c + 1/M_e$), which in turn determines the measured D_{res}. This interpretation was corroborated by a nonzero y intercept when plotting $D_{res} \propto 1/M_c^{DQ}$ vs $1/M_c^{sw}$ from swelling experiments.[37,44] This means that in an inverse representation M_c^{DQ} should reach a plateau value. In contrast, more recent theoretical work has shown that D_{res} rather scales as $1/(M_c M_e)^{0.5}$ at low cross-linking when $M_c \gg M_e$.[50] However, this behavior is not easily observed experimentally, as the very slow terminal relaxation in lowly cross-linked networks formed by long entangled precursor chains leads to a finite D_{res} at finite temperature. If observable, M_c^{DQ} should thus scale as $M_c^{0.5}$ at high M_c^{DQ}. Since the accuracy of the D_{res} determination is challenged at low cross-linking degress, it is not possible to distinguish the two scenarios with the given data. In any way, entanglement contributions can explain the bend at high M_c^{DQ}, and could also partially explain an underestimation of M_c^{DQ} (decreased slope).

As to entanglements, it should be stressed that the given samples, based upon nonentangled precursors, are not really dominated by entanglement effects at low cross-link conversions just above the gel point. In this regime, the elastically active network fraction consist of complex chain-extended and branched but weakly entangled structures that are embedded in a similarly complex mixture of isotropically mobile dangling material. At present, we do not have a sufficient theoretical understanding of the low NMR-determined D_{res} in such a system, reminding the reader that in Figure 7 it is shown that D_{res} reaches a near-zero value close to the gel point.

The overall good agreement of M_c^{DQ} and M_c^{MM} should be discussed in the context of the ambiguities related to the derivation of the constant of proportionality used in eq 6, which relies on spin dynamics simulations of the local spin system and a few model assumptions related to the geometry of local conformational fluctuations and the definition of the Kuhn segment.[37] It should be kept in mind the most highly cross-linked samples, with M_c of 5 kg/mol and less, still contain around 25−35% of defects (see Figure 6). These are part of the average D_{res} measured on the dry sample, so we can expect that D_{res} may be biased toward lower values, corresponding to higher M_c^{DQ}. Without the defects, M_c^{DQ} would be even lower, thus increasing the deviation. We therefore take this as another

hint that the defect contribution to D_{res} is minor and assign the lower slope of 0.73 mainly to shortcomings of the underlying model.

Last but not least, we address the direct correlation of DQ NMR and swelling results. This time, we choose the representation in terms of effective cross-link densities, $1/M_c^{DQ}$ vs $1/M_c^{sw}$, as already discussed above, see Figure 9c. As expected, the deviation in the linear representation is about a factor of 2. In this case, as opposed to our earlier work on vulcanized diene rubbers,[37,44] the y intercept related to entanglements is hardly visible. This can be explained by the high M_e of PDMS and the correspondingly low y intercept, and the limited accuracy for networks with low D_{res}. In principle, this third correlation offers no new insights, and we just summarize that the factor of 2 deviation is, to roughly equal parts, due to inadequacies of the Flory−Rehner model and the DQ NMR calibration factor.

An issue of practical relevance is that the weight-average functionality f_{wa} is not routinely available, since the numerical Miller−Macosko calculations are not at everybody's disposal and are further based upon the molecular weight distribution and the density of functionalized monomers ρ_{vinyl} of the prepolymers, the exact extent of reaction from MAS NMR, and the experimental sol content. This poses the question to which extent the results are challenged when the swelling or DQ NMR experiments are evaluated without taking defects into account. Therefore, Figure 9c also contains data for which both M_c^{DQ} and M_c^{sw} were evaluated using a constant $f = 4$ and (for the latter) the as-determined polymer volume fraction ϕ_p. It is seen that, superficially, the corresponding data follow a similar trend as the data taking full account of the network defects. However, the agreement of the slopes is mainly due to the trivial fact that the phantom model introduces the very same f-dependence for the two results, see eq 6 and eq 13, which essentially cancels when just the quality of a linear correlation between the two quantities is discussed. The arrow in Figure 9c shows that data for one and the same sample do not deviate by more than 10−20% at high cross-link densities, which however is deceiving, as the relative deviation becomes very large (300−400%) for lowly cross-linked samples, an effect which is concealed close to the origin of this favorable representation. The main effect of the neglect of $\phi_{p,e}$ is an upward shift of the uncorrected data, implying an apparently higher entanglement contribution (y intercept).

Finally, it is noteworthy that the $1/M_c^{DQ}$ vs $1/M_c^{sw}$ correlation becomes almost perfect (unity slope) when the f-dependent correction factor for DQ NMR, which is 2 for when a constant $f = 4$ is used, is simply omitted from eq 6. This is of course not permissible as we have proven the validity of the Phantom model by reference to the unbiased Miller−Macosko calculations. However, the use of an analogue of eq 6 for natural rubber without the correction was exactly the state of knowledge at the time of publication of our earlier work, ref 44, where a slope of around 1 was observed when the swelling data was analyzed on the basis of the phantom model. Note that using a constant $f = 4$ is a good approximation for rubbers based on very long precursor chains over a wider range of cross-link densities. This means that the seemingly good previous correlation must be revised, suggesting that probably also for natural rubber, the same limitations of the Flory−Rehner model and the model-dependent DQ NMR calibration factor hold. In addition, it should be checked whether the omission of $\phi_{p,e}$ in swelling analyses is also responsible for systematic errors

related to the apparent entanglement contribution (y intercept) in such samples.

■ CONCLUSIONS

In this work, we have studied randomly cross-linked PDMS networks by ^{1}H double-quantum low field NMR, equilibrium swelling experiments, and Miller−Macosko calculations based upon a number of well-defined experimental input parameters, in order to assess their microstructure, with emphasis on network defects and the molecular weight between cross-links, M_c.

The defect fraction of the polymer networks has been investigated by double-quantum NMR. In the dry state, chain packing correlations or topological restrictions impede sufficiently fast isotropic motions of dangling structures and loops. Thus, a fraction of the defects is observed as elastically active chains on the experimental time scale of the double-quantum experiment, and the defect fraction is thus underestimated. The restrictions are released and the segmental dynamics is sped up by swelling of the networks with a suitable solvent, leading to fast isotropic motions, and the defect fraction determined in swollen networks is considerably higher as in the corresponding dry networks. The almost perfect agreement of the so-determined defect fraction with results of the Miller−Macosko calculations demonstrates that double-quantum NMR experiments on swollen samples provide a reliable measure of the elastically active and inactive fractions of polymer networks.

On the basis of the extracted sol known from the swelling experiments, the Miller−Macosko calculations yield the weight-averaged functionality of cross-links f_{wa}, which is found to be significantly smaller than the expected value of four, varying substantially between 3.6 and 2.5 depending on the degree of cross-linking. Another quantity related to network defects is the volume fraction of elastically active chains in the swollen state $\phi_{p,el}$, which is obtained from the polymer volume fraction at equilibrium swelling after correction using the correct defect fraction determined by NMR on swollen samples. Both quantities can be used for a proper evaluation of equilibrium swelling experiments, and a comparison of the resulting M_c with results from Miller−Macosko calculations clearly demonstrates the importance of the consideration of defects. A linear correlation between the M_c obtained from the two approaches is only observed when f_{wa} and $\phi_{p,el}$ are taken into account.

The absolute M_c values obtained by equilibrium swelling are 40% larger than the results from the Miller−Macosko calculations, and the deviations are assigned to the known inadequacies of the Flory−Rehner model. In comparison, double-quantum NMR experiments on dry samples, which also yield reliable results for M_c, underestimate it by 30%, which is assigned to minor inadequacies of the model underlying the determination of the calibration factor used to analyze such data. At high M_c, entanglement effects or slow dynamics in branched defect structures start to dominate the NMR results, and the correlation with the known M_c is no longer linear.

The fact that the network samples in this study exhibit different effective functionalities allowed for a rigorous test of the Phantom model of rubber elasticity. The assumption of phantom (rather than affine) behavior leads to strongly functionality-dependent results for both swelling as well as NMR experiments, as both methods are sensitive to fluctuations of the network chains. Since the results from the Miller−Macosko calculations are independent of such considerations,

we have demonstrated that the linear correlation of the M_c from either swelling or NMR with the Miller–Macosko results constitute a validity test of the phantom model.

■ APPENDIX

Miller–Macosko Calculations

In this section we describe the computations of the sol fraction, the dangling material, and the average lengths of active strands of the randomly cross-linked networks. Let us assume independence of all reactions, equal reactivity among all monomers, and that cross-linking occurs by a pairwise connection of arbitrary selected monomers out of the reaction bath. Under these assumptions, the distribution $P(f,N)$ of branches f per polymer of N monomers is given[55] by the binomial distribution

$$P(f, N) = \binom{N}{f} p^f (1 - p)^{N-f} \tag{A1}$$

based upon the probability p that an arbitrary selected monomer is reacted. Let n_N denote the mol fraction of molecules containing N monomers. For the polydisperse samples of our study with weight fractions w_N of molar masses, equation (A1) implicitly defines a weight distribution of polymer having f branches. The weight fraction of polymers with f branches is then given by

$$w_f = \sum_N P(f, N) M_N / \sum_N n_N M_N$$

whereby $M_N = N M_{mon}$ is the molar mass of the N-mer, M_{mon} the mass of a monomer. The number-average degree of polymerization of chains having f branches N_f is given by

$$N_f = \sum P(f, N) n_N N$$

The mol fractions of branches a_f on polymers of f branches is computed via

$$a_f = \frac{f \sum_N n_N P(f, N)}{\sum_f f \sum_N n_N P(f, N)}$$

Let Q denote the probability that a given branching monomer on a chain is the start of a *finite* chain.[61] Q is computed recursively by numerically solving

$$Q = \sum_f a_f Q^{f-1}$$

If all f branches of a given polymer lead to a dangling end, then the chain is part of the sol. Thus, the weight fraction of sol is given by

$$w_{sol} = \sum_f w_f Q^f$$

The above treatment assumes no intra-molecular reactions in finite species, which is certainly not the case. Intra-molecular reactions in finite species lead to a fraction of non-branching reactions that increase the weight fraction of sol. Therefore, we introduce a fraction of reacted monomers p_b (out of the fraction of p reacted monomers) that lead to ideal branching reactions following mean field theory, while the remaining fraction $1 - p_b$ is involved in intra-molecular reactions in finite species. Since the molecular weight

distribution and the fraction of reacted monomers is known, we leave p_b as the only parameter to match the experimental sol content as a function of $p' = p_b p$ with our predictions above.

After p' is determined, we compute the length distribution of strands between these ideally branching monomers and the weight fraction of dangling material following refs 32 and 55 and the above results based on p'. Since Q denotes the probability that a given branch leads to a finite chain, we can compute the probability that a chain of f branches contains k connections which are not finite

$$P(X_{k,f}) = \binom{f}{k} Q^{f-k} (1 - Q)^k$$

The weight fraction of dangling material is all polymer attached to gel $k \geq 1$ that is not between the first and last of these k active branches along the chain. Since k branches divide a chain into $k + 1$ sections, there is a fraction of $2/(k + 1)$ dangling material per chain. Thus, the weight fraction of dangling material is given by

$$w_{dang} = \sum_f 2 N_f P(X_{2,f}) / (k + 1)$$

and the weight fraction of active material is then

$$w_{act} = 1 - w_{sol} - w_{dang}$$

The number fraction of branches that are active p_{act} is the number fraction of branches with at least three independent connections to the network

$$p_{act} = \sum_{f=3}^{\infty} \left(P(f, N) \sum_{k=3}^{f} P(X_{k,f}) \right)$$

Thus, there is a number fraction of $p_{act} p'$ monomers inside the active material that is an active branch and the average active strand length is given by

$$N_{act} = \frac{w_{act}}{p_{act} p'} \tag{A2}$$

with a molecular weight distribution that is quickly converging from the high molecular weight wing of the precursor weight distribution to a most probable weight distribution[55] of the above average and a polydispersity index of 2.

Let us introduce the active functionality f_a, which is given by the number of independent active connections of a junction to the network, and the weight fraction w_{f_a} of junctions with f_a active connections. The weight-average of the active functionality is then

$$f_{wa} = \sum_{i=3}^{\infty} i w_{f_a} / \sum_{i=3}^{\infty} w_{f_a}$$

If an active cross-link connects to a neighboring active cross-link, the connected cross-links are selected proportional to the number of active connections. Thus, the weight-average active functionality f_{wa} determines the average functionality of the surrounding network that is experienced by an active cross-link.

NMR Order Parameter and Phantom Model

The estimate for the average dynamic segmental order parameter will be performed in a pre-averaged manner by using the number-average length of an active strand $\bar{N}_{act}$ and

following the phantom model as discussed in ref 50. To this end, we have to compute the length of the corresponding combined chain that allows to map the phantom model onto the affine model. Let us consider an active chain that is connected to two active junctions, each of average functionality f. Then, the average fluctuations of the cross-links without the chain in between can be modeled by attaching virtual chains of

$$ K_a \approx \frac{\bar{N}_{act}}{f - 2} $$

monomers to the non-fluctuating elastic background. The corresponding combined chain of the affine model consists of

$$ N_{comb} \approx \bar{N}_{act} \frac{f}{f - 2} $$

monomers. Below we denote ensemble averages by $[...]$. For the affine model using a large set of chains of N monomers with Gaussian end-to-end distribution and segments of length b it is known that in general the (ensemble average) vector order parameter $[m]$ is proportional to the tensor order parameter $[s]$

$$ [m] = \frac{[R^2]}{b^2 N^2} = \frac{1}{N} = \frac{5}{3}[s] $$

using the Gaussian result $[R^2] = b^2 N$. Following the arguments of ref 50, we replace N by N_{comb} and use the average size of the combined chain to obtain the tensor order parameter as a function of the number-average active chain length and the weight-average active functionality

$$ s \approx \frac{3}{5} \frac{f - 2}{f} \frac{1}{\bar{N}_{act}} $$

The tensor order parameter s is directly proportional to the NMR-determined residual dipolar interaction, $D_{res} = s\, D_{ref}$, where D_{ref} is a pre-averaged dipolar coupling constant characterizing the spin arrangement and local motions within a statistical (Kuhn) segment.[37]

■ AUTHOR INFORMATION

Corresponding Author
*E-mail: (W.C.) walter.chasse@physik.uni-halle.de; (K.S.) kay.saalwaechter@physik.uni-halle.de.

■ REFERENCES

(1) Patel, S. K.; Malone, S.; Cohen, C.; Gillmor, J. R.; Colby, R. H. Elastic modulus and equilibrium swelling of poly(dimethylsiloxane) networks. *Macromolecules* **1992**, *25*, 5241−5251.

(2) Arndt, K. F.; Schreck, J. Netzwerkcharakterisierung durch dampfdruckosmotische Messungen. *Acta Polym.* **1985**, *36*, 56−57.

(3) Tan, Z.; Jaeger, R.; Vancso, G. Crosslinking studies of poly-(dimethylsiloxane) networks: a comparison of inverse gas chromatography, swelling experiments and mechanical analysis. *Polymer* **1994**, *35*, 3230−3236.

(4) Falcão, A. N.; Pedersen, J. S.; Mortensen, K. Structure of randomly crosslinked poly(dimethylsiloxane) networks produced by electron irradiation. *Macromolecules* **1993**, *26*, 5350−5364.

(5) Folland, R.; Charlesby, A. Pulsed NMR studies of crosslinking and entanglements in high molecular weight linear polydimethylsiloxanes. *Radiat. Phys. Chem.* **1977**, *10*, 61−68.

(6) Mark, J. E.; Sullivan, J. L. Model Networks Of End-Linked Polydimethylsiloxane Chains 0.1. Comparisons Between Experimental And Theoretical Values Of Elastic-Modulus And Equilibrium Degree Of Swelling. *J. Chem. Phys.* **1977**, *66*, 1006−1011.

(7) Falender, J. R.; Yeh, G. S. Y.; Mark, J. E. The effect of chain length distribution on elastomeric properties. 1. Comparisons between random and highly nonrandom networks. *J. Am. Chem. Soc.* **1979**, *101*, 7353−7356.

(8) Erman, B.; Mark, J. E. Rubber-Like Elasticity. *Annu. Rev. Phys. Chem.* **1989**, *40*, 351−374.

(9) Mark, J. E.; Llorente, M. A. Model networks of end-linked polydimethylsiloxane chains. 5. Dependence of the elastomeric properties on the functionality of the network junctions. *J. Am. Chem. Soc.* **1980**, *102*, 632−636.

(10) Llorente, M. A.; Andrady, A. L.; Mark, J. E. Chemical analysis of vinyl-crosslinked poly(dimethylsiloxane) model networks and use of the resulting structural information in the interpretation of their elastomeric properties. *J. Polym. Sci. Polym. Phys. Ed.* **1980**, *18*, 2263−2270.

(11) Mark, J. E. Elastic Properties Of Model Polymer Networks. *Pure Appl. Chem.* **1981**, *53*, 1495−1503.

(12) Sommer, J. U.; Lay, S. Topological Structure and Nonaffine Swelling of Bimodal Polymer Networks. *Macromolecules* **2002**, *35*, 9832−9843.

(13) Flory, P.; Rehner, J. Statistical mechanics of cross-linked polymer networks. *J. Chem. Phys.* **1943**, *11*, 521−527.

(14) Flory, P. Statistical Mechanics of Swelling of Network Structures. *J. Chem. Phys.* **1950**, *18*, 108−111.

(15) Flory, P. *Principles of Polymer Chemistry*; Cornell University Press: New York, 1953.

(16) Brotzman, R. W.; Eichinger, B. E. Volume dependence of the elastic equation of state. 2. Solution-cured poly(dimethylsiloxane). *Macromolecules* **1981**, *14*, 1445−1448.

(17) Brotzman, R. W.; Eichinger, B. E. Volume dependence of the elastic equation of state. 3. Bulk-cured poly(dimethylsiloxane). *Macromolecules* **1982**, *15*, 531−535.

(18) Brotzman, R. W.; Eichinger, B. E. Swelling of model poly(dimethylsiloxane) networks. *Macromolecules* **1983**, *16*, 1131−1136.

(19) Hermans, J. Deformation and swelling of polymer networks containing comparatively long chains. *Trans. Faraday Soc.* **1947**, *43*, 591−600.

(20) Wall, F. T.; Flory, P. J. Statistical Thermodynamics of Rubber Elasticity. *J. Chem. Phys.* **1951**, *19*, 1435−1439.

(21) James, H. M.; Guth, E. Theory of the Elastic Properties of Rubber. *J. Chem. Phys.* **1943**, *11*, 455−481.

(22) James, H. M.; Guth, E. Theory of the increase in rigidity of rubber during cure. *J. Chem. Phys.* **1947**, *15*, 669−683.

(23) Gottlieb, M.; Gaylord, R. J. Experimental tests of entanglement models of rubber elasticity. 2. Swelling. *Macromolecules* **1984**, *17*, 2024−2030.

(24) Andrady, A. L.; Llorente, M. A.; Sharaf, M. A.; Rahalkar, R. R.; Mark, J. E.; Sullivan, J. L.; Yu, C. U.; Falender, J. R. Model networks of end-linked polydimethylsiloxane chains. XII. Dependence of ultimate properties on dangling-chain irregularities. *J. Appl. Polym. Sci.* **1981**, *26*, 1829−1836.

(25) Vega, D. A.; Villar, M. A.; Alessandrini, J. L.; Vallés, E. M. Terminal Relaxation of Model Poly(dimethylsiloxane) Networks with Pendant Chains. *Macromolecules* **2001**, *34*, 4591−4596.

(26) Acosta, R. H.; Monti, G. A.; Villar, M. A.; Vallés, E. M.; Vega, D. A. Transiently Trapped Entanglements in Model Polymer Networks. *Macromolecules* **2009**, *42*, 4674−4680.

(27) Bastide, J.; Picot, C.; Candau, S. The influence of pendent chains on the thermodynamic and viscoelastic properties of swollen networks. *J. Polym. Sci., Polym. Phys. Ed.* **1979**, *17*, 1441−1456.

(28) Bibbó, M. A.; Vallés, E. M. Influence Of Pendant Chains On The Loss Modulus Of Model Networks. *Macromolecules* **1984**, *17*, 360−365.

(29) Villar, M. A.; Bibbó, M. A.; Vallés, E. M. Influence of pendant chains on mechanical properties of model poly(dimethylsiloxane) networks 0.1. Analysis of the molecular structure of the network. *Macromolecules* **1996**, *29*, 4072−4080.

(30) Villar, M. A.; Vallés, E. M. Influence of pendant chains on mechanical properties of model poly(dimethylsiloxane) networks 0.2. Viscoelastic properties. *Macromolecules* **1996**, *29*, 4081−4089.

(31) Urayama, K.; Kawamura, T.; Kohjiya, S. Structure-mechanical property correlations of model siloxane elastomers with controlled network topology. *Polymer* **2009**, *50*, 347−356.

(32) Macosko, C. W.; Miller, D. R. A New Derivation of Average Molecular Weights of Nonlinear Polymers. *Macromolecules* **1976**, *9*, 199−206.

(33) Chalk, A. J.; Harrod, J. F. Homogeneous Catalysis. II. The Mechanism of the Hydrosilation of Olefins Catalyzed by Group VIII Metal Complexes1. *J. Am. Chem. Soc.* **1965**, *87*, 16−21.

(34) Weese, J. A Reliable And Fast Method For The Solution Of Fredholm Integral-Equations Of The 1st Kind Based On Tikhonov Regularization. *Comput. Phys. Commun.* **1992**, *69*, 99−111.

(35) Chassé, W.; Valentín, J. L.; Genesky, G. D.; Cohen, C.; Saalwächter, K. Precise dipolar coupling constant distribution analysis in proton multiple-quantum NMR of elastomers. *J. Chem. Phys.* **2011**, *134*, 044907.

(36) Saalwächter, K.; Ziegler, P.; Spyckerelle, O.; Haidar, B.; Vidal, A.; Sommer, J. U. [1]H multiple-quantum nuclear magnetic resonance investigations of molecular order distributions in poly(dimethylsiloxane) networks: Evidence for a linear mixing law in bimodal systems. *J. Chem. Phys.* **2003**, *119*, 3468−3482.

(37) Saalwächter, K.; Herrero, B.; Lopez-Manchado, M. A. Chain order and cross-link density of elastomers as investigated by proton multiple-quantum NMR. *Macromolecules* **2005**, *38*, 9650−9660.

(38) Saalwächter, K. Proton multiple-quantum NMR for the study of chain dynamics and structural constraints in polymeric soft materials. *Prog. Nucl. Magn. Reson. Spectrosc.* **2007**, *51*, 1−35.

(39) Bueche, A. M. Interaction of polydimethylsiloxanes with swelling agents. *J. Polym. Sci.* **1955**, *15*, 97−103.

(40) Hecht, A. M.; Guillermo, A.; Horkay, F.; Mallam, S.; Legrand, J. F.; Geissler, E. Structure and dynamics of a poly(dimethylsiloxane) network: a comparative investigation of gel and solution. *Macromolecules* **1992**, *25*, 3677−3684.

(41) Mallam, S.; Horkay, F.; Hecht, A. M.; Rennie, A. R.; Geissler, E. Microscopic and macroscopic thermodynamic observations in swollen poly(dimethylsiloxane) networks. *Macromolecules* **1991**, *24*, 543−548.

(42) Soni, V. K.; Stein, R. S. Light-Scattering-Studies of Poly(dimethylsiloxane) Solutions and Swollen Networks. *Macromolecules* **1990**, *23*, 5257−5265.

(43) Horkay, F.; Hecht, A. M.; Geissler, E. Thermodynamic Interaction Parameters In Polymer-Solutions And Gels. *J. Polym. Sci., Part B: Polym. Phys.* **1995**, *33*, 1641−1646.

(44) Valentín, J. L.; Carretero-González, J.; Mora-Barrantes, I.; Chassé, W.; Saalwächter, K. Uncertainties in the Determination of Cross-Link Density by Equilibrium Swelling Experiments in Natural Rubber. *Macromolecules* **2008**, *41*, 4717−4729.

(45) Graf, R.; Heuer, A.; Spiess, H. W. Chain-order effects in polymer melts probed by ^{1}H double-quantum NMR spectroscopy. *Phys. Rev. Lett.* **1998**, *80*, 5738−5741.

(46) McLoughlin, K.; Szeto, C.; Duncan, T. M.; Cohen, C. End-Linked Poly(dimethylsiloxane) Elastomer Structure: 2H-NMR Transverse Dephasing Data Compared to Predictions of Statistical and Thermodynamic Models. *Macromolecules* **1996**, *29*, 5475−5483.

(47) Valentín, J.; Posadas, P.; Fernández-Torres, A.; Malmierca, M. A.; González, L.; Chassé, W.; Saalwächter, K. Inhomogeneities and Chain Dynamics in Diene Rubbers Vulcanized with Different Cure Systems. *Macromolecules* **2010**, *43*, 4210−4222.

(48) Sommer, J.-U.; Chassé, W.; Valentín, J. L.; Saalwächter, K. Effect of excluded volume on segmental orientation correlations in polymer chains. *Phys. Rev. E* **2008**, *78*, 051803.

(49) Saalwächter, K.; Kleinschmidt, F.; Sommer, J.-U. Swelling Heterogeneities in End-Linked Model Networks: A Combined Proton Multiple-Quantum NMR and Computer Simulation Study. *Macromolecules* **2004**, *37*, 8556−8568.

(50) Lang, M.; Sommer, J.-U. Analysis of Entanglement Length and Segmental Order Parameter in Polymer Networks. *Phys. Rev. Lett.* **2010**, *104*, 177801.

(51) McKenna, G. B.; Flynn, K. M.; Chen, Y. Experiments on the elasticity of dry and swollen networks: implications for the Frenkel-Flory-Rehner hypothesis. *Macromolecules* **1989**, *22*, 4507−4512.

(52) Flory, P. Thermodynamics of High Polymer Solutions. *J. Chem. Phys.* **1941**, *9*, 660−661.

(53) Huggins, M. Solutions of Long Chain Compounds. *J. Chem. Phys.* **1941**, *9*, 440.

(54) Schuld, N.; Wolf, B. A. Solvent quality as reflected in concentration- and temperature-dependent Flory-Huggins interaction parameters. *J. Polym. Sci., Part B: Polym. Phys.* **2001**, *39*, 651−662.

(55) Lang, M.; Göritz, D.; Kreitmeier, S. Length of Subchains and Chain Ends in Cross-Linked Polymer Networks. *Macromolecules* **2003**, *36*, 4646−4658.

(56) Plazek, D. J. Effect of Crosslink Density on the Creep Bahavior of Natural Rubber Vulcanizates. *J. Polym. Sci., A-2: Polym. Phys.* **1966**, *4*, 745−763.

(57) Curro, J. G.; Pearson, D. S.; Helfand, E. Viscoelasticity of Randomly Crosslinked Polymer Networks. Relaxation of Dangling Chains. *Macromolecules* **1985**, *18*, 1157−1162.

(58) Vaca Chávez, F.; Saalwächter, K. Time-Domain NMR Observation of Entangled Polymer Dynamics: Universal Behavior of Flexible Homopolymers and Applicability of the Tube Model. *Macromolecules* **2011**, *44*, 1549−1559.

(59) Oyerokun, F. T.; Schweizer, K. S. Microscopic theory of rubber elasticity. *J. Chem. Phys.* **2004**, *120*, 9359−9370.

(60) Saalwächter, K.; Gottlieb, M.; Liu, R.; Oppermann, W. Gelation as Studied by Proton Multiple-Quantum NMR. *Macromolecules* **2007**, *40*, 1555−1561.

(61) Rubinstein, M.; Colby, R. *Polymer Physics*; Oxford University Press: New York, 2003.

3.3. Thermodynamics of Swollen Networks As Reflected in Segmental Orientation Correlations

The article investigates the validity of the classical Flory-Rehner (FR) model for the description of the *thermodynamic properties* of swollen polymer networks. The equilibrium swelling degree of randomly- and end-linked PDMS networks with different cross-link density was measured over a broad range of temperatures for various solvents ranging from the bad solvent regime over theta solvents up to good solvent regime. The results are analyzed in terms of a novel construction of solvent-independent swelling master curves. Therefore the temperature-dependent swelling degrees of the different solvents of a given sample are plotted vs a reduced temperature, $(1 - \theta/T)$, using the θ-temperature as shift parameter with respect to an unshifted reference solvent so as to achieve the best data overlap. The so-obtained swelling master curves are fitted by the FR equation showing a rather well agreement when the fit is limited to low swelling degrees obtained in the range of poor solvents to slightly above the θ-condition. For higher swelling-degrees obtained in the good-solvent regime the fit fails completely.

Equilibrium swollen samples were investigated by ^{1}H double-quantum (DQ) NMR over a broad range of temperatures above and below the θ-temperature. The comparison of the two experimentally accessible quantities, the backbone order parameter and the equilibrium swelling degree, allows conclusions on the validity of the classical FR theory in terms of scaling theory, leading to the same results as obtained by the swelling experiments.

Authors Contributions. W.C. planned the study, prepared the samples, performed the measurements and, together with K.S. and J.-U.S., analyzed the data. J.-U.S. and K.S. designed research and wrote the manuscript.

Thermodynamics of Swollen Networks As Reflected in Segmental Orientation Correlations
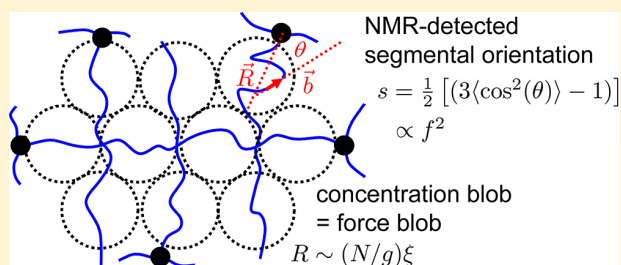
Walter Chassé and Kay Saalwächter*

Institut für Physik — NMR, Martin-Luther-Universität Halle-Wittenberg, Betty-Heimann-Str. 7, D-06120 Halle, Germany

Jens-Uwe Sommer*

Leibniz-Institut für Polymerforschung Dresden e.V., Hohe Strasse 6, D-01069 Dresden, Germany

Technische Universität Dresden, Institute for Theoretical Physics, Zellescher Weg 17, D-01069 Dresden, Germany

ABSTRACT: We show that segmental orientation correlations, arising from network constraints and reflected in NMR observables such as the apparent proton residual dipolar coupling constant (RDCC), are sensitive to the thermodynamic state of a swollen network. The RDCC is proportional to a dynamic tensor order parameter of the network chain, which depends upon the fluctuation statistics of a network chain subject to swelling-induced stretching and excluded-volume interactions. The correlation of its value at swelling equilibrium with the corresponding degree of swelling for different networks directly reflects the value of the thermodynamic interaction parameter. A description of the phenomenon based on scaling theory allows for conclusions on the limited validity of the classical Flory−Rehner (FR) model for the good-solvent case. Our study is supplemented by temperature-dependent swelling experiments of different PDMS networks in various solvents, analyzed via a novel construction of solvent-independent swelling master curves, which also emphasize deviations from the FR model for good solvents and further confirm previous reports on concentration- or cross-linking-dependent interaction parameters. We rationalize the failure of the FR model for the good-solvent case in terms of the ratio of the network correlation length and the thermal blob size.

NMR-detected segmental orientation
$$s = \tfrac{1}{2}\left[(3\langle\cos^2(\theta)\rangle - 1)\right]$$
$$\propto f^2$$

concentration blob = force blob
$$R \sim (N/g)\xi$$

I. INTRODUCTION

Thermodynamic properties of molecules in solution are immediately reflected in their equilibrium fluctuations, and local concentration fluctuations are for instance the central condition for the occurrence of neutron or light scattering phenomena.[1,2] Consequently, besides direct and often tedious thermodynamic measurements, scattering techniques are among the most popular methods to assess the thermodynamics of polymer solutions.[3−5] The thermodynamics of polymers is further directly related to their conformational entropy;[6] thus, in this case, conformational fluctuations are the cornerstone of the classic thermodynamic theories of rubber elasticity[7] and swelling.[8] We here discuss the use of NMR spectroscopy, which in fact provides a direct measure of conformational fluctuations in terms of segmental orientation correlations, to assess the thermodynamic state of swollen networks. We demonstrate that NMR results, which are sensitive to time-averaged tensorial interactions such as dipole−dipole couplings and which can be obtained on simple low-field instruments,[9−11] in comparison with swelling experiments, yield consistent information on the thermodynamic properties of the given polymer−solvent system. We give a detailed theoretical account of the phenomena and are able to draw important conclusions on the applicability and the well-

known limitations of the classical Flory−Rehner (FR) model for network swelling.[12−15]

A profound understanding of the swelling of polymer networks is one of the major outstanding problems of polymer physics. Although first theoretical approaches based on mean-field-like models and Gaussian statistics of chains such as the FR model[8] have been proposed early on, these models led to serious discrepancies with experimental observations for swelling in good solvents, the most prominent observation being the so-called *swelling anomaly*.[12,16] Notably, the most striking feature of this anomaly, namely the apparent maximum of the swelling activity parameter (also called dilational modulus), has recently been shown to likely be an artifact related to inappropriate smoothing of data with limited accuracy.[15] However, the fact that the dilational modulus still decreases with increasing degree of swelling $Q = V/V_0 = 1/\phi$ is not consistent with the simple FR model, and ad-hoc approaches such as a concentration- and cross-linking-dependent interaction parameter χ[17−20] and specific models for the elasticity contribution, e.g. the constrained-chain model of

Flory and Erman,[21,22] can be considered. We note that the limit $Q \gg 1$ of the FR model can be rederived using scaling arguments, which take into account properly the excluded volume induced correlations in a solution of overlapping chains,[23,24] which represent an alternative viewpoint and will be addressed herein.

The FR model combines the Flory−Huggins (FH) model with an affine model of network deformation. Within the FR model, polymer chains are considered as random walks on a lattice and finite concentration of segments is taken into account as mean field. The free energy per lattice site in units of kT (k denotes the Boltzmann constant) can then be written as the sum of the solvent entropy, the energy part of the monomer−monomer interaction, and the Gaussian network elasticity:

$$f = f_s + f_\chi + f_{el} = (1 - \phi) \ln(1 - \phi) + \chi\phi(1 - \phi)$$
$$+ ng_f \frac{3}{2}\phi(\phi^{-2/3} - 1) \tag{1}$$

Here, $\phi = 1/Q$ defines the monomer number per lattice site (polymer volume fraction), χ denotes the Flory−Huggins interaction parameter, and n gives the number density of network strands in the dry state (cross-link density). On the FH lattice we have $n = 1/N$, where N denotes the length of the network stands. The factor g_f refers to the network model (affine: $g_f = 1$; phantom: $g_f = (1 - 2/f_x)$, with the cross-link functionality f_x). The network properties can be taken into account in more detail leading to other expressions for g_f. However, within the validity of Gaussian conformation statistics, the exponents of ϕ remain the same (ignoring subtle effects of ϕ on the fluctuations of cross-links). Swelling equilibrium is given by zero overall osmotic pressure $\Pi = \partial F/\partial V = 0 = \partial(fV)/\partial V = f - \phi(\partial f/\partial\phi)$, where $df/dV = (df/d\phi)(d\phi/dV)$ is used. This leads to the following nonlinear equation:

$$^2\ln(1 - \phi) - \frac{1}{2}v\phi^2 + ng_f\phi^{1/3} = 0 \tag{2}$$

The first term $^2\ln(1 - \phi) = \ln(1 - \phi) + \phi + \frac{1}{2}\phi^2$ represents all higher-order virials. The effective interaction parameter (second virial coefficient) is denoted by

$$v = \frac{1}{2}(1 - 2\chi) = B\frac{T - \theta}{T} \tag{3}$$

The last expression defines the θ-temperature, at which the volume repulsion between the segments is exactly compensated by solvent-induced attraction. The parameter B should be considered as empirical parameter since it also contains the mapping of the segments' volume onto the FH lattice. The solution of eq 2 provides the equilibrium degree of swelling $\bar{Q}(v,ng_f) = 1/\bar{\phi}(v,ng_f)$ as a function of temperature and cross-link density. An overbar will henceforth be used to denote quantities considered/measured at swelling equilibrium. We note that in the general case $\bar{Q}(v,ng_f)$ can only be obtained numerically while the inverse solutions $n(\bar{Q})$ and $N(\bar{Q})$ can be obtained explicitly.

The additivity of mixing and elasticity in eq 1 as a major hypothesis of the FR model has been intensively debated in the literature.[17−20,25−27] The apparent increase of the χ parameter in polymer networks as compared to the corresponding linear-chain solutions is a major finding arising from the use of standard models of rubber elasticity and the FR additivity

assumption. A possible solution from the thermodynamic point of view is to assume an ad-hoc concentration or cross-linking dependence of the χ parameter.[17−20] In these and related works it is already realized that the cross-link dependency of the χ parameter is most likely due to the failure of the additivity assumption. For instance, in ref 19 it has been shown that a cross-linking-dependent χ parameter can explain the unusual swelling behavior of networks in their own melt, but this can also be explained by assuming a nonaffine swelling deformation of the network (see also refs 19 and 28). In ref 20 the authors have compared the apparent χ parameter of networks and solutions of star polymers. Interestingly, for higher concentrations star polymers display no increased χ parameter, which illustrates that localized cross-links cannot be exclusively responsible for the apparent increase the χ parameter. These authors therefore conclude that "the difference in interaction parameter is mainly due to an extra entropic contribution in the networks".

Here, we study the validity of the classic FR relations on a series of PDMS networks with different topology (end-linking vs random cross-linking) prepared at different polymer concentrations swollen to equilibrium $\bar{Q}$ with a variety of solvents in a wide temperature range, covering the range from well below to well above θ-conditions. We show that, using the FR model, a direct relation between two independently observable parameters can be derived and tested on the given sample series. This allows us to reconsider the question of the effective interaction parameter in polymer networks in the limit of validity of Gaussian chain statistics, i.e., for temperatures below or slightly above the θ-point.[25−28] The two observables are the equilibrium degree of swelling $\bar{Q}$ and the average local segmental orientational order parameter

$$s = \frac{1}{2}[(3\langle\cos^2(\theta)\rangle - 1)] \tag{4}$$

where $\langle...\rangle$ denotes the thermal average over all conformations of a network chain and $[...]$ denotes the structural average over all segments in the sample. The angle θ refers to the instantaneous segmental orientation with respect to the end-to-end vector of the given chain. The quantity s is most reliably measured by proton multiple-quantum (MQ) NMR,[11] which is a probe of the effective dipole−dipole coupling between the protons of a given monomer unit. These are orientation-dependent and averaged to zero in isotropic liquids, but the thermal average over the network chain as constrained by its fixed ends leads to a finite residual dipole−dipole coupling constant (RDCC), which is directly proportional to s.

Our approach is motivated by the work of Cohen-Addad, who was the first to study an NMR measure of s in swollen networks.[9,29,30] It was found that the change of s with increasing Q up to equilibrium is complex and strongly subaffine, and we could later refine this picture by also measuring the distribution function of s in swollen samples, revealing strong swelling inhomogeneities.[31] Restricting the discussion to an ensemble-averaged s, Cohen-Addad found a unique relation $\bar{s} \sim \bar{Q}^{-1.5}$ for samples swollen to equilibrium.[30] This relation turned out to be rather general, as it applies to very different network samples, end-linked and randomly cross-linked in bulk and in the diluted state.[24]

Cohen-Addad interpreted the relation $\bar{s} \sim \bar{Q}^{-1.5}$ as a proof of de Gennes' c^* theorem, which states that swelling equilibrium corresponds to the overlap concentration c^* of the equivalent free network chains.[32] We could, however, show that this is

incorrect, as the FR model in fact predicts the same relation,[24] and thus further draw a few conclusions on the compatibility of the FR and c^* models, which will be taken up below. While Cohen-Addad's NMR studies were restricted to good solvents, our preliminary results taken under θ-conditions indicated a qualitatively different behavior.[24] This issue is taken up herein, where we now take a comprehensive approach and study a wide range of thermodynamic conditions. As we will show, the NMR-detected relation $\overline{s}(\overline{Q})$, which arises from a comparison of two well-defined experimental quantities taken on a series of networks with different cross-link densities, is a unique measure of solvent quality. We provide a quantitative theoretical treatment, which allows us to critically asses the validity of certain assumptions in the different theoretical approaches

II. THEORETICAL BACKGROUND

A. Segmental Order Parameter and Conformational Statistics of Network Chains. We here present a condensed version of our previously published first general treatment of the effect of conformational statistics on segmental orientation correlations in swollen networks.[24] As mentioned above, RDCCs can be related to the tensor order parameter

$$s = \left[\sqrt{\frac{3}{2}\mathrm{Tr}\langle S \rangle^2} \right] \tag{5}$$

Here, S denotes the orientation tensor of a given segment $S_{\alpha\beta} = \langle b_\alpha b_\beta \rangle - \frac{1}{3}\delta_{\alpha\beta}$, where b_α are the Cartesian components of the unit vector of segment orientation.[31,33] The brackets $\langle ... \rangle$ denote the average over all conformations (thermal average), and $[...]$ denote the average of the ensemble of segments which is considered (structural average). When the orientation is caused by a uniaxial and invariant symmetry break described by a director $\vec{e}$, one obtains eq 4 defined above, in which $\cos\theta = \vec{b}\cdot\vec{e}$. In the following, we consider the case that orientational order is caused by fixing the chain ends with a given end-to-end vector, $\vec{R}$ (see Figure 1), with $\vec{e} = \vec{R}/R$ and $R = |\vec{R}|$. In order to calculate the averages in eq 4 for the segment with the index $1 \leq k \leq N$ along the chain, the conditional probability $P(z_k|R,N)$ needs to be considered. Here and in the following we use the notation $z = \cos\theta$.

We consider a chain in a semidilute solution which corresponds to the most important case for network swelling. The end-to-end distribution of chains is then Gaussian[32] and is given by

$$P(\vec{R}, R_0; N) = \left(\frac{3}{2\pi R_0^2} \right)^{3/2} \exp\left(-\frac{3}{2}\frac{R^2}{R_0^2} \right) \tag{6}$$

where R denotes the actual end-to-end distance of the chain composed of N flexible repeat units (Kuhn segments) and R_0 is
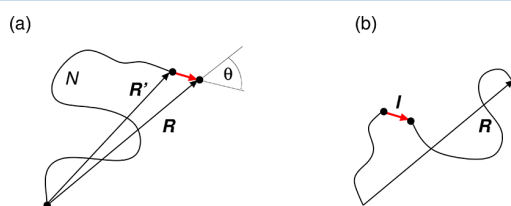
Figure 1. Orientation of a segment within a chain of fixed end-to-end vector for (a) a segment located at the chain's end and (b) a segment located inside the chain.

the average end-to-end distance in free solution. The order parameter can be directly obtained for a segment located at the end of the chain, as displayed in Figure 1a. In this case, the orientation of the segment is caused by a chain of length $N-1$ which is fixed at the end position $\vec{R} - \vec{l}$, where $\vec{l}$ denotes the vector of the segment, i.e., $\vec{l} = \vec{b}\cdot l$. The segment length l can be considered as small as compared to R, and the calculation can be performed by expanding $P(\vec{R} - \vec{l}, R_0; N)$ with respect to zR/R_0^2. In the case of the Gaussian distribution function, however, the calculation can be carried out exactly, leading to

$$s = \frac{3}{5}\left(\frac{lR}{R_0^2} \right)^2 \tag{7}$$

This last result allows us to draw a link between thermodynamic properties of unentangled polymer networks and the tensor order parameter:[24] The origin for the segment orientation is the force acting on the segment by restricted fluctuations of the rest of the chain. As sketched in Figure 1, the chain pulls the segment in the direction parallel to the end-to-end vector in oder to maximize the number of conformations. This is very similar to the effect of a magnetic field on spin orientations in a magnetic material. The dimensionless force acting on the chain end is given by

$$f_N = 3lR/R_0^2 \tag{8}$$

where we use energy units ($kT = 1$). We use the symbol f_N for the force, which should not be confused with the free energy per volume unit, f, as used above. Thus, we obtain

$$s = \frac{1}{15}f_N^2 \tag{9}$$

This relates the tensor order parameter with a thermodynamic property. In order to obtain the structural average in eq 4 along a given chain, also the result for segments inside the chain have to be obtained (see Figure 1b). In the absence of good solvent there is no other contribution to the force acting inside of the chain than just connectivity, and the obtained results are exactly the same for all values of the segment index k along the chain. Under good-solvent conditions the situation is different since both subchains also interact via excluded volume forces in addition to the tension inside the chain.

We have so far considered this situation for the case of a single chain in good solvent.[24] This situation corresponds to the c^* limit of a swollen network.[32] First, we have shown that a relation similar to eq 9 holds, the derivation of which is based on the so-called Fisher distribution function,[32,34,35] leading to $f_N \sim (R/Nl)^{\nu/(1-\nu)}$, where the prefactor depends on parameters of the distribution function.[24] Here, $\nu \simeq 3/5$ denotes the Flory exponent. Using Monte Carlo simulations, we have studied the average order parameter s and its scaling behavior for chains of various length under athermal solvent conditions. We found very good agreement with the predicted behavior of the end segments

$$s \sim \left(\frac{R}{Nl} \right)^a \quad \text{with } a \simeq \frac{2\nu}{1-\nu}$$

The best fit to simulation data was obtained with $a \simeq 2.7$, close to 2.85 according to ideal scaling of the end segments, corresponding to the best-known value for $\nu \simeq 0.588$.[24] Therefore, we can also assume end-segment scaling of the order parameter throughout the chain for the case of semidilute

solutions (assuming that the excluded-volume effect is restricted to the blob size of the solution). We note that a rigorous proof for this result in terms of field-theoretical methods is still missing; see a related problem solved by Schäfer and Elsner.[36]

On the basis of these results, we conclude that the tensor order parameter s for a network chain in the semidilute state is given by

$$s = \frac{3}{5} A_0 \frac{R^2 l^2}{R_0{}^4} \tag{10}$$

where the prefactor A_0 is related to the average of the order parameter over all monomers (which is unity for the chain ends and increasing for segments inside the chain), but also to the fluctuations of cross-links in the network. In a simplified phantom model, the latter can be described simply by effectively prolonged network chains.[37] We note that both contributions tend to compensate each other.

In the Results and Discussion section, we will follow up on these considerations, relating the chain dimensions with the equilibrium degree of swelling $\bar{Q}$ and comparing poor-, θ-, and good-solvent conditions, where specific scaling arguments need to be applied in the latter case.

III. EXPERIMENTAL SECTION

A. Samples. Different network samples based upon random vinyl-functionalized (r) or divinyl-end-functionalized (e) PDMS precursor polymers and the appropriate cross-linker molecules with two or four Si—H functionalities, respectively, using a Pt-based catalyst were prepared and characterized following previously published procedures.[38,39] All components were purchased from ABCR company and used as-received. The PDMS precursor sample numbering corresponds to their lot number of the supplier: rPDMS-431 (M_w = 29.4K, PD = 2.6, 4.3 mol % vinyl), rPDMS-731 (M_w = 32.2K, PD = 2.6, 7.8 mol % vinyl), ePDMS-21 (M_w = 22.8K, PD = 2.1), and ePDMS-25R (M_w = 9.4K, PD = 2.0).

Table 1 summarizes the different network samples and results of their characterization. The "r" samples were prepared with 20 wt % toluene to facilitate mixing, and the amount of difunctional cross-linker was varied to realize different cross-link densities. The last part of the sample name cXXX indicates the percentage of reacted vinyl units. The "e" samples were prepared using a stoichiometric amount of a 4-functional cross-linker in solutions containing different amounts of toluene, with tXXX indicating the relative weight of toluene in % as

Table 1. Results of the Characterization of PDMS Network Samples

sample		$D_{res}/2\pi{}^a$ (Hz)	$\omega_{def,dry}{}^a$ (%)	$\omega_{def,sw}$ (%)	ω_{sol} (%)
rPDMS-731	c100	765	0.6		1.3
	c075	633	0.7	19	1.7
rPDMS-431	c090	410	2.7	27	5.4
	c060	240	5.6	36	8.2
ePDMS-21	t000	381	3.9		3.0
	t020	306	1.0		4.0
	t100	227	1.4		3.6
	t200	189	1.6	20	4.2
	t400	147	1.5		4.2
	t700	123	1.5		3.7
ePDMS-25R	t050	180	0.7		3.3
	t100	136	0.6		3.8
	t400	097	1.7		2.8

^{a}Determined by MQ NMR on dry samples.

Table 2. Thermal Properties of PDMS[42] and the Different Solvents Used for the Swelling Experiments

substance	θ^a (K)	$\rho(T\ [°C])$ (g/cm³)
PDMS		$0.9919 - 8.925 \times 10^{-4}T + 2.65 \times 10^{-7}T^2 - 3.0 \times 10^{-11}T^3$
toluene	240	$0.886 - 9.12 \times 10^{-4}T - 4.23 \times 10^{-7}T^2$
ethyl acetate	278	$0.925 - 0.00141T + 6.53 \times 10^{-6}T^2$
butanone	293	$0.828 - 0.0011T$
styrene	308	$0.924 - 9.18 \times 10^{-4}T$
phenetole	363	$0.984 - 9.33 \times 10^{-4}T$
1-propanol	398	$0.818 - 6.63 \times 10^{-4}T - 2.08 \times 10^{-6}T^2$

^{a}The θ-temperatures are for solutions of linear PDMS taken from ref 40, except for the styrene value that is published in ref 41.

compared to the weight of PDMS. Detailed partial-swelling studies on these latter samples, for which the amount of trapped entanglements is expected to vary, will be published shortly. We here just note that the results obtained for the equilibrium-swollen state that are addressed herein do not differ qualitatively within the series and as compared to the bulk end-linked samples. The samples can simply be considered as having different effective cross-link densities.
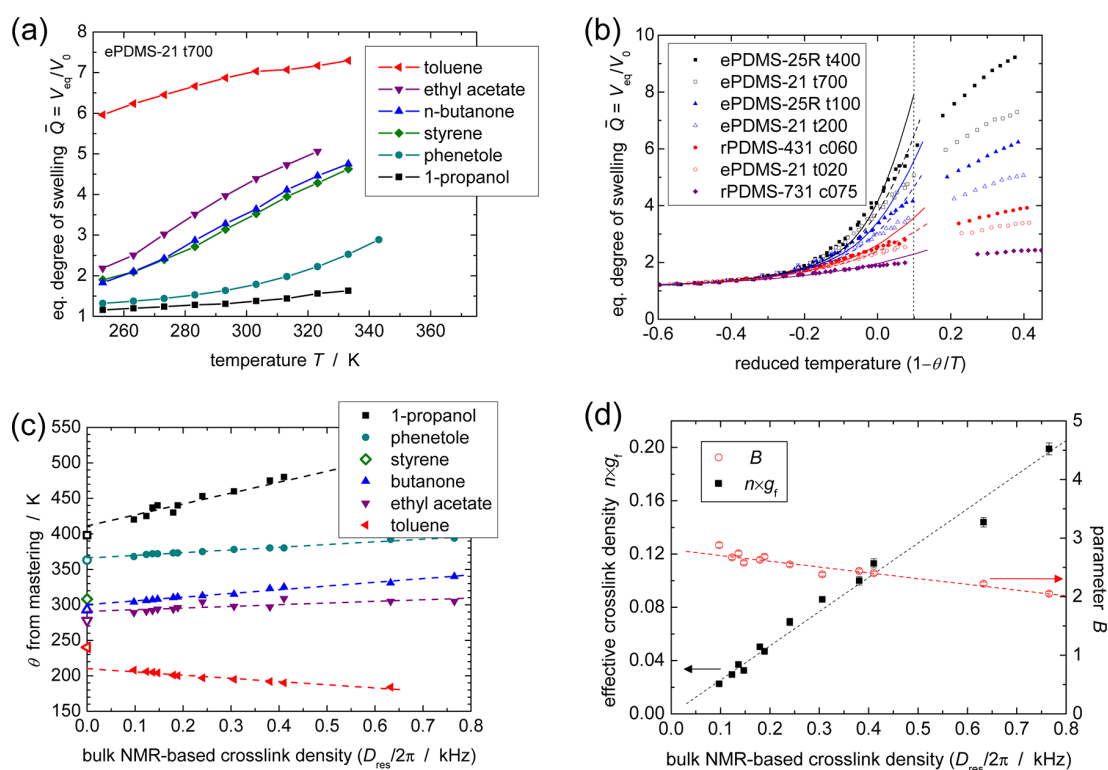
B. Equilibrium Swelling Experiments. The equilibrium swelling experiments were carried out over a wide range of temperatures between 250 and 350 K using different solvents, the properties of which are listed in Table 2. Five pieces of each sample were weighed in the dry state ($m_0 \approx 50$ mg) and swollen for 4 days to equilibrium. The swelling kinetics was checked in several cases, and equilibrium was found to be reached already after several hours in most cases. Swollen samples were blotted with tissue paper to remove the excess of solvent and weighed immediately (m_{sw}). Finally, the swelling solvent was evaporated carefully from the networks over a couple of days, and the dry samples were weighed again (m_{dry}). The sol content ω_{sol} is the fraction of polymer chains not coupled to the network after the cross-link reaction and was extracted from the samples during swelling. The sol fraction ω_{sol} was estimated by comparing the weight of the networks as-prepared m_0 and the weight of the dry networks m_{dry} corresponding to $\omega_{sol} = (m_{dry} - m_0)/m_0$. The equilibrium degrees of swelling $\bar{Q}$ were calculated according to eq 11 using the PDMS density ρ_p and the respective solvent density ρ_s given in Table 2:

$$\bar{Q} = \frac{V_{sw}}{V_{dry}} = \frac{m_{dry}/\rho_p + (m_{sw} - m_{dry})/\rho_s}{m_{dry}/\rho_p} \tag{11}$$

C. NMR Spectroscopy. Proton MQ time-domain solid-state NMR experiments were carried out on a Bruker minispec mq20 spectrometer operating at a resonance frequency of 20 MHz with a 90° pulse length of 2.8 μs and a dead time of 13 μs. The experiments and the analysis of the measured raw data were performed following the previously published procedures.[11,38,43] NMR experiments yielding the distribution-averaged RDCC, D_{res}, were performed at 313 K on the dry network samples to characterize their cross-link density ($D_{res} \propto 1/M_{c,app}$) and in the different solvents at various temperatures at swelling equilibrium, where $\bar{D}_{res}$ reflects the state of stretching of the elastically active chains and thus the thermodynamic properties. The segmental dynamic tensor order parameter is in all cases obtained according to

$$s = \frac{D_{res}}{2\pi \times 7580\ \text{Hz}} \tag{12}$$

where the reference coupling of a Kuhn segment of PDMS in the denominator is taken from ref 44. It should be mentioned that the "NMR cross-link density" D_{res} determined in the bulk includes the action of entanglements and "packing constraints", which are partially relieved in the swollen state. This is not a problem here, since the bulk D_{res} is only used as a gauge and does not enter the data analyses, which focuses only on properties measured in swelling equilibrium. An in-depth discussion of this issue is presented in ref 38.

Figure 2. Results from equilibrium swelling experiments (color online). (a) Equilibrium degrees of swelling $\bar{Q}$ for one of the samples in the different solvents as a function of temperature. (b) Solvent-independent swelling master curves of the data in (a) for each given network, obtained by shifting the data in the different solvents along an abscissa given by $(1 - \theta/T)$, varying θ to obtain the best match. The lines are fits to eqs 2 and 3 for all data $(1 - \theta/T) < 0.1$, as indicated by the dotted vertical line. Note that the fits were performed in an inverse representation, plotting reduced temperature vs $\bar{Q}$. (c) Apparent θ-temperatures obtained from the shifting procedure vs cross-link density. The open symbols on the ordinate are the literature values for θ of solutions of linear PDMS. (d) Results from the fits shown in (b) as a function of cross-link density. The dashed lines in (c) and (d) are linear fits.

An analysis of the different MQ NMR signal functions also yields the apparent defect fraction ω_{def} of material that is not part of the elastically active network, as reflected in slowly relaxing signal tails. In the swollen state, this quantity is dominated by the solvent signal. Some of the samples were swollen and measured in deuterated toluene in order to determine the exact content of elastically ineffective network defects $\omega_{def,sw}$. The defect content in the given type of networks is indeed considerable but is in very good agreement with computer simulations[45] and theoretical calculations based on the theory of statistical cross-linking (see ref 38 for a detailed study of the given samples). On the basis of the qualitative correlation between $\omega_{def,dry}$ and $\omega_{def,sw}$ (see Table 1), we can estimate the defect content to about 20% or lower in most ePDMS samples. Note that the defects in principle act as a second component of the swelling solvent. However, all relevant conclusions are drawn from samples with $\bar{Q}$ in excess of 2, at which the given defect content is an admixture on the 10% scale. We have thus chosen to neglect this issue, but note that some systematic error may arise.

VI. RESULTS AND DISCUSSION

A. Equilibrium-Swelling Experiments. We first address, experimentally, the applicability of FR theory, eq 2. We primarily focus on the phenomenological temperature dependence of the excluded-volume parameter as given by eq 3, by determining the equilibrium degree of swelling $\bar{Q}$ over a wide temperature and solvent range (see Figure 2a for the data taken for one network sample). Corresponding swelling experiments in all solvents over a wide temperature range were conducted for all samples.

Noting the expected temperature dependence $(1 - \theta/T)$, which should be a good approximation for temperatures sufficiently close to θ, we attempt to construct solvent-independent *swelling master curves*, combining all data of one given network sample in *all solvents* in a single data set. As the unshifted reference, we chose the data taken for styrene, which was shown to be a θ-solvent at 35 °C.[41] Thus, keeping $\theta_{styrene}$ constant at 308 K, the equilibrium degrees of swelling of a given sample in the other solvents were plotted vs $(1 - \theta/T)$, varying θ so as to achieve the best overlap of $\bar{Q}(1 - \theta/T)$. As is apparent from Figure 2b, which shows examples for seven different samples, shifting and master-curve construction works rather well, in particular for the data taken around θ-conditions and in poor solvents. The good-solvent range represented by toluene is somewhat less reliable due to the lack of data overlap, as we were not able to identify a suitable in-between solvent.

The shifting procedure yields apparent absolute-value estimates for the θ-temperatures of all solvents, except the styrene reference, in the different network samples. Figure 2c presents these results for the different solvents as a function of the NMR-determined cross-link density measured in the dry state, which of course has an inverse relation with $\bar{Q}$ and thus a direct positive relation with the polymer concentration at swelling equilibrium. Within the accuracy of our data, we see that for all solvents with θ-temperatures not too far from the reference solvent styrene (phenetole, butanone, and ethyl acetate) the correlations of the apparent θ with the cross-link density are rather weak. Note that these observations are

potentially convoluted with a cross-link-density dependence of θ of the reference solvent styrene, which, as further discussed below, is assumed to be weak or even absent.

An important consistency check is represented by the linear back-extrapolations to zero cross-link density, which reproduce the literature values for θ (indicated by the open symbols on the ordinate) within about 10 K. We stress that the largest deviation between the back-extrapolated apparent θ and the corresponding literature value is observed for toluene, which is a good solvent. This already demonstrates that the simple mean-field ansatz, locating the temperature dependence only in the FH term, is problematic. This will be taken up below, where we address the problems related to using FR theory for good solvents.

In order to assess the applicability of the simple FR eqs 2 and 3, we have fitted the master curves in Figure 2b with the effective cross-link density ng_f and the parameter B as the only free variables. Since eq 2 cannot be solved for $\overline{Q} = 1/\phi$ analytically, we have performed the fits with $\overline{Q}$ as the abscissa and $(1 - \theta/T)$ as the ordinate. Note that only now, as opposed to our simple shifting procedure, we implement the typical assumptions of FR theory concerning a specific model for the elastic response and the additivity of osmotic and elastic contributions to the free energy. We have restricted the fits to the range $(1 - \theta/T) < 0.1$, in agreement with the well-known fact that the applicability of FR theory, being a mean-field theory, is of course best for low $\overline{Q}$ as further discussed below. The fits indeed describe the range below $\overline{Q} \approx 4$ and the range from poor solvents to slightly above θ-conditions rather well but fail completely to account for the good-solvent region.

The results shown in Figure 2d nicely confirm that the FR equations provide a good measure of the cross-link density ng_f and thus appear to be well-applicable in the poor- and θ-solvent regimes. Using appropriate and literature-known apparent (concentration- and cross-linking-dependent) χ parameters in applications of FR theory to determine the cross-link density from swelling experiments, we have previously obtained similar good-quality linear correlations with NMR-based absolute-value determinations of the cross-link density in natural rubber[14] and PDMS elastomers.[38]

However, here χ is not taken as an input parameter, but can be estimated from eq 3, $\chi \approx {}^{1}/_{2} - B(1 - \theta/T)$, using the apparent θ temperatures from Figure 2c and the fitted dimensionless parameter B, which exhibits a clear decreasing trend with values ranging from about 2.9 to 2.1 upon increasing the cross-link density. Apparent χ parameters are plotted as a function of the NMR-based cross-link density in Figure 3, taking room temperature as a reference. For all solvents except toluene, the estimated χ parameters are well within the range reported in the literature[46] and exhibit relative variations with cross-link density which are comparable to what is reported in the literature for networks swollen in poor or θ solvents.[14,17,20] Since $\overline{Q}$ (= inverse concentration) depends on the cross-link density, it is not possible here to decide whether this trend is related to a variation with either the degree of cross-linking or just the concentration. Notably, the variations are mostly due to the trends seen for θ in Figure 2c, while the influence of the variable B on χ is rather weak over the given value range of B. This again hints at the general limitations of FH (mean field) theory in describing the thermodynamic state of polymer solutions. To conclude, the most important observation from our swelling experiments is the complete failure of FR theory to account for data at high $\overline{Q}$ (Figure 2b)
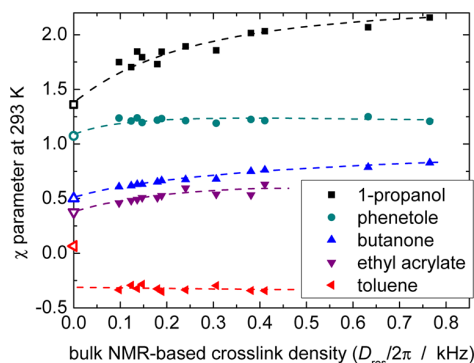
Figure 3. Apparent χ parameters calculated from eq 3, $\chi \approx {}^{1}/_{2} - B(1 - \theta/T)$, using the apparent θ temperatures from Figure 2c and the fitted dimensionless parameters B. The dashed lines are just guides to the eye, and the open symbols on the ordinate are calculated from the literature values for θ of solutions of linear PDMS. Note the unrealistically low values for toluene, which demonstrate the inapplicability of FR theory.

and the discrepancy of the apparent θ from the literature (solution) values for the good solvent toluene. Its χ parameter estimated from our data for room temperature is actually negative, as opposed to a literature value in the range of 0.45.[5] The thermodynamics of a network swollen in good solvent thus differs qualitatively from the mean-field picture of the FH and FR theories.

B. Order Parameters at Equilibrium Swelling. We now address the general relation between the NMR-detected order parameter $\overline{s}$ measured at swelling equilibrium and $\overline{Q}$. We aim at a universal relation that is independent of the cross-link density $n \sim 1/N$ appearing in eq 2. As mentioned, this equation cannot be solved for $\overline{\phi} = 1/\overline{Q}$. However, the inverse solution $N(\overline{Q}, v)$ is straightforwardly obtained:

$$N(\overline{Q}, v) = 1/n(\overline{Q}, v) = g_f \frac{\overline{Q}^{5/3}}{\frac{1}{2}v - {}^{2}\ln(1 - 1/\overline{Q})\overline{Q}^2}$$

(13)

From this expression the limiting case for high degrees of swelling $\overline{Q} \gg 1$ can be read off directly. In good solvent, $v > 0$, and we obtain the well-known result $\overline{Q} \sim N^{5/3}$. For the θ-point, $v = 0$, we take into account the leading-order term ${}^{2}\ln(1 - \phi) \simeq -{}^{1}/_{3}\phi^3$, leading to $\overline{Q} \sim N^{3/8}$. We note that both conditions—high degree of swelling and $T = \theta$—are difficult to match experimentally, which means that low-concentration approximations must not be used.

1. Poor- and θ-Solvent Cases: Order Parameter at Low Degrees of Swelling. The FH model can in fact be assumed to be rather good for *low degrees of swelling*,[32] which is usually the case for swelling of polymer networks in poor and θ-solvents. As a consequence, the full nonlinear solution has to be considered. We note that a poor solvent does not lead to changes in the Gaussian statistics but only to a low degree of swelling. Therefore, the poor-solvent case meets the conditions of the FR model best.

For swelling up to the θ-temperature, the order parameter is given by eq 10 with $R_0^2 = l^2N$. If we introduce the linear stretching ratio $\lambda = R/R_0 = Q^{1/3}$ (the latter relation refers to affine deformation), we obtain

$$s = \frac{3}{5}A_0\frac{1}{N}Q^{2/3} \tag{14}$$

We again note that the phantom model can be mapped onto the affine case by simple rescaling of the effective network chain length,[37] which, along with g_f, can be absorbed into A_0. Now, using the exact solution of the FR model, eq 13, leads to

$$\overline{s} = \frac{3}{5}A_0\overline{Q}^{-1}\left\{\frac{1}{2}v - {}^2\ln(1 - \overline{Q}^{-1})\overline{Q}^2\right\} \tag{15}$$

This equation relates *two directly measurable quantities*, namely the residual dipole–dipole coupling (expressed by the order parameter $\overline{s}$) and the degree of equilibrium swelling $\overline{Q}$. The limiting cases for $\overline{Q} \gg 1$ are given by

$$\begin{cases} \overline{s} \sim \overline{Q}^{-1} & T > \theta \\ \overline{s} \sim \overline{Q}^{-2} & T = \theta \end{cases} \tag{16}$$

However, we note that the former case cannot be considered correct, since excluded-volume effects are not properly taken into account for good solvent and $\overline{Q} \gg 1$.[24] For $T < \theta$, no asymptotic solution with a distinct power-law exponent can be obtained. In this case, the limit $\overline{Q} \gg 1$ cannot be reached.

In Figure 4, we display the experimental results obtained for all PDMS networks in styrene solutions, in which the range of investigated temperatures covers a wide range from well below to above θ. We have fitted the data with a fixed $\theta = 308$ K, which corresponds to θ of linear-polymer solutions, as evidenced by ideal chain dimensions.[41] Here, only two free parameters, $A_0 = 0.9$ and $B = 2.4$, have been used in a simultaneous fit to all data sets. A good fit to all data sets from poor-solvent conditions up to the θ-point and slightly above it can be achieved. Gratifyingly, the result for the parameter B is fully compatible with the value range estimated from the swelling master curves covering a larger range of solvent conditions (see Figure 2d).

In the good-solvent region the fit quality deteriorates, as the predictions for athermal solvents lie far above the data range. As will be discussed below, in the good-solvent range, eq 14 does not hold, and the general relation given by eq 10 has to be used,
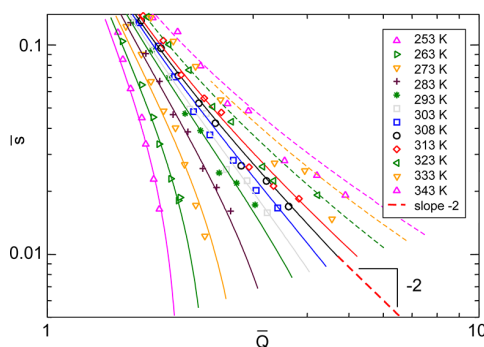
Figure 4. Comparison of the segmental order parameter at equilibrium swelling $\overline{s}$ as obtained by NMR as a function of $\overline{Q}$ and eq 15 in a broad range of temperatures for PDMS networks in styrene, covering the range from well below to above θ. The lines are from a simultaneous fit yielding $A_0 = 0.9$ and $B = 2.4$, using a constant $\theta = 308$ K. The limiting slope for the θ-temperature according to eq 16 is indicated. Results for temperatures far above θ, which were not included in the fit, are plotted as dashed lines. Different colors denote different temperatures.

which takes into account the solvent effect for chain stretching, which reduces the segmental order parameter at a given Q.[24] We note that the trick of shifting the (apparent) θ-point can be formally applied in order to improve the fit for the data at higher temperatures. However, the fit then deteriorates for all data sets at lower temperatures. Such results would be in contrast with both the expected range of validity of the FH model and the expected corrections to the order parameter due to excluded-volume effects.

We thus conclude that the θ-point of PDMS networks swollen in styrene is most likely not shifted as compared to the solution state; i.e., our data can be explained by a constant χ parameter. This is remarkable, considering that the literature value for θ of solutions of linear PDMS has been used and that the data covers a large range of cross-link densities. The deviations for swelling at $T > \theta$ are due to the improper use of Gaussian statistics for segment orientations.

2. Good-Solvent Limit. The swelling of polymer networks in good solvent changes both values of R and R_0 in eq 10. Let us reconsider the FR model for the present case. Again, we assume stretching of the chain due to swelling from the dry network state according to $R = N^{1/2}Q^{1/3}$. Using the well-known result for $R_0^2(N,Q) = A_R l^2 N Q^{1/4}$ (A_R being a numerical constant) in the semidilute state (considering the Flory exponent $\nu_F = 3/5$, which is sufficiently accurate in the present context), we obtain from eqs 10 and 13 in the limit $Q \gg 1$

$$\overline{s} = \frac{3}{5}\frac{Av}{2g_f}\overline{Q}^{-3/2} \tag{17}$$

Here, the numerical prefactor is given by $A = A_0/A_R^2$. The power-law decay with an exponent of $-3/2$ is in marked contrast to the FR result without correction of the solvent effect for the order parameter, $\overline{s} \sim \overline{Q}^{-1}$ (see eq 16); however, as shown previously, it is in excellent agreement with experimental data for different types of networks in the good-solvent regime.[24] This study was restricted to a single temperature, and in order to test eq 17 in a wider range of temperatures, we have estimated the asymptotic slopes of the order parameter in the log–log plot of Figure 4 for the case of styrene and combined these results with equivalent results for toluene, now also taken over a wide temperature range. The results are plotted as a function of the reduced temperature $(1 - \theta/T)$ in Figure 5. It can be observed that the effective exponents approach the athermal-solvent value of $-3/2$ but never reach any higher value even for the highest temperatures displayed for toluene (340 K), which is a rather good solvent for PDMS already at room temperature. Note that the $(1 - \theta/T)$ temperature scaling assumed in mean-field theory may well break down in the good-solvent limit (see Figures 2 and 3). This is also the reason for the slight misfit in the trends for the two series of data points in Figure 5. However, we stress that the effective exponent determined from the slope in a log–log plot of $\overline{s}$ vs $\overline{Q}$ taken for a series of networks with different cross-link density reflects the solvent quality very reliably.

3. Flory–Rehner vs c* Model. It is instructive to compare the result for equilibrium swelling in athermal solvent with the predictions of de Gennes' c* model.[32] In this case the equilibrium degree of swelling is just given by the overlap threshold of the network chain, $\overline{Q} \sim Q^* \sim N^{3\nu-1}$. Considering eq 10 for $R = R_0$, we obtain $s \sim R_0^{-2}$ and in the limit of overlap swelling
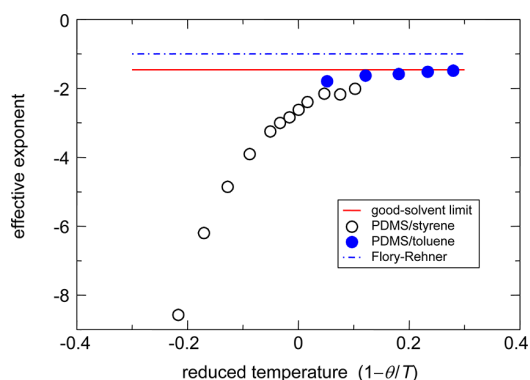
Figure 5. Effective exponents for PDMS in two solvents as a function of the reduced temperature. The literature values for θ have been used for the reduced temperature, which explains the overlap of its value ranges. Note the discrepancy to Figure 2b, where it was shown that the apparent (shifted effective) θ temperatures for toluene deviate substantially from the literature value.

$$\overline{s} \sim \overline{Q}^{-2\nu/(3\nu-1)} \tag{18}$$

This results agrees with the prediction of eq 17 for $\nu_F = 3/5$. Interestingly, by rederiving the FR swelling result using scaling arguments,[47,48] one obtains $\overline{Q} \sim N^{3(2\nu-1)/4}$ instead of $\overline{Q} \sim N^{5/3}$ (see eq 13), which leads in combination with eq 10 again to eq 18.[24]

This surprising coincidence of the FR and c^* models can be better understood if we rewrite eq 18 in terms of the correlation length $\xi \sim Q^{\nu/(3\nu-1)}$

$$\overline{s} \sim \xi^{-2} \tag{19}$$

This result is now valid for semidilute solution (FR) and at the overlap threshold. It relates the order parameter directly with the correlation length of the network at equilibrium swelling, as can also be obtained by scattering experiments. Using des Cloizeaux's relation $\xi^3\Pi \sim kT$, where Π denotes the osmotic pressure, we obtain

$$\overline{s} \sim (\Pi/kT)^{-2/3}$$

Again, this is a direct relation between two measurable quantities, the validity of which can be assessed experimentally.

The reason why the relations coincide for both models is straightforwardly explained by the high stretching of chains in the FR model. While the elastic contribution in the FR free energy is of the order of kT per chain, the mixing free energy is proportional to the number of monomers in the chain. At swelling equilibrium the chains are fully extended strings of Pincus blobs,[32] the size of which corresponds to ξ (see Figure 6). The chain extension is given by $R \sim (N/M)\xi \sim N^{(3\nu+1)/4}$, where M denotes the number of monomers within a blob. The last result leads to the well-known relation $R \sim N^{7/11}$ by using $\nu = 3/5$ (see also ref 49). As a consequence, segmental orientation fluctuations can only take place within a blob, and the swollen network is in fact equivalent to a c^* gel at the corresponding degree of swelling. Thus, NMR experiments on equilibrium-swollen networks provide a direct measure of the blob size.

C. Is the θ-Point Accessible in Swollen Polymer Networks? The results in Figure 4 show that the asymptotic behavior $\overline{s} \sim \overline{Q}^{-2}$ expected for the θ-temperature is not reached for the system studied. This is because the degree of swelling
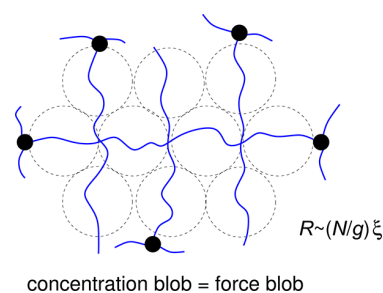
Figure 6. Sketch of network chains at equilibrium swelling according to the Flory−Rehner model. The chain corresponds to a fully extended string of concentration blobs which at the same are Pincus (force) blobs.

under θ-conditions is rather low and higher virial coefficients contribute to the general result of eq 15. Thus, the θ-point itself, which is defined as the asymptotic state for $v = 0$ and $\overline{Q} \gg 1$, is not observed in our experiments.

The thermal blob size $\xi_T \sim 1/v$ is defined as the crossover from Gaussian statistics to excluded-volume dominated (or collapsed in the case of $v < 0$) conformations. It can be obtained both from the Flory result of the excluded-volume chain or from a Lifshitz-type argument for self-contacts in Gaussian chain statistics. For $\xi < \xi_T$, excluded volume effects are only weak. In this region we assume the classical correlation length $\xi \sim (Q/v)^{-1/2}$. At the crossover we obtain $\xi \sim \overline{Q}^{-1}$. We further assume the degree of equilibrium swelling is given by $\overline{Q} \sim N^{3/8}$ (see eq 13). Thus, we obtain a crossover relation for the excluded-volume dominated, good-solvent limit which depends on the cross-link density

$$v_n \sim N^{-3/8} \sim n^{3/8}$$

This defines a line in the n,T-diagram which separates the good- from the poor-solvent region (see Figure 7). It defines a smooth crossover above the θ-temperature. By lumping all unknown constants into C, we obtain

$$T_n = \theta(1 + Cn^{3/8}) \tag{20}$$

Let us call T_n the network temperature. The θ-point can only be reached in the limit $n \to 0$, that is, at very low cross-link
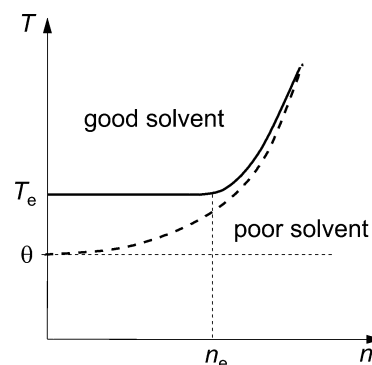
Figure 7. Phase diagram of a polymer network at equilibrium swelling. Good-solvent states are separated from poor-solvent states by a continuous crossover above the θ-temperature, as indicated by the dashed line. In entangled polymer networks, n_e denotes the density of entanglements, and the crossover becomes independent the network density, as indicated by the solid line.

densities. At higher values of n, the crossover to the apparent θ-state (Gaussian statistics) is reached already at higher temperatures (corresponding to a higher χ-parameter), and higher orders of the virial coefficient are important if $\overline{Q}$ is low.

Real networks contain entanglements, and the fraction that is topologically trapped provides a constant contribution to n at swelling equilibrium and thus limits $\overline{Q}$. This leads to

$$T_e = \theta(1 + Cn_e^{3/8}) \tag{21}$$

where n_e indicates the density of trapped entanglements . Thus, the θ-point cannot be reached at all, and transitions between good- and poor-solvent states proceed without signature of the θ-point. This might put the discussions about the apparent shift of the θ-temperature and the concentration (cross-link-density) dependence of χ for polymer networks swollen in good solvents into a different perspective. Instead of a sharp transition with a well-defined limiting case of $T \rightarrow \theta$, a broad and smooth crossover between good and poor solvent regimes is expected.

We point out again the behavior of the apparent θ-temperatures obtained from master curve constructions for different solvents in Figure 2c, which suggests systematic deviations from the literature values, which are rather small around θ and correspond to the weak concentration- or cross-linking-dependence of the χ parameter. Now, being in the poor- or good-solvent regions in our phase diagram does or does not, respectively, imply the applicability of eq 2 for the analysis of swelling results. The predicted behavior, in particular the effect of entanglements, implies a favorably larger applicability range even for temperatures above θ. This will of course break down for rather good solvents, which is the origin of the large deviations apparent in Figure 2 for data obtained for PDMS swollen by the best solvent studied, toluene.

D. Validity of the Flory−Rehner Model. We note that most commonly FR theory is applied outside of its actual validity limit, i.e., for swelling in good solvents. Here, large equilibrium degrees of swelling, $\overline{Q}$, violate the mean-field assumption inherent to the FH model for the free energy of mixing. This may partially explain the common need for using an apparently concentration- and (thus) cross-link density-dependent values of the apparent χ parameter,[17−20] related with an apparent shift in the θ-temperature as compared to non-cross-linked samples. However, as we have seen that variations in χ also arise in the poor- and θ-solvent range, more subtle limitations of mean-field (FH) theory, along with a violation of the additivity assumption, may play a role. Another complication arises from the assumption of affine deformation of chains during swelling. This leads to maximum stretching of chains at the given concentration (see Figure 6). At high degrees of equilibrium swelling, entropy can be gained by, at least partial, desinterspersion of chains, which, in the extreme case, corresponds to the c^*-state of the network.

We remind that even though the most prominent feature of the "swelling anomaly" appears to be resolved,[15] standard FR theory still cannot account for the apparently nonconstant swelling activity parameter. This feature can, however, be successfully modeled by using, as mentioned, a concentration- or cross-linking dependent χ parameter,[17−20] in combination with modifications of the network deformation model, where constrained-chain approaches[21,22] have been successfully used.[15] It appears well possible that the nontrivial chain statistics described above represents an alternative explanation, in particular for the elastic contribution. This issue clearly deserves more attention in future research.

In contrast, swelling in poor solvents and close to the θ-point leads to low degrees of equilibrium swelling $\overline{Q}$, and both the assumption of Gaussian elasticity and the mean-field mixing free energy are expected to be rather good approximations. However, because of the low degree of swelling, this requires the use of the full analytical form of the FR expression without any low-concentration approximations. Relating two directly accessible quantities, the equilibrium degree of swelling and the orientational order parameter of the segments in a range around and below θ-conditions, good agreement between FR predictions and our experimental results is indeed found, at least for the given case in which the θ-temperature of the styrene/PDMS network system does not appear to be much different from that of the linear polymer solution. However, because of the limitation of the correlation length in polymer networks by cross-links and entanglements, a clear signature of the θ-point is absent, and a smooth crossover to the poor solvent regime occurs above the θ-point.

V. CONCLUSIONS

NMR experiments performed on swollen polymer networks provide an alternative test for theoretical models of network swelling via their sensitivity to segmental orientation correlations, as quantified by the local, dynamic tensor order parameter that is defined with respect to the end-to-end vector of the network chains. In this work, we have considered the Flory−Rehner model for network swelling, as combined with predictions for the tensor order parameter based upon the Gaussian approximation for the chain statistics. This leads to a prediction for the relation between two directly measurable quantities: the equilibrium degree of network swelling and the tensor order parameter measured in this state. An explicit estimation of the cross-link density is not necessary. Experiments on different PDMS networks swollen in styrene (θ-solvent at 308 K) at different temperatures are in very good agreement with the theoretical predictions for temperatures below and near the θ-point, where the θ-temperature is found to be unchanged with respect to the non-cross-linked polymer. In contrast, in the good solvent regime, associated with large degrees of swelling, this approach is not valid. Here, only explicit and rather unrealistic shifts of the apparent θ-temperature can enforce a fit between the experimental results and the theoretical predictions.

The direct observation of the equilibrium degrees of swelling as a function of temperature in different solvents concurs with this result. We have measured solvent- and temperature-dependent swelling data, and for each network sample, the data for different solvents were suitably combined into a swelling master curve as a function of reduced temperature, $\overline{Q}(1 - \theta/T)$, taking styrene as a reference. A consistent fit of these master curves using the standard FR-model is not possible over the full range of temperatures but can be achieved for temperatures below and also slightly above the θ-point. As an independent consistency check, the apparent θ-temperatures obtained from the shifting procedure for a variety of solvents are also in good agreement with corresponding literature data, with the exception of the good solvent toluene, for which large deviations are apparent.

On the basis of these results, we conclude that FR theory is well applicable provided that the θ-point is not shifted very much, which is the case for the PDMS/styrene system studied in this work. For the case of good solvent the FR model is clearly stretched beyond its theoretical limitations, as can be

inferred from the deviations of our NMR data from the predictions and also from the direct observation of the equilibrium degrees of swelling as a function of temperature in this regime, which do not comply with the FR prediction. In order to correctly predict the segmental order parameter in the this case, excluded-volume effects on the chain statistics have to be included, as already shown in previous work. We finally note that a direct observation of the θ-point in swelling of polymer networks is not easily possible, since finite length scales due to cross-linking and entanglements shift the apparent crossover between the good- and poor-solvent regimes to temperatures above θ. Future studies will have to show whether the nontrivial chain statistics in good solvent can serve as an input for improved predictions of the thermodynamics of networks swollen in good solvent.

■ AUTHOR INFORMATION

Corresponding Authors
*E-mail: kay.saalwaechter@physik.uni-halle.de.

*E-mail: sommer@ipfdd.de.

Notes

■ REFERENCES

(1) Smoluchowski, M. v. Molekular-kinetische Theorie der Opaleszenz von Gasen im kritischen Zusatande, sowie einiger verwandter Erscheinungen. *Ann. Phys.* **1908**, *25*, 205−226.

(2) Einstein, A. Theorie der Opaleszenz von homogenen Flüssigkeiten und Flüssigkeitsgemischen in der Nähe des kritischen Zustandes. *Ann. Phys.* **1910**, *33*, 1275−1298.

(3) Yamakawa, H. *Modern Theory of Polymer Solutions*; Harper & Row: New York, 1971.

(4) Huglin, M. B., Ed.; *Light Scattering from Polymer Solutions*; Academic Press: London, 1972.

(5) Horkay, F.; Hecht, A.-M.; Geissler, E. Thermodynamic Interaction Parameters in Polymer Solutions and Gels. *J. Polym. Sci., Part B: Polym. Phys.* **1995**, *33*, 1641−1646.

(6) Flory, P. J. *Principles of Polymer Chemistry*; Cornell University Press: Ithaca, NY, 1953.

(7) Flory, P. J.; Rehner, J., Jr. Statistical Mechanics of Cross-Linked Polymer Networks I. Rubberlike Elasticity. *J. Chem. Phys.* **1943**, *11*, 512−520.

(8) Flory, P. J.; Rehner, J., Jr. Statistical Mechanics of Cross-Linked Polymer Networks II. Swelling. *J. Chem. Phys.* **1943**, *11*, 521−526.

(9) Cohen-Addad, J. P.; Domard, M.; Herz, J. NMR observation of the swelling process of polydimethylsiloxane networks. Average orientational order of monomeric units. *J. Chem. Phys.* **1982**, *76*, 2744−2753.

(10) Cohen-Addad, J. P. NMR and Fractal Properties of Polymeric Liquids and Gels. *Prog. Nucl. Magn. Reson. Spectrosc.* **1993**, *25*, 1−316.

(11) Saalwächter, K. Proton Multiple-Quantum NMR for the Study of Chain Dynamics and Structural Constraints in Polymeric Soft Materials. *Prog. Nucl. Magn. Reson. Spectrosc.* **2007**, *51*, 1−35.

(12) Gottlieb, M.; Gaylord, R. J. Experimental Tests of Entanglement Models of Rubber Elasticity. 2. Swelling. *Macromolecules* **1984**, *17*, 2024−2030.

(13) McKenna, G. B.; Flynn, K. M.; Chen, Y. Swelling in crosslinked natural rubber: experimental evidence of the crosslink density dependence of χ. *Polymer* **1990**, *31*, 1937−1945.

(14) Valentín, J. L.; Carretero-González, J.; Mora-Barrantes, I.; Chassé, W.; Saalwächter, K. Uncertainties in the Determination of Cross-Link Density by Equilibrium Swelling Experiments in Natural Rubber. *Macromolecules* **2008**, *41*, 4717−4729.

(15) Xu, B.; Di, X.; Mckenna, G. B. Swelling Behavior of Cross-Linked Rubber: Explanation of the Elusive Peak in the Swelling

(16) Neuburger, N. A.; Eichinger, B. E. Critical Experimental Test of the Flory-Rehner Theory of Swelling. *Macromolecules* **1988**, *21*, 3060−3070.

(17) McKenna, G. B.; Horkay, F. Effects of crosslinks on the thermodynamics of poly(vinyl alcohol) hydrogels. *Polymer* **1994**, *35*, 5737−5742.

(18) McKenna, G. B.; Crissman, J. M. Temperature and Crosslinking Effects on the Swelling of Poly(isoprene) in Isopiestic Conditions. *J. Polym. Sci., Part B: Polym. Phys.* **1997**, *35*, 817−826.

(19) Russ, T.; Brenn, R.; Geoghegan, M. Equilibrium Swelling of Polystyrene Networks by Linear Polystyrene. *Macromolecules* **2003**, *36*, 127−141.

(20) Horta, A.; Pastoriza, M. A. The interaction parameter of crosslinked networks and star polymers. *Eur. Polym. J.* **2005**, *41*, 2793−2802.

(21) Flory, P. J.; Erman, B. Theory of Elasticity of Polymer Networks. 3. *Macromolecules* **1982**, *15*, 800−806.

(22) Erman, B.; Monnerie, L. Theory of Elasticity of Amorphous Networks: Effect of Constraints along Chains. *Macromolecules* **1989**, *22*, 3342−3348.

(23) Rubinstein, M.; Panyukov, S. Elasticity of Polymer Networks. *Macromolecules* **2002**, *35*, 6670−6686.

(24) Sommer, J.-U.; Chassé, W.; Valentín, J. L.; Saalwächter, K. Effect of excluded volume on segmental orientation correlations in polymer chains. *Phys. Rev. E* **2008**, *78*, 051803.

(25) Sommer, J. U.; Vilgis, T. A.; Heinrich, G. Fractal properties and swelling behaviour of polymer networks. *J. Chem. Phys.* **1994**, *100*, 9181−9191.

(26) Bastide, J.; Candau, S. J. *Structure of Gels as Investigated by Means of Static Scattering Techniques*; John Wiley: New York, 1996; Chapter 5, pp 143−210.

(27) Sommer, J. U.; Lay, S. Topological Structure and Nonaffine Swelling of Bimodal Polymer Networks. *Macromolecules* **2002**, *35*, 9832−9843.

(28) Sommer, J. U.; Russ, T.; Brenn, B.; Geoghegan, M. Scaling model for the anomalous swelling of polymer networks in a polymer solvent. *Europhys. Lett.* **2002**, *57*, 32−38.

(29) Cohen-Addad, J. P.; Domard, M.; Lorentz, G.; Herz, J. Polymeric gels. NMR study of elementary chain swelling. Effect of trapped topological constraints. *J. Phys. (Paris)* **1984**, *45*, 575−586.

(30) Cohen-Addad, J. P. Polymeric-gel swelling: NMR evidence for the $c*$ theorem. *Phys. Rev. B* **1993**, *48*, 1287−1290.

(31) Saalwächter, K.; Kleinschmidt, F.; Sommer, J.-U. Swelling Heterogeneities in End-Linked Model Networks: A Combined Proton Multiple-Quantum NMR and Computer Simulation Study. *Macromolecules* **2004**, *37*, 8556−8568.

(32) de Gennes, P. G. *Scaling Concepts in Polymer Physics*; Cornell University Press: Ithaca, NY, 1979.

(33) Sommer, J.-U.; Saalwächter, K. Segmental Order in Endlinked Polymer Networks: A Monte Carlo Study. *Eur. Phys. J. E* **2005**, *18*, 167−182.

(34) Des Cloizeaux, J.; Jannik, G. *Polymers in Solution*; Oxford University Press: Oxford, 1989.

(35) McKenzie, D. S.; Moore, M. A. Shape of self-avoiding walk or polymer chain. *J. Phys. A* **1971**, *4*, L82−L86.

(36) Schäfer, L.; Elsner, K. Calculation of the persistence length of a flexible polymer chain with short-range repulsion. *Eur. Phys. J. E* **2004**, *13*, 225−237.

(37) Lang, M.; Sommer, J.-U. Analysis of Entanglement Length and Segmental Order Parameter in Polymer Networks. *Phys. Rev. Lett.* **2010**, *104*, 177801.

(38) Chassé, W.; Lang, M.; Sommer, J.-U.; Saalwächter, K. Cross-Link Density Estimation of PDMS Networks with Precise Consideration of Networks Defects. *Macromolecules* **2012**, *45*, 899−912.

(39) Kovermann, M.; Saalwächter, K.; Chassé, W. Real-time observation of polymer network formation by liquid- and solid-state

NMR revealing multi-stage reaction kinetics. *J. Phys. Chem. B*, DOI: 10.1021/jp302745a.

(40) Mark, J. E., Ed.; *Physical Properties of Polymers Handbook*; Springer: New York, 2007.

(41) Lapp, A.; Strazielle, C. Un nouveau solvant theta pour le polydimethylsiloxane. Comportement au voisinage des conditions theta et facteur dexpansion. *Makromol. Chem., Rapid Commun.* **1985**, *6*, 591−596.

(42) Shih, C.-S.; Alben, R. Lattice Model for Biaxial Liquid Crystals. *J. Chem. Phys.* **1972**, *57*, 3055−3061.

(43) Chassé, W.; Valentín, J. L.; Genesky, G. D.; Cohen, C.; Saalwächter, K. Precise dipolar coupling constant distribution analysis in proton multiple-quantum NMR of elastomers. *J. Chem. Phys.* **2011**, *134*, 044907.

(44) Saalwächter, K.; Herrero, B.; López-Manchado, M. A. Chain order and crosslink density of elastomers as investigated by proton multiple-quantum NMR. *Macromolecules* **2005**, *38*, 9650−9660.

(45) Gilra, N.; Cohen, C.; Panagiotopoulos, A. Z. A Monte Carlo study of the structural properties of end-linked polymer networks. *J. Chem. Phys.* **2000**, *112*, 6910−6916.

(46) Favre, E. Swelling of Crosslinked Polydimethylsiloxane Networks by Pure Solvents: Influence of Temperature. *Eur. Polym. J.* **1996**, *32*, 1183−1188.

(47) Obukhov, S. P.; Rubinstein, M.; Colby, R. P. Network Modulus and Superelasticity. *Macromolecules* **1994**, *27*, 3191−3198.

(48) Rubinstein, M.; Colby, R. H. *Polymer Physics*; Oxford University Press: New York, 2003.

(49) Pütz, M.; Kremer, K.; Everaers, R. Self-Similar Chain Conformations in Polymer Gels. *Phys. Rev. Lett.* **2000**, *84*, 298−301.

3.4. Real-Time Observation of Polymer Network Formation by Liquid and Solid-State NMR Revealing Multistage Reaction Kinetics

This work aims at the very basic and often researched question of the mechanistic details of network *formation*. In many cases, surprisingly little detailed knowledge is available, thus the reaction kinetics of the cross-linking of end-functionalized PDMS by a four functional cross-linker was studied in-depth. The conversion of the functional groups was determined by high resolution liquid-state NMR in dependence of the reaction temperature. The results show that the reaction has at every stage the same activation energy indicating that it is governed by the same local mechanism throughout the whole cross-linking process. The very high time resolution of the performed experiments reveals a complex dependence of the reaction rate on the reaction turnover. The latter is related to a different reactivity of the cross-linker molecules in dependence on the number of already reacted functional sites. This reasons the observed non-uniform overall reaction order of the cross-linking process whereas the different cross-linker species react corresponding first order reaction kinetics. The results are used to conclude on a three stage model of the reaction kinetics.

Authors Contributions. W.C. and M.K. designed the study. W.C. prepared the samples, performed the measurements and analyzed the data. W.C. and K.S. interpreted the data , and W.C. wrote the manuscript.

Real-Time Observation of Polymer Network Formation by Liquid- and Solid-State NMR Revealing Multistage Reaction Kinetics

Michael Kovermann,[†] Kay Saalwächter,[‡] and Walter Chassé*[,‡]

[†]Institut für Physik—Biophysik, Martin-Luther-Universität Halle-Wittenberg, Betty-Heimann-Str. 7, D-06120 Halle, Germany
[‡]Institut für Physik—NMR, Martin-Luther-Universität Halle-Wittenberg, Betty-Heimann-Str. 7, D-06120 Halle, Germany

ABSTRACT: The reaction rate for the end-cross-linking process of vinyl-terminated poly(dimethylsiloxane) by a cross-linker with four Si–H functionalities in the presence of solvent was studied by ^{1}H liquid-state NMR in dependence of the reaction temperature. The properties of the resulting polymer networks, i.e., the gel-point and the formation of the elastically effective network, were monitored *in situ* during the reaction by single-evolution-time ^{1}H double-quantum (SET-DQ) low-field NMR. It was found that the cross-linking kinetics shows no uniform reaction order for the conversions of the functional groups before the topological gelation threshold of the polymer network. The two NMR methods are combined to investigate the formation of the elastically effective network in dependence of the conversion of the functional groups of the precursor polymers and the cross-linker. The high chemical and time resolution of the experiments enabled an in-depth analysis of the reaction kinetics, allowing us to conclude on a multistage model for PDMS network formation by hydrosilylation-based end-linking in the presence of solvent. We found that the nonuniform network formation kinetics originates from a dependence of the apparent reaction rate on the number of the Si–H groups of the cross-linker that have already reacted during the progress of the reaction. The fastest overall reaction rate is observed in a range until each cross-linker has reacted once on average, and a uniform apparent overall reaction order of unity with respect to cross-linker concentration is only found at a later stage, when multiply reacted cross-linker molecules with similar reactivity dominate.
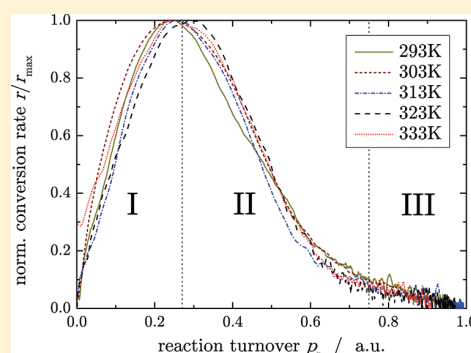
INTRODUCTION

Poly(dimethylsiloxanes) (PDMS) are prominent examples for the versatility of current polymer network materials. The resistance to light degradation, chemical attack, and high temperatures, and of course the extraordinary mechanical properties, render PDMS-based materials applicable as sealant, adhesive, and anticorrosion materials, especially for biomedical uses.

PDMS networks are typically formed by covalent cross-linking of randomly or end-functionalized polysiloxanes and multifunctional cross-linkers with complementary reactive groups. These networks are often used as so-called model networks in studies of rubber elasticity and structure–property relations due to their well-defined cross-link chemistry. A very efficient and frequently used approach is the Pt-catalyzed hydrosilylation[1] of vinyl-terminated poly(dimethylsiloxane) by cross-linkers with silane functionalities. The permanent cross-links are established by addition of the silane-hydrogen to the carbon–carbon double bond, forming an ethylene connection between polymer and cross-linker. The reaction is commonly described by the Chalk–Harrod[2] or the modified Chalk–Harrod[3] mechanism.

The hydrosilylation reaction has been the subject of intense investigations. Many studies show a strong dependence of the reaction kinetics on the molecular structure and type of the catalyst[4−6] and the initial concentration of the functional groups and their stoichiometry.[7] Usually the kinetics are monitored by observation of the chemical conversion of specific functional groups with spectroscopic methods, e.g., FTIR[8] and NMR.[5,6,9] Especially for the reaction order, different results are reported.[5,6,10]

In this work, we present an in depth study of the cross-linking and network formation kinetics of the end-linking process of vinyl-terminated PDMS by a four-functional cross-linker in the presence of solvent. An equal-molar formulation of the polymer and cross-linker is investigated at different reaction temperatures to obtain information about the relevant activation energy. The conversion of the terminal vinyl-groups and the Si–H groups is monitored by high-resolution ^{1}H liquid-state NMR. The high time resolution of the performed experiments allows a detailed discussion of the conversion rates and the reaction order of the hydrosilylation.

The formation of the elastically effective network is investigated by ^{1}H double-quantum (DQ) NMR. This approach uses the fact that the NMR response changes during the cross-link process. In melts, and especially in the presence

of solvent, polymers behave like liquids unless their molecular weight is not far above the entanglement molecular weight M_e. Inter- and intra-monomer dipolar couplings between ^{1}H spin-pairs are completely averaged out by fast segmental fluctuations of the polymer chain. Restrictions, i.e., chemical cross-links and entanglements, constrain the polymer motions. They become anisotropic, and weak residual dipolar couplings persist. Thereby, the anisotropy of the motions is directly proportional to the nature and severity of topological restrictions in which the polymer chains are involved. In this way, the detectable residual dipolar couplings correlate with the physical and chemical cross-link density of polymer networks. In this study, a single-point detection technique for the DQ intensity[11] is used to investigate the formation kinetics of the networks, since the recording of full DQ build-up curves leads to an insufficient time resolution. Combining the observations of the kinetics in terms of chemical conversion and in terms of elastic network-chain formation as a function of temperature, we are able to draw conclusions on the rate-limiting steps in the end-linking reaction by hydrosilylation.

■ EXPERIMENTAL SECTION

Sample Preparation. In this study, a commercially available (ABCR) vinyldimethylsiloxy-terminated poly-(dimethylsiloxane), ePDMS21, and a nominally 4-functional cross-linker, tetrakis(dimethylsiloxy)silane, were used. The prepolymer was characterized by gel permeation chromatography (GPC) using a polystyrene standard. The determined average molecular weight was $M_n \approx 4.8$ kg/mol with a polydispersity of about 2. The average functionality of the cross-linker, turning out to be 3.6 by the ratio of the methyl and Si−H groups, and the precise ratio of the vinyl-functionalized terminal monomers to the dimethylsiloxy monomers were both determined by ^{1}H liquid-state NMR. The catalyst, *cis*-dichlorobis(diethylsulfide)platinum(II),[12,13] was dissolved in 98% toluene.

For the investigation of the cross-link kinetics by ^{1}H liquid-state NMR and ^{1}H low-field DQ NMR, all samples were prepared following the same protocol. The un-cross-linked polymer was dissolved in 200 wt % deuterated toluene with respect to the used amount of polymer and mixed by a shaker at 1200 rpm for about 5 min. This corresponds to a semidilute solution with a polymer concentration about 10 times higher than the overlap concentration ($c^* \approx 0.035$ wt %) and significantly reduced viscosity, facilitating the fast mixing of the reactants. The 3.6-functional cross-linker was added to this solution in a stoichiometric ratio and shaken again. The necessary amount of cross-linker was calculated with regards to the results of the sample characterization by liquid-state NMR. From this parent solution, 700 μL was filled into the NMR sample tubes. For liquid-state and solid-state NMR experiments, 5 and 10 mm tubes, respectively, were used. The sample tubes were placed for about 5 min in the preheated spectrometer for temperature equilibration. After adding 2.5 μL of the catalyst solution, the tubes were sealed carefully with Teflon strips and the measurements were immediately started.

^{1}H Liquid-State NMR Experiments. All ^{1}H liquid-state NMR experiments were performed on a Bruker Avance III 600 MHz spectrometer, using a deuterium lock to avoid and compensate field drifts during the long-time experiments. The cross-link reaction was followed by a pseudo-2D experiment composed of consecutive 1D ^{1}H free induction decay (FID) experiments. The time resolution of the liquid-state NMR

experiments was adjusted with respect to the cross-linking temperature T_{cr} by changing the number of scans used for the acquisition of a single FID. The time increments were in the range of 11−60 s for reaction temperatures of 343−293 K, respectively. The recorded 1D experiments of a cross-link reaction were separately processed for reasons of data quality.

^{1}H Solid-State NMR Experiments. The ^{1}H DQ solid-state NMR experiments were carried out on a Bruker minispec *mq*20 spectrometer operating at a ^{1}H resonance frequency of 20 MHz with a 90° pulse length of 2.2 μs and a dead time of 13 μs. The experiments and the analysis of the measured raw data were performed following the previously published procedures.[14,15]

In this study, we used ^{1}H DQ low field NMR to determine the residual dipolar couplings. Several publications have shown that ^{1}H DQ NMR is a robust and versatile tool for the quantitative investigation of the structure of polymer networks.[14,16−18] The main advantage of this method is the acquisition of two time-dependent sets of data, the double-quantum build-up and the reference decay curve, by different phase cycling schemes in the pulse sequence with a variable evolution time τ_{DQ} for the excitation and reconversion of multiquantum coherences. The intensity of the double-quantum signal $I_{DQ}(\tau_{DQ})$ contains the $(4n + 2)$-quantum coherences and comprises the structural information of the network. The intensity of the reference signal $I_{ref}(\tau_{DQ})$ contains the dipolar modulated longitudinal magnetization and all $4n$-quantum coherences. Additionally, isotropic mobile fractions of the polymer networks, i.e., network defects, contribute to I_{ref}. The defect fraction has a rather slow relaxation as compared to elastically active network components,[19] which allows a precise identification and subtraction of the contribution to I_{ref}. With the two measured signal intensity curves, it is possible to remove the relaxation effects by a point-by-point division of I_{DQ} by the sum of both signals.

$$I_{nDQ} = \frac{I_{DQ}}{I_{DQ} + I_{ref} - \text{defects}} \tag{1}$$

After a proper subtraction of the defect contribution, the normalized double-quantum build-up I_{nDQ} (eq 1) is dominated by pure dipolar interactions that are only related to the network structure. The information about the residual dipolar couplings and their distributions are obtained by fitting functions or numerical inversion procedures. In this study, we used the recently introduced improved Tikhonov regularization procedure to determine the average residual dipolar coupling constant D_{res} of the investigated samples.[15]

The recording of a complete DQ build-up curve takes about 20−60 min. Thus, the method is not suited for the investigation of fast cross-linking processes. To overcome this limitation to the observation of very slow reactions, we use a single point detection to investigate the network formation.[11] This approach is based on the notion that the DQ intensity exclusively arises from contributions of the elastically effective network. The DQ intensity is recorded at a fixed single evolution time (SET) during the whole cross-linking reaction.

In order to test the validity and reliability of this approach, a cross-link reaction at 313 K was investigated by SET-DQ NMR and completely recorded DQ build-up curves (full-DQ). At this temperature, the network formation is just slow enough to be followed by a full-DQ experiment with minimum recycle delay. The results of the full-DQ measurements were evaluated according to the procedure which was explained above. The
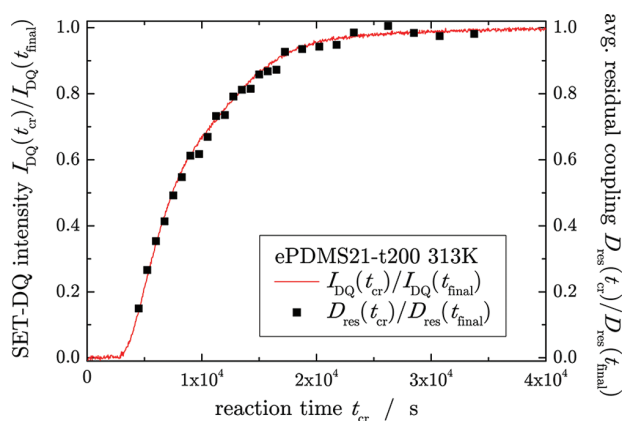
Figure 1. Normalized SET-DQ intensity nI_{DQ} and scaled average residual dipolar coupling constant nD_{res} in dependence of the reaction time of a cross-linking reaction performed at 313 K.

Figure 2. ^{1}H liquid-state NMR spectra acquired during the first 20 min during a cross-link reaction at 333 K showing the functional groups, vinyl (6.3...5.7 ppm) and silane (~5 ppm), and the α and β addition products of the reaction in the aliphatic region at 1.35...1.2 and 0.8...0.6 ppm, respectively. The small signal at 4.6 ppm, rising further at longer raction times, is an unknown side product.
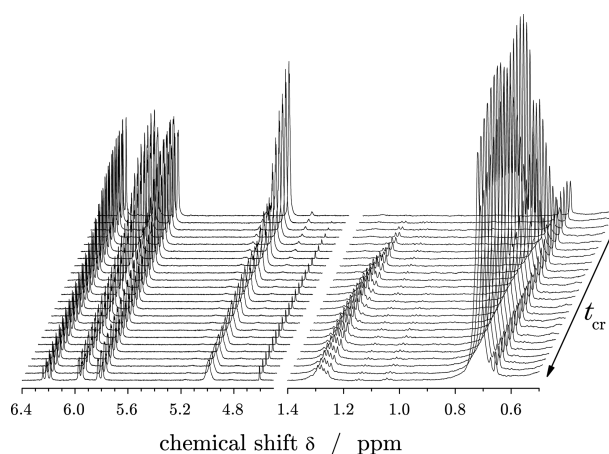
results of both methods, SET-DQ intensities and residual dipolar couplings, respectively, are shown in Figure 1 and are both normalized by the results for the fully cured samples. The very good agreement of the dependence on the reaction time t_{cr} confirms that both methods are equally suitable for the investigation of gelation kinetics. The clear advantage of the SET-DQ approach is the much higher time resolution, which allows for the investigation of the sol–gel transition. In contrast to the full-DQ measurements, no information about the sol fraction and the coupling constant distribution is obtained during the cross-link reaction. Below, we demonstrate that all reactions, independent of the reaction temperature, show a comparable progress of the DQ intensity with the reaction turnover obtained from liquid-state NMR. Therefore, it can be assumed that distributions and sol-fractions obtained at a certain reaction turnover by full-DQ experiments during slow reaction also reflect these in fast reactions at the same reaction turnover.

Finally, we point out again that the SET-DQ intensity represents no quantitative estimate for the residual dipolar coupling strength, since it is measured in arbitrary units and is not normalized. The presented dependency of the SET-DQ intensity on the cross-link time t_{cr} just yields information about the relative change of the effective cross-link density.

■ RESULTS AND DISCUSSION

In the present work, the end-linking of vinyl-terminated PDMS in the presence of solvent reducing the viscosity and enabling better mixing at the initial stages was investigated in dependence on the reaction temperature T_{cr}. First, we will show the results of the high-resolution liquid-state NMR measurements of the reaction kinetics. The reaction-time-dependent formation of the resulting elastically effective network is discussed in the second part. Finally, we investigate the coupling constant distributions and the defect fractions of the obtained PDMS networks and demonstrate the universality of the network formation process.

Reaction Kinetics of Semidilute PDMS Solutions. In order to study the cross-linking kinetics and the reaction rate constants in the semidilute PDMS systems, the conversions of the functional groups of the vinyl-terminated precursor polymers and the (nominally) four-functional cross-linker were estimated by liquid-state NMR. Figure 2 shows ^{1}H

NMR spectra obtained for a semidilute PDMS/cross-linker solution of 33 wt % polymer at different reaction times t_{cr}. The signals of the vinyl-group protons (6.3...5.7 ppm) and the silane proton (~5 ppm) of the cross-linker are well-defined, and the different chemical shift allows an independent evaluation of the conversion of the functional groups. It is important to stress that the liquid-state NMR observations remain quantitative up to the gelation threshold of the systems. While network-like components (characterized by finite residual dipolar couplings) may be broadened beyond detection in the high-resolution spectra, isotropically mobile dangling structures remain visible even above gelation. This is why vinyl group signals (which are always attached to a sol or a dangling chain) are visible throughout the whole reaction, and the good agreement of the vinyl signal with the total cross-linker signal (see below) shows that indeed also the multiply reacted cross-linker remains quantitatively visible up to high conversions.

The integrated signals of the vinyl and silane groups directly reflect their concentration in the semidilute system, and have the expected ratio of 3:1 according to the different number of protons belonging to the functional groups. This ratio was observed to be approximately constant for all investigated reactions. Therefore, the impact of potential competitive secondary reactions, i.e., the formation of Si−OH groups by oxidation or hydrolysis of the silane-group with oxygen or water, respectively, on the conversion of the silane groups is minor or even negligible. For vinyl groups, no secondary reactions are reported in the literature for the temperature range used in this work. Therefore, the conversion of the terminal vinyl groups is taken to represent the overall conversion p_r for the study of the kinetics, ensuring that only primary network-forming reactions are investigated.

The signals at 1.35...1.2 ppm and 0.8...0.6 ppm in Figure 2 belong to the two different kinds of cross-links which are formed during the hydrosilylation reaction. The Markovnikov process (α addition) leads to a 1,1-ethylene cross-link, and the anti-Markovnikov process (β addition), to an 1,2-ethylene cross-link. The analysis of the recorded kinetics shows that 14−18% of the cross-links were formed by the α addition, which corresponds to values observed for hydrosilylation reactions in

7568

dx.doi.org/10.1021/jp302745a | J. Phys. Chem. B 2012, 116, 7566−7574
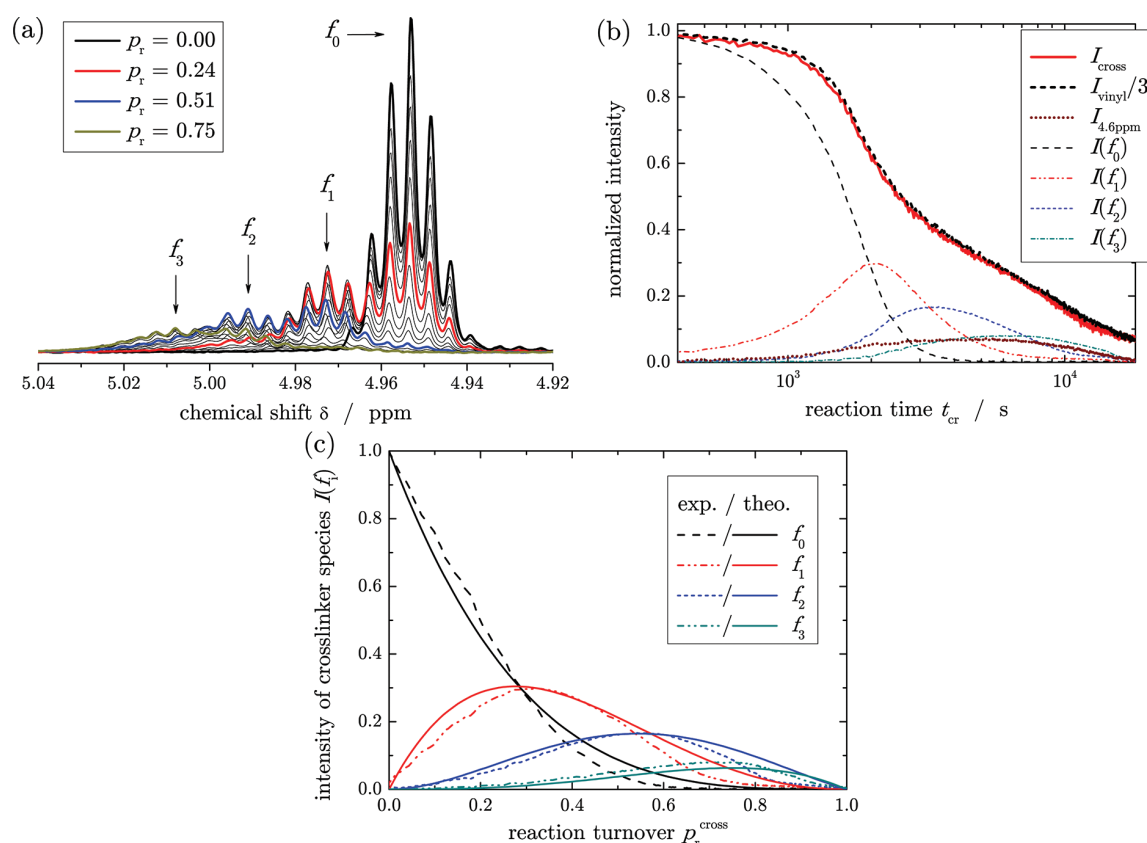
Figure 3. (a) Evolution of the cross-linker ^1H signal during a cross-linking reaction at 313 K. f_i indicates the central spectral line of the i-fold reacted cross-linker. (b) Time-dependent intensities of the cross-linker, vinyl group, and side product (4.6 ppm) signal, as well as the fractions f_i of I_{cross} (thin lines), normalized with respect to $I_{cross}(t_{cr} = 0)$. (c) Comparison of the relative signals of the different cross-linker species determined during the cross-link reaction, along with theoretical predictions based on Bernoulli statistics in dependence on the reaction turnover of the cross-linker p_r^{cross}.
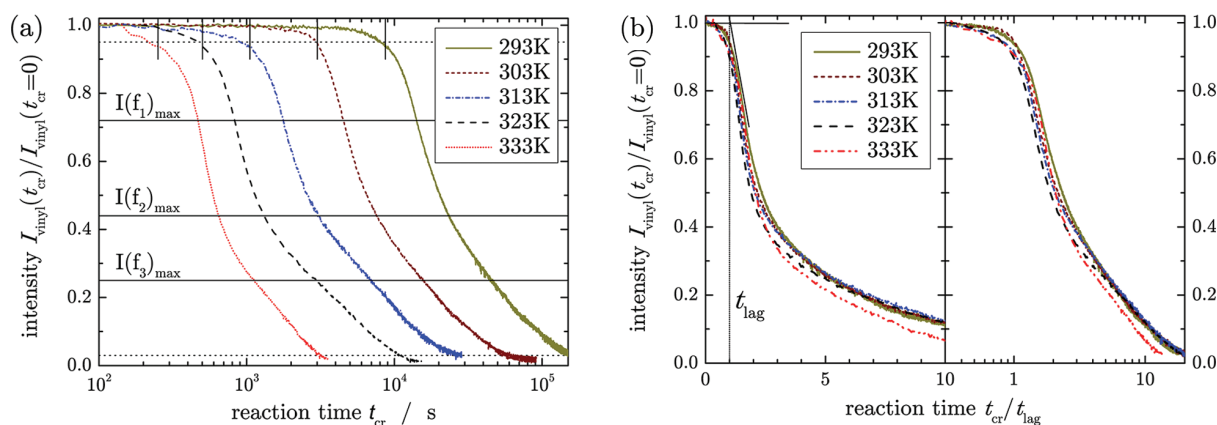
Figure 4. (a) Evolution of the integrated vinyl intensity determined by ^1H liquid-state NMR during the end-linking process in the PDMS/toluene system in dependence on reaction time t_{cr}. The intensities are normalized to the intensity at $t_{cr} = 0$, and lag times t_{lag} are indicated by vertical bars. (b) Vinyl intensity I_{vinyl} vs linear (left) and logarithmic (right) reaction time t_{cr}, scaled with respect to t_{lag}, as determined from the intercept of the steepest tangent with $y = 1$ in the linear representation, as indicated by the lines in the left panel in part b.

the literature.[20] The fraction of formed β products slightly increases at higher cross-link temperatures. Additionally, a signal of rather low intensity, attributed to a side product, is observed at 4.6 ppm in Figure 2.

Figure 3a shows a detailed view of the cross-linker Si–^1H resonances recorded during a cross-link reaction at 313 K at different reaction times. The signal of the remaining Si–H

groups of an i-times reacted cross-linker molecule is obviously shifted in dependence of the number of reacted functional sites. Each of the subsignals is the septed expected for a single Si–H J-coupled to 6 methyl protons. We attribute this shift to changes in the overall conformational dynamics when different numbers of chains are attached.

The equivalent dependence of the vinyl- and Si–H intensity on the reaction time shown in Figure 3b demonstrates that both are consumed in equal amounts during the cross-link reaction, and the observed dependencies yield no clear information about the origin of the additional signal at 4.6 ppm, which reaches about 10% with respect to the initial cross-linker signal and vanishes again by the end of the overall reaction. We currently have no explanation for this significant side product, but point out that the corresponding signal is not "missing" in the overall signal balance; the signal of all vinyl groups is at any time identical to 3 times the total cross-linker signal, and the aliphatic signals of the formed cross-links are at any time the exact intensity complement.

The progress of the reacted functional sites of the cross-linker is shown in Figure 3b and c, where in the latter it is plotted as a function of the reaction turnover of the cross-linker p_r^{cross}. The data on the relative amounts were obtained by integration of the central lines of the respective septets marked in Figure 3a, which does not lead to significant errors related to the overlap of the multiplets. In Figure 3c, this data is compared with theoretical predictions based on simple Bernoulli statistics, assuming statistically independent reaction probabilities for the four sites of the cross-linker, and equating these probabilities p_r with the reaction turnover. For example, the fraction f_1 is given by $4(1 - p_r)^3 p_r$. For the theory lines in Figure 3c, it was taken into account that the signals for the fractions f_i correspond to $(4 - i)$ protons. The higher f_i are thus underrepresented (f_4 is not detectable, as it has no Si–H anymore). Finally, it was further considered that the average functionality of the cross-linker is actually 3.6, which means the data can be thought of as being represented by 60 and 40% 4- and 3-functional linker molecules, respectively. With all these details considered, we observe very satisfactory agreement of the experimental data and the predictions, confirming a well-behaved cross-linking reaction.
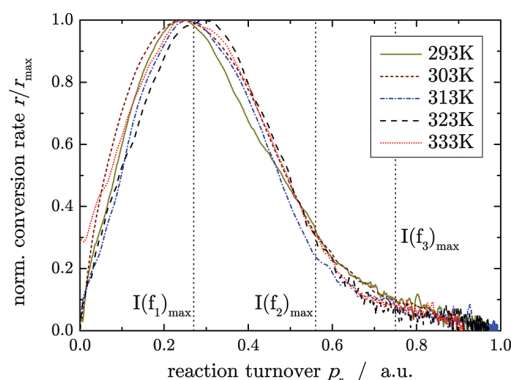
Figure 4a shows the integrated vinyl group intensities I_{vinyl} of the ^1H NMR spectra measured *in situ* during the end-cross-linking process in dependence of the reaction time t_{cr} for different temperatures T_{cr}. The results were normalized with respect to their initial intensity $I_{vinyl}(t_{cr} = 0)$ and plotted on a logarithmic time scale to amplify the different stages of the reaction. Three main periods can be identified in Figure 4a for the conversion of the vinyl groups. This corresponds to results reported in the literature for platinum complex-catalyzed hydrosilylation reactions.[21,22] In the first part of the reaction, the induction period, the active species of the catalyst is formed. This is followed by the reaction period, in which the majority of the vinyl-groups is consumed in a fast exothermic reaction. In the final postcuring period, the reaction is very slow due to the low concentration of the reactants and steric hindrances. The different reaction periods can also be distinguished by the horizontal solid lines in Figure 4a, which represent the turnovers for which each of the stepwise reacted cross-linker species is maximal.

The induction period is characterized by a rather slow conversion of the functional groups. Such an induction period was also observed in previous kinetic studies[21] but never analyzed in more detail due to the lack of experimental accuracy (mainly time resolution). The length of the induction period, the lag time t_{lag}, can be identified by a steepest-tangent construction; see Figure 4b. The so-obtained lag times are used as a scaling factor for the reaction time in the same figure. The comparable dependence of I_{vinyl} on the scaled reaction time

clearly demonstrates the uniform progress of the cross-link reaction at all investigated temperatures. Obviously, the whole reaction kinetics follow more or less the same temperature dependence, which is at the earliest stage reflected in t_{lag}. The rather small deviations can be attributed to minor inaccuracies during the preparation of the semidilute PDMS/cross-linker solution. The evaluation of the lag time t_{lag} in dependence on the reaction temperature in an Arrhenius plot yields an activation energy of about $E_a \approx 74$ kJ/mol for the rate-limiting step of the investigated reaction.

The conversion profiles of the vinyl-groups in the reaction period show a complex dependence on the reaction time t_{cr}. The data in Figure 4a and b already indicate that the overall reaction kinetics cannot be described by a simple single exponential first-order or power-law-type second-order rate equation. In order to obtain more information about the conversion rate constants, the reaction kinetics were explicitly evaluated according to a first-order reaction as well to a second-order reaction. For both, no uniform dependence of the conversion rate on the reaction time and the turnover was observed over the entire reaction period. Especially between 5 and 75% conversion of the vinyl groups, the measured kinetic profiles clearly deviate from the typical behavior of first- and second-order reaction kinetics. An analysis in terms of reaction rate constants was thus not possible.

Figure 5 shows the conversion rate r of the vinyl groups in dependence on the fraction of vinyl groups consumed during

Figure 5. Normalized conversion rate r vs reaction turnover p_r of the terminal vinyl-groups. Conversion rates were determined by a direct time derivative of the integrated vinyl intensities shown in Figure 4. The vertical dotted lines indicate the dominant i-times reacted cross-linker species.

the cross-linking process, the reaction turnover p_r. The conversion rate is directly obtained by the derivative of the integrated vinyl intensity with respect to the reaction time, $r = dI_{vinyl}(t_{cr})/dt_{cr}$, and normalized by the respective maximum rate r_{max}. Independent on the reaction temperature T_{cr}, the investigated cross-link reactions all have the same dependence of the normalized conversion rate on the reaction turnover. At the start of the cross-linking process, the conversion rate rapidly increases and reaches its maximum rate r_{max} at reaction turnovers of about 25%. This feature is particularly indicative of a complex process without a well-defined reaction order. In the later stages of the reaction, the conversion rate continuously decreases. At first, a very rapid decay of the rate r is observed beyond the maximum. This decay distinctly decelerates at roughly 60% reaction turnover. For reaction turnovers above

75%, only a slow near-linear decrease of the conversion rate is observed.

Discussion of the Complex Reaction Kinetics. We assume that the observed behavior of the conversion rate r can solely be attributed to the number of *residual functional sites* of the cross-linker molecules in the polymer/solvent system. For times larger than t_{lag}, the dependence of the intensity (=concentration) of the completely nonreacted cross-linker $I(f_0)$ on the reaction time t_{cr} shown in Figure 3b can indeed be described by a first-order reaction, i.e., by a singly exponential decay. The observation of a first-order reaction is expected from the published mechanism,[2,3] where the initial stage involves a homolytic cleavage of the Si–H bond of the cross-linker and binding of both fragments to the metal center. A dependence on the vinyl concentration is then not expected, and the observation of a (pseudo-) first-order reaction with respect to the vinyl concentration is a mere consequence of the stoichiometry. Our observations thus allow for conclusions on the rate-limiting step.

Along with the decay of $I(f_0)$, the cross-linker species with less residual functional sites f_1, f_2, and f_3 populate in a stepwise manner, as also shown in Figure 3b. Initially, the reaction involves the addition of unreacted cross-linker molecules to single vinyl functionalities. At around 25% reaction turnover, all cross-linker molecules have reacted once on average, and this indeed coincides well with the observed maximum intensity of the once-reacted species of the cross-linker, $I(f_1)_{max}$. The latter is observed at approximately 27% reaction turnover, which can be attributed to the estimated average functionality of 3.6 of the used cross-linker. The ongoing reaction of the once-reacted cross-linker after the rate maximum (where f_0 is almost completely gone) follows again a first-order decay but with a lower apparent rate. The same behavior is observed for the intensities of the cross-linker species with two or one residual functional sites, $I(f_2)$ and $I(f_3)$, respectively. Despite the observed first-order kinetics of the different cross-linker species $I(f_i)$, this behavior is not reflected in the *overall* conversion of cross-linker, and also not in the vinyl group concentration of the polymer chains, as shown in Figure 4a. This can be rationalized by the coexistence of the different cross-linker species, which therefore appear to feature different apparent reaction rates. The overall conversion of the functional groups as observed in the total NMR intensity only yields the average conversion rate for all species.

The recorded complex overall reaction kinetics of the vinyl groups obviously arises from the different reaction rates associated with the cross-linker species that are mostly populated in different stages of the reaction, as indicated by the vertical dotted lines in Figure 5. This is why the conversion of the functional groups can be described only partially by first-order reactions with different reaction rates. Especially at low reaction turnovers ($p_r < 0.5$), the distinctly different populations of the different cross-linker species preclude a description of the overall reaction kinetics by a simple singly exponential first-order rate equation. In particular, the unreacted (f_0) and the once-reacted cross-linker (f_1) appear to have a larger reactivity. The decaying apparent reactivity may simply be related to the decreasing number of close-by reactive groups; in other words, the Si–H concentration is locally increased in an as-yet unreacted four-functional cross-linker. The increasingly bulky nature of the substituents of the Si atom of the cross-linker unit that binds to the catalytic center may also play an indirect role.

As is apparent from Figure 3b, the induction period is mainly characterized by an increase of the conversion rate of the unreacted cross-linker f_0. The maximum rate is observed when 30–50% of it are consumed. The origin of this autocatalytic feature remains unclear at present; we can only state that it cannot be explained by an increased local concentration of Si–H groups around a given metal center, since it is observed for the unreacted and not for the once-reacted cross-linker. A viable hypothesis would be that the catalyst in its initial state must go through one catalytic cycle, thus changing its structure and becoming more reactive. From the consideration of the activation energies below, this first cycle must, however, have the same rate-limiting step as the ensuing cycles.

At higher reaction turnovers ($p_r > 0.75$), the number of the residual functionalities of the cross-linker molecules decreases significantly below two on average. The f_1 species then loses more and more of its dominant influence on the conversion rate, while f_2 and f_3 appear to have more similar reactivities. Only in this range, the apparent reaction order can indeed be estimated from a double-logarithmic representation of the *total* conversion rate r versus the concentration of vinyl groups, $1 - p_r$. Linear fits to the data in the region between 75 and 95% reaction turnover yield slopes between 0.95 and 1.09. The slope in such a representation directly reflects the reaction order of the investigated process, which thus follows approximately a uniform first-order reaction kinetics. In this range, the same dependence is observed for the conversion of the Si–H groups. As mentioned, we attribute the observation of a pseudo-first-order reaction with respect to the vinyl concentration to be due to the fixed stoichiometry

At this point, we propose a three-stage model to describe the kinetics of an end-linking process with multifunctional cross-linkers in the presence of solvent. In the first stage, the increasing conversion rate is determined by an autocatalytic process involving mainly a reaction with the unreacted cross-linker f_0, and the increasing conversion of this and the once-reacted cross-linker species. When the conversion rate of the f_0 species has reached its maximum, its ensuing reaction is well described by first-order kinetics. In the second state beyond the maximum overall conversion rate, the apparently more reactive zero- and once-reacted cross-linkers diminish, and multiply reacted and apparently less reactive cross-linker species become dominant, but still no uniform overall reaction order can be observed. This is followed by the third stage, during which the conversion of multiply reacted cross-linker species dominates and follows a first-order reaction kinetics, as does the overall conversion of vinyl groups.

Activation Energy of the Cross-Link Reaction. The investigated hydrosilylation reaction in the presence of solvent exhibits a complex progress of the conversion of the functional groups with the reaction time t_{cr}, as shown above. This of course prevents an evaluation of the reaction kinetics with respect to global conversion rates. Therefore, the conversion rates at certain reaction turnovers p_r were used to estimate the activation energy of the reaction. Figure 6 shows the conversion rates at several reaction turnovers as an Arrhenius plot. For all selected reaction turnovers, a linear dependence of $\ln(r)$ on the inverse reaction temperature T_{cr}^{-1} is observed. The figure shows again the large difference in the conversion rates at different points of the cross-link reaction. A global linear fit to the data yields an activation energy of $E_a = 73.7 \pm 2.2$ kJ/mol. The latter is within the error equal to the activation energy obtained above by evaluation of the length of the induction period, and
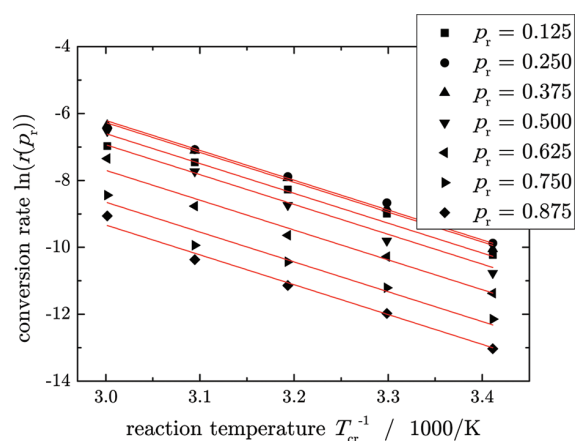
Figure 6. Dependence of the vinyl group conversion rates r at different reaction turnovers on the reaction temperature T_{cr}^{-1}. The rates were obtained by direct time-derivation of the vinyl intensities.

Figure 7. Evolution of normalized DQ intensities nI_{DQ} at a fixed DQ-evolution time, $\tau_{DQ} = 1.317$ ms, for different cross-link temperatures T_{cr} in dependence on reaction time t_{cr}.

corresponds to values given in the literature.[10] The global fit shows a remarkably good agreement with the data for all investigated reaction turnovers. This confirms that the reaction is in *every* stage rate-limited by the same reaction step that is of course part of a complex multistep mechanism.

The simplest a priori assumption explaining the uniform activation energy and the complexity of the cross-linking reaction would actually be to assume diffusion control. Then, the nonuniform reaction rates beyond the maximum could be related to the changing large-scale mobility of the cross-linking components, and the activation energy would characterize the rate-limiting basic process of molecular transport through the semidilute solution. This option must, however, be ruled out on the basis of the high value of the activation energy. It is distinctly higher than the activation energy E_a^D for the diffusion coefficient of PDMS in toluene, that is reported to be around 14 kJ/mol.[23] We have performed additional pulsed-gradient NMR diffusion experiments on the PDMS and toluene components of our semidilute solutions, and confirmed that E_a^D in our system is almost equal for the two components and of similar magnitude as the literature value, further confirming a possible description on the basis of a common effective friction coefficient. This leaves us with the above-discussed combination of an autocatalytic initial stage and decreasing reactivity for multiply reacted cross-linker species as the origin of the overall rate profile shown in Figure 5. Since we observe well-defined first-order kinetics for the concentration of the Si−H groups of the unreacted cross-linker after the induction time, we conclude that the rate-limiting step of the reaction with the given activation energy involves the homolytic cleavage of the Si−H bond upon binding to the catalytic metal center.

Formation of the Elastically Effective Network. The evolution of the elastically effective polymer network was investigated by low-field ^{1}H single-evolution-time double-quantum (SET-DQ) NMR. The DQ evolution time τ_{DQ} used for the measurements during the cross-linking process was obtained from a complete DQ build-up curve recorded for a fully cured ePDMS21 sample. The time at which the normalized DQ intensity reaches 50% of its maximum was used as DQ evolution time τ_{DQ}. The latter was kept constant for all measurements.

Figure 7 shows the results of the real-time SET-DQ NMR experiments during the cross-link reaction in dependence on
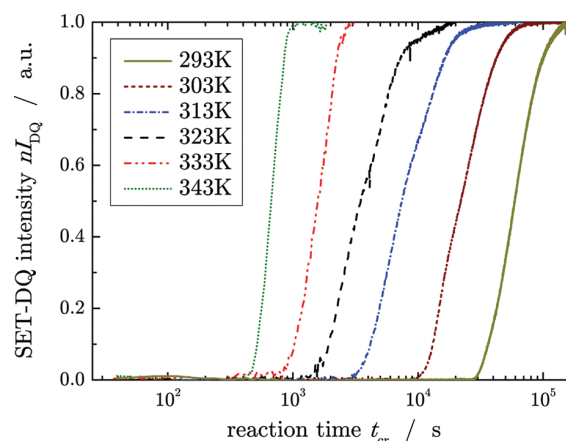
the reaction time t_{cr} for a series of different reaction temperatures T_{cr}. The results were normalized with respect to the DQ intensities of the fully cured gels and plotted on a logarithmic time scale to clarify the strong temperature dependence of the investigated gelation process. The reaction times at which the final extent of the cross-link reaction is observed range from 15 min at $T_{cr} = 343$ K up to 40 h at $T_{cr} = 293$ K.

The recorded formation kinetics can be separated into three main stages. In the first part of the reaction, the *pregel phase*, the measured DQ intensity is equal to zero. Orientation dependent dipole−dipole couplings are averaged out completely by the fast isotropic motions of the short and unentangled polymers. In the *formation period*, the NMR response of the polymers is partially solid-like. The formation of a network due to the chemical linkage of the polymer chains by permanent covalent bonds leads to restrictions of the polymer mobility. The latter becomes anisotropic, and some dipolar couplings persist. The strength of these observable residual dipolar couplings is directly proportional to the number of restrictions which the polymer chains are subject to. The contribution of entanglements and/or packing effects to the DQ intensity I_{DQ} can be assumed as negligible, since the cross-linking is performed under conditions of dilution by solvent, and the molecular weight of the used precursor polymers is far below M_e. Therefore, the recorded DQ intensity $I_{DQ}(t_{cr})$ directly reflects the evolution of the cross-link density of the elastically effective network. Finally, a very slow *postcuring process* is observed, which is characterized by small changes of I_{DQ} at very long reaction times, until no further notable increase is detected. This stage corresponds to the last stage observed for the vinyl-group conversion by the ^{1}H liquid-state NMR experiments.

The build-up of the DQ-intensity in the *formation period* in Figure 7 was analyzed by an exponential rate equation, $I_{DQ} \sim e^{-k_{gel}t_{cr}}$. The evaluation of the so-obtained gelation rates, k_{gel}, in dependence on the reaction temperature in an Arrhenius plot yields an activation energy of $E_a = 74.3 \pm 3.6$ kJ/mol. This is again in very good agreement with the activation energies obtained from the investigation of the lag times and the conversion rates of the terminal vinyl groups. The equal temperature dependence of the conversion rate r and the gelation rate k_{gel} demonstrates that indeed the DQ-intensity directly reflects the cross-link density of polymer networks.

Estimation of the Gel-Point. The transition between the liquid- and solid-like NMR response of the polymer chains is equivalent to the sol−gel transition and is characterized as an apparent gelation time. For a detailed investigation of the gelation process, and especially the gel point, the results obtained by the two NMR methods are combined. Figure 8
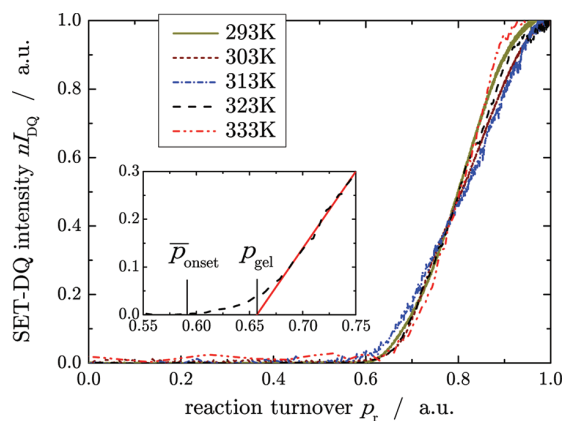
Figure 8. Formation of the elastically effective network in dependence on the reaction turnover. The inset shows an enlargement of the sol−gel transition region for a sample cross-linked at T_{cr} = 323 K. p_{gel} indicates the gel point obtained by linear extrapolation (dotted line).

shows the evolution of the SET-DQ intensity as a function of the reaction turnover p_r. Only above a certain reaction turnover of around 65%, a noticeable DQ intensity is observed, which exhibits a continuous crossover into a near-linear dependence on the reaction turnover. This behavior, which is clearly illustrated by the inset in Figure 8, is observed for all investigated cross-link temperatures. We assume that the continuous sol−gel transition can be attributed to the formation of small network-like domains or microgels in the solution which raise detectable residual dipolar couplings. Therefore, the topological gelation threshold is not straightforwardly reflected by the first observation of a recognizable DQ intensity at $\bar{p}_{onset}$, as loosely defined in ref 11. For a more precise estimation, the observed and expected linear dependence of the DQ intensity on the reaction turnover is used to determine the gel-point, p_{gel}, by linear extrapolation. The evaluation of the temperature dependence of the corresponding gelation times t_{gel} in an Arrhenius representation yields an activation energy of again E_a = 72.1 ± 3.3 kJ/mol. This is in very good agreement with all activation energies determined during this study and confirms again that the reaction proceeds in every stage with the same local reaction mechanism.

Network Characterization. The network structure of the fully cured samples was investigated by low-field ^{1}H DQ NMR. The average residual dipolar coupling constant, D_{res}, and its variance, σ, were determined by numerical analysis (regularization) of the normalized DQ build-up curves. The experiments were performed on dry network samples after complete and careful evaporation of the solvent. The defect fraction, $\omega_{def,sw}$, of the networks was determined by ^{1}H DQ NMR experiments on equilibrium swollen samples.[24]

The results of the network characterization (see Table 1) show a very good agreement for the determined properties of the networks, which were cured during the high- and low-field NMR studies of the reaction kinetics. The observed deviations are within the experimental error of the DQ experiment or can

Table 1. Results of Network Characterization by ^{1}H Low-Field DQ Experiments on Fully Cured Networks Previously Investigated by High-Field (hf) and Low-Field (lf) NMR Experiments after Evaporation of the Toluene-d_8[a]

T_{cr} (K)	$D_{res}/2\pi$ (kHz)		σ/D_{res}		$\omega_{def,sw}$	
	hf	lf	hf	lf	hf	lf
293	0.164	0.165	0.31	0.23	0.18	0.18
303	0.159	0.173	0.28	0.26	0.18	0.20
313	0.161	0.161	0.31	0.26	0.22	0.20
323	0.160	0.166	0.31	0.28	0.21	0.16
333	0.163	0.159	0.25	0.31	0.16	0.20

[a]D_{res} and σ were obtained by regularization of I_{nDQ}. $\omega_{def,sw}$ was determined in an equilibrium swollen sample.

be attributed to slight inaccuracies in the preparation of the samples. Overall, this demonstrates that networks with nearby equal properties are formed during the cross-link reaction independent on the cross-link temperature.

■ CONCLUSIONS

In this study, the reaction kinetics of the hydrosilylation and the formation of the elastically effective network were investigated during the end-cross-linking process in a semidilute PDMS system. For the first time, we could identify deviations from a simple exponential time dependence of the conversion on the reaction time, as reflected in the concentration of the vinyl groups at the PDMS chain ends and the four Si−H units of the cross-linker molecule. The precise estimation of the conversion of the terminal functional groups of the polymers by real-time ^{1}H liquid-state NMR and the high time resolution of the experiments enabled a direct investigation of the conversion rates during the entire progress of the reaction and thus an in-depth analysis of the reaction kinetics.

The results show a complex dependence of the overall conversion rate on the reaction turnover, revealing an induction period and a maximum rate at around 25% conversion (stage I), and an apparently nonuniform reaction order also beyond the conversion rate maximum (stage II). The constantly changing number of residual reaction sites of the cross-linker molecules leads to different dominating species throughout the reaction, and the reactivity (apparent conversion rate constant) of these species is found to decrease with an increasing number of already reacted Si−H sites. Only at higher reaction turnovers (stage III), an apparent first-order reaction kinetics can be observed for the overall conversion of either the total amount of Si−H or vinyl groups, presumably because multiply reacted cross-linker molecules show similar apparent reactivity.

The consistent observation of the same activation energy derived from the different observables taken at different stages and from different experiments based on molecular conversion, or chain dynamics revealing the topological network formation, confirms that the network formation is rate-limited by the same local mechanism. Diffusion control and flow activation as a possible origin can be ruled out on the basis of the high value of the activation energy of about 74 kJ/mol. Since the conversion of the Si−H groups of the unreacted cross-linker molecules at the early stage after the induction period also follows a first-order kinetics, we assign the rate-limiting step to the homolytic cleavage of the Si−H groups upon binding to the catalytic metal center. The observation of a pseudo-first-order reaction

kinetics for the vinyl group conversion is merely a consequence of the stoichiometry.

■ AUTHOR INFORMATION

Corresponding Author
*E-mail: walter.chasse@physik.uni-halle.de.
Notes
The authors declare no competing financial interest.

■ ACKNOWLEDGMENTS

■ REFERENCES

(1) Speier, J. L.; Webster, J. A.; Barnes, G. H. *J. Am. Chem. Soc.* **1957**, *79*, 974−979.

(2) Chalk, A. J.; Harrod, J. F. *J. Am. Chem. Soc.* **1965**, *87*, 16−21.

(3) Chung, L. W.; Wu, Y.-D.; Trost, B. M.; Ball, Z. T. *J. Am. Chem. Soc.* **2003**, *125*, 11578−11582.

(4) Dez-González, S.; Nolan, S. P. *Acc. Chem. Res.* **2008**, *41*, 349−358.

(5) Caseri, W.; Pregosin, P. *J. Organomet. Chem.* **1988**, *356*, 259−269.

(6) Coqueret, X.; Wegner, G. *Organometallics* **1991**, *10*, 3139−3145.

(7) Esteves, A.; Brokken-Zijp, J.; Laven, J.; Huinink, H.; Reuvers, N.; Van, M.; de With, G. *Polymer* **2009**, *50*, 3955−3966.

(8) Hammouch, S. O.; Beinert, G. J.; Herz, J. E. *Polymer* **1996**, *37*, 3353−3360.

(9) Bonnet, J.; Bounor-Legaré, V.; Boisson, F.; Mélis, F.; Cassagnau, P. *J. Polym. Sci., Part A: Polym. Chem.* **2011**, *49*, 2899−2907.

(10) Antíc, V. V.; Antíc, M. P.; Govedarica, M. N.; Dvorníc, P. R. *J. Polym. Sci., Part A: Polym. Chem.* **2007**, *45*, 2246−2258.

(11) Saalwächter, K.; Gottlieb, M.; Liu, R.; Oppermann, W. *Macromolecules* **2007**, *40*, 1555−1561.

(12) Roulet, R.; Barbey, C. *Helv. Chim. Acta* **1973**, *56*, 2179−2186.

(13) Horn, G. W.; Kumar, R.; Maverick, A. W.; Fronczek, F. R.; Watkins, S. F. *Acta Crystallogr., Sect. C* **1990**, *46*, 135−137.

(14) Saalwächter, K. *Prog. Nucl. Magn. Reson. Spectrosc.* **2007**, *51*, 1−35.

(15) Chassé, W.; Valentín, J. L.; Genesky, G. D.; Cohen, C.; Saalwächter, K. *J. Chem. Phys.* **2011**, *134*, 044907.

(16) Saalwächter, K.; Herrero, B.; López-Manchado, M. A. *Macromolecules* **2005**, *38*, 9650−9660.

(17) Graf, R.; Heuer, A.; Spiess, H. W. *Phys. Rev. Lett.* **1998**, *80*, 5738−5741.

(18) Valentín, J. L.; Carretero-González, J.; Mora-Barrantes, I.; Chassé, W.; Saalwächter, K. *Macromolecules* **2008**, *41*, 4717−4729.

(19) McLoughlin, K.; Szeto, C.; Duncan, T. M.; Cohen, C. *Macromolecules* **1996**, *29*, 5475−5483.

(20) Mukbaniani, O.; Titvinidze, G.; Tatrishvili, T.; Mukbaniani, N.; Brostow, W.; Pietkiewicz, D. *J. Appl. Polym. Sci.* **2007**, *104*, 1176−1183.

(21) Stein, J.; Lewis, L. N.; Smith, K. A.; Lettko, K. X. *J. Inorg. Organomet. Polym.* **1991**, *1*, 325−334.

(22) Stein, J.; Lewis, L. N.; Gao, Y.; Scott, R. A. *J. Am. Chem. Soc.* **1999**, *121*, 3693−3703.

(23) Rauch, J. Ph.D. thesis, Universität Bayreuth, 2006.

(24) Chassé, W.; Lang, M.; Sommer, J.-U.; Saalwächter, K. *Macromolecules* **2012**, *45*, 899−912.

3.5. Solution Cross-linked Networks

This and the following section deal with the *structure* of polymer networks in dependence of their preparation condition and swelling properties of end- and randomly cross-linked polymer networks. PDMS networks are investigated in dry and equilibrium swollen state and the alternation of the network *structure* within these two extremes is studied at various well-defined swelling degrees below equilibrium.

In this section the influence of the polymer volume fraction $\varphi_{\mathrm{p,c}}$ during the cross-link reaction of end-functionalized PDMS precursor polymers on the network *structure* is investigated. Polymers cross-linked in solution show an increased extensibility in comparison to networks prepared by the corresponding polymers in bulk [77, 78] which is referred to as 'superelasticity' [79]. Several studies investigate the elastic properties of polymer networks on the conditions of their *formation* in solution [80, 81, 82] and discuss the results in terms of trapped entanglements [83]. However, there is little knowledge about *structure* properties like the sol fraction, network defect fraction and the distribution of network strand lengths and their dependence on the solvent content during preparation. Therefore, two series of end-linked PDMS networks, ePDMS-21 and ePDMS-25R, cross-linked at well-defined polymer volume fractions, $\varphi_{\mathrm{p,c}}$, were investigated by equilibrium swelling and ^{1}H double-quantum NMR experiments. The studied ePDMS-21 and ePDMS-25R networks were prepared according the procedure stated in the Experimental Details.

Figure 3.2 represents the results of the equilibrium swelling experiments of the ePDMS-21 and ePDMS-25R networks obtained by the end-cross-linking process at different polymer volume fractions. The equilibrium degree of swelling, Q_{eq}, continuously increases with decreasing polymer fraction $\varphi_{\mathrm{p,c}}$ for both sample series indicating a reduction of the cross-link density γ_{c}. Especially the ePDMS-25R networks exhibit a pronounced increase of Q_{eq} at very low polymer fractions ($\varphi_{\mathrm{p,c}}$<0.1). In order to compare the two sample sets, the volume fraction of polymer during the cross-link process of the ePDMS-25R samples was scaled with respect to the ratio r of the radii of gyration of the precursor polymer ePDMS-21 to ePDMS-25R in a good solvent using the number average molecular weight, M_{n}, obtained by GPC.

$$\varphi_{\mathrm{p,c}}^{\mathrm{ePDMS\text{-}25R}}(\text{scaled}) = \frac{r_G^{\mathrm{ePDMS\text{-}21}}}{r_G^{\mathrm{ePDMS\text{-}25R}}}\, \varphi_{\mathrm{p,c}}^{\mathrm{ePDMS\text{-}25R}} = \left(\frac{M_{\mathrm{n}}^{\mathrm{ePDMS\text{-}21}}}{M_{\mathrm{n}}^{\mathrm{ePDMS\text{-}25R}}} \right)^{0.6} \varphi_{\mathrm{p,c}}^{\mathrm{ePDMS\text{-}25R}} \qquad (3.0)$$

The equilibrium degree of swelling of the so-scaled ePDMS-25R series coincidences with that of the ePDMS-21 series revealing a similar dependence on the polymer fraction dur-
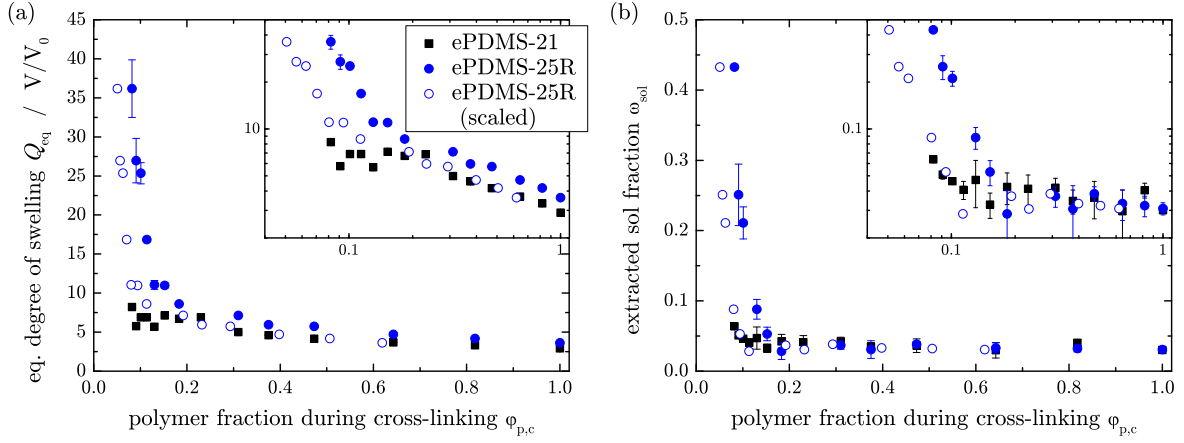
Fig. 3.2.: (a) Dependence of the equilibrium degree of swelling Q_{eq} of the ePDMS-21 and ePDMS-25R networks on the polymer fraction during the cross-link reaction, $\varphi_{p,c}$, and (b) extracted sol fraction, ω_{sol}, during swelling experiments. The insets show the same data as log-log plot.

ing cross-linking. This already indicates that the networks properties exhibit a distinct dependence on the overlap of the chains in the solution during the network *formation*.

The extracted sol fraction, ω_{sol}, of the ePDMS-21 and ePDMS-25R networks does not increase significantly up to polymer fractions of $\varphi_{p,c} \approx 0.12$ and $\varphi_{p,c} \approx 0.18$, respectively (see Figure 3.2b). The scaled ePDMS-25R series again shows a good agreement with the ePDMS-21 series. At lower polymer fractions, more close to the overlap concentration φ^*, ω_{sol} increases considerably. The low local concentration of terminal functional groups belonging to different chains leads presumably to a higher probability of loop *formations* [25] and small subnetworks not attached to the infinite gel. However, the rather low extracted sol fractions demonstrate that both network series are characterized by a very good conversion of the precursor chains over a broad range of dilutions during the cross-link reaction. This is also confirmed by nearby complete consumption of the cross-linker and the terminal vinyl-groups observed during the investigation of the kinetics of the network *formation* [52]. The error bars of the sol fraction can be interpreted as small inhomogeneities of the networks caused by insufficient mixing of the reactants throughout the progress of the cross-link reaction.

Figure 3.3 shows the results of the ^{1}H DQ NMR measurements of the dry network series. The average residual dipolar coupling constant, D_{res}, decreases continuously with increasing fraction of diluent during the network *formation*. Thereby both network series show the same dependence on the decreasing polymer fraction during cross-linking, $\varphi_{p,c}$,
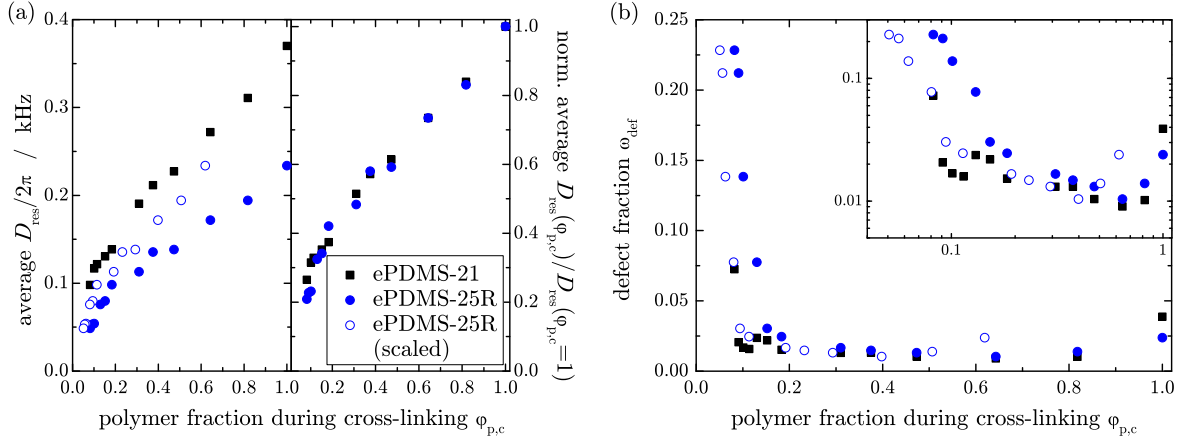
Fig. 3.3.: (a) Relationship between the residual dipolar coupling constant, D_{res}, measured in dry ePDMS-21 and ePDMS-25R samples and the polymer fraction $\varphi_{\mathrm{p,c}}$ and (b) fraction of network defects measured by DQ NMR of the same samples. The inset shows the same data as log-log plot.

as demonstrated by the normalized coupling constants, $D_{\mathrm{res}}(\varphi_{\mathrm{p,c}})/D_{\mathrm{res}}(\varphi_{\mathrm{p,c}} = 1)$, in the right panel of Figure 3.3a. However, the above introduced scaling (Eq. 3.5) does not lead to a coincidence of the data (left panel Figure 3.3a). In this case an agreement of the two sample sets is observed when $\varphi_{\mathrm{p,c}}$ of the ePDMS-25R networks is scaled by the ratio of the corresponding molecular weights, M_{n}, of the prepolymers. This indicates that the apparent residual dipolar coupling constant is distinctly dependent on the co-monomer concentration of the terminal functional groups during the network *formation*.

The residual dipolar coupling constant, D_{res}, is directly related to the effective cross-link density, $D_{\mathrm{res}} \sim \gamma_{\mathrm{c}}$. Thus, the data shows that the cross-link density γ_{c} is reduced distinctly at lower polymer fractions $\varphi_{\mathrm{p,c}}$, despite similar conversions of the reagents during the cross-link reaction. The latter is confirmed by the approximately constant extracted sol fraction and a rather low estimated defect fraction, ω_{def}, of roughly $2\,\%$ as shown in Figure 3.3b, over a broad range of dilutions. This dependence of the cross-link density is also substantiated by the concurrent increase of the equilibrium degree of swelling, as shown above. The observed behavior corresponds to results in the literature [83, 84, 85, 86] where the decrease of the cross-link density is attributed to trapped entanglements, which decrease in number when the cross-link reaction is performed at lower polymer concentration, due to the reduced overlap and with that increased center-of-mass distance of the polymer coils in the solution [87], and to the consumption of cross-link sites for the *formation* of elastically ineffective loops [88, 89]. The latter can
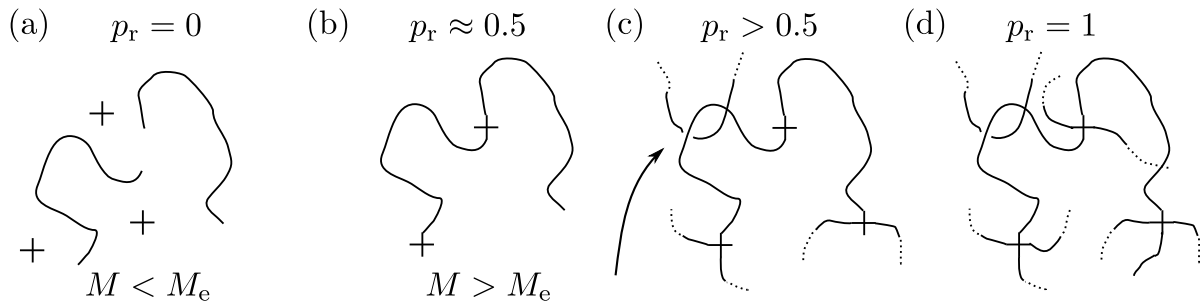
Fig. 3.4.: Schematic sketch of trapped entanglement *formation* at different reaction turnover p_r during cross-link reaction.

emerge as intra-chain loops and higher rank cyclizations [89].

The number average molecular weight, M_n, of the ePDMS-25R precursor chains matches approximately the entanglement molecular weight. In combination with the rather broad molecular weight distribution the *formation* of trapped entanglements during cross-linking is reasonable. However, the ePDMS-21 precursor chains have an average molecular weight of about $5\,\mathrm{kg/mol}$ which is far below the entanglement molecular weight of $M_e \approx 12\,\mathrm{kg/mol}$ of PDMS [90]. Nevertheless, about 30 % of the chains exhibit a molecular weight larger than M_e as shown by the molecular weight distribution obtained by the GPC characterization (Figure A.1b). The cross-link reaction is dominated by the once and twice-reacted cross-linker species at conversions up to 60 % [52] whereas the twice-reacted cross-linker leads primarily to chain extensions. Thus the linear polymer chains in the solution have a higher average molecular weight at this stage of the reaction in comparison to the precursor chains [25] which leads to an increased probability of the *formation* of trapped entanglements, since the number of the latter increases linearly with the length of the subchains [87].

The *formation* of trapped entanglements, which arise by entangled chains connected to the infinite gel, is schematically illustrated in Figure 3.4 for the scenario stated above. At the start of the reaction (a) the precursor molecular weight is too low for entanglements. The latter increases due to chain extensions in the progress of the reaction (b). The higher molecular weight of chains, with potentially un-reacted cross-link sites on their backbone, may give rise to entanglements (c) which are trapped at higher conversions p_r. At the final stage of the reaction (d) the residual functional sites of the cross-linker molecules react, leading to trapped entanglements at network strands with lower molecular weight than the critical entanglement molecular weight. This might elucidate the emergence of trapped entanglements during the *formation* of networks obtained by
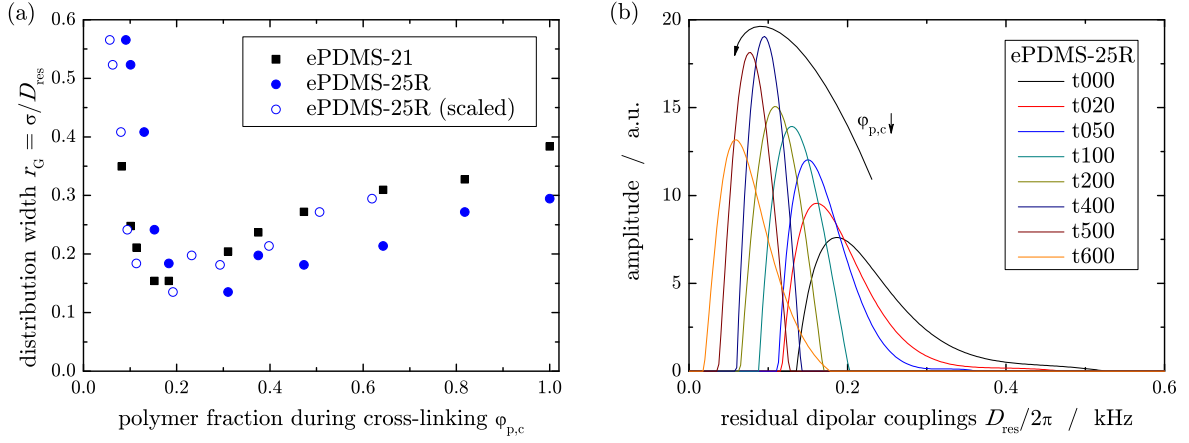
Fig. 3.5.: (a) Variation of the relative width of the distribution of coupling constants as a function of polymer fraction $\varphi_{p,c}$ for samples ePDMS-21 and ePDMS-25R and (b) residual dipolar coupling distributions of ePDMS-25R samples cross-linked in presence of different amount of diluent.

precursor polymers despite the effective M_n is below the entanglement molecular weight. For cross-link reactions performed in more and more dilute solution, the polymer coils overlap less reducing the number of trapped entanglement [87]. In conclusion, the decrease of the cross-link density can be attributed to a combination of less formed trapped entanglements and a strong increased probability of loop *formation* whereas the latter should be assumed as dominating influence at higher dilutions.

For a more detailed investigation of the network *structure*, the relative distribution width, r_G, of the residual dipolar coupling constant distributions of the ePDMS-21 and ePDMS-25R networks are analyzed in dependence of the polymer fraction $\varphi_{p,c}$ during the cross-link reaction. The results are illustrated in Figure 3.5a. For both sample series a comparable dependence on $\varphi_{p,c}$ is observed, as deduced from the compliant behavior of the ePDMS-21 and the scaled ePDMS-25R networks. The apparent relative distribution width, yielding information about the spatial distribution of cross-links, features a complex dependence on the amount of diluent during cross-linking. Thereby, the latter can be subsumed roughly in two regions. In the first region, ranging from bulk up to polymer fractions of $\varphi_{p,c} \approx 0.14$ and $\varphi_{p,c} \approx 0.2$ for ePDMS-21 and ePDMS-25R, respectively, the distribution width is narrowed continuously with decreasing polymer fraction $\varphi_{p,c}$. Here, the narrowest observed distributions widths are about 0.15 and 0.13 for ePDMS-21 and ePDMS-25R, respectively, which is less than half of the distribution width of the respective bulk cross-linked samples. These rather small values, usually

just observed for natural rubber prepared of high molecular weight precursor chains [44], indicate an increase of the network homogeneity through cross-linking in presence of diluent. In the second region an opposite dependence is observed. The distribution width increases strictly at lower polymer fractions $\varphi_{p,c}$ exceeding the values of the bulk cross-linked samples. These two regions are also nicely exemplified by the coupling constant distributions of the ePDMS-25R networks shown in Figure 3.5b. The maximum of the distributions is shifted towards lower coupling constants at lower volume fractions. Thereby it becomes more pronounced up to a certain volume fraction as mentioned above, and the high coupling tail of the distribution vanishes. This corresponds to the first region. At increasing dilution the maximum is distinctly less pronounced and the high coupling tail rises.

The observed behavior can be attributed mainly to two competing mechanisms during the cross-link reaction in presence of solvent, which show a different dependence on the amount of diluent. In bulk, a certain fraction of trapped entanglements is established during the network *formation*. The concentration of the latter is reduced continuously for networks cross-linked in solution with increasing solvent content [87]. This, in combination with the more facilitated homogeneous mixing of the reagents during the cross-link reaction, leads to the observed increased homogeneity of the networks. Additionally this region is characterized by low sol and defect fractions. On the other hand loop *formation* and higher-rank cyclizations become more important with decreasing volume fractions. The *formation* of microgels and local sub-networks, caused by concentration fluctuations, which are interconnected by cross-linking at later stages of the reaction, leads to again larger network heterogeneities. This is clarified by the high extracted fraction of sol during the equilibrium swelling experiments and NMR-detected defect fraction.

In conclusion, the presented results show that the network properties are highly dependent on the condition of their *formation*. Thereby the investigated properties, except the cross-link density, reveal a dependence on the overlap of the polymer chains in the solution during the *formation* as demonstrated by the coincidence of the ePDMS-21 and scaled ePDMS-25R network samples. To complete this study, the samples will be investigated at swelling equilibrium by ^{1}H double-quantum NMR in order to obtain further information about the defect fraction and coupling constant distribution.

3.6. Partial Swelling of Networks

In this section the influence of the swelling degree below equilibrium on the order parameter is investigated. This study essentially closes the gab between the investigation of the *structure* of dry polymer networks in section 3.1 and 3.5, and the *thermodynamic properties* of equilibrium swollen networks in section 3.3. The work is motivated by previously published results of Cohen-Addad and co-workers [91, 92], and our group [51, 93]. Cohen-Added discusses the progressive swelling of gels in terms of a two step process. In the first part, starting from the dry gel, the Gaussian properties of the network chains are unaffected by the desinterspersion of the chains due to swelling. In the second part, the radius of gyration of the chains increases due to rising excluded volume effects. However, theoretical considerations show that swelling by good solvents affects the chain statistics already at low and intermediate swelling degrees due to the reduced excluded volume screening leading to a reduction of the order parameter [51]. At higher swelling degrees the order parameter increases due to the network deformation upon swelling [51] whereas the latter is observed as subaffine process which is attributed to swelling heterogeneities [93]. In this context randomly and end-linked PDMS-networks are investigated at systematically varied well-defined swelling degrees by ^{1}H double-quantum NMR in order to elucidate the influence of the swelling solvent on the backbone order parameter as reflected by residual dipolar couplings and the affinity of the network deformation.

Figure 3.6 shows the results of the NMR experiments performed on several ePDMS-21 networks, cross-linked at different polymer fractions, at various degrees of swelling. All samples show a comparable dependence of the evolution of the residual dipolar coupling constant, D_{res}, with respect to the swelling degree. However, for better discussion the swelling curves can be subsumed into two parts. In the first part, at low swelling degrees, in comparison to the degree of equilibrium swelling, Q_{eq}, varying dependencies are observed. For networks with a low coupling constant in dry state, a decrease of the coupling constant with increasing swelling degree is determined up to a certain swelling degree. With increasing coupling constant in dry state this becomes less pronounced and turns into a slight increase of the coupling constant upon swelling as shown in Figure 3.6a. The second region is characterized by an obvious, continuous monotonic increase of the coupling constant in dependence on the swelling degree. In a log-log representation of the data it becomes obvious that the samples show a comparable scaling of the average residual dipolar coupling constant on the swelling degree, $D_{\mathrm{res}} \sim Q^{\nu_{\mathrm{def}}}$, with ν_{def} as deformation scaling exponent, in this region. This behavior is observed for all
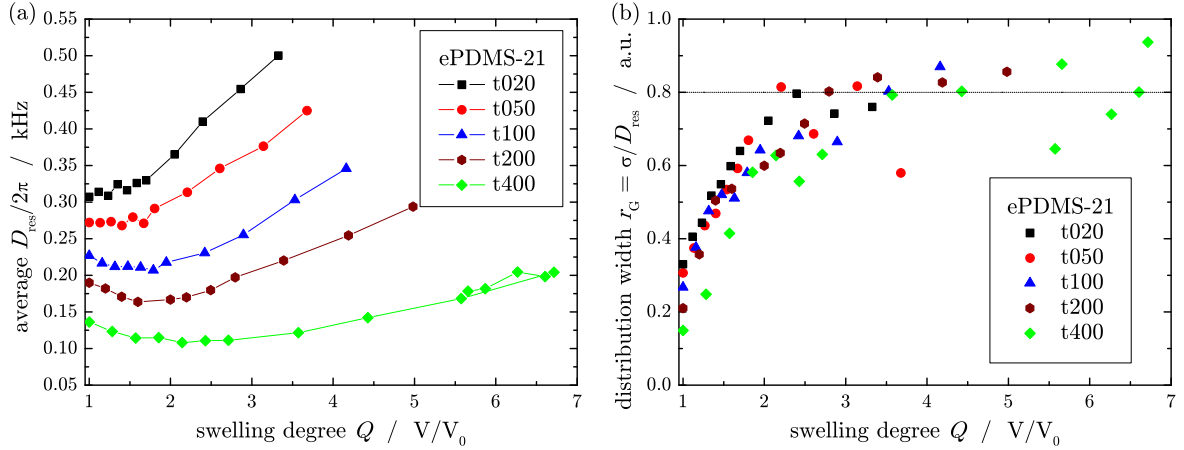
Fig. 3.6.: (a) Residual dipolar coupling constants, D_{res} and (b) distribution widths, r_G determined by evaluation of coupling constant distributions obtained by regularization of the normalized DQ build-up curves measured at different degrees of swelling, Q.

investigated networks and will be examined in detail later. The transition between the two regions is continuous.

The Gaussian chain statistics predicts a strict monotonic increase of the residual dipolar coupling with the swelling degree of networks. Assuming an affine deformation of the network due to swelling which yields $\nu_{def} = 2/3$, the affine prediction $D_{res} \sim Q^{2/3}$ is obtained [51]. However, the experimental results in the first region of the swelling curves in Figure 3.6a show a deviating behavior. The residual dipolar coupling constant does not reflect the fact that the spatial separation of the cross-links, as characterized by the end-to-end distance of networks strands, increases. This indicates a non-affine deformation of the network and corresponds to observations in the literature for low and intermediate swelling degrees [92, 94, 93] where this is attributed to desinterspersion effects and the release of entanglement or packing constraints. At higher swelling degrees the residual dipolar coupling constant reveals a power-law dependence on the swelling degree as mentioned above. This will be evaluated explicitly in the next section.

For a more detailed understanding of the network swelling, especially at low and intermediate swelling degrees, the distributions of the dipolar couplings were investigated. Figure 3.6b represents the evolution of the apparent relative distribution width, r_G, in dependence of the swelling degree, Q. For all samples a distinct broadening of the distribution is observed upon swelling and thus the distribution width is increased. This observation is restricted to low and intermediate Q values. Thereby, the distribution
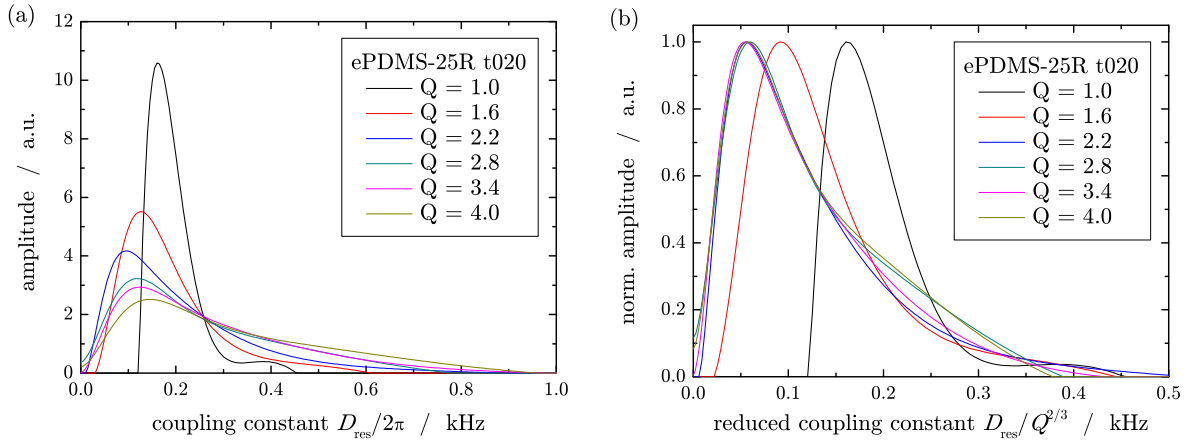
Fig. 3.7.: (a) Coupling constant distribution of ePDMS-25R t020 determined at different swelling degrees, Q, and (b) the same distributions normalized to their maximum amplitude plotted vs a coupling constant reduced with respect to an affine deformation.

width increases about 2-4 times in comparison to the respective of the dry network samples. The samples differ widely in their coupling constants in the dry state. Nevertheless, all networks show a comparable dependence of the distribution width on the swelling degree. Up to a certain swelling degree, the distribution width of all networks increases continuously to approximately the same magnitude. The latter stays more or less constant at higher degrees of swelling as indicated by the doted line in Figure 3.6b. The swelling degree ranges in which the different dependencies of the distribution width are observed correspond to the regions introduced above and will be discussed later. Similar results were obtained during the investigation ePDMS-25R and the randomly cross-linked networks where the data is not shown here.

The approximately constant distribution width at higher swelling degrees is indicative for an affine deformation in this range. For a precise examination of the network deformation, the change of the coupling constant distribution upon swelling is investigated directly. Figure 3.7a shows the determined coupling constant distributions of ePDMS-25R t020 at different swelling degrees. The dry network ($Q = 1$) features a rather narrow distribution of coupling constants with a Gaussian shape, indicating a homogeneous network *structure*, and a small tail towards higher couplings. By swelling, the observed shape of the distribution changes clearly. The distributions are broadened, involving higher and lower coupling constants with respect to the dry sample. Especially the high coupling contribution rises which reveals the increased residual order

caused by stretching of network strands due to the deformation of the network upon swelling. At low and intermediate swelling degrees the maximum of the distribution, representing the most probable chain order, is shifted slightly towards lower coupling constants. At higher swelling degrees the opposite is observed. The maximum is slightly shifted towards higher coupling constants. This turnaround of the shift of the maximum coincidences with the observation of an approximately constant distribution width. In order to compare the coupling constant distributions at different degrees of swelling, the distributions are normalized with respect to their maximum amplitude and plotted in dependence of a reduced coupling constant in Figure 3.7b. Thereby, the coupling constants were scaled by $Q^{-2/3}$ using the respective swelling degree, which corresponds to the assumption of an affine deformation. The distributions at low and intermediate swelling degrees, $Q = 1.6$ and $Q = 2.2$, respectively, deviate distinctly from that of the dry network. In combination with the above discussed increase of the distribution width, this confirms clearly a non-affine deformation of the network and shows that swelling in this range is a rather heterogeneous process. However, at higher swelling degrees, starting from $Q = 2.2$, the coupling constant distributions are in very good agreement. Especially for the low coupling part of the distribution up to $D_{\mathrm{res}}/Q^{2/3} = 0.15\,\mathrm{kHz}$ a nearby perfect coincidence is observed. Only for higher values of the reduced coupling constant minor discrepancies between the distributions become obvious. Nevertheless, this is a strong indication that the network is deformed affinely at higher swelling degrees. The same behavior was also observed for several other end- and randomly cross-linked networks used in this study.

The analysis of the coupling constant distributions in Figure 3.7b reveals a strong non-uniform deformation of the networks upon swelling over the entire range of the investigated swelling degrees. This also corresponds to the observed dependence of the average residual dipolar coupling constant and the relative distribution width on the swelling degree. Overall the deformation behavior of the investigated networks due to swelling can be subsumed into two stages as already discussed above. In the first stage, at low and intermediate swelling degrees, the network deformation is non-affine. This is characterized by constant or even decreasing average coupling constant, D_{res}, a strong increase of the relative distribution width, r_{G}, and the highly distinctive shapes of the coupling constant distributions. Especially for D_{res} different evolutions with the swelling degree are observed in dependence on the coupling constant of the dry network whereas the distribution width shows a comparable tendency for all samples. In the second stage, ranging from intermediate up to equilibrium swelling degrees, the network deformation
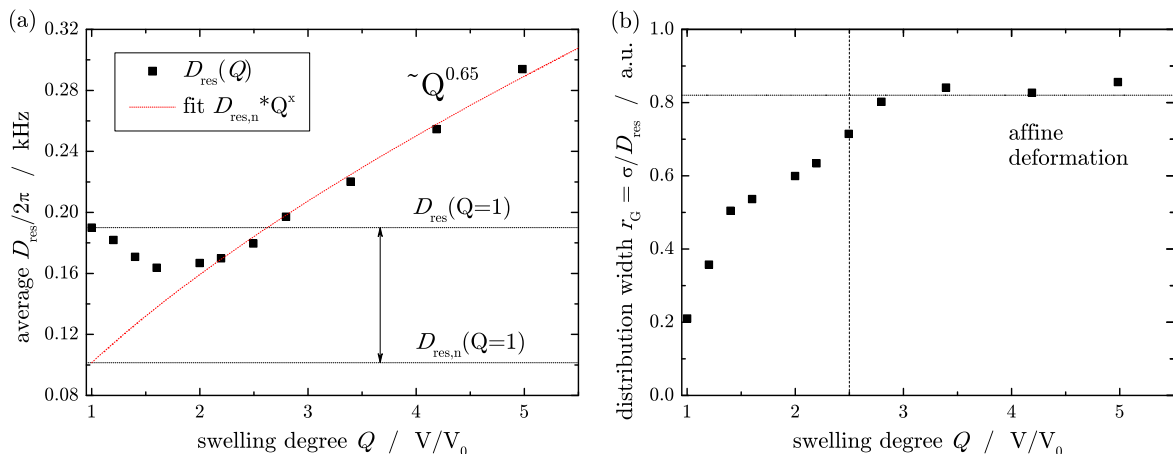
Fig. 3.8.: (a) Residual dipolar coupling constant, D_{res}, and (b) distribution width, r_{G}, of ePDMS-21 t200 in dependence of the swelling degree, Q. The dotted red line represents a power-law fit to the range of swelling degrees with affine network deformation as indicated in (b).

can be considered as affine or at least as nearby affine. This is confirmed by a roughly constant distribution width and equal-shaped coupling constant distribution. Additionally a comparable increase of the average coupling constant with respect to swelling degree is observed for all networks revealing a similar power-law dependence in a log-log representation.

The dependence of the coupling constants on the swelling degree, which is a measure of relative network deformation, so far does not reveal any universality, as essentially expected by the Gaussian chain statistics. In order to derive a consistent relation between the order parameter, represented by D_{res}, and the network deformation, the observed two stage swelling behavior is integrated in the data evaluation. The second stage of the swelling curves, which shows an affine deformation upon swelling, is fitted to a power-law according Eq. 3.6 using the deformation exponent ν_{def} and $D_{\text{res,n}}$ as free parameters.

$$D_{\text{res}}(Q) = D_{\text{res,n}} Q^{\nu_{\text{def}}} \tag{3.0}$$

The fitting region is determined by the swelling degrees which exhibit no major changes of the distribution width as shown in Figure 3.8b. In this treatment, $D_{\text{res,n}}$ is the back-extrapolated coupling constant of a dry network with assumption that the entire swelling process is affine. In Figure 3.8a it shown that $D_{\text{res,n}}$ clearly deviates of the coupling constant experimentally determined in the dry network, $D_{\text{res}}(Q = 1)$. The latter is higher as $D_{\text{res,n}}$ which is reasonable, since it was shown that the first stage of the swelling process
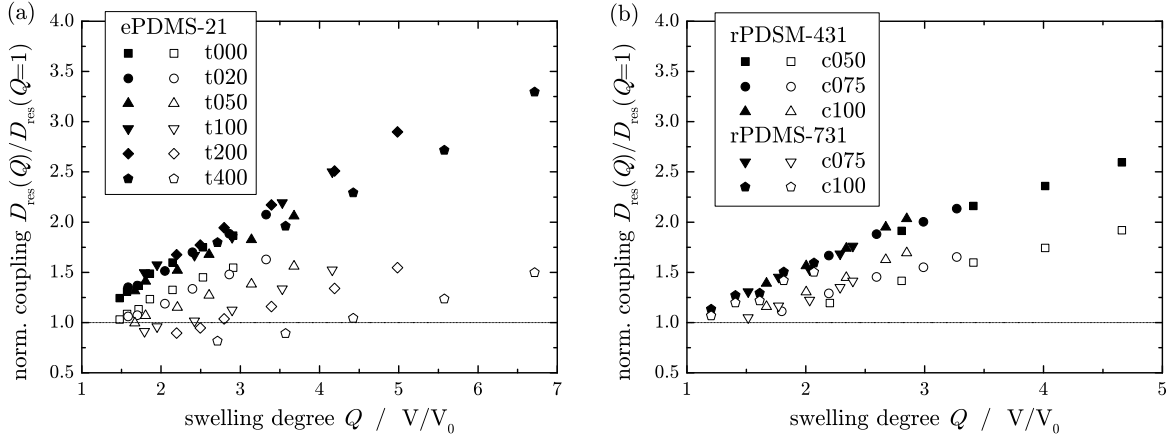
Fig. 3.9.: Dependence of the coupling constants of (a) ePDMS-21 and (b) rPDMS networks on the swelling degree, Q, in the affine stage of the swelling process. The coupling constants, D_{res}, were normalized with respect to $D_{res}(Q = 1)$ of the dry networks (open symbols) and the back-extrapolated $D_{res,n}$ (filled symbols).

is non-affine. Possible reasons for this difference will be discussed later.

Figure 3.9 displays the evolution of the coupling constants of randomly- and end-linked networks in dependence of the swelling degree. In this representation, the shown coupling constants are restricted to that determined in the second stage of the swelling process, where the affine deformation was observed. The latter are normalized with respect to the coupling constants measured in the dry network, $D_{res}(Q = 1)$, in order to investigate the relative change upon deformation and depicted by the open symbols in Figure 3.9. The data reveals no uniform dependence of residual order of the network chains in dependence of the deformation for end- and randomly-linked networks, ePDMS-21 and rPDMS, respectively. Thereby some of the ePDMS-21 networks in fact have a lower residual order as in their respective dry state, as demonstrated by the data points below the dotted line in Figure 3.9a. The filled symbols in Figure 3.9 show the same data normalized with respect to back-extrapolated coupling constant, $D_{res,n}(Q = 1)$, obtained by the power law fit to the affine deformation region. Hence, all swelling series of the end- and randomly-linked networks combine, revealing a uniform dependence of the normalized apparent residual dipolar coupling constant on the swelling degree and with that on the deformation.

In Figure 3.10 the final results of the partial swelling studies are summarized. The apparent change of the residual dipolar coupling constant upon swelling coincidences for all investigated networks. Thereby, a nearby affine deformation behavior is observed, as
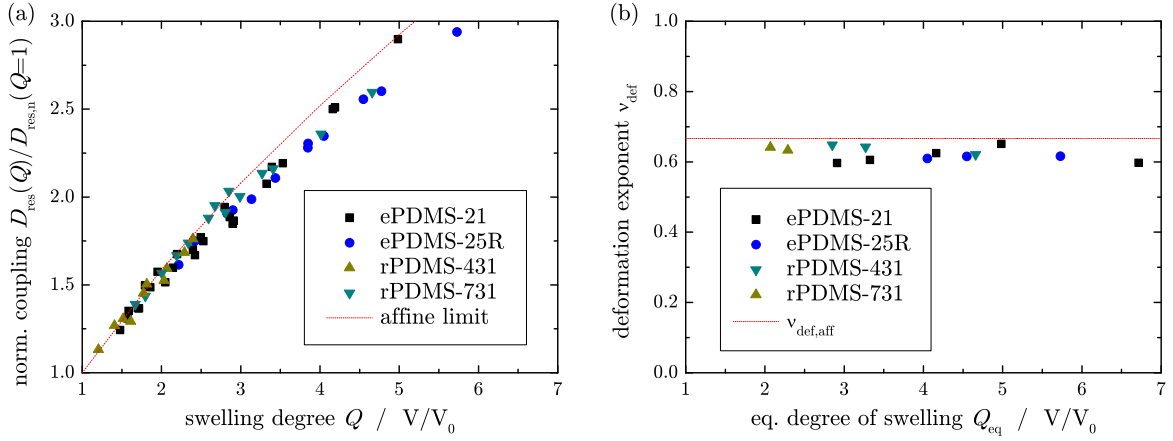
Fig. 3.10.: (a) Evolution of the normalized coupling constant in dependence of the swelling degree and (b) deformation exponents, ν_{def}, obtained by the power-law fit to the region of affine deformation in dependence on the degree of equilibrium swelling, Q_{eq}, of the respective samples. The red dotted line indicates the theoretical affine case, $\nu_{\text{def}} = 2/3$.

demonstrated by the comparison of the data and the theoretical affine behavior indicated by the red dotted line in Figure 3.10a. Also the determined deformation exponents, ν_{def}, are close to that of the affine deformation, $\nu_{\text{def,aff}} = 2/3$. However, the deformation exponents of all networks determined by the power-law fit are slightly lower, as the one of an affine deformation as shown in Figure 3.10b.

The slight deviations of the observed deformation behavior to the affine prediction may be explained with respect to the Flory-Huggins solution theory. The latter assumes no volume change upon mixing polymer and solvent meaning that their volumes are simply additive. This assumption is used for the determination of the equilibrium degree of swelling by gravimetric measurements. However, an attractive interaction between the solvent molecules and the polymer segments, as present in polymer networks swollen by a good solvent, should lead to a (presumably small) negative volume change with respect to the sum of the pure component volumes. A smaller overall volume of a swollen network results in a higher volume fraction of the polymer, φ_{p}, at equilibrium and thus in a lower swelling degree, $Q_{\text{eq}} = 1/\varphi_{\text{p}}$. This would lead to a more pronounced increase of the residual dipolar coupling constant, D_{res}, with respect to the swelling degree, Q, and with that to higher values for the deformation exponents, ν_{def}. This discussion is of course hypothetical since also inaccuracies during the preparation, i.e., evaporation of solvent during sealing of the sample tubes, might originate the same observation. At

this point it has to be mentioned that the experiments are rather challenging due to the small added volumes of solvent at low swelling degrees and the limitation of the usable amount sample. The latter is determined by the diameter of the sample tubes (8 mm) and the range where the static magnetic filed of the spectrometer is approximately constant (5 mm). Thus, especially measurements at high degrees of swelling feature a reasonable experimental noise.

Finally, the observed behavior of the coupling constant, D_{res}, in the non-affine deformation region at low swelling degrees has to be discussed. In the literature this effect is often addressed to a desinterspersion process [95, 96], which can be interpreted as a topological unfolding. The latter is induced by the swelling solvent. The solvent molecules replace monomer units of the networks chains which were swollen by each other in the dry polymer networks [95] separating the individual network strands. Thereby it is assumed that the network can swell up to certain degree without any change of the conformation of the network chains due to topological rearrangements [97, 98] meaning that the radius of gyration of the individual network strands does not change. The unfolding of the network leads to a release of topological constraints, i.e., entanglements, and thus to a reduction of the residual order [95]. This explanation is at least ambiguously for the investigated samples since rather short precursor polymers were used for the preparation of the networks.

On the other hand, the initial decay of the coupling constant is explained as solvent effect. Starting from the dry state of the network to very low swelling degrees the excluded volume repulsion is less screened due to the increase of the solvent monomer contacts. This leads to a reduction of the order parameter despite the increasing separation of the cross-links due to the expansion of network by excluded volume forces up to a certain threshold [51]. However, the investigation of samples swollen in a theta-solvent give rise to doubts about this interpretation [95]. Figure 3.11a shows the results of DQ NMR measurements on ePDMS-21 t400 swollen in toluene and styrene. The latter is a theta-solvent for PDMS at 308 K [99]. The coupling constants determined at this temperature show at low swelling degrees a similar dependence on the latter as compared to the results obtained by swelling with the good solvent. Since in the theta state the repulsive excluded volume effects are compensated completely by the attractive solvent-monomer interactions, the above discussed solvent effect, i.e., the removal of the excluded volume screening, can not be used solely for the explanation of the decreasing coupling constant.

However, the observed behavior can be explained by the presence of solvent during the *formation* of most of the investigates samples. The solvent was evaporated after
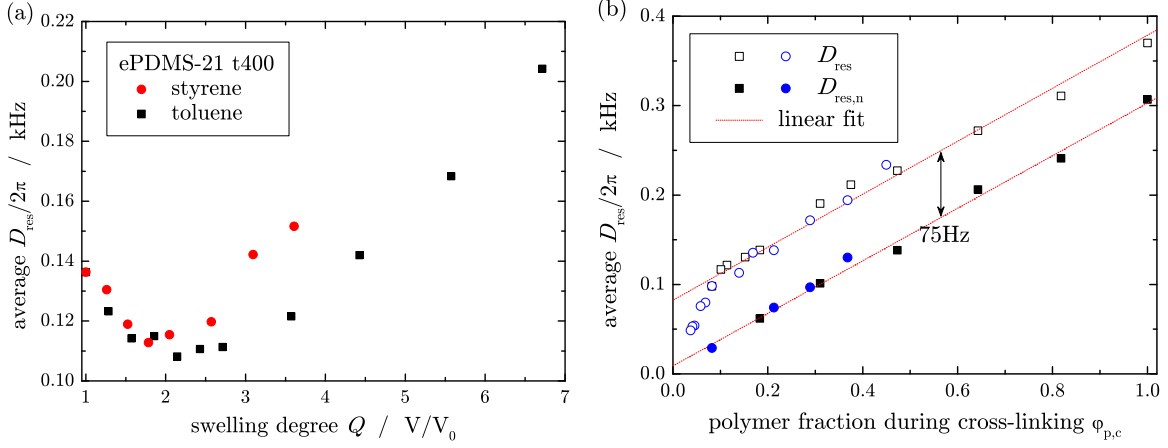
Fig. 3.11.: (a) Evolution of the residual dipolar coupling constant, D_{res}, of ePDMS-21 t400 swollen in a good solvent (toluene) and a θ-solvent (styrene) at θ-conditions in dependence of the swelling degree, and (b) dependence of D_{res} on the polymer fraction during cross-linking, $\varphi_{p,c}$, measured in dry network samples and obtained by back-extrapolation of the affine region.

the completed cross-link reaction. During this deswelling process the overall volume of the networks decreases in order to keep the density almost constant and thus the chain conformations collapse [78]. This contraction of the chains in the network due to the removal of the solvent is called 'supercoiling' [58]. Thereby it is assumed that supercoiled chains feature a contracted chain conformation in comparison to Gaussian chains. By swelling the supercoiled conformation is more and more abolished with increasing amount of solvent. In that way it can be assumed that a theta solvent induces a comparable solvent effect as the good solvent since the supercoiled chains do not feature the conformation as expected for the unperturbed reference state. This leads to a decrease of the coupling constant until the chains adopt their respective common conformation. Beyond the swelling degree at which the latter is adopted the coupling constant increases monotonously. This assumption is clearly supported by the data in Figure 3.11a. For the samples swollen by the theta-solvent an increase of the coupling constant is observed at lower swelling degrees in comparison to the samples swollen in the good solvent which corresponds to the fact that polymer coils in a theta solvent feature smaller coil expansions as in good solvents. Furthermore, this interpretation is encouraged by the stronger relative decrease of the coupling constant for samples cross-linked at lower polymer volume fractions, $\varphi_{p,c}$, as shown in Figure 3.6a. The difference of the coupling constants of the samples swollen in the θ-solvent and good-solvent at higher swelling degrees, Q,

100

shown in Figure 3.11a reflects thus nicely the impact of the solvent quality on the chain statistics.

The dipolar coupling constant, D_{res}, determined in dry samples and the back-extrapolated coupling constant, $D_{\text{res,n}}$, of the ePDMS-21 samples are displayed in Figure 3.11b in dependence of the polymer volume fraction during cross-linking, $\varphi_{\text{p,c}}$. The two coupling constants differ roughly about 70-80 Hz. This difference was also observed for all other investigated networks yielding no obvious dependence on the preparation procedure.

In conclusion, the presented data shows that swelling is a highly complex process. The dependence of the average residual dipolar coupling constant and its distribution width on the swelling degree allows for a subdivision of the swelling process into a non-affine and an affine region. The affine region is characterized by an approximately constant distribution width. Thereby the affine deformation is confirmed by comparison of the shapes of coupling constant distributions at different swelling degrees. The data of all experiments is superposed by using a back-extrapolated coupling constant obtained by a power-law fit to the coupling constants determined in the affine region. The so-obtained reduced coupling constants coincidence for all investigated networks over a broad range of swelling degrees revealing a nearby affine deformation. In the non-affine region at low swelling degrees nearby constant or decreasing coupling constants are observed. This can presumably be attributed to a combination of a solvent effect and the release of topological constraints. Nevertheless the swelling behavior in the non-affine region is not yet fully understood and requires further investigation. Therefore further experiments should be performed, i.e., partial swelling studies on samples cross-linked in presence of bad- or θ-solvents.

4. Summary

In this work the *structure*, *formation* and *thermodynamic properties* of polymer networks were investigated by NMR and equilibrium swelling experiments. For that purpose polymer networks were prepared by cross-linking end- and randomly functionalized PDMS precursor chains at various systematically changed well-defined reaction conditions.

The *structure* of randomly cross-linked networks was studied by ^{1}H double-quantum low-filed NMR and by absolute-value Miller-Macosko calculations. The results were used to investigate the impact of the network *structure*, i.e., the defect fraction and the functionality of cross-links, on the evaluation of equilibrium swelling experiments in terms of the Flory-Rehner model regarding the molecular weight between two cross-links. The *thermodynamic properties* of swollen networks as described by the Flory-Rehner theory were studied by solvent- and temperature-dependent swelling experiments of different PDMS networks and DQ NMR experiments on equilibrium swollen samples at different temperatures. The results were compared to predictions of the Flory-Rehner theory for the relation between these two quantities and the swelling experiments were evaluated in terms of a novel construction of solvent-independent swelling master curves. This allowed for conclusions about the influence of excluded volume effects on the predictions of the Flory-Rehner model in the good solvent regime and the concentration-dependence of Flory-Huggins interaction parameter. The cross-link kinetics of the end-cross-linking process in presence of solvent and the *formation* of the elastically effective network were investigated temperature-dependent by high resolution liquid-state and DQ low-field NMR. The results revealed mechanistic details of the cross-link process and were summarized in a multi-stage model for the description of the network *formation*. The deformation behavior of PDMS networks upon swelling was studied by DQ NMR experiments on samples at well-defined swelling degrees. The results were evaluated with respect to the influence of the solvent quality on the chain statistics at low swelling degrees and the universality of the deformation at higher swelling degrees.

A. Experimental Details

In this chapter the characterization and preparation of the samples and the experimental methods used in this work are explained. At first details of gel permeation chromatography (GPC) and liquid-state NMR measurements of the unprocessed pre-polymers are shown. This is followed by a detailed description of the preparation of the polymer networks. In the second part the experimental basics of the applied equilibrium swelling and NMR experiments are presented. This particulary focuses on details of the data acquisition and processing.

A.1. Poly(dimethylsiloxane)

Polysiloxanes are polymers whose backbone consists of oxygen-bridged silicon atoms. The free valences of the silicon are usually saturated by organic groups, e.g., methyl-groups in poly(dimethylsiloxane). Poly(dimethylsiloxane) exhibits a high thermal stability due to the high binding energy of the oxygen–silicon and carbon–silicon bond of about 370 and 326 kJ/mol, respectively. The combination of the latter and the chemical resistance of the C–Si bond of the attached methyl groups, enables a vast variety of possible industrial applications, i.e., biomedical devices, surfactants, lubricants, adhesives and cosmetics. Networks are typically formed by covalent cross-linking of PDMS chains with functional groups, i.e., hydroxyl or vinyl groups, and multi-functional crosslinkers with complementary functional groups. These crosslinks are very stable and show nearly no degradation due to irradiation of light in contrast to sulfur-vulcanized natural rubber. Additionally, PDMS has a rather low glass transition temperature, $T_\mathrm{g} \approx 150\,\mathrm{K}$, and characteristic ratio of $C_\infty = 6.8$. Due to these properties, PDMS networks are applicable for the investigation of rubber-elasticity, network *structure* and *thermodynamic properties* over a broad range of temperatures. Therefore end-linked PDMS networks are used in many studies as so-called 'model networks' [100].

A.2. Sample Characterization

In this study commercially available end- and randomly functionalized PDMS precursor polymers were used for the preparation of networks. All polymer samples and cross-linker were purchased from ABCR company and used as-received. The precursor polymers were characterized by gel permeation chromatography (GPC) and liquid-state NMR in order to obtain information about the average molecular weight and the polydispersity.

The GPC experiments were performed using a polystyrene standard and a diluted solution of the PDMS precursor polymers with tetrahydrofuran (THF) as solvent. The latter is a good solvent for PDMS. The liquid-state NMR experiments were performed on a Bruker Avance III 600 MHz spectrometer. For the experiments about 20 mg of the precursor polymers were diluted by 700 μl deuterated toluene and filled in 5 mm NMR sample tubes. The used cross-linker were investigated analogously using 5 μl sample volume for the NMR measurements.

The results of the investigation of the end-functionalized precursor polymer samples, a vinyldimethylsiloxy-terminated poly-(dimethylsiloxane), further referred as ePDMS, are shown in Figure A.1. The sample numbering corresponds to their lot number of the supplier. The ^{1}H liquid-state NMR spectra (Figure A.1a) are restricted to the chemical shift range around the signal of the methyl-groups and the terminal vinyl-groups. The intensity of the measured signals is directly proportional to the amount of protons at the respective groups. Thus, the comparison of the integrated signals allows a precise estimation of the average number of dimethylsiloxane monomers between two terminal vinyl-groups and with that the number average molecular weight, M_n, of the polymer

polymer	NMR		GPC		
	M_n/kDa	ρ_{vinyl}	M_n/kDa	M_w/kDa	M_w/M_n
ePDMS-21	5.20	-	4.77	9.37	1.97
ePDMS-25R	12.62	-	10.61	22.75	2.16
ePDMS-35R	35.29	-	24.81	52.01	2.10
rPDMS-431	-	0.0426	11.19	29.38	2.63
rPDMS-731	-	0.0776	12.55	32.15	2.56

Tab. A.1.: Results of the polymer sample characterization by ^{1}H liquid-state NMR and GPC.

Fig. A.1.: (a) ^{1}H spectra of ePDMS precursor samples; For clarity, the vinyl signal region is amplified 200 times over the methyl signal. (b) Molecular weight distribution of the same samples obtained by GPC. The inset shows the same results as log-log representation. The dotted line indicates the entanglement molecular weight M_e [90].

chains. The latter and the GPC results are stated in Table A.1.

The number average molecular weight obtained by NMR is for all ePDMS precursor polymers higher as compared to the results of the GPC measurements. This indicates that the purchased samples contain a certain fraction of polymer chains with just one or even without functional groups. These fractions lead to dangling chains or sol, respectively, during the *formation* of the networks.

The ^{1}H liquid-state NMR characterization of the vinylmethylsiloxane-dimethylsiloxane trimethyl-siloxy-terminated random precursor copolymers, further referred as rPDMS, yields information about the vinyl-methylsiloxane co-monomer concentration, ρ_{vinyl}, on the polymer backbone. The latter is determined by the ratio of the integrated signals of the vinyl- and methyl-groups. The copolymer density of the functionalized monomers differs roughly about a factor of two for the two used samples which have nearby same molecular weight and polydispersity as obtained by GPC (see Table A.1).

Finally, the cross-linker, tetrakis(dimethylsiloxy)silane and 1,1,3,3-tetradimethyl-di-siloxan, which have 4 and 2 functional sites, respectively, were investigated by ^{1}H liquid state NMR in order to obtain information about their functionality. For that purpose the integrated signal intensity of the Si-H protons was compared to that of the methyl-groups. Per reactive site both cross-linker have two methyl-groups containing 6 protons and one Si-H proton. Thus, the ratio of the signals is expected to be 6:1.

However, the observed ratio yields a higher amount of methyl-groups as expected for both cross-linker. This can most likely be attributed to trimethyl-siloxy impurities in the cross-linker molecules which have no functionality. In the case of the 2-functional cross-linker this assumption leads to a fraction of roughly 5 % mono-functional cross-linker molecules. The latter do not contribute to the *formation* of a polymer network and reduce the average functionality of the cross-linker to 1.95. For the 4-functional cross-linker it is unlikely that a cross-linker molecule has more than one impurity. With this assumption, the methyl/Si-H ratio yields a fraction of approximately 7 % 3-functional cross-linker molecules leading to an average functionality of 3.93.

A.3. Sample Preparation

In this section the preparation of the investigated end- and randomly cross-linked PDMS networks is reviewed shortly.

The chemical cross-link process of the above introduced pre-polymers and cross-linker molecules is based on a Pt-catalyzed hydrosilylation [101], wherein an electrophilic addition of the silane-hydrogen of the cross-linker molecule occurs to the carbon-carbon double bond of the vinyl-functionality. The reaction is commonly described by the Chalk-Harrod mechanism [102] and establishes permanent cross-links via the ethylene connection between polymer and cross-linker. The C-C bond has a binding energy of about 340 kJ/mol which is comparable to the binding energies in the PDMS chain and reasons the high mechanical and chemical stability of the networks. The used catalyst, cisdichlorobis(diethylsulfide)platinum(II) [103], was dissolved in 98 % toluene.

The randomly cross-linked networks were all prepared following the same protocol. 3 g of the rPDMS-431 and rPDMS-731 prepolymers were weighed with a precision of ± 5 mg and placed in a roll edge glass. Afterwards 20 wt% of toluene were added with respect to the used amount of polymer in order to facilitate homogeneous mixing of the components and the solution was mixed by a shaker at 1200 rpm for about 5 min. The nominal 2-functional cross-linker (1,1,3,3-tetradimethyl-di-siloxan) was added to this solution and shaken again. The amount of cross-linker was chosen so as to react with a defined percentage of the vinyl groups whereas the used amounts of cross-linker are based upon the known density of vinylmethylsiloxane co-monomers, ρ_{vinyl}, from the sample characterization by the liquid-state NMR measurements, as shown above. Additionally, the used amount of cross-linker was corrected for the fraction of mono-functional cross-linker molecules. The percentage of reacted vinyl groups is indicated by cXXX in the last part

of the sample name. After adding $7.5\,\mu$l of the catalyst solution, the sample glasses were sealed and shaken again for about 10 min. The samples were stored for 7 days at room temperature, opened and the toluene was evaporated carefully over several days in a fume hood.

The end-linked networks were cross-linked using the same sequence of steps as for the preparation of the randomly cross-linked networks. 3 g of the ePDMS-21 and ePDMS-25R prepolymers were weighed with a precision of ±5 mg and placed in a roll edge glass. Afterwards, a well-defined amount of toluene ranging from 0 wt% up to 1000 wt% was added with respect to the used amount of polymer and the so-obtained solutions were mixed by a shaker at 1200 rpm for about 5 min. The relative weight of toluene in % is indicated by tXXX in the last part of the sample name. The nominal 4-functional cross-linker (tetrakis(dimethylsiloxy)silane) was added in a stoichiometric ratio to this solution and shaken again. The necessary amount of cross-linker was calculated with regards to the results of the sample characterization by liquid-state NMR and additionally corrected with respect to the fraction of cross-linker molecules having a lower functionality. After adding $7.5\,\mu$l of the catalyst solution, the sample glasses were sealed and shaken again for about 10 min. The samples cross-linked in bulk (0 wt% toluene) were shaken for about 30 min in order to ensure a homogeneous mixing of the reactants. The samples cross-linked in presence of up to 300 wt% toluene were stored for 7 days at room temperature. All samples cross-linked at higher solvent content were stored for 14 days at the same temperature. The filling level of the sample glasses was marked and stayed approximately constant during the cross-linking process confirming that just rather small amounts of the toluene evaporated. At the end of the cross-linking time the whole sample volume was gelled. Even for the networks cross-linked at very high solvent contents no free solvent was observed. After the sample glasses were opened, the toluene was evaporated carefully in a fume hood. Completely dry network were obtained within 2 days up to 14 days in dependence of the weight fraction of the solvent.

Finally, it has to be mentioned, that the equilibrium degree of swelling, Q_{eq}, of the ePDMS-21 samples cross-linked at 600 wt% toluene and higher, is smaller as the corresponding solvent-uptake during the preparation. This has to be attributed to a kind of post-curing of the networks during the solvent evaporation due to the reduction of the spatial distance of the not yet consumed functional groups.

A.4. Equilibrium Swelling Experiments

In this section the execution and evaluation of the equilibrium swelling experiments are explained shortly. The latter were performed in order to obtain information about the equilibrium degree of swelling, Q_{eq}, which is the experimental basis for the description of the *thermodynamic properties* of polymer networks in terms of the Flory-Rehner model. Additionally, the sol content of the networks, ω_{sol}, which is the fraction of polymer chains not coupled to the network after the cross-link reaction, is determined by this experiment.

The standard equilibrium swelling experiments were carried out at room temperature (21 °C) using toluene (density $\rho_s = 0.87\,\mathrm{g/cm^3}$) as swelling solvent. From each network sample, 10 pieces of different size were cut out from the as-prepared networks and used for the investigation. The pieces were weighed in the dry state (m_0) and swollen for 4 days to equilibrium in sealable glasses in an excess of solvent (at least 10 ml). The swelling kinetics was checked for several samples, and equilibrium was found to be reached already within a day which is in agreement with results in the literature [95] and demonstrates that the used swelling time is sufficiently long. The swollen samples were carefully taken out the swelling solvent, blotted with tissue paper to remove the excess of solvent and weighed immediately (m_{sw}). Thus, the weight of the swollen sample, m_{sw}, characterizes the solvent uptake of the network. Finally, the swollen samples were placed in a fume hood, the swelling solvent was evaporated from the networks over a couple of days, and the dry samples were weighed again (m_{dry}).

The swelling of networks in large amounts of solvents allows for the extraction of network components not coupled permanently to the infinite gel leading to a drop in weight of the dry samples in comparison to the samples as-prepared. Thus the sol fraction, ω_{sol}, was estimated by comparing the weight of the networks as-prepared, m_0, and the weight of the dry networks corresponding to Eq. A.4.

$$\omega_{sol} = \frac{m_{dry} - m_0}{m_0} \tag{A.0}$$

The reliability of the so-obtained sol fraction was checked by swelling some samples to equilibrium again. The comparison of sample weights before swelling and after evaporation of the solvent revealed just minor changes of the weight which were less than 2 % demonstrating the almost complete extraction of the sol during a single equilibrium swelling experiment.

The volume of a swollen network sample, V_{sw}, is the sum of the volume of the dry

network, V_0, and the volume of the solvent absorbed in the swollen network, V_s, corresponding the Flory-Huggins theory of polymers in solution which assumes no volume change upon mixing. Thus, the equilibrium degree of swelling, Q_{eq}, and with that the volume fraction of polymer in the swollen network, φ_p, were calculated according to Eq. A.4 using $\rho_p = 0.97\,\mathrm{g/cm^3}$ for PDMS.

$$Q_{eq} = \frac{1}{\varphi_p} = \frac{V_{sw}}{V_0} = \frac{V_0 + V_s}{V_0} = \frac{m_{dry}/\rho_p + (m_{sw} - m_0)/\rho_s}{m_{dry}/\rho_p} \tag{A.0}$$

For the temperature-dependent swelling experiments 5 already sol extracted pieces of each network were used. The samples were swollen in an excess of solvent in sealable glasses placed in a thermostated oil-bath. The weight of the swollen samples was obtained as stated above and the equilibrium degree of swelling was calculated according Eq. A.4 using the corresponding temperature-dependent densities for PDMS and the swelling solvents.

A.5. Double-Quantum NMR Experiments

The ^{1}H double-quantum solid-state NMR experiments were carried out on a Bruker minispec $mq20$ spectrometer operating at a ^{1}H resonance frequency of 20 MHz with a 90° pulse length of $2.2\,\mu$s and a dead time of $2.2\,\mu$s. For the experiments the modified Baum-Pines pulse-sequence shown in Figure 2.6b was used with $n_c = 2$ for the excitation and reconversion. The defect fraction was determined by plotting $I_{ref} - I_{DQ}$ and fitted to a single-exponential decay function. The normalized DQ intensity, I_{nDQ}, was evaluated by *ftikreg* according to the procedure presented in section 3.1. For measurements on swollen samples with $Q > 5$, five consecutive experiments were accumulated due to data quality reasons.

Bibliography

[1] K. Little. Irradiation of linear high polymers. *Nature*, 170(4338):1075–1076, 1952.

[2] A. Charlesby. Effect of high-energy radiation on long-chain polymers. *Nature*, 171(4343):167–167, 1953.

[3] R. Folland and A. Charlesby. Pulsed nmr studies of radiation-induced crosslinking and gel formation in linear polydimethy siloxane. *International Journal for Radiation Physics and Chemistry*, 8(5):555 – 562, 1976.

[4] M.J. Maryanski, J.C. Gore, R.P. Kennan, and R.J. Schulz. Nmr relaxation enhancement in gels polymerized and cross-linked by ionizing radiation: A new approach to 3d dosimetry by mri. *Magnetic Resonance Imaging*, 11(2):253 – 258, 1993.

[5] A. M. Bueche. The curing of silicone rubber with benzoyl peroxide. *Journal of Polymer Science*, 15(79):105–120, 1955.

[6] P.R. Dluzneski. Peroxide vulcanization of elastomers. *Rubber Chemistry and Technology*, 74(3):451–492, 2001.

[7] A. M. Kotliar and S. Podgor. Evaluation of molecular size distributions and molecular weight averages resulting from random crosslinking and chain-scission processes. *Journal of Polymer Science*, 55(162):423–436, 1961.

[8] G.S. Grest and K. Kremer. Statistical properties of random cross-linked rubbers. *Macromolecules*, 23(23):4994–5000, 1990.

[9] S.Y. Hobbs, M.E.J. Dekkers, and V.H. Watkins. Effect of interfacial forces on polymer blend morphologies. *Polymer*, 29(9):1598 – 1602, 1988.

[10] P. Ghosh and A. Chakrabarti. Conducting carbon black filled epdm vulcanizates: assessment of dependence of physical and mechanical properties and conducting

character on variation of filler loading. *European Polymer Journal*, 36(5):1043 – 1054, 2000.

[11] H. Yang, X. Zhang, C. Qu, B. Li, L. Zhang, Q. Zhang, and Q. Fu. Largely improved toughness of pp/epdm blends by adding nano-sio2 particles. *Polymer*, 48(3):860 – 869, 2007.

[12] R. Ullman. An essay on the molecular theory of rubber elasticity. *Journal of Polymer Science: Polymer Symposia*, 72(1):39–44, 1985.

[13] J.J. Hermans. Deformation and swelling of polymer networks containing comparatively long chains. *Transactions of the Faraday Society*, 43:591–600, 1947.

[14] F.T. Wall and P.J. Flory. Statistical thermodynamics of rubber elasticity. *The Journal of Chemical Physics*, 19(12):1435–1439, 1951.

[15] H.M. James and E. Guth. Theory of the elastic properties of rubber. *The Journal of Chemical Physics*, 11:455–481, 1943.

[16] H.M. James and E. Guth. Theory of the increase in rigidity of rubber during cure. *The Journal of Chemical Physics*, 15:669–683, 1947.

[17] G. Ronca and G. Allegra. An approach to rubber elasticity with internal constraints. *The Journal of Chemical Physics*, 63(11):4990–4997, 1975.

[18] S. F. Edwards. The statistical mechanics of polymerized material. *Proceedings of the Physical Society*, 92(1):9, 1967.

[19] M. Rubinstein and S. Panyukov. Nonaffine deformation and elasticity of polymer networks. *Macromolecules*, 30(25):8036–8044, 1997.

[20] M. Rubinstein and S. Panyukov. Elasticity of polymer networks. *Macromolecules*, 35(17):6670–6686, 2002.

[21] M. Gottlieb and R.J. Gaylord. Experimental tests of entanglement models of rubber elasticity. 2. swelling. *Macromolecules*, 17(10):2024–2030, 1984.

[22] J. E. Mark and J. L. Sullivan. Model networks of end-linked polydimethylsiloxane chains .1. comparisons between experimental and theoretical values of elastic-modulus and equilibrium degree of swelling. *Journal of Chemical Physics*, 66(3):1006–1011, 1977.

[23] S.K. Patel, S. Malone, C. Cohen, J.R. Gillmor, and R.H. Colby. Elastic modulus and equilibrium swelling of poly(dimethylsiloxane) networks. *Macromolecules*, 25(20):5241–5251, 1992.

[24] M. Schulz and J.U. Sommer. Monte carlo studies of polymer network formation. *The Journal of Chemical Physics*, 96(9):7102–7107, 1992.

[25] J. L. Braun, J. E. Mark, and B. E. Eichinger. Formation of poly(dimethylsiloxane) gels. *Macromolecules*, 35(13):5273–5282, 2002.

[26] W. Paul, K. Binder, D.W. Heermann, and K. Kremer. Dynamics of polymer solutions and melts. reptation predictions and scaling of relaxation times. *The Journal of Chemical Physics*, 95(10):7726–7740, 1991.

[27] E.R. Duering, K. Kremer, and G.S. Grest. Structure and relaxation of end-linked polymer networks. *The Journal of Chemical Physics*, 101(9):8169–8192, 1994.

[28] K. Kremer and G.S. Grest. Dynamics of entangled linear polymer melts: A molecular-dynamics simulation. *The Journal of Chemical Physics*, 92(8):5057–5086, 1990.

[29] I. Carmesin and K. Kremer. The bond fluctuation method: A new effective algorithm for the dynamics of polymers in all spatial dimensions. *Macromolecules*, 21(9):2819–2823, 1988.

[30] K. Schmidt-Rohr and H.W. Spiess. *Multidimensional Solid-State NMR and Polymers*. Academic, New York, 1994.

[31] J. P. Cohen-Addad. Effect of the anisotropic chain motion in molten polymers: The solidlike contribution of the nonzero average dipolar coupling to nmr signals. theoretical description. *The Journal of Chemical Physics*, 60(6):2440–2453, 1974.

[32] J.P. Cohen-Addad. Nmr and fractal properties of polymeric liquids and gels. *Progress in Nuclear Magnetic Resonance Spectroscopy*, 25(1-3):1 – 316, 1993.

[33] P. Sotta, C. Fulber, D. E. Demco, B. Blumich, and H. W. Spiess. Effect of residual dipolar interactions on the nmr relaxation in cross-linked elastomers. *Macromolecules*, 29(19):6222–6230, 1996.

[34] R. C. Ball, P. T. Callaghan, and E. T. Samulski. A simplified approach to the interpretation of nuclear spin correlations in entangled polymeric liquids. *The Journal of Chemical Physics*, 106(17):7352–7361, 1997.

[35] R. Graf, D.E. Demco, S. Hafner, and H.W. Spiess. Selective residual dipolar couplings in cross-linked elastomers by 1h double-quantum nmr spectroscopy. *Solid State Nuclear Magnetic Resonance*, 12(2-3):139 – 152, 1998.

[36] K. Saalwächter. Proton multiple-quantum nmr for the study of chain dynamics and structural constraints in polymeric soft materials. *Progress in Nuclear Magnetic Resonance Spectroscopy*, 51(1):1 – 35, 2007.

[37] W. Chassé, M. Lang, J.U. Sommer, and K. Saalwächter. Cross-link density estimation of pdms networks with precise consideration of networks defects. *Macromolecules*, 45(2):899–912, 2012.

[38] H. Luo, M. Klüppel, and H. Schneider. Study of filled sbr elastomers using nmr and mechanical measurements. *Macromolecules*, 37(21):8000–8009, 2004.

[39] M. G. Brereton. Nmr transverse relaxation function calculated for constrained polymer-chains - application to entanglements and networks. *Macromolecules*, 23(4):1119–1131, 1990.

[40] K. Saalwächter. Artifacts in transverse proton nmr relaxation studies of elastomers. *Macromolecules*, 38(4):1508–1512, 2005.

[41] P. T. Callaghan and E. T. Samulski. Molecular ordering and the direct measurement of weak proton-proton dipolar interactions in a rubber network. *Macromolecules*, 30(1):113–122, 1997.

[42] R. Graf, A. Heuer, and H. W. Spiess. Chain-order effects in polymer melts probed by h-1 double-quantum nmr spectroscopy. *Physical Review Letters*, 80(26):5738–5741, 1998.

[43] K. Saalwächter, P. Ziegler, O. Spyckerelle, B. Haidar, A. Vidal, and J. U. Sommer. H-1 multiple-quantum nuclear magnetic resonance investigations of molecular order distributions in poly(dimethylsiloxane) networks: Evidence for a linear mixing law in bimodal systems. *Journal Of Chemical Physics*, 119(6):3468–3482, 2003.

[44] K. Saalwächter, B. Herrero, and M. A. López-Manchado. Chain order and cross-link density of elastomers as investigated by proton multiple-quantum nmr. *Macromolecules*, 38(23):9650–9660, 2005.

[45] J.L. Valentín, P. Posadas, A. Fernández-Torres, M. A. Malmierca, L. González, W. Chassé, and K. Saalwächter. Inhomogeneities and chain dynamics in diene rubbers vulcanized with different cure systems. *Macromolecules*, 43(9):4210–4222, 2010.

[46] P.J. Flory. Thermodynamics of high polymer solutions. *The Journal of Chemical Physics*, 9:660–661, 1941.

[47] M.L. Huggins. Solutions of long chain compounds. *The Journal of Chemical Physics*, 9:440, 1941.

[48] P.J. Flory and J. Rehner. Statistical mechanics of cross-linked polymer networks. *Journal Of Chemical Physics*, 11:521–527, 1943.

[49] W. Chassé, J.L. Valentín, G.D. Genesky, C. Cohen, and K.Saalwächter. Precise dipolar coupling constant distribution analysis in proton multiple-quantum nmr of elastomers. *The Journal of Chemical Physics*, 134(4):044907, 2011.

[50] W. Chassé, K. Saalwächter, and J.U. Sommer. Thermodynamics of swollen networks as reflected in segmental orientation correlations. *Macromolecules*, 45(13):5513–5523, 2012.

[51] J.U. Sommer, W. Chassé, J.L. Valentín, and K. Saalwächter. Effect of excluded volume on segmental orientation correlations in polymer chains. *Physical Review E*, 78, 2008.

[52] M. Kovermann, K. Saalwächter, and W. Chassé. Real-time observation of polymer network formation by liquid- and solid-state nmr revealing multistage reaction kinetics. *The Journal of Physical Chemistry B*, 116(25):7566–7574, 2012.

[53] P.J. Flory. The configuration of real polymer chains. *The Journal of Chemical Physics*, 17(3):303–310, 1949.

[54] M.E. Fisher. Shape of a self-avoiding walk or polymer chain. *The Journal of Chemical Physics*, 44(2):616–622, 1966.

[55] D.S. McKenzie. Polymers and scaling. *Physics Reports*, 27(2):35 – 88, 1976.

[56] J. C. Le Guillou and J. Zinn-Justin. Critical exponents for the *n*-vector model in three dimensions from field theory. *Phys. Rev. Lett.*, 39:95–98, 1977.

[57] P.J. Flory. Thermodynamics of dilute solutions of high polymers. *The Journal of Chemical Physics*, 13:453–465, 1945.

[58] P.G. De Gennes. *Scaling concepts in polymer physics.* Cornell University Press, Ithaca, New York, 1979.

[59] T. P. Lodge and M. Muthukumar. Physical chemistry of polymers: Entropy, interactions, and dynamics. *The Journal of Physical Chemistry*, 100(31):13275–13292, 1996.

[60] Jr. P.E. Rouse. A theory of the linear viscoelastic properties of dilute solutions of coiling polymers. *The Journal of Chemical Physics*, 21(7):1272–1280, 1953.

[61] J.D. Ferry. *Viscoelastic properties of polymers.* John Wiley & Sons Inc, 1980.

[62] P.G. de Gennes. Reptation of a polymer chain in the presence of fixed obstacles. *The Journal of Chemical Physics*, 55(2):572–579, 1971.

[63] F. Vaca Chávez and K. Saalwächter. Nmr observation of entangled polymer dynamics: Tube model predictions and constraint release. *Phys. Rev. Lett.*, 104:198305, 2010.

[64] F. Vaca Chávez and K. Saalwächter. Time-domain nmr observation of entangled polymer dynamics: Universal behavior of flexible homopolymers and applicability of the tube model. *Macromolecules*, 44(6):1549–1559, 2011.

[65] M. Lang and J.-U. Sommer. Analysis of entanglement length and segmental order parameter in polymer networks. *Phys. Rev. Lett.*, 104(17):177801, 2010.

[66] W. Kuhn and F. Grün. Beziehungen zwischen elastischen konstanten und dehnungsdoppelbrechung hochelastischer stoffe. *Colloid & Polymer Science*, 101:248–271, 1942.

[67] C.P. Slichter. *Principles of magnetic resonance.* Springer Verlag, New York, 3rd edition, 1990.

[68] J. Baum and A. Pines. Nmr-studies of clustering in solids. *Journal Of The American Chemical Society*, 108(24):7447–7454, 1986.

[69] K. McLoughlin, C. Szeto, T.M. Duncan, and C Cohen. End-linked poly(dimethylsiloxane) elastomer structure: 2h-nmr transverse dephasing data compared to predictions of statistical and thermodynamic models. *Macromolecules*, 29(16):5475–5483, 1996.

[70] J. Weese. A reliable and fast method for the solution of fredholm integral-equations of the 1st kind based on tikhonov regularization. *Computer Physics Communications*, 69(1):99–111, 1992.

[71] J. Weese. A regularization method for nonlinear ill-posed problems. *Computer Physics Communications*, 77(3):429 – 440, 1993.

[72] S.C. Chinn, C.T. Alviso, E.S.F. Berman, C.A. Harvey, R.S. Maxwell, T.S. Wilson, R. Cohenour, and W. Saalwächter, K.and Chassé. Mq nmr and spme analysis of nonlinearity in the degradation of a filled silicone elastomer. *The Journal of Physical Chemistry B*, 114(30):9729–9736, 2010.

[73] J. Bastide, C. Picot, and S. Candau. The influence of pendent chains on the thermodynamic and viscoelastic properties of swollen networks. *J. Polym. Sci. Polym. Phys. Ed.*, 17(8):1441–1456, 1979.

[74] C.W. Macosko and D.R. Miller. A new derivation of average molecular weights of nonlinear polymers. *Macromolecules*, 9(2):199–206, 1976.

[75] P.J. Flory. Statistical mechanics of swelling of network structures. *The Journal of Chemical Physics*, 18(1):108–111, 1950.

[76] J. Fried. *Polymer science and technology*. Pearson Education, 2003.

[77] K. Urayama and S. Kohjiya. Uniaxial elongation of deswollen polydimethylsiloxane networks with supercoiled structure. *Polymer*, 38(4):955 – 962, 1997.

[78] K. Urayama and S. Kohjiya. Extensive stretch of polysiloxane network chains with random- and super-coiled conformations. *The European Physical Journal B - Condensed Matter and Complex Systems*, 2:75–78, 1998.

[79] S.P. Obukhov, M. Rubinstein, and R.H. Colby. Network modulus and superelasticity. *Macromolecules*, 27(12):3191–3198, 1994.

[80] V.G. Vasiliev, L.Z. Rogovina, and G.L. Slonimsky. Dependence of properties of swollen and dry polymer networks on the conditions of their formation in solution. *Polymer*, 26(11):1667 – 1676, 1985.

[81] K. Urayama and S. Kohjiya. Crossover of the concentration dependence of swelling and elastic properties for polysiloxane networks crosslinked in solution. *The Journal of Chemical Physics*, 104(9):3352–3359, 1996.

[82] K. Sivasailam and C. Cohen. Scaling behavior: Effect of precursor concentration and precursor molecular weight on the modulus and swelling of polymeric networks. *Journal of Rheology*, 44(4):897–915, 2000.

[83] A. Dubault, B. Deloche, and J. Herz. Effects of trapped entanglements on the chain ordering in strained rubbers - a deuterium magnetic-resonance investigation. *Macromolecules*, 20(9):2096–2099, 1987.

[84] J.E. Mark. Experimental comparison of the theories of elasticity of polymer networks. *Journal of the American Chemical Society*, 92(25):7252–7257, 1970.

[85] S. Wang and J.E. Mark. Unimodal and bimodal networks of poly(dimethylsiloxane) in pure shear. *Journal of Polymer Science Part B: Polymer Physics*, 30(8):801–807, 1992.

[86] M. Beltzung, C. Picot, and J. Herz. Investigation of the chain conformation in uniaxially stretched poly(dimethylsiloxane) networks by small-angle neutron scattering. *Macromolecules*, 17(4):663–669, 1984.

[87] W. Michalke, M. Lang, S. Kreitmeier, and D. Goritz. Comparison of topological properties between end-linked and statistically cross-linked polymer networks. *The Journal of Chemical Physics*, 117(13):6300–6307, 2002.

[88] A.E. Tonelli and E. Helfand. Elastically ineffective cross-links in rubbers. *Macromolecules*, 7(1):59–63, 1974.

[89] J.E. Elliott and C.N. Bowman. Kinetics of primary cyclization reactions in cross-linked polymers: An analytical and numerical approach to heterogeneity in network formation. *Macromolecules*, 32(25):8621–8628, 1999.

[90] J. E. Mark. *Physical Properties of Polymers Handbook*. Springer, New York, 2007.

[91] J. P. Cohen-Addad, M. Domard, and J. Herz. Nmr observation of the swelling process of polydimethylsiloxane networks - average orientational order of monomeric units. *Journal Of Chemical Physics*, 76(5):2744–2753, 1982.

[92] J.P. Cohen-Addad, M. Domard, G. Lorentz, and J. Herz. Polymeric gels. nmr study of elementary chain swelling. effect of trapped topological constraints. *J. Phys. France*, 45(3):575–586, 1984.

[93] K. Saalwächter, F. Kleinschmidt, and J.U. Sommer. Swelling heterogeneities in end-linked model networks: A combined proton multiple-quantum nmr and computer simulation study. *Macromolecules*, 37(23):8556–8568, 2004.

[94] J. P. Cohen-Addad. Polymeric-gel swelling: Nmr evidence for the c* theorem. *Phys. Rev. B*, 48(2):1287–1290, 1993.

[95] J.P. Cohen-Addad, M. Domard, G. Lorentz, and J. Herz. Polymeric gels. nmr study of elementary chain swelling. effect of trapped topological constraints. *J. Phys. France*, 45(3):575–586, 1984.

[96] B. Deloche and E. T. Samulski. Rubber elasticity: a phenomenological approach including orientational correlations. *Macromolecules*, 21(10):3107–3111, 1988.

[97] J. Bastide, C. Picot, and S. Candau. Some comments on the swelling of polymeric networks in relation to their structure. *Journal of Macromolecular Science, Part B*, 19(1):13–34, 1981.

[98] C. Schmit and J. P. Cohen-Addad. Nmr approach to the characterization of the swelling process of polyethylene networks. *Macromolecules*, 22(1):142–146, 1989.

[99] A. Lapp and C. Strazielle. Un nouveau solvant theta pour le polydimethylsiloxane. comportement au voisinage des conditions theta et facteur d'expansion. *Die Makromolekulare Chemie, Rapid Communications*, 6(9):591–596, 1985.

[100] J. Mark. The use of model polymer networks to elucidate molecular aspects of rubberlike elasticity. In Karel Dusek, editor, *Polymer Networks*, volume 44 of *Advances in Polymer Science*, pages 1–26. Springer Berlin / Heidelberg, 1982.

[101] J.L. Speier, J.A. Webster, and G.H. Barnes. The addition of silicon hydrides to olefinic double bonds. part ii. the use of group viii metal catalysts. *Journal of the American Chemical Society*, 79(4):974–979, 1957.

[102] A. J. Chalk and J. F. Harrod. Homogeneous catalysis. ii. the mechanism of the hydrosilation of olefins catalyzed by group viii metal complexes1. *Journal of the American Chemical Society*, 87(1):16–21, 1965.

[103] G. W. Horn, R. Kumar, A. W. Maverick, F. R. Fronczek, and S. F. Watkins. Structure of cis-dichlorobis(dimethyl sulfide)platinum(ii). *Acta Crystallographica Section C*, 46(1):135–137, 1990.

List of Publications

[E1] J.U. Sommer, W. Chassé, J.L. Valentín, K. Saalwächter. Effect of excluded volume on segmental orientation correlations in polymer chains. *Physical Review E*, 78(5), 051803, 2008

[E2] J.L. Valentín, J. Carretero-González, I. Mora-Barrantes, W. Chassé, K. Saalwächter. Uncertainties in the Determination of Cross-Link Density by Equilibrium Swelling Experiments in Natural Rubber. *Macromolecules*, 41(13), 4717–4729, 2008

[E3] J.L. Valentín, P. Posadas, A. Fernández-Torres, M.A. Malmierca, L. González, W. Chassé, K. Saalwächter. Inhomogeneities and Chain Dynamics in Diene Rubbers Vulcanized with Different Cure Systems. *Macromolecules*, 43(9), 4210-4222, 2010

[E4] S.C. Chinn, C.T. Alviso, E.S.F. Berman, C.A. Harvey, R.S. Maxwell, T.S. Wilson, R. Cohenour, K. Saalwächter, W. Chassé. MQ NMR and SPME Analysis of Non-linearity in the Degradation of a Filled Silicone Elastomer. *The Journal of Physical Chemistry B*, 114(30), 9729-9736, 2010

[E5] W. Chassé, J.L. Valentín, G.D. Genesky, C. Cohen, K. Saalwächter. Precise dipolar coupling constant distribution analysis in proton multiple-quantum NMR of elastomers. *The Journal of Chemical Physics*, 134(4), 044907, 2011

[E6] W. Chassé, M. Lang, J.U. Sommer, K. Saalwächter. Cross-Link Density Estimation of PDMS Networks with Precise Consideration of Networks Defects. *Macromolecules*, 45(2), 899-912, 2012

[E7] M. Kovermann, K. Saalwächter, W. Chassé. Real-Time Observation of Polymer Network Formation by Liquid- and Solid-State NMR Revealing Multistage Reaction Kinetics, *The Journal of Physical Chemistry B*, 116(25), 7566-7574, 2012

[E8] W. Chassé, K. Saalwächter, J.U. Sommer. Thermodynamics of Swollen Networks As Reflected in Segmental Orientation Correlations. *Macromolecules*, 45(13), 5513-5523, 2012

Lebenslauf

Persönliche Daten

Name:	Chassé
Vorname:	Walter
Geburtsdatum:	31.07.1981
Geburtsort:	Halle/Saale
Nationalität:	Deutsch
Familienstand:	ledig

Ausbildung

07/2000	Abitur, Landesgymnasium Latina August Hermann Francke, Halle/Saale
08/2000-07/2001	Zivildienst
10/2001-09/2007	Martin-Luther-Universität Halle-Wittenberg
	Studiengang "Physik"
	Abschluss: Diplom-Physiker
	Thema der Diplomarbeit: "NMR - Multiquantenspektroskopie an Polydimethylsiloxan - Netzwerken unterschiedlicher Topologie"
seit 9/2007	Martin-Luther-Universität Halle-Wittenberg
	Promotion in der Fachgruppe NMR
	Fachgruppenleiter: Prof. Dr. Kay Saalwächter

Eidesstattliche Erklärung

Hiermit erkläre ich gemäß der Promotionsordnung der Naturwissenschaftlichen Fakultäten I,II,III der Martin-Luther-Universität Halle-Wittenberg vom 13.06.2012, dass ich die vorliegende Arbeit

Structure, Formation and Thermodynamic Properties of Polymer Networks as Studied by NMR

selbständig und ohne fremde Hilfe verfasst, andere als die von mir angegebenen Quellen und Hilfsmittel nicht benutzt und die den benutzten Werken wörtlich oder inhaltlich entnommenen Stellen als solche kenntlich gemacht habe. Ich erkläre die Angaben wahrheitsgemäß gemacht und die vorliegende Dissertation an keiner anderen wissenschaftlichen Einrichtung zur Bewerbung eines Doktorgrades eingereicht zu haben.

Halle (Saale), September 27, 2012

Walter Chassé